Development of Novel Imaging and Image Modeling Techniques for the Assessment and Quantification of Inter-Vertebral Motion Using MRI

A dissertation presented to

the faculty of

the College of Arts and Sciences of Ohio University

In partial fulfillment

of the requirements for the degree

Doctor of Philosophy

Niladri Kumar Mahato

August 2016

This dissertation titled

Development of Novel Imaging and Image Modeling Techniques for the Assessment and Quantification of Inter-Vertebral Motion Using MRI

by

NILADRI KUMAR MAHATO

has been approved for

the Department of Biological Sciences

and the College of Arts and Sciences by

Brian C. Clark

Professor of Biomedical Sciences

Robert Frank

Dean, College of Arts and Sciences

Abstract

MAHATO, NILADRI KUMAR, Ph.D., August 2016, Biological Sciences

Development of Imaging and Image Modeling Techniques for the Assessment and Quantification of Inter-Vertebral Motion Using MRI

Director of Dissertation: Brian C. Clark

Low back pain (LBP) is the leading cause of disability worldwide with more than eight hundred billion dollars of direct and indirect costs associated with LBP being incurred annually in the US alone. About 80-90% of all LBP patients do not have a definitive diagnosis of the etiology of pain, and are grouped under the non-specific LBP cohort. A group of such patients with unspecified etiology for their back pain are believed to have their LBP due to un-controlled and often, more than normal segmental motion involving one or more of their lumbar vertebrae. As such, many surgical treatments for LBP are directed at reducing inter-vertebral motion at and around an affected segment. The most common approaches for quantifying vertebral motion are based on radiographic assessments, which in many cases preclude scientific inquiry (e.g., use of high radiation equipment is not permitted for scientific investigations in some states, and, even when permitted, presents a major roadblock for serial assessments). This project was undertaken to develop and examine the feasibility, reliability and accuracy of a technique that used magnetic resonance (MR) images, custom built 3-D models and animations of spine-segment motion to quantify displacements in a calibrated imaging space.

Experiment 1 explored the feasibility of developing an MRI-based spine kinematics quantification technique that involved (i) creating MRI compatible solid-body objects, (ii) scanning axial images of the objects in the MRI machine to create static 3-D virtual models of the solid-bodies, (iii) scanning the solid bodies as they were displaced

within the MR imaging space through pre-determined magnitudes, and (iv) using images from the displacement trials to create background 'scenes' in an animation software where the user performed an image-to-model matching. This process called 'rotoscoping', resulted in reliable quantification of the displacements achieved with the technique developed in this aim (see Chapter 3 for full results).

Experiment 2 examined the accuracy and reliability of the MRI-based quantification technique developed in experiment 1. Porcine spine segments were used for quantification of spine motion using a standard T_1 weighted sequence and a novel 2D HYCE S (streaming) sequence. The spine segments were moved through specified measures within a custom-built device that was used to move the spine segments relative to each other through precise magnitudes of translation and rotation displacements. The images from the motion trials were used to create 3-D animations for quantifying inter-vertebral motion (translation and rotation) in the sagittal and coronal planes. The results from this experiment show that fairly accurate and reliable quantification of inter-vertebral motion can be performed using this technique (see Chapter 4 for full results).

The analysis performed in the third experiment explored the potential for weight-bearing MRI using T_2 weighted images and a semi-automated segmentation technique developed for quantifying and comparing changes in sagittal plane translation, rotation and spinal canal morphology under different loading conditions of the spine. Results from this case study showed that compressive loading induced appreciable changes in vertebral translation and rotation, spinal canal cross sectional area, lateral foraminal morphology between supine, standing upright, and upright with additional loading (10% of body mass) in a patient with recurrent disc herniation.

Together, the results from these three experiments provide evidence and support to the feasibility of developing an exclusive technique based on MR imaging, image modeling and animation technique to quantify inter-vertebral motion. This work represents one of the first attempts to apply an MRI-only technique for quantification of inter-vertebral motion with 3-D modeling and animation. This work provides insights into the usage of dynamic/streaming imaging sequences that may be used to scan real-time motion trials for quantification of real-time spine motion. Evidence from this work also supports the notion that supine vs. standing vs. standing and loaded spine-positions are associated with quantifiable changes in inter-vertebral morphological parameters. These findings indicate that the development of automated segmentation based 3-D modeling of MR images acquired with advanced sequences may be able to perform fast multi-planar, real-time vertebral motion quantification in the near future to investigate, optimize treatment and rehabilitation strategies in LBP.

Dedication

To Dr. Abhijit Mahato

Whose memories take me through this journey

&

To my dear parents

Acknowledgments

Dr. Brian Clark has been a great mentor and an inspiration to me right throughout the program. I have learnt so much from him, every step and every time, always with a smile. I am sincerely grateful for his decision to accept me as his student and helping me patiently and wholeheartedly to fulfill all requirements of the program. I am grateful to him for providing me all the resources, his time and support for the accomplishment of this work. I am appreciative for the faith placed in me to permit me to invest my efforts in essentially what was a technique development work for my dissertation. Thank you.

I would also like to express my sincere gratitude to the members of my dissertation committee, Dr. Susan Williams, Dr. Robert Staron, Dr. James Thomas, and Dr. John Cotton for their thoughtful guidance and encouraging feedback all through the program. I have learnt a lot from each one of them. I convey my thanks to Dr. Stephane Montuelle from Dr. Susan William's laboratory for helping me understand nuances of the animation software used in this work. I also thank the wonderful OMNI staff who were available whenever I needed their help for the project.

I express my heartfelt gratitude to all OU faculty, staff, students and friends in the Athens community who made me feel at home, always. My special thanks to the OU Alden Library Staff for promptly providing resources needed for my work.

Finally, I would like to acknowledge the immense support extended to me by my parents with their unconditional patience, sacrifice and blessings, and my wife Seema who has stood by me every moment as the proverbial friend, philosopher and guide, while living up to the commitments and expectations of her own career and profession.

Table of Contents

Page

List of Tables

Page

List of Figures

Page

List of Abbreviations

AJX: anatomical joint axis

DICOM: digital imaging and communications in medicine

DLT: direct linear transformation

EMG: electromyography

ES: erector spinae muscle

GUI: graphical user interface

ISB: international society of biomechanics

JCS: joint co-ordinate system

LBP: low back pain

LDH: lumbar disc herniation

MEL: maya embedded language

MF: multifidus muscle

MRI: magnetic resonance imaging

fMRI: functional magnetic resonance imaging

RLDH: recurrent lumbar disc herniation

STC: standardization and terminology committee

T_1: T_1 weighted sequence

TIFF- tag index file format

VBM: voxel based morphometry

XROMM: x-ray reconstruction of moving morphology

2D HYCE S: two dimensional hybrid contrast enhanced streaming sequence

2-D: two dimension/dimensional

3-D: three dimension/dimensional

Chapter 1. Introduction

Background and Significance

Low back pain (LBP) is a leading cause of physical disability in the world with $850+ billion spent annually as direct and indirect costs in the US alone (108, 280, 343, 405). Acute or chronic LBP may result from a myriad of etiologies or may arise from a non-detectable cause (322). Regardless of the etiology, LBP has been associated with aberrant vertebral motion (45, 178, 338). To this end, many of the expensive surgical treatments and rehabilitation programs directed towards mitigation of spine pain are focused towards reducing, and often obliterating, inter-vertebral motion in a spine segment (176). The most common approaches for quantifying vertebral motion are based on radiographic examination and/or clinician palpation (1, 20, 145, 185, 322), and a few use MRI, for a 2-D assessment of spine kinematics (254). The vast majority of current approaches for quantifying spine kinematics require exposure to high levels of x-ray radiation (e.g., quantitative fluoroscopy and functional radiography), which in many cases preclude scientific inquiry (e.g., use of high radiation equipment is not permitted for scientific investigations in some states, including Ohio) (398, 467). Moreover, more sophisticated radiography techniques for mapping spine kinematics are not sufficiently developed for routine use in clinics. These findings underscore the need to develop techniques that can investigate complex spine motion without the use of ionizing radiation (246, 256, 350, 427, 472).

Although aberrant inter-vertebral motion has been reported in a large number of patients with LBP, attempts to mechanistically and etiologically link vertebral motion (commonly referred to as instability by clinicians) and LBP have been mostly inconclusive (45, 178, 298, 338, 391). (143, 360, 361). Although studies have

documented co-existence of aberrant vertebral motion with degenerative disc disease (38, 178, 235, 336), there is very little agreement between clinically determined LBP, characteristics of radiologically determined spine motion or the degree of disc degeneration (1, 20, 113, 239, 325, 451, 480). This discrepancy exists for three primary reasons. Firstly, truly determining the interrelationship between LBP and segmental vertebral motion is difficult as investigations are hampered due to a lack of techniques to reliably and accurately quantify vertebral motion (38, 235, 239, 451, 480). Secondly, most of these techniques use high doses of ionizing radiation exposure, which ultimately limit their use. Thirdly, lack of availability of techniques for 3-D and real-time (dynamic) evaluation of spine motion restricts investigation of derangement of complex spine motion patterns to LBP. It has been understood that the availability of a multi-planar, real-time assessment technique will improve the accuracy of quantification of inter-vertebral motion and will enhance our understanding of the association between abnormal vertebral motion and LBP (215, 424). The purpose of this work was to develop novel techniques and approaches to ultimately quantify motion of the spine using non-ionizing magnetic resonance imaging (MRI).

This work represents one of the first attempts to apply a MRI-only technique for quantification of inter-vertebral motion with 3-D modeling and animation. The two-fluoroscope orthogonal imaging techniques such as a dual fluoroscope imaging system (DFIS) or radio stereo-photogrammetry (RSA) performing real-time motion analyses in spine segments motion require exposure to ionizing radiation, and at times, implantation of metallic markers in the skeletal tissues. Therefore, the need for an improved and safer technique has motivated me to undertake this project. Accordingly, this research work envisages accomplishing quantification of spine motion using only-MR imaging and

image modeling technique. This work is a pioneering attempt to, in the long-term, develop an animation based quantification technique for the human lumbar spine *in vivo*.

The research question. *Is it possible to reliably and accurately quantify 3-dimensional inter-vertebral motion in the lumbar spine using an MRI-only based imaging, modeling and animation technique?*

Specific aims.

Specific aim 1. To develop and test the reliability of an MRI-based technique for quantifying translational and rotational motion of solid body objects. Hypothesis: Quantification of solid-body motion using MR imaging and 3-D modeling is feasible and can be performed reliably. Approach: Solid-body objects that can be moved in the MR imaging space through pre-determined magnitudes were created and the imaging volume to conduct the motion trials was custom-calibrated. The solid bodies were then moved in the MRI while imaging them with a T_1 and a contrast-enhanced hybrid (2D HYCE S) streaming sequence. Next, 3-D models of the solid bodies and images from the displacement trials were imported into the Maya animation software. The animator then performed a model-to-image matching that quantified motion in the solid bodies the desired plane of analysis.

Specific aim 2. To develop a reliable and accurate MRI-based technique for quantifying translational and rotational motion of spine segments in an *ex vivo* porcine spine model. Hypothesis: Quantification of porcine spine motion will be highly reliable and accurate. Approach: Virtual 3-D models were built from MR images acquired from dissected porcine spine segments. The scanning volume within the imaging space was calibrated and the spine segments were fit into a custom-built device that allowed precise control of motion. Images of the porcine spine motion were acquired using a standard T_1 weighted sequence and a novel dynamic 2D HYCE S sequence. The

images from the motion trials were used to create real-time 3-D animations for quantifying inter-vertebral motion.

Experiments. Experiment 1 addressed Specific Aim 1 using a combination of MR imaging and 3-D modeling and animation techniques to quantify inter-vertebral motion in a pair of solid-body objects. A pair of solid-body models made of solid wood blocks were built with hour-glass shaped hollows created inside the cubes to represent landmarks. These landmarks were later used for animation. The wooden models were first scanned axially with a T_1 sequence to create 3-D models of the objects. The volume of a selected MRI coil was calibrated with a custom-built calibration grid. Next, the solid bodies were displaced (translated and rotated) relative to each other within the MRI coil through specific magnitudes. At each displaced position, the solid bodies were scanned using a standard T_1 and a dynamic contrast enhanced streaming 2D HYCE S sequence. Images from the displaced scans and the 3-D model were imported into an animation software. The images from the displacement trials were processed and displayed in the animation as background ‘scenes’. The user then applied a model-to-image matching technique to ‘fit’ the 3-D models to their outlines visible in the ‘scenes. This process recreated the motion trial in the animation software that quantified the displacements in any plane of motion selected for analysis (154).

Experiment 2 addressed Specific Aim 2 using an MRI-based 3-D modeling technique developed in Specific Aim 1 to quantify inter-vertebral motion in a disarticulated porcine spine-segment model. 3-D models of the porcine vertebrae were created by a ‘segmentation’ technique from axial T_1 weighted scans of the spine segments. Thawed out porcine spine segments were mounted in a custom-built MRI compatible motion control device. The vertebrae were then moved (translated and rotated) through specified magnitudes of displacements and scanned at each displaced

position using a T_1 and a novel streaming sequence to image the displacement trials. Spine motion trials were performed in the flexion-extension (sagittal) and lateral-bending (coronal) planes. Finally, the images and the 3-D spine models were used to perform a model-to-image matching technique to recreate the motion trials in the animation platform to quantify inter-vertebral motion in the porcine spine model.

Exploratory aim 3. To explore the potential for weight-bearing MRI to detect changes in sagittal plane vertebral translation and rotation, and in spinal canal morphology under different loading conditions. *Hypothesis*: Compressive loading would be associated with changes in vertebral translation and rotation, spinal canal cross sectional area, lateral foramina dimensions and inter-vertebral morphology. *Approach*: T_2 weighted images were acquired in different loading conditions (supine, standing upright, and upright with additional 10% of body mass) in a patient with recurrent disc herniation. Image analysis will be performed using proprietary software (OrthoCAD®, Esaote SpA) and morphological parameters across loading conditions compared.

Experiment 3 addressed the Exploratory Aim 3 with acquisition of T_2 weighted MR images of the lumbar spine in different axial loading conditions in a weight-bearing open-MRI machine. Semi-automated segmentation of the images was performed using a proprietary software to quantify changes in inter-vertebral morphological properties (linear, angular and cross sectional areas) in the sagittal 2-D plane. Assessment of inter-vertebral morphology is usually performed using radiographic techniques in un-loaded condition of the spine (78, 243, 273). This case study provides MRI based analysis of compressive axial loading (in the upright standing position) of the spine in a patient with unilateral recurrent lumbar disc herniation. Most studies reporting effects of spine loading in such conditions are usually imaged in the supine position with axial

compression applied with loading devices used in the recumbent position (93, 144, 156, 224, 264, 265, 310, 472).

Significance. To date, imaging vertebral motion has primarily been restricted to analyzing positional changes in vertebrae from images acquired at the end-ranges of bending movement. There are virtually no techniques available that allow visualization and analysis of spine movement in a dynamic context, especially applying MR imaging. This project addressed a major scientific problem of not being able to safely and accurately assess spine segmental motion in physiologic weight-bearing position, which is a barrier for optimizing therapeutic strategies in LBP. Development of an accurate and reliable MRI-based motion analysis technique was the goal of this project. The results from this work are impactful because, in the long term, they should result in the development and validation of a novel, non-radiation based, 3-D image analysis protocol for quantification of real-time inter-vertebral motion. Further, this work will also explore the clinical utility of a similar 3-D segmentation based semi-automated technique to detect inter-vertebral morphological alterations in lumbar disc herniation.

Innovation

The proposed work is innovative for three reasons, as enumerated below. This represents one of the pioneering efforts to develop a quantification technique for assessment of solid-body motion in 3-D that was based exclusively on a MR imaging platform. This technique is particularly innovative as it will (i) use a porcine spine model fit in a custom-designed apparatus to permit precise control of inter-vertebral movement and thus establish accuracy of the proposed method, as well as (ii) use a novel contrast-enhanced streaming (2D HYCE S) pulse sequence that permits scanning of moving objects (55). The images acquired will be used to animate the trials of spine

displacements using an animation software. Lastly (iii), the innovative use of physiological weight-bearing MRI, especially in context of investigating changes in inter-vertebral morphology secondary to differential axial loading of the spine, is a new approach to detect clinically meaningful changes in symptomatic disc herniation patients. The use of a two-camera orthogonal perspective (biplanar visualization) to enhance assessment accuracy of and detecting out-of-plane motion in the solid bodies, and the use of multiple anatomical landmarks for rotoscoping are highly innovative approaches not reported prior. The technique offers the potential of setting up multi-planar imaging that can be used to view vertebral coupled allowing analysis of more complex spine motion.

In the long-term, improving the imaging technique (e.g., using higher resolution images, faster multi-planar image acquisition) with automation of image segmentation will facilitate accurate quantification of joint kinematics. Availability of better visualization techniques of spine motion have the potential to change the concepts of diagnosis and treatments in the fields of physical medicine and rehabilitation, orthopedics, physical therapy, especially in context of LBP.

Assumptions Limitations and De-Limitations

Assumptions. (i) Equipment employed in this work, such as the MRI scanner and the motion control device, were in proper working condition, and all data collected from such equipment was accurate.

(ii) The solid bodies and the porcine spine did not undergo mechanical deformation between displacements (22).

Limitations. Current MRI technology restricts image acquisition to a single perspective (view) at a time. This image acquisition perspective, or view, was flipped

orthogonally to create the ‘second view’ of the biplanar displacements in the solid-body mode experiment to improve the accuracy of the quantification and to allow the detection of out-of-plane motion in the models. Development of advanced sequences may allow simultaneous, multi-planar imaging of dynamic motion trials in the future. However, the technique presented in this study, in its current form, is capable of acquiring serial multi-slice multi-planar images at any given position allowing quasi-dynamic assessment of motion (154). The inability to obtain simultaneous orthogonal images from a trial is currently a limitation of this technique.

The apparatus used to displace the motion-segments was custom made as an MRI-compatible device. The design of the device was kept very simple and could be used to move linked objects independently through all degrees of freedom except translation in the vertical axis. The vertebral elements in AIM 2 were disarticulated to (i) keep the design of the device simple, MR compatible and, (ii) get precise measures of displacements to check the accuracy of the technique, and (iii) permit quantification of uniplanar displacements in a one-at–a-time format and to avoid analysis of complex coupled rotations in the porcine spine models. Additionally, a number of studies investigating spine kinematics quantification techniques have used completely disarticulated cadaveric spine specimens (70, 398, 459). While this approach is justified scientifically, it should be noted that uncoupling the spine segments reduces the external/ecological validity of our model.

Delimitations. Custom-made solid-body systems were used to accomplish AIM 1 due to convenience of testing the feasibility of the technique and to avoid any biohazards. Porcine spine models were used for AIM 2 experiments as these biological specimens were easy to procure and are considered closer analogues to the human spine (205, 267). The cost of MR imaging and the time constraints for testing the

feasibility and then working on the refinement of the technique did not permit me to increase the number of spine samples and the number of displacement data points used in this study. In AIM 3, classification of disc degeneration in the patient was not performed as it was out of the scope of the work. The main aim here was to quantify inter-vertebral morphology across the three loading conditions used in the experiment.

Chapter 2. Review of the Literature

The following sections in this chapter provides an overview of the available literature related to the different aspects of the human spine and spine kinematics as related to the scope of this dissertation work. There are five sections or parts in this chapter. Part I discusses the structural elements of the spine. Part II deals with the functional lumbar motion-segment components. Part III covers the biomechanical and clinical perspectives of aberrant lumbar spine motion that enables us to understand the basic mechanistic relationship between the structural integrity in the normal spine and changes associated with LBP. The next to last section (Part IV) focusses the range of techniques available for imaging inter-vertebral static and dynamic spine displacements. The concluding section (Part V) examines the background for developing the current work that aims to quantify lumbar spine segmental motion based on an MRI-only technique without using any ionizing radiation.

(Note: Alphabetic subheadings of all figures related to this chapter presented in the figures section are provided at the bottom of the figure panels).

Part I. Structural Determinants of the Lumbar Motion-Segment

The basic structural and functional unit of the spine is a single spinal segment (motion-segment) defined as two adjacent articulated vertebrae with the intervening intervertebral disc. These structures are articulated with the help of several ligaments and short and long segmental muscles. Anatomical experimental models of the spine have been used to investigate the attributes of mechanical forces that tend to disrupt natural spinal stability at susceptible and specific locations. Additionally, simulation experiments on mathematical models of the spine constructed based on the data obtained from mechanical testing of biological spine models have yielded important

insights and closer approximation of the functioning of the spine *in-vivo* during static load bearing as well as during dynamic movements of the spine (338, 341). Accordingly, different therapeutic interventions directed to mitigate symptoms arising from aberrant spine segmental motion are often directed toward the preservation, restoration, or replacement of the normal spine anatomy in order to combat pain and to reinstate physiological function of the intervertebral discs, the vertebral endplates and the facet joints (67, 236, 358, 368, 381).

The absolute range of motion (ROM) in any degree of freedom at any given lumbar motion segment is regulated by passive (bones and ligaments) and active elements (muscles) (341). This classification has also divided motion at different spine-segments in terms of sections or 'zones' within the entire ROM. Vertebral joint movements have been found to be freely executable without any intrinsic opposition to motion at the mid-ranges of the ROM, close to the neutral position of the joint. This zone of relatively unopposed motion has been termed as the Neutral Zone (340, 341). On both sides beyond the neutral zones, movements are intrinsically restricted to a greater extent than that experienced in the neutral zones, by surrounding joint tissues and by active contractions of segmental muscles. This area of the ROM is defined as the (b) Elastic Zone. As the joint movement approaches the end range of physiological motion, greater degrees of resistance are experienced by the moving segments with eventual cessation of further motion as the bony elements in the joints come in close apposition. The sizes of these two zones have been hypothesized to vary dynamically depending upon the magnitude of loading, spine motor control and in presence of spine tissue injury (341). The sizes of the two zones add up to constitute the absolute ranges of motion at each spine level (Figure 1). Anatomical structures that determine structural integrity of

the vertebral segments are the: (a) inter-vertebral discs (IVD), (b) facet joints, (c) the lumbar musculature and (d) spinal ligaments. Each of these are discussed below.

Inter-vertebral discs (IVD). Each IVD has a gelatinous core (nucleus pulposus) made up of randomly arranged collagen fibers and radially disposed elastin fibrous shell embedded in a highly hydrated aggrecan-containing gel (368) (Figure 2). Cells in the nucleus look like chondrocytes (368). The peripheral part of the disc (annulus fibrosus) is made up of a series of concentric collagenous lamellae. About 15-25 lamellar sheets surround the nucleus angled at about 60º to the vertical axis and directed either left or right to the vertical axis in adjacent lamellae (10, 358, 368). Elastin fibers are present between these lamellae and the tough concentric lamellae of the annulus fibrosus create a water-tight zone at the center of the vertebral body. When a compressive load is subjected to the vertebral body, the central nuclear gel expands and generates a tensile hoop stress in the annulus that facilitates uniform loading of the endplates and prevents aberrant motion such as twisting, bending and shearing in the inter-vertebral segments (10, 19, 196, 260, 328, 368). Structural degeneration from perpetual mechanical overloading is often associated with disc degeneration and LBP (10, 341, 368). Loss of gel-like characteristics, increase in fibrotic content and reduction in the hydrostatic pressure zone created by the tight nuclear gel region characterizes disc degeneration (19, 75). Additionally, nerve and cell proliferation is also seen at the sites of the degeneration (177, 217, 383). Formation of new blood vessels (neo-vascularization) and new nerves (neo-neuralization) are observed at the disc-centers as these areas exhibit a loss of pressure. The loss of pressure allows cellular proliferation due to accompanying enzymatic changes that result in the loss and breakage of collagen and an increase in disc fibronectin. The increase in fibronectin content makes the disc fragmented and with

additional loss of the proteoglycan content, the disc demonstrates changes in its loading behavior. Further, a loss of aggrecan allows free movement of large molecules like serum proteins and cytokines through the disc matrix. The loss of disc aggrecan accelerates neural ingrowth in to the disc connective tissue matrix (30, 100, 177, 266, 281, 302, 326, 381, 445). Infiltration of nerves and capillaries into the center of the nucleus pulposus have been considered two major factors that result in chronic disc-related LBP, associated muscle spasm and aberrant segmental motion. Imaging studies and tests in sedated LBP patients demonstrate significant correlation between the severity of back pain and degree of disc degeneration, facet joint arthropathy and spine ligament injury (59, 67, 100, 138, 188, 242, 338). Evidence suggests that improper disc loading, as seen with associated degeneration, result in inflammation, fibrosis and loss of annular structure at the periphery of the discs. Abnormal loading in spine motion segments is characterized by changes in the instantaneous axis of rotations (IAR) during dynamic spine movements, pain, loss of agonist-antagonist muscle control (116, 159, 282, 316, 356, 357, 402).

There are two major hypotheses that have attempted to address disc degeneration in humans and in experimental animals. (a) The overload or 'wear and tear' hypothesis proposes that a more demanding mechanical environment produces localized trauma of the disc that leads to progressive accumulation of micro-trauma resulting in weakens of the disc and lumbar vertebral endplates (18, 445). (b) The 'mechanical pathogenesis' hypothesis suggests that hypo-mobility of the disc resulting from the initial traumatic assault produces adaptive changes that may cause metabolically initiated tissue weakness and degeneration secondary to the inactivity-related reduction in disc cells and altered metabolic composition (169, 206, 384). Typically, recent-onset degeneration may be associated with relative hypo-mobility at the

affected motion segment early and in the later stages of degeneration (304, 317). However, the middle phase of degeneration is believed to demonstrate a transient change in vertebral motion with an increase of laxity around the neutral zone, predisposing end-plate spinal injury even with low magnitudes of loading. In the later stages of degeneration, excessive motion at the degenerative segment is believed to be restricted with formation of osteophytes at the facet-edges and at the endplates borders with occasional ossification of ligaments (304, 317, 341, 417). Additionally, alteration in mechanical load bearing at a primary affected motion segment is believed to induce pathological changes at adjacent vertebral joints depending on the duration, location, and stiffness of the primary lesion (72, 98, 124, 143, 211). Asymmetric loading seen in scoliosis also leads to tissue deformation, nutritional impairment and altered disc composition as evidenced with adaptive disc remodeling secondary to experimental immobilization or overload induced alteration in material properties and structural disc-failure (72) (226, 331).

The facet or zygapophyseal joints. Anatomically the spinal motion segment comprises a three-joint complex, namely the secondary cartilaginous joint (inter-vertebral discs connecting the vertebral bodies), and the two pillars represented by the synovial facet joints (3, 51). The size and orientation of the facet joints vary throughout the backbone with changing angular orientation of the articular surfaces that allow specific and limited range of axial rotation at different regions of the spine (15, 125, 232, 332-335, 459) [Table 1]. Typically, the inter-vertebral disc gets loaded in forward flexion of the spine and the zygapophyseal joints are loaded in extension and lumbar rotation (16, 357, 358, 368, 471). It is estimated that ~ 8% of the total compressive load incumbent on a lumbar vertebra in the neutral position of the spine is shared by the facet joints (Figure 2 C), and the share of this load increases as the spine bends backwards (extended) (9,

11-13, 17, 358). Rich nociceptive innervation of the facets makes them one of the primary sites of pain generation in a subset of LBP patients demonstrating load-related disc degeneration and degenerative spondylolisthesis (13, 57, 60, 63, 131, 167, 379, 395, 471). Therapies directed to mitigate LBP often target to stall the process of degeneration at the facet joints (379, 393, 395). Facet sensory innervation is usually derived from the medial divisions of the dorsal rami that also innervate surrounding ligaments (Figure 3A). The motor branches to the small inter-segmental Multifidus (MF) muscles are derived from the dorsal ramus as well and segmentally control inter-vertebral motion at the joint segment (60, 63, 67, 236, 379, 393, 432) (Figure 4). However, certain structures close the facets like the posterior margin of the intervertebral disc, the posterior longitudinal ligament, and the dura-mater are innervated by branches from the ventral primary ramus (the sinu-vertebral nerve) instead of the dorsal rami (62, 63, 210, 471) (Figure 3A & 4). Therefore, a wide range of sensory-motor reflex loops may potentially be activated depending upon the tissue origin of the LBP (60, 63, 307, 393, 394, 396). Anatomical facet joint asymmetry (topism) (Figure 3B) and nerve entrapment have been recognized as two primary reasons for facetogenic pain accounting for 15 - 40% of all chronic and diagnosed LBP (51, 210, 288, 389, 394). Injuries to the pars inter-articularis (spondylolysis), posterior ligament defects and para-spinal muscle deficiencies result in facet joint stress and pain that is often worsens on standing and lumbar extension (with radiation to ipsilateral buttock and posterior thigh) and a feeling of relief on sitting and forward flexion or anesthetic ‘blocking’ of the medial branch of the dorsal rami (259, 288, 320, 379).

Spondylolisthesis is defined as the slipping of one vertebra on top of the lower one. The cause for such slippage could range from a dysplastic facet, elongation, trauma or fracture of the pars inter-articularis or may result from a primary degeneration

of the facet or from a generalized bone disorder (119, 125, 232, 236, 259, 471). As a result, abnormal joint stress leads to adaptive osteophyte formation, degenerative capsular laxity, ligament instability, overriding and subluxation of the facets (106, 307, 342, 358). Progressive deterioration of joint ROM, neutral zone changes, pathological end-range motion, velocity/acceleration control of joint motion may all lead to facet arthropathy and aberrant joint motion (28, 58, 131, 389, 396).

The range, pattern and trajectory of spine motion depend upon the level of the lumbar segment and can also be influenced by the variability of the facet joint anatomy and degree of muscle control. Invariably, quantification of spine motion forms an important topic of objective investigation to triangulate possible links between spine anatomy, spine-motion motor-control and if present, the concomitant LBP.

Local segmental and global lumbar muscles. The complex role of muscles in determining spine motion in response to physiological loading and adaptation to injury has been studied extensively. However, despite identifying factors such as alterations in onset of muscle-activation, latencies, activation patterns and deficiencies in para-spinal muscle co-activation as some of the major causes of chronic LBP, it has not yet been conclusive if these changes are etiologically linked to the pain or if they constitute compensatory neuro-musculoskeletal changes in response to mitigate LBP (82, 150, 201, 247). Additionally, altered muscle activation patterns have been recognized as adaptive responses to expected or unexpected experimental trunk perturbations (149, 150, 345). Reviewing trunk muscle activation patterns in the context of the two alternate LBP-related hypotheses of muscle activation discussed earlier, *van* Dieen and co-workers have brought forward some interesting aspects of muscle activation in LBP patients (448). According to this review, the “pain-spasm-pain” hypothesis of LBP suggests that spine pain leads to voluntary or involuntary complete ‘splinting’ of the

affected spine segment from all expected or unexpected segmental motion where any incumbent motion is perceived to be potentially painful. On the other hand, the 'pain adaptation' hypothesis proposes an increase in antagonist muscle activation that slows down spine motion to guard against the exacerbation of existing pain. This controlled and selective slowing down of spine motion is achieved by controlling segmental stiffness by the MF at individual spinal levels. At the same time the larger global muscles like the ES controlled the overall movement and orientation of the lumbar spine in space. This selective activation of muscles is facilitated by the precise attachments of the superficial and the deep groups of back muscles and their specific innervations (60, 270, 271, 388).

The bulk of the back extensor muscles comprise the Erector Spinae (ES) (Figure 5). These muscles are larger, lateral and more superficial than the MF that are smaller, more medial and relatively deeper to the ES. The ES muscle mass is composed of a medial (longissimus) and a lateral division (ilio-costalis) (Figure 5). On each side, both these divisions of the ES cover the thoracic as well as the lumbar regions and hence are named according to their locations in the thoracic (pars thoracic) and lumbar (pars lumborum) (Figure 6A and 6B) regions (269). All four components of the ES caudally attach to the dorsal aspects of the sacrum and the ilium. The complexity of the ES lies in the overlapping nature of its long fascicles that successively fan out upwards towards the ribs. For functional reasons, both the cranial and the caudal ends of the ES muscle fibers become largely aponeurotic close to their osseous attachments (221).

The medial division of the ES (longissimus) is made up of about five long fascicles that arise from the lumbar accessory and the transverse processes (Figure 6A). Some fibers of the longissimus also arise from the dorsal part of the iliac crest. On the other hand, the L1-L4 fascicles arising from the respective vertebral processes are

covered on their lateral sides by an aponeurotic barrier (the lumbar intermuscular septum) separating the lumbar longissimus from the ilio-costalis part of the ES. The lateral division of the ES (iliocostalis) has both lumbar (iliocostales pars lumborum) and thoracic parts. The lumbar ilio-costalis lies lateral to the longissimus pars lumborum (Figure 6B) and arises from the tip of the upper four lumbar vertebrae extending to the dorsal segment of the iliac crest. The fibers are mostly fleshy without prominent tendons at their osseous attachments. The wider attachments of the cranial end of the ES pars lumborum assist the ES to function more as the global muscle of the trunk that controls the movement of the trunk as a whole (269).

The MF constitutes the most medial smaller and shorter group of muscles situated in the osseous groove formed by the spinous process and the laminae of the lumbar vertebrae (Figure 5, 6 & 7). The MF belongs to the transverso-spinalis group of muscles that run in short vertical segments cranio-caudally deep and medial to the ES. The lumbar MFs arise as five short individual bands from each of the bases of the L1-L4 spinous processes. The shortest fascicle in each band is also the most medial one. The lower parts of each MF fascicle gets attached to the mammillary process of the vertebrae located one-to-two segmental levels below their origins. The longer, lateral and more superficial fascicles reach and insert onto mammillary processes or the dorsal surface of the sacrum. The L5 MF band comprises of only one fascicle that inserts onto the dorsal sacrum. The rotatores and the inter-transversii (between successive transverse processes) muscles and inter-spinales (between spinous processes of adjacent vertebrae) muscle groups are situated deep to the MF and like the MF, control inter-segmental curvature and small segmental movements of the lumbar spine (74, 110, 137, 230, 269, 480). Typically, the primary dorsal rami of the spinal nerves innervate the intrinsic layers of the lumbar region (Figure 4). The medial motor branches of the dorsal

rami innervate the MF segmentally, whereas the intermediate and lateral branches of the dorsal rami form plexuses to supply the larger, ES muscles (60, 62) (Figure 4). The segmental nature of MF innervation permits greater fascicular control of the MF elements (204, 308, 416). On the other hand, ES innervation demonstrates larger collateralization via intersegmental communicating loops (60). Accordingly, MF activates segmental rigidity and the ES generates the torques required for moving the spinal column in space [Table 2]. Typical orientation of the fascicles in the superficial and deep back muscles enable application of a range of force vectors depending on the direction of the muscle fascicles (268, 269). Additionally, complex interaction between the pulls of the ES and MS muscles help to sustain complex spine movements fine-tuned by the proprioceptive feedback loops connecting the passive and active spine sub-systems to control segmental motion (61).

In addition to the anatomy of the motion-segment articulation and the gross structure of the back muscles, the properties of the muscle fibers have been thought to play an important role in influencing the onset and prognosis of LBP. In terms of muscle fiber properties, essentially two types of fibers are present in the back musculature, namely the Type I (slow twitch) and the Type II (fast twitch) fibers. Type I fibers have high oxidative capacity capable of long-lasting and sustained contractions, and demonstrate greater tonic action at lower intensities of activation. The other broad category of muscle type is the Type II (fast twitch) fibers that show high glycolytic capacity and are recruited when a fast and vigorous contraction is necessary. The Type II muscles fatigue quicker but can perform work against relatively higher loads (387, 410). Generally, different group of back muscles are made up of different and varying proportions of muscle fiber types in them (Figure 9). The relative number and proportion (by size) of Type I and Type II fibers within a muscle mass depend, to a large extent, on

the nature of function of that muscle (410, 411). Kalimo *et al*. reported that the MF contained 61.5% and 57.7% of Type I fibers in men and women respectively, as observed in patients undergoing surgical treatment for lumbar disc herniation. Mattila *et al*. reported 62.5% and 60.8% of Type I fibers in men and women respectively (221, 284) [Table 3]. An ATP-ase dependent histochemical study noted no major differences in the relative percentage of Type I (62 vs 57%), Type IIA (20 vs 22%) or Type IIB fibers (18 vs 22%) between MF and the longissimus portion of ES muscles, nor detected any significant difference in the absolute size of fibers between them (range of mean diameter= 58 to 66 μm) (440) [Table 3]. Although some studies demonstrate relatively larger cross sectional areas of Type I fibers in females (70-75% in females vs. 54-58% for the males), the number of Type I vs Type II fibers have been demonstrated to be largely the same in both genders (410, 411). In fact, the female back muscles exhibit smaller size of the Type II fibers, and therefore, a higher Type I/Type II area ratio in female biopsy samples (ratio=1.70-1.90 in female vs 0.88-0.92 for male) suggesting differences in functional capacity of back muscles (159). Interestingly, MF and the ES fiber composition do not show fiber type differences between the thoracic and lumbar parts of these muscles (279). Mannion *et al*. reported insignificant difference in gender related fiber proportions (percentage distribution) between the two components of MF and ES. The same study indicated larger slow twitch Type I fiber areas in women indicating their role as long-acting postural muscles (279, 369). Additionally, reduced numbers of Type II fibers reported in women may be physiological adaptations in response to use-dependent and load-induced activities (221, 279, 369). Lifestyle activities and loading intensity of the spine have been thought to help regulate characteristic muscle-type isoform synthesis in these muscles (354, 411).

Fiber-type constitution of the back muscles has been investigated in context of the origin, progression and outcomes of LBP. Patients after disc herniation surgery have shown good clinical recovery if their Type II muscle fibers regained their expected normal size with adequate physical activity and exercise. On the contrary, a selective Type II fiber atrophy has been noted in patients with persisting LBP (284). However, Mannion *et al.* has reported differences in muscle fiber sizes between thoracic and the lumbar regions (with no differences in fiber-type percentages between the regions) observed and compared between the T-10 and L-3 spine levels (278, 279) (Figure 9). Rantanen *et al*., in a study of post-mortem MF and ES microscopic specimens, have reported regionally uniform to slightly larger and numerically superior Type 1 fibers in males (369) [Table 3]. Additionally, switching of muscle fiber types have been reported in adult back muscles (134, 135). Switch in fiber-type composition has been well documented in back muscles both during embryogenesis and in early life. These events are regulated by innervation patterns and neural activity in these muscles (354, 370, 408, 409). In addition to the ES and MF, abdominal wall muscles, especially the transversus abdominis (TA), are connected to the lumbar vertebrae via the lumbar fascia and apply transverse pull on the spine in axial rotation or in side-bending (34, 192, 193, 415, 477). The other major player in lumbar spine motion is the psoas major (PM) that acts as a major flexor of the trunk (32, 33, 353). The TA and PM in young and healthy individuals exhibit within-subjects as well as inter-subject variations in fiber composition with about 55-58% of type I, 15-23% of type IIA, 21-28% of type IIB, and 0-1% of type IIC fibers, suggesting Type I > Type II fibers in these muscles (166). The PM shows Type I, IIA and IIX fibers with predominance of Type IIA fiber (59.28%) and larger Type IIA sectional area as compared to Type I fibers (40.72%) (32). Some studies have also

demonstrated small side-related variations in fiber types in PM and age-related Type IIA atrophy in PM with aging (31, 32).

Spine ligaments. Ligaments form fundamental anatomical links between the vertebral elements and play an important role in defining the structural integrity of the spine and in determining overall range of spine motion (459) (Figure 10). Most of these ligaments possess rich distribution of mechanoreceptors for precise proprioceptive feedback to the central nervous system for regulating muscular control of spinal movements (358) (Figure 10B). The anterior longitudinal ligament (ALL) is a thick, flat, band of ligament that connects the anterior aspects of all vertebrae like a strap and resists hyper-extension moments on the lumbar spine (315). The posterior longitudinal ligament (PLL) is thinner and narrower than the ALL and binds the posterior aspects of the vertebral bodies and assists restriction of hyper-flexion of the vertebral segments. The ligamentum flavum (LF) connects the spinal laminae and protects the spinal canal from the posterior aspect. The inter-spinous ligament (ISL) spans between the spinous processes of the lumbar vertebrae and the supra-spinous ligaments (SSL) connect the tips of the spinous processes along the spine. Both these ligaments and the LF limit flexion of the spine and they are densely populated with mechanoreceptors and supply proprioceptive feedback of motion in the motion segments (17, 37).

A number of novel spinal devices and instrumentation techniques have been developed in recent years to treat LBP and to restore the functional anatomy of the spine (123, 262, 458). Devices like rods, cages, screws and procedures like prosthetic replacements with artificial disc replacement aim to restore or replace normal anatomical structures, and physiological function at the spine joints (2, 28, 37, 111, 165). Additionally, outcomes of novel cell-based therapies have attempted to regenerate new tissue dependent on the host-specific mechanical environment at the motion-segments

being treated (24, 446). Most of these techniques are directed to restore the normal range of vertebral motion or to abolish abnormal motion patterns at diseased spinal joints by fusion. However, unfavorable outcomes of fusion techniques may deleteriously alter motion at the adjacent segments resulting in adjacent-segment disc-disease in the long run (37, 48, 111, 140, 183). The current work, therefore, importantly presents a technique that may be applicable in the long run to investigate complex spine motion for detecting the integrity of the structural components in the spine.

In summary, so far, I have reviewed that structural integrity of the spine depends not only upon the incumbent loading, but also upon the tissue property, mobility or stiffness of the segments, and associated static and dynamic neuro-muscular control. Invariably, quantification of *in-vivo* spine motion (or the lack of it) may provide insights into the quality of spine motion and its relationship with pain, degeneration and outcomes of therapeutic intervention.

Part II. Mechanics of Lumbar Motion and Preservation of Structural Integrity

The previous section reviewed the structure of the spinal column. This section will discuss mechanisms that actively maintain the structural integrity of the spine at rest or during routine and complex motion. Since the human spine is a segmented column, it needs to be supported at individual segments in order to prevent angular buckling on static loading, as well as during dynamic movements with or without extraneous loading (14, 50). Experimental models have shown that the buckling behavior of the spine depends considerably upon the integrity of its ligament system (104, 105). Cadaver simulations and theoretical experimental spine models demonstrate that a force of about 88 Newtons (N) (~ 20 lbs) can buckle the spine segments when all ligaments are removed from them (50, 103). Results from these studies also show that spine segments

in general resist any attempt to buckle in the sagittal plane by virtue of the strong ligaments and the lordotic curvature in the sagittal plane. However, with further increase in the magnitude of axial loading, the segments exhibit axial rotation and eventually fail in the coronal plane (105). It has been observed that progressive and step-wise removal of spinal ligaments facilitates buckling even with lesser magnitudes of loading (105). Mathematical models show that for a given initial stiffness assigned to the model, greater forces are required to buckle the spine with intact ligaments than without them (105, 297, 465). However, far greater loads are applied to our spines in day-to-day activities than that would be required to disrupt a ligament-only spine (with all muscles removed). The question is how does our spine then resist destabilizing loads? More specifically, I will discuss the role of local and the global para-spinal muscles (the 'active' sub-system) in sustaining structural integrity of the spine. Additionally, studies have shown that loading may have variable outcomes at different spine levels in the same individual. Magnetic Resonance Imaging (MRI) spine imaging in the relaxed upright weight-bearing position can detect decrease in the overall length of the spine (spine shrinkage) and lumbosacral responses to loading such as increased sagittal rotations at different segments (465). While the L2-L4 motion segments show extension on spine loading in the vertical position, the L5 tends to flex more on such loading with the discs from L2 through L4 demonstrating an anterior translation and the L5 disc showing a posterior translation (465). It has been documented that even day to day flexion-extension, lateral bending or rotation can bring about significantly high bending moments in the spine regardless of any external loading (220, 414). Additionally, concomitant movement of limbs necessitates the spine to behave like a semi-rigid column requiring greater activation levels in the para-spinal muscles possibly resulting in further accentuation in overall axial loading (194, 293, 404).

The current definition and characterization of ‘spinal stability’ has mostly evolved from the reductionist approach based on elasto-static concepts developed by Bergmark’s studies on mathematical spine models (50, 376, 404). The current concept of stable functioning of the spine is understood predominantly on the ability of the spine to stiffen itself on loading, as displayed by the load-displacement relationship of its segments (Figure 11). However, the definition of spine stability has varied depending on its usage from the perspectives of classical physics, biomechanics or in the clinical setting (173, 237). Biomechanical models have elegantly explained spine stability in terms of joint stiffness and its complex control by segmental muscles (90, 341). Concepts of energy wells have offered us a theory for stability that attempts to define the role of bones, ligaments and muscle components to control joint stability (373). This idea has further enhanced the concept of spine stability in terms of the Potential Energy (PE) content of a system (Figure 12). This concept of stability proposes that systems (or objects) with a definite mass possess certain PE by virtue the position of the mass above a given baseline. Similarly, systems that are elastic can ‘store’ certain magnitudes of PE by being elastically deformed under loading. Accordingly, PE stored in systems either due to the height of the mass (with respect to a baseline) or due to any elastic deformation, can be released or recovered when such objects either fall from higher to a lower position or as the object returns to an un-deformed state when the incumbent load is removed, respectively. Essentially, the ‘energy wells’ and PE concepts represent a force-displacement relationship in the systems. A closer inspection of the ball-bowl example shown in Figure 12A will reveal that the ball gets progressively unstable as one moves from condition (a) to (d). It is the force-displacement relationship that changes from (a) to (d) at each level, despite the balls being placed at the bottom of the respective bowls. This means that as we move from (a) to (d) in the example given, it

seems apparent that less and less is required to displace the ball sideways from the position of maximum stability at the ground zero in each situation. Accordingly, one may infer that the stability of the ball inside a bowl could be augmented by increasing the steepness of the sides of the bowl by increasing the height of the side-walls (the boundary conditions). Classically from a joint analogy, accentuation of the steepness of the side-walls of the bowl has been equated to ‘increasing’ the stiffness of the concerned joint that apparently increases its stability (49, 372, 376). Mathematically, it implies with increase in the steepness of the well walls, more and more energy will be required to displace the ball from its position of minimum PE at the bottom of the bowl, and progressively harder to eventually force the ball out of the system.

The other noticeable parameter in the given example would be the ‘flatness’ of the base of the bowl. This feature of the system determines the force-displacement relationship of the ball-bowl system as progressive flattening of the base of the bowl may conceptually require less and less energy to push the ball around at, or out of, the base regardless of the height of the side-walls of a bowl. On the other hand, the flatter we make the base, the likelihood for the ball to revert back to its initial position on the base after a perturbation is removed, becomes proportionality lesser. In biomechanical terms, the example of a more flat-base bowl has been considered to be a less ‘robust’ system than one with a relatively less flat baser. As such, two attributes: (a) energy requirements for moving the ball out of equilibrium and eventually out of the system (steepness of side-walls), and (b) likelihood of returning to the baseline (flatness of the base), define respectively, the stability and robustness of a system. However, the relationship of the stability and the robustness of any system may not be proportional. Accordingly, a stable and robust system at the same time will not only require greater forces to move a ball out of the position of the minimum PE, but will also possess the

intrinsic capacity for the ball to roll back to its original position of maximum neutrality once the perturbation force is withdrawn [system in Figure 12 A (a) is more stable and robust than Figure 12 B (b)]. Thus, from the ball and bowl analogy, mathematical stability and the robustness of a joint system are determined by the inclination and dimension of the side-walls as well as the by the shape of the base-surface (292, 373, 376).

The previous analogy of the ball moving inside the bowl only allows motion of the ball in a single plane (e.g., flexion-extension of a hinged joint). On the other hand, a ball and socket joint has 3 degrees of freedom in 3 different planes. Therefore, in terms of the lumbar spine with 5 segmental joints each capable of rotating in 3 planes, a bowl with more than 15 side-wall dimensions would be required (total of 15 degrees of freedom) to represent the lumbar spine in a mathematical ball-bowl model. This model could then simulate the effects of altering the ‘steepness’ and ‘height’ properties of the side-walls that represent different anatomical equivalents in the spine (373, 376, 404). Additionally, the PE concept postulates that the stability of a system depended upon the height-width ratios of specific sidewall-base relationship of the system that regulates the amount of torque required to topple the system (376).

In terms of PE, spine stability is defined as a function of stiffness and the stored elastic energy within the system. Musculoskeletal systems rely on such stiffness-derived elastic potential energy of constituent joint structures and their capacity to store elastic potential energy on application of displacing forces. In context of the spine, stiffness is attributed to physical properties of bony articulations, discs, capsules, ligaments and segmental muscle activity that dynamically initiated and sustained the resistance against motion at different stages of the ROM (341). With spine loading, segments not only become unstable at static positions, the segments also become unbalanced and fails to demonstrate a smooth motion through the ROM and may, in some situations, present a

catastrophic end-range failure if the perturbation force applied to the spine exceeds the stored potential energy in the system created by joint elastic properties (117, 341).

The role of muscles in maintaining lumbar structural integrity in static and dynamic conditions has been studied extensively either with the use of *in-vitro* biomechanical models of the spine, *in-vivo* human muscle-activation studies on segmental and global muscle groups of the lumbar spine or with mathematical modeling (103, 104, 367, 447, 463). Analysis of dynamic muscle action simulation, MF has been shown to exert the maximum influence on segmental ROM and to determine the size of the neutral zones at individual segments (463). Tonic contractions of para-spinal muscles (stiffness modulators) actively augment the stiffness of the segments in addition to the 'passive' stiffness imparted to the segments by the bony articulations and associated ligaments (197, 341, 461) (Figure 13). It has been hypothesized that the bone and ligaments control segmental motion ROM mostly at the end-range of motion, whereas the muscles provided 'working' stiffness at regions within the ROM, specifically around the NZ of joint motion (341). Contractions as low as 25% of maximum isometric capacity of the spinal muscles can support heavy spine loading and generate sufficient stiffness without compromising motion (88, 291, 292, 341). Co-contraction of synergists and antagonists muscle groups plays a critical role in stabilizing lumbar joints, at the same time allowing movements in the spine with concurrent and accurate processing of mechanoreceptor afferent inputs (proprioception) from tissues like ligaments, inter-segmental muscles and discs (10, 214, 321, 383) (Figure 13B). Muscles controlling spine joint motion are recruited in a pattern depending upon the structural and molecular characteristics of its constituent fibers. This principle is called the Henneman's size principle, which postulated that with increasing contraction intensity, there is an orderly recruitment of moto-neurons with the smaller neurons being recruited first with larger

and larger neurons getting progressively recruited thereafter, with increasing drive. The reverse order followed in de-recruitment with motor units recruited first being deactivated at the end. This recruitment pattern was termed the 'size principle' (180-182, 184). The Type I muscle fibers are recruited first and are called the slow twitch fibers. These fibers and the associated motor neurons comprise the slow-twitch motor units (MUs) that are responsible for slow, low intensity tasks. These fibers produce small forces for a longer period of time, and are relatively fatigue resistant quickly (303). The slow twitch (ST) fibers are designated as the Type I fibers with associated nerve fibers forming the motor units that are designed for extended, slow fatiguing activity (158). The ST fibers are classically recruited at a later stages of sustained muscle contractions. However, orderly MU recruitment may not always follow the classical size principle but may show divergence in recruitment patterns e.g., depending upon complex interactions between proprioceptive feedback systems (44, 412). Additionally, the proportion of fiber types within a muscle mass, muscle capillary density, enzyme activities and associated metabolism of fibers decide the fatigability of a muscle (158, 261, 278). In context of the spine, sustained isometric contractions is maintained by slow twitch Type I fiber activation that is economical as it utilizes less energy to maintain the same relative force for the duration of a contraction, in comparison to fast twitch fibers (278, 387).

A newer concept has attempted to define stability in more dynamic terms where a functional and effective 'system' helps to prevent spine injuries that may occur even with very small errors in motor system activation and function or even from very small magnitudes of adjustment errors that control interaction of muscle forces (e.g. back injuries resulting from a task such as picking up a pin) (376). This concept emphasizes the necessity of precise and varying levels of stiffness operating at the spine motion-segments during motion. This idea points to a more energy-efficient system instead of

mere presence of an unregulated and generalized stiffness (373, 377). This definition proposes interactive, dynamically changing inter-segmental coordination of spine stiffness. Cholewicki and McGill studying precise segmental motion in power lifters demonstrated that even while flexing the spine to lift a weight off the ground, each lumbar segment involuntarily and actively maintained some degree of inter-segmental extension (2–3 degrees short of full flexion) though the lumbar spine apparently looked fully flexed while lifting the weight off the ground. Dynamic spine motion in this study was recorded with a single fluoroscopic view of the spine while lifting very heavy weights (87). Reeves and Cholewicki have proposed that this approach of defining stability necessities the spine system first to be stable in order to fulfill its intended goal i.e., to bear loads. Next, a controlled and graded motion is required at individual spine segment to fulfill the load-bearing task without risking injury and pain. According to this definition, the complex interplay between the anatomical components of the motion segment is based on a feedback control system. Accordingly, the authors suggest that a multiple-afferent input system including the visual system and related mechanoreceptor apparatus interact with the central nervous system (CNS) during each stage of the activity to relay information about the spatial orientation of the body (375, 376) (Figure 14). Depending upon the direction of an incoming afferent stimulus, feedback can be characterized as positive (muscle force acting in the same direction as the displacement) or negative feedback (muscle forces directed in the opposite direction to the original displacement, often larger than the force) (376).

The performances of spine motion and stability control systems take some time to become efficient and ergonomically viable. Optimal functioning of the feedback mechanisms with appropriate adjustments in the ‘gain’ of systems, determination and utilization of the appropriate feedback responses is initially poor but improve with

learning from repeated usage. The chief controller in the system is the central nervous system (CNS). The CNS gradually gets tuned to the requirements of feedback gain and activates suitable response reflex loops depending upon the physical and emotional changes in the environment. This mechanism of spine stability proposes precise, moment-to-moment, dynamic and goal-orientated corrections of the system (376). This system of spine motion is thought to be operational both in the static as well as in the dynamic contexts. Specifically, in the static context a perturbation disturbing the stationary equilibrium of the spine system deviates the spine from its initial equilibrium position to a new 'disturbed' position. Accordingly, on cessation of the perturbing force, the trajectory of spine motion induced by the perturbation attempts to revert back to the original or starting equilibrium position as the effect of the perturbation gets neutralized. On the other hand, in the dynamic context (like while catching a thrown ball), if a perturbation is applied to the spine segments directly or indirectly while the person is in the action of catching the ball, a dynamic adjustment generated in response to the perturbation. This response does not revert the spine back to a static neutral position when the perturbation is removed, but instead, the response allows the perturbed trajectory to slowly resolve into a trajectory of motion that was initiated and intended to accomplish the original task of catching the ball, even before the perturbation was applied (376, 404) (Figure 15). This idea indicates to probable mechanism that not only prevents injury to the spine by making it asymptotically stable, but also allows dynamic adjustments brought about by the interaction of multiple feedback loops in the spine. Although stability can be restored with the application of several feedback loops, stability is ensured with the use of a minimum number of operational feedback loops (292). Thus, these systems with their added redundancies enhance robustness to the system and

therefore theoretically permit lowering some of the stiffness parameters of the system without compromising its stability (292, 374, 376, 414).

Accordingly, it may be presumed that stability in such a system may be achieved even with transient lowering of the stiffness between some of the joint components. Specifically, stability may not always get compromised with lowering of spine stiffness, changing the PE stored in the system or with the introduction of subtle changes in the load-displacement relationship (173, 174). Physiologically, reflexive feedback controls from intrinsic pathways involving joint capsules and tendon endings act instantaneously and earlier than mechanoreceptor mediated muscle stretch reflex (complex poly-synaptic feedback control loops) and voluntary muscle contraction pathways. The later examples are associated with small but significant temporal delays in system initiation in response to a perturbation (374-377). Studies have indicated neuromuscular delay errors are related to loss of spine motor control and subsequently to the development of injury and LBP (163, 291, 454, 464, 465). Additionally, perception of threat of injury and of impending pain may also predispose unstable behavior in the spine response system with delayed onset of muscle activation and inappropriate agonist-agonist, agonist-antagonist muscle co-ordination during in task accomplishment (388, 437, 438, 450). On a broader context, numerous studies have reported the association between impairments of muscle co-activation patterns, disturbances in joint proprioception, alteration in muscle fatigue properties and injury-induced changes in ligament and bone mechanical properties with spine and back pain, whereas some have proposed etiological relationship between them (40, 103, 104, 157, 184, 195, 238, 248, 263, 292, 339, 364, 425). Accordingly, strategies enhancing spine stability have mostly focused on augmenting direct or indirect control of segmental motion properties, improving precise spine motor control (101, 195, 248, 309, 374, 439). Therefore, availability of spine-

motion quantification techniques may be of great assistance in diagnosing aberrant segmental motion, in the evaluation of treatment outcomes in spine pain or in the assessment of changes in spine motion with physiological loading, limb motion, muscle fatigue, cognitive behavioral training, dynamic exercises and even to investigate with training and detraining effects (86, 157, 161, 184, 191, 425, 443, 461). Given the abundance of factors influencing spine motion characteristics and thereby linking it, mechanistically, with LBP, the ability to assess spine motion patterns may objectively be used to further quantitatively investigate the relationship between spine motion, motor control and back pain.

In summary, dynamic and integrated functioning of the para-spinal muscles based on a feedback system facilitates the maintenance of the structural integrity of the complex lumbar spine in motion. Additionally, the stiffness of the spine has been considered to be dynamically, adjusted to optimize the stability of the spine. The potential role of a spine motion quantification system that could potentially uncover the relationship between segmental motion patterns in LBP has been underlined. The next section will discuss why quantification of spine motion deserves merit and how could such assessment be achieved.

Part III. Why Do We Need to Quantify Vertebral Displacements?

The widely accepted definition of clinical spine instability postulated by Pope and Panjabi attempts to objectively encompass both the clinical (tissue damage, pain and deformity) and bio-mechanical (abnormal inter-vertebral displacements on loading) views of spine instability (360). However, there is very little evidence suggesting that all biomechanically exaggerated spine movements are associated with LBP, or all clinically detected LBP demonstrate hyper or hypo mobility of the spine (361). This section

discusses (i) certain aspects of the biomechanical spine stability and how biomechanical stiffness characteristics and the load-displacement relationship may possibly be etiologically related to LBP, (ii) the probable reasons for the lack of agreement and inconsistencies observed between the clinical evidence of back pain, degree of clinically detected spine stability and the bio-mechanical concept of loss of stiffness being the primary etiology of LBP, and lastly (iii) discusses the importance of objective evaluation of spine motion, inter-vertebral displacement quantification and their application in basic and clinical science research.

Although a change in the load-displacement behavior in spine-segments may suggest altered stiffness properties in the segment, it may not always be conclusive in etiologically explaining the clinically observed LBP (102, 148, 173). Changes in spine stiffness parameters may not always be pathological and may arise from the needs of adaptive changes in neuromuscular properties of paraspinal muscles. Also, from a biomechanical perspective, physiological changes occurring in segment stiffness properties may vary at different time-points along the entire ROM of a joint, often suggesting a non-linear character of the load-displacement curve. Regardless of the nature of the load-displacement relationship at a vertebral segment, LBP has often been associated with a laxity of anatomical structures in the joint segment, loss of motor control regulating the joint stability leading to exaggerated joint motion specifically with an increase in the NZ and ROM ranges.

On the other hand, clinical assessment of LBP encompasses testing segmental laxity of the spine with a passive palpatory approach that helps in the assessment of inter-segmental mobility. Additionally, direct visualization of anatomical inter-vertebral displacements is performed mainly from end-of-range spine radiographs. These radiographs are essentially sagittal films of the spine acquired at the end-range of

flexion-extension motion that are compared. A criteria of >4 mm of inter-vertebral translation and/or >20 degrees of sagittal plane rotation translation has been standardized for a clinical diagnosis of spinal instability, with or without back pain (338). Despite the purported association of clinically detected hyper-mobility or hypo-mobility of segments, clinical evidence of loss of motor-control of segmental motion and LBP, there are no studies that have quantified and validated results of these clinical assessments with direct visualization of the spine in motion or with appropriate bio-mechanical tests. Regardless, a great many cases diagnosed as clinical 'instability' are followed up with attempts to restore physiological load-displacement relationship, often with variable outcomes (5, 59, 108, 176, 244).

Despite the increasing direct and indirect costs of LBP at more than $624 billion per year in the USA alone, the existing clinical and imaging expertise in the field permits only about 15% of LBP patients to be diagnosed accurately to have a specific etiology for their LBP (276, 460). Precise diagnosis of pain remains unknown in 80-90% of all LBP patients who are clustered together as a non-specific LBP (NSLBP) cohort (108, 258). Approximately 20-30% of the NSLBP patients are diagnosed as having some sort of abnormal motion responsible for their LBP, and hence requires specialized medical attention to alleviate the associated pain (361, 362). Though the relationship of an altered (pathological) pattern of segmental motion and LBP has not yet been completely understood, and with sophisticated surgical procedures performed for restricting anomalous spine motion with inter-vertebral fusions, efforts to develop new and precise techniques for visualization of *in–vivo* real-time spine motion has not deserved the required attention.

Fritz *et al*. while reviewing the biomechanical and clinical approaches for the assessment of lumbar spine functional stability expressed that the currently available

definitions for spinal instability may not be adequate and also may not be very helpful in determining appropriate treatment strategies for NSLBP since the basic model for such evaluations was based upon mathematical spine models proposing loss of stiffness characteristics as the only primary deterministic factor for LBP (50, 139, 185, 376, 404). Although these models can simulate the role of different anatomical structures that influence spine motion with each of the elements being represented by each 'dimension' of, e.g., the ball-bowl model, these models may not be able to simulate dynamic interactions between all muscle, tendon, ligament and bony elements of the spine (50, 376, 377, 404). Moreover, from a kinematic perspective, these models may fail to determine and quantify the moment to moment variations in inter-vertebral displacements during real-time motion, as may be possible with an *in-vivo* spine motion imaging technique (59, 231).

Since central nervous system (CNS) feedback loops play an important role in the neuromuscular control of the spine stiffness, the ability of mapping of subtle adjustments in dynamic inter-vertebral relationship within the ROM may permit us to investigate precise and timely neural control mechanisms that regulate dynamic motor control of segmental motion in normal and symptomatic spines (91, 136, 173, 174, 290, 292, 341). Several researchers have demonstrated the importance of the role of inter-vertebral motion control in determining the overall normal functioning of the spine. Cholewicki *et al*, Gardener-Morse *et al*. and others have delineated the role of the inter-segmental small muscles controlling the motion-segment stiffness and in regulating overall spine motion with mathematical modeling (91, 254, 290, 414, 415). As we discussed earlier, Panjabi *et al*. emphasized the loss of control of the ROM mid-zone (neutral-zone/ NZ) stiffness as the proposed mechanism that initiates an injury-laxity-injury cycle leading to LBP. This same hypothesis proposed that within the entire ROM, the NZ encountered

minimum resistance to motion. This NZ stiffness is thought to be primarily controlled actively by muscle contractions. The spine joints stiffness characteristically increased progressively towards the end of the ROM. This end-ROM stiffness was supposed to be controlled by passive elements like the ligaments and the bony articulations (341). As McGill put it: "Functionally, a patient must be able to maintain sufficient stability during necessary daily activities: …tasks of daily living, is not compromised by insufficient strength but rather points to the importance of endurance", indicating that low levels of muscle co-contraction of the synergists, and hence low levels of stiffness were hypothetically sufficient to maintain spine stability for daily activities and fatigue resulting from over activation in muscles may be another responsible mechanism for loss of spine stiffness and resultant segmental spine pain (91, 136, 151, 249). Moreover, from a clinical viewpoint, detection of abnormal and excessive displacements in motion segments around the neutral position (roughly representing the NZ) with palpatory methods have been reported to co-exist with LBP presentation to the clinic (341). Accordingly, clinical decision-making on lumbar spine instability in the clinical setting has been supplemented with sagittal-plane static imaging of the spine at the end-of–range flexion-extension position. Visual assessment of >4 mm or a 15% vertebral body length slippage of one vertebra over the lower one, as compared between flexion-extension inter-vertebral displacements or, a > 20 degrees' rotation between segments have been defined as criteria for the diagnosis of spinal instability. This clinical approach for the diagnosis of instability apparently does not take into account the dynamic nature of spine motion or the inconsistent nature of the force-displacement relationship at the lumbar segments on active spine loading. Neither of the clinical or the bio-mechanical approaches have applied *in-vivo* visualization of dynamic adaptations in physiological segmental motion or impairments secondary to the injury or pain.

Contrary to the views of spine stability, some observers have fundamentally challenged the validity of such a concept of stiffness derived spine stability. Hasan *et al*. questioned the very concept of conventional spine stability suggesting that the response to perturbations in many situations 'assist' rather than 'resist' the trajectory of the disturbance caused by the perturbation, and therefore the response being more of a destabilizing reaction than a stabilizing one (173, 174). Hasan proposed that functionally, the spine motor control system may not always implement and enforce strict stiffness response secondary to a mechanical perturbation and may even promote exaggerated motion in an already potentially unstable spine system where a high degree of maneuverability was necessary to restore stability and attenuating pain, an idea similar to an earlier observation by Crisco & Panjabi (102). Some authors have also suggested that a spine system may be stable even if intrinsically not in equilibrium e.g., while executing limb movements during active spine motion (160, 173, 441). According to Hasan, delays in stretch reflex responses may precipitate or exacerbate clinical instability, and accordingly, the lag property of muscles, nerve conduction intervals, and properties of tendon compliance delays may impact spine stability if all these systems simultaneously attempted to kill spine motion secondary to a perturbation (175). It has been argued that if an extension-moment initiated by activation of the spindle reflex action (at the dorsal spine) subjected to a flexion perturbation arrives late, it may bring about further instability (hyper-extension) of the joint toward the extensor side. Further, this delay might activate both the short or long latency reflex actions using a continuous feedback system thereby destabilizing the joint even further through potential oscillation associated with this delay (6, 237, 476). Regardless of the pitfalls in the biomechanical definitions of spine instability or existent gaps in understanding the exact neurophysiological mechanisms clinically detected LBP, the proposed importance of

precise control of spine segmental motion in the resting state or the dynamic motion cannot be overestimated (173). Additionally, taking into consideration the number of adjustments required for a task-specific motor control of the lumbar spine, assessment of the entire ROM for understanding subtle inter-segmental relationship has been under–represented as a diagnostic entity in context of non-specific LBP patients (455).

In light of the importance of mapping inter-vertebral motion patterns (across the ROM) in investigating the regulation of spine stiffness and motor control properties in the pain-free individual or in LBP patients, the argument in favor of developing *in vivo* visualization techniques for quantitative assessment of spine motion becomes very strong. The case becomes even stronger if this assessment could be performed while the spine was in the normal physiological weight bearing state, and if possible, while in a state of dynamic motion (143, 361, 472). Such examination of vertebral kinematics in addition to clinical testing of vertebral hyper- or hypo mobility with or without LBP would have helped to explain or validate specific clinical findings as detected by direct palpation, the straight leg raise and a number of other such techniques (102, 234, 361). However, visualization of spine motion can be challenging in several ways. Direct imaging of the spine has used almost all available depended on imaging modalities like x-rays, ultrasound, CT and MRI. Most spine imaging has been performed in the static context, with dynamic imaging being performed mainly with x-ray fluoroscopy. Typically, fluoroscopic imaging of the spine has been practiced mostly for instrumentations in the spine segments where this imaging were done in a single plane. More recently, the roentgen stereo-photogrammetry (RSA) techniques have been developed that use biplanar fluoroscopic imaging to detect shift in implanted prosthetic devises at limb joints(245, 429, 479). The details of this technique and its applications are discussed later in Chapter 6. Some of these RSA techniques have also relied on 3-D models

created from static CT or MRI images of the boney articulation by superimposing these 3-D models over the moving images captured (with fluoroscopy) during real-time movement of these joint within a previously calibrated imaging volume (68). Despite recent upgradation of these techniques, they have rarely been used in context of objective assessment of spine segment motion despite the fact that clinicians have long postulated that abnormal spine motion may be an important cause of LBP and despite the fact that many treatment options have been based on the predication that they alter spine segmental motion (59, 136, 292, 359). The current quantification techniques of spine motion are not optimal in several ways. Techniques based on fluoroscopy are associated with exposure to x-ray radiation and therefore cannot be used for serial assessments in all individuals or in pregnant women (229, 250, 300). Some of the techniques based on dynamic fluoroscopic imaging only quantify spine motion in single-plane of motion (mostly sagittal plane flexion-extension). Additionally, some of these techniques are not sufficiently sensitive to detect segmental motion at the required resolution and yield a 3-D analysis of segmental motion (257). Though some of the recently reported fluoroscopy and 3-D based techniques quantifying spine kinematics have been fairly accurate (467, 468). However, these techniques had used experimental biplanar fluoroscopic imaging that may not be ideal for routine use in the clinical context (474). In addition, the availability of a safe and reliable non-ionizing radiation based technique may be very useful in the validation of clinical findings and quantification of real-time spine motion in LBP patients that can be routinely used for identification of precise kinematic derangement responsible for spine-segment stress, injury and LBP. In the following section I discuss the role of imaging techniques that have been proposed to quantify spinal motion and the current state of development and scope of application of these imaging techniques.

Part IV. Role of Imaging and Imaging-Based Modeling Platforms in Evaluating Segmental Lumbar Spine Form and Function: LBP and Inter-Vertebral Relationships

This section focusses on the application of different imaging techniques for evaluating spine motion quantification in general and imaging approaches being developed to investigate LBP from a vertebral kinematics perspective. Specifically, this section focuses on the currently used MRI based tools for detecting musculoskeletal dysfunction and injury and in diagnosing LBP and spine pain (186, 419, 468). In addition to discussing the advancement in the field of MRI based computational techniques used to study segmental lumbar vertebral motion, the application of other techniques for similar purposes is discussed (253, 327, 344, 468).

To start with, an overview of the use of MRI and other imaging techniques for evaluating muscle size and function given in the following paragraph. These images are acquired for a structural and functional status of the superficial and deeper paraspinal muscles, the parameters that are often associated with pathological changes occurring with chronic LBP. The evaluation of the muscle size entails quantification of muscle cross sectional area (CSA) from static images acquired at different levels of the spine. Different imaging modalities including radiographs and ultrasound have been used for quantifying CSAs of the ES and MF muscles to primarily (i) to determine any cause-effect relationship or correlation between muscle size and the presence of LBP, (ii) to investigate correlation between muscle size of and muscle activity, as studied through comparison of static muscle images and surface EMG recordings acquired during voluntary force generation, and (iii) to investigate the effects of therapeutic interventions on the size of muscle groups responsible for controlling segmental spine motion (189, 289, 306, 365, 403, 416). The application of MRI for evaluation of muscle function and

muscle activation levels involves the use of T_2 'relaxometric' sequences. These sequences are able to assess muscle function on the basis of comparative activity-dependent differences in the T_2 relaxation times of osmolite protons in muscles. These sequences essentially calculate the relaxation time of the spinning hydrogen nuclei, compared between two images of a muscle acquired at two time-points set apart by tens of milliseconds, as they to lose their magnetic induction (decay in magnetization). Thus T_2 relaxometric maps are generated for each muscle groups at the same set two time-points within the imaging protocol. T_2 relaxation time have been documented to be longer in muscles that have been subjected to higher levels of activity such as resistance exercises when compared to muscles kept at the resting state prior to the imaging or different between muscle depending upon the differences in their intrinsic metabolic rates (96, 285, 444). Muscle activity levels studied by T_2 relaxo-metric imaging and P31 magnetic resonance spectroscopy have been, to a limited extent, quantitatively verified by electromyography (EMG) analysis (286, 435, 436, 449, 478).

Basic principles of MRI. In this section I briefly discuss the basic principles of magnetic resonance imaging (MRI) (55). Principally, MR imaging is based on an orchestrated agitation of water molecules within a given tissue. Once the agitation is withdrawn, the energy released by the protons forming the nuclei of the water molecules, is received and measured as signals by the MR coil. These signals are converted to gray-scale MR images that we use for diagnosis of disease. A variety of MR 'sequences' are used to agitate the proton molecules in different ways to obtain diverse signal intensities that generate a wide variety of images. 'Weighting' image gray-scale intensities based on relaxation times of protons in different tissues can delineate soft tissue anatomy with high resolution and clarity, in MR images.

Agitation of water molecules. Generally, in a non-magnetized tissue, the hydrogen nuclei within the water molecules rotate like a spinning top around their axes that are randomly oriented in space. When a body part is placed within a sufficiently strong magnetic field, such as the core magnet of an MRI machine, the axes of all the protons in the tissue water molecules are forced to align more or less along the dipole net magnetization of the core magnet (called the B_0) (Figure 16). The perfection of this alignment mainly depends upon the strength of the core magnet B0 and upon to the presence of any interference from other magnetic field present in the surrounding environment. At this juncture, the protons spin around their axes parallel to the B_0 and also, at the same, time sway/wobble like a spinning top (a phenomenon called precession). The axes of all protons are now almost parallel to the long axis of the core magnet. This is referred to as the state of primary magnetization. Once a steady nuclear rotation of proton spins in the core magnet is achieved, a secondary radiofrequency (rf) pulse is applied to 'excite' a specific tissue slice (volume) selected with the help of the secondary magnet coils that surround the subject (Figure 16B). This impulse forcibly pushes the protons to flip the axes of the precessing by 90 degrees (the value of this flip angle may differ based on the type of 'sequence' used). The new position of the flipped protons represents the new state of magnetization referred to as the B_1. The protons spin around their own axes and rotate in a plane perpendicular to the direction of the primary magnetization, called the transverse plane (Figure 17).

Magnetic induction decay (Figure 17). The vector of magnetization in this transverse plane is detected as 'signals' by the body coils acting as receivers. As the rf pulse is withdrawn, this transverse magnetization vector (B_1 or TM) slowly decays as the magnetization vector of the transversely rotating and spinning nuclei gradually return from this transverse plane back to the long axis of the primary magnetization i.e., to the

B_0 (known as Free Induction Decay). The two changes in the magnetization are visualized or quantified as two connected events. One is the reduction or decay in the TM and the other is a proportional 'recovery' of the B_0. These two events are measured in two time constants, the T_1 and the T_2 constants. Principally, MR images are acquired from the signals obtained from these two time constants. The protons in the tissue of interest are excited within a given body structure moving from slice to slice. Each slice is selected with the application of 'slice selection' gradients using a set of secondary (gradient) magnetic coils located in the inner shell of the main magnet frame. These slice 'selecting' magnetic gradients allow to accurately focus a magnetization gradient across the long axis of the imaging object thereby 'creating' a slice of choice for the imaging. Once a slice is selected, another set of gradient magnets create a couple of magnetic gradients in the same plane of the slice, but perpendicular to each other.

Phase, frequency and resolution (Figure 18). One of these gradients (and its direction) in the plane of the slice is called the phase encoding gradient (direction) and the other gradient (and its direction) perpendicular to the phase encoding gradient is known as the frequency encoding gradient (direction). Once the slice is elected, the phase and the frequency encoding gradients are set, the body coil of the MRI system applies rf pulses to the slice and changes the net magnetization vector of the protons in the selected slice from the B0 to the B1 direction. Once this pulse is withdrawn, the magnetic induction in the protons decay and the signal time constants of these signals are used to construct the MR images. A single rf pulse is applied to agitate all the water molecules of the slice for each phase or frequency encoding gradient value. Additional rf pulses are applied for each change introduced in the phase or field encoding gradient of the slice. This process of pulsing the slice undergoes several iterations with changing values of both the encoding gradients in an ascending order of magnitude. The number

of phase and field encoding gradient changes determines the pixel size of the image resolution. It is therefore evident that with each change of the phase and field gradients, the effect of the rf pulse, and therefore the induction decay time and intensities of the precessing water molecules, is altered. The receiver coil detects the signal from the entire slice for each value of the frequency gradient is recorded in a time series called the ‘k’ space (frequency encoded time-series signal). Since the phase and frequency gradients are changed in an orderly and ascending fashion, each recorded signal can be attributed a specific location within the slice of interest. The size of this ‘location’ within the slice is determined by the number of phase encoding gradients used for the selected field of view. The beak-up of the field of view in terms of phase and frequency encoding numbers is called the matrix of the image. The size of this area within the slice, in essence, determines the resolution of the images. Repeated excitation of the same slice at different ‘phases’ essentially alters the rate of deceleration of interacting protons (dephasing) that allows faster return of the protons to the B0 with simultaneous decay of the TM. Signals with changing phase are recorded as additional ‘lines’ in the ‘k’ space (phase encoded time-series signal) (Figure 17). Thus, when the pre-decided number of phase iterations is accomplished as per the sequence programmed, the information in the ‘k’ space is converted from the time series data into the frequency domain with Fourier transformation. Such transformation is applied both for the frequency encoding and the phase encoding data. Since these signals have fixed locations within the slice, a Fourier transformation generates a gray-scale image from the signals recreating visual representation of the structures in the slice. The ability to generate contrast between tissue elements depends upon the judicious ‘weighting’ of the two time constants, T_1 or T_2, to create the images. This ‘weighting’ is manipulated by selecting the appropriate window of time when the signals are picked up from the relaxing protons, according to

the requirement for the best visualization of the tissue components within the slice. This weighting generates optimum contrasts between the tissues in question depending upon rate and time of signal sampling (55).

As we have seen earlier, the receiver coils record signals after execution or delivery of each pulse. Additionally, the number of pulses delivered for each slice depends upon the number of phase encoding gradient applied to cover the field of view of the object being scanned. The time interval between each applied pulse is called the Repetition Time or the TR. After the application of a pulse, the time allowed for the protons to relax until the recording of the signals is initiated, is called the Echo Time or the TE (Figure 19). Therefore, the total scan time required to completely scan an object of interest depends upon the cumulative duration of several factors such as: (i) the number of phase encoding iterations performed to fill up the 'k' space for each slice. This parameter also determines the spatial resolution of the image; (ii) the time interval allowed after the application of the rf to start recording the TM signal (TE=Echo time), as performed in a Spin Echo (SE) sequence (Figure 19B); (iii) The time interval TR fixed between application of two consecutive pulses (delivered at gradually increasing intensities of the 'phase encoding gradient'); (iv) the number of slices selected for scanning. Imaging time can be reduced by several techniques that are briefly enumerated in the following paragraph. (i) Using a very short TE allows shortening of TRs and eventually, the overall scan time. Typically, images acquired with a short TE are T_1 weighted and are generated by signals collected with the recovery of the magnetization in the B_0 direction. However, each TE has to be followed by the application of the next rf pulse that flips the magnetization vector of the protons again from the B_0 to the transverse 90º position. As the protons precess in the transverse

plane, the magnetization vector (TM) of each proton decays with time. Additionally, any two TM vectors arising from two protons spinning in the transverse plane start out spinning in 'phase' immediately after the 90º flip. However, with time the two vectors slowly lose their coherence and move out of 'phase' as the electrical interactions with their surrounding structures and also as a result of the decay of the TM on to the B_0 direction influence these individual vectors. Therefore, loss of TM necessitates the delivery of the next 90º pulse to generate the next quanta of signal at a different phase encoding gradient to write up the next line in the k-space. (ii) However, generating signals from the protons may not need the application a 90º rf pulse each time and wait to record the recovering magnetization vector in the B_0 direction. Some sequences detect signals only from the transverse magnetization (TM). These images are essentially T_2 weighted and quantify signals only from the transverse magnetization. The speed of signal generation in the transverse plane can be expedited by flipping the protons repeatedly though 180º within the transverse plane from one side to the other, after a single pulse (i.e, within a single TR). The timing of such 180º flips is synchronized so that the dephasing transverse magnetization vectors of the nuclei again start to rephrase after the 180º flip. Such flips are repeated till the TMs become weaker and weaker and return to the B_0 direction. It is the time that a next 90º pulse is applied again. Thus, several lines of the k-space can be written within a single TR thereby reducing the overall scan time. These 180º flips create 'echo' of signals as the spins flip back from a dephasing to a rephrasing state. This technique is called the Fast Spin Echo (Figure 19C) and can apply a train of such flips within a given TR. (iii) Fast changes in phase encoding also can be performed with the help of gradient magnets within a single TR. A series of these phase changes allow accommodating more number of TEs within the

given TR to reduce the scan time. These sequences are faster and are called Gradient Echo sequences. (iv) Some techniques use simultaneous phase and frequency changes within TRs across inter-leaved slices that helps to reduce the scan time appreciably without compromising the filling of the k-space. (v) Application of tissue specific pulse angles to generate appropriate and selective tissue TM vectors enables the detection of desired magnitudes of tissue-specific TMs (steady states). Some of these angles are short and specific, and require less scan time. Such sequences are sometimes referred to as Short T sequences.

Selective enhancement of tissue signals can be performed to increase the contrast between different structures visible in the slice. This augmentation of contrast is achieved with selective enhancement of the 'recovery' of magnetization of a desired tissue with the application of an 'inversion recovery' sequences (IR) (Figure 19D). Typically, the magnetization vector of choice, in this sequence, is recovered in the transverse plane. Therefore, instead of delivering a 90º pulse at the outset, an 180º rf pulse is applied to flip the longitudinal magnetization vector in the B_0 direction in the diametrically opposite direction ('inverted' in the $-B_0$ direction). After the flip is delivered, the magnetization gradually recovers to the original B_0 direction as this vector gradually involutes through the long axis of the magnetization. Magnetization vectors of different tissue protons gradually decay along the $-B_0$ axis to become zero at the intersection with the transverse axis. Further, the vectors gradually recover again in the $+B_0$ direction till the signals are completely recovered. However, different tissues take different time to 'recover' their individual magnetizations and, therefore, take different time for their signals to involute through the $-B_0$ long axis and reach the zero value. Let us consider the example of recovering vectors of two tissues A and B having different material

properties, with the vector A having faster recovery time than B. Say ‘t’ milliseconds after the delivery of the 180º pulse, vector A recovers some of its magnitude in the $+B_0$ direction while the vector B has just involutes to the zero mark. At this precise moment if a 90º rf pulse is applied to the recovering vectors, only the vector A gets flipped to the transverse plane. Since there is no effective B_0 vector for the tissue B (being zero at the time of the 90º pulse), no transverse magnetization (TM) develops for tissue B. Therefore, all the signals forming the image are contributed only by tissue A giving it a sharp contrast against the tissue B. The timing of this 90º flip can be manipulated in such a way that signals from a specific tissue (fluid or fat) can be suppressed by timing the 90º pulse when the tissue is at the state of ‘zero’ recovery of the longitudinal magnetization in the B_0 direction. Typically, a short inversion recovery time before the 90º pulse suppresses fat transverse magnetization. Sequences that use short recovery times suppress fat that appears dark and are called Short T Inversion Recovery (STIR) sequences. The FLAIR (Fluid Attenuated Inversion Recovery) sequences, on the other hand, use the same ‘inversion recovery’ technique with application of a relatively late rf pulse after the delivery of the initial 180º inversion pulse. These sequences specifically suppress all signals except those coming from the fluid components like water/CSF (55).

Advanced MR sequences designed to discern very subtle signal variations in the tissue magnetization depending on the oxygenation status of the tissues, especially used for scanning the brain, permit functional brain MRI. Image-maps of specific brain areas activated on performance of specific tasks are created using functional MRI (fMRI) techniques. These techniques use advanced MRI sequences that can compare voxel based signal intensities from minute areas within the brain by detecting the differences in blood oxygenation levels in brain tissue with the use of blood oxygenation level

dependent (BOLD) sequences. Additionally, subtle diffusion of water molecules can be tracked along the brain or other tissue areas by using sequences that are specifically designed to identify the phase differences of signal vectors of moving water molecules at different scan time points. Complex computation of the phase changes in the signals collected from slices can define contrast between areas of physiological or pathological (e.g., post-infarct) diffusion rate differences in water molecules. Such imaging sequences are used for Diffusion Weighted Imaging (DWI). Analysis of the direction of the phase changes accumulated in the spins of diffusing water molecules moving along specific direction (e.g., along white matter tracts in the brain) from a tissue may be used to reconstruct 3-D images of the brain fibers (Tractography) or to re-create 3-D anatomy of complex structures using Diffusion Tensor Imaging (DTI) (23, 95, 130, 132, 133, 219, 233, 287).

The MR imaging techniques that we discussed so far yield images in the 'static' form (i.e., the images are stationary representations of body slices or volumes). Additionally, these techniques were developed only to image stationary objects and not applied to scan objects that moved with respect to any reference frame (e.g., a moving hand within the imaging coil or a pulsatile heart within the thoracic cavity, respectively). However, real-time visualization of moving objects or body parts can be accomplished by using very fast MR sequences having extremely short TEs. These sequences utilize the phenomenon of accumulation of phase differences in proton magnetization vectors in a tissue moving in and out of the fixed plane of rf excitation of the selected slice volume. The difference in the phase magnitudes acquired by the proton spins of different tissue elements depends upon the position and material properties of the element as it moves in and out of the plane of imaging. Thus the signals used for these real-time image formations contain phase-contrast or phase-difference information that rapidly fill

the time-domain k space and then Fourier transformed for the frequency and phase domains to create real-time dynamic images. The sequences used in such imaging are often referred to as ‘kinematic’ sequences and the imaging as kinematic MRI or the Cine-MRI imaging. The application and limitations of such real-time MR imaging in context of lumbar motion assessment will be comprehensively discussed in the next section. The following paragraphs describe some of the other imaging techniques applied for assessment of *in-vivo* spine motion in experimental and clinical settings.

Use of imaging in studying lumbar vertebral segmental motion. The use of static and kinematic imaging has provided insight into vertebral motion under different load bearing conditions as well as pathological states. Additionally, it has aided in understanding the role of active and passive components in stabilizing the spine (144, 256, 296, 401, 426, 468, 472). An array of imaging modalities including static X-rays, ultrasound, fluoroscopy, CT scans and MR imaging have been used to determine range of motion (ROM), alterations in the center of rotation (COR), changes in the instantaneous axis of vertebral rotation (AOR) and other biomechanical parameters at different spinal levels of the lumbar spine in health and in disease. In the clinical setting, assessment of translation and rotation displacements between adjacent lumbar vertebrae is performed by manual palpation or by the use of goniometric measurements on the skin surface (Figure 20A). From a radiographic perspective, end-plate measures from end-of-range sagittal plane images has been considered the standard approach for the diagnosis of lumbar instability and for deciding surgical interventions (Figure 20B). Typically, inter-vertebral translations of >4 mm measured between adjacent vertebral end-plates comparing two static images, one taken at the full extension and one performed at the full flexed position of the lumbar spine have been considered suggestive of unstable motion at the segment. Although several combinations of coronal,

oblique and axial plane imaging have been used for such clinical decision making, imaging for such purposes have essentially been restricted to quantitative two-dimensional evaluation of sagittal plane radiographs, CT or MRI scans. Experimental radiography for the assessment of three dimensional inter-vertebral motion using biplanar, static, end-of-range flexion-extension motion was attempted about three decades ago using elaborate x-ray equipment and set-up in an experimental setting by Pearcy *et al*. (Figure 20C). The advent of fluoroscopy permitted low-resolution imaging of skeletal motion. Several studies have utilized single-plane fluoroscopy for mapping skeletal motion including the lumbar spine for static imaging and rarely, biplanar or the dual fluoroscopy imaging system (DFIS) for 3-D imaging of the lumbar spine (Figure 21). Commonly used methods like X-rays, MRI or US used in clinical or experimental settings to analyze segmental vertebral motion apply specified inter-vertebral co-ordinate systems for analysis (Figure 22).

Since static end-of-range image analysis do not capture events occurring during dynamic motion of the spine, these techniques don't capture any out-of-plane motion. Given the limitation of radiation-based techniques, the scope of application of three-dimensional imaging techniques to study complex spine motion has been very limited. The next section discusses some of the strategies that have attempted 3-D analysis of lumbar spine motion, specifically the DFIS system.

Biplanar fluoroscopy and modelling technique for real time spine motion assessment. The technique described here is closely based on the XROMM (X-Ray Reconstruction of Moving Morphology) technique developed over the past decade at Brown University (154). This technique has largely been used for experimental studies to study animal locomotion patterns possibly due to the associated amount of radiation exposure that occurs during testing. However, a select number of investigations have

utilized similar techniques in the humans with biplanar fluoroscopy to capture real-time motion and using superimposition of 3-D models on the fluoroscopic images (257, 344, 468, 472). The technique, as applied to the lumbar spine, involves the following steps: (i) Lumbar spine motion is captured using orthogonal fluoroscopes (using low dose X-rays) (Figure 23). The individual being tested is instructed to move the spine by flexion-extension, lateral bending or axial rotation of the spine within the imaging volume. This system is called the Dual Fluoroscopic Imaging System (DFIS) and has been used for imaging motion within a volume of ~30 cm^3. This imaging space allows positioning the lumbar spine of the subject standing within this imaging space. For imaging lumbar spine motion, the person being imaged moves the lumbar spine in predetermined directions (bending) in the imaging volume with the pelvis or the hips restrained. The fluoroscope produces a stream of images on the DFIS image intensifiers and video-recorded as hundreds of sequential snapshots. Since the images are 2-D representations of the spine, these have to be corrected for optical distortions. Additionally, the imaging volume is calibrated for the accurate quantification of vertebral motion during the movement trials. (b) 3-D Modeling: Axial CT or MR spine scans are used to create the 3-D models of the spine segments. Segmentation software is used to create virtual 3-D models of the vertebral bodies and inter-vertebral discs that are shaped accurately with all contours represented as present in the actual spine images. (c) Next, the video-recorded images from two fluoroscopes are processed to create two separate series of image sequences that represent the perspective of the motion trial as viewed through that fluoroscope. These image sequences are then imported into the animation software and set-up in the software viewing system as if these two images are being viewed through two cameras as orthogonal background images. The details of this arrangement are given in the next Chapter 6. (d) Image Analysis: The 3-D model is first imported into the animation

software and then the models are manually rotated to ‘match’ both the background images acquired by the two fluoroscopes. Once ‘matching’ of the fluoroscopic images with the outlines of the 3-D models is accomplished in the first frames of the background images, the models are ‘registered’ with a joint coordinate system assigned between the vertebral elements. This process of ‘matching’ between the models and images is performed manually, one by one, for each image frame in the background. This process is termed as ‘rotoscoping’ and is completed by assigning joint coordinated systems in each motion-segment (39, 68). The software then calculates translational and rotational displacements between vertebral segments in all six degrees of freedom, a matrix for all frames of the background images. Additionally, one can also calculate the ROMs, IARs and CORs of the lumbar spine motion segments across the entire range of the recorded spine motion. Recent reports by Li *et al*., have quantified 3-D knee and coupled lumbar spine motion using the techniques that involved orthogonal fluoroscopic imaging of motion, 3-D models built from static axial scans of the body parts (468, 472). The development of biplanar spine imaging for quantification has been developed over the last couple of decades to expand from diagnostic and interventional usage to be used as a motion quantifying application. However, the uses of x-rays in such procedures have limited the repeated application of this technique in humans, especially in women of the childbearing age. However, radiological assessment of segmental spine stability has regularly been used in the clinical settings to detect ‘shifts’ of vertebral positions between two or more 2-D images (327). In addition to linear displacements and rotations, estimation of the instantaneous axis of rotation (IAR) between two vertebrae (calculated as the point of intersection of the perpendicular bisectors of two points on a rigid body) is used to determine rotation patterns in the joint segment or is performed to calculate translation along the angular bisector between the two end-plate angles. As mentioned

earlier, these assessments use 2-D sagittal plane images for the evaluation of abnormal and exaggerated spine segment motion, in the clinical setting. In addition to x-rays, single-plane fluoroscopy has also been reported to study real-time lumbar spine motion. Typically, fluoroscopic image resolution is lower but allows real-time visualization of the dynamically moving spine (253). The use of two orthogonal fluoroscope system has been developed in the last decade specifically as a tool for quantifying spine kinematics.

The use of MRI has been attempted for assessing lumbar spine segmental displacements. Although MRI is free from the usage of ionizing radiation, MR imaging techniques however, have been restricted to the analysis of end-of-range 2-D sagittal plane static images (Figure 24). Since MR images are typically acquired in the supine position, these images do not effectively represent physiological weight-bearing in the tested individuals and may be the reason for poor correlation between the finding from the analysis of static flexion-extension images with the levels of LBP or discomfort (144, 426). Typically, inter-vertebral translation and rotation are compared between end-of-range flexion-extension images. One advantage of using MR techniques is that additional information on degenerative disc changes can be obtained in the spine being evaluated. Using MRI for the evaluation of structural pathology in the lumbar spine is safe as unlike x-ray and CT imaging, it does not use ionizing radiation. However, commonly used MRI sequences only allow spine imaging in the stationary position. Additionally, due to weight-bearing limitations of the conventional recumbent MR scanner, it becomes a challenge to scan the lumbar spine at the flexion-extension end-of-range position because of the limited space available within the imaging coil and also due to the supine (non-weight bearing) position of the individual being scanned. However, quantification of 3-D lumbar and cervical inter-vertebral motion has been attempted using static-position imaging along the ROM using MRI (144, 207) (Figure

25). Nonetheless, MR sequences commonly used for diagnostic imaging only allow scanning of stationary objects and do not permit real-time imaging of the spine. Therefore, single-plane static and supine MR imaging may not be an ideal tool for quantifying dynamic inter-vertebral displacements.

The significance of 'coupled' lumbar vertebral motion. Movement at the spine segments demonstrates a 'coupled' behavior. This means that due to the anatomy of the articulating surfaces of the facets joints between the vertebral elements, movement in the spine is not restricted in a single plane of motion e.g., a lateral bending of the spine in the coronal plane is associated with a twisting axial motion in the transverse plane. Similarly, primary axial rotation of the spine is associated with varied degrees of secondary lateral bending within the motion-segments depending upon the part of the spine in question. Additionally, flexion-extension moments of the spine may induce lateral bending and/or axial rotation in the lumbar spine. This characterizes the complex multi-planar nature of spine motion. Invariably, 3-D motion tracking of the spine becomes imperative to analyze complex motion characteristics of the spine during flexion–extension, rotation, lateral bending or a combination of these motions. Studies have attempted complete axial scanning of the lumbar spine at discrete static positions of a rotation task to quantify and characterize coupled motion at different segments from L1/2 to L5/S1 (144, 294). A number of these static positioning studies have generated data on the complex behavior of the lumbar spine and explaining the functional anatomy of the lower spine in health and disease (59, 221, 263, 277, 382, 406). Additionally, some studies have attempted to quantify the effects of pain reducing stability exercises on spine motion from static image analysis (190, 221). Some of the other reports have documented the outcomes of different modalities of non-surgical treatment interventions on the potential changes of lumbar spine motion and LBP (111, 190, 382, 422). Despite

a variety of techniques available for 2-D lumbar spine motion, there are hardly any techniques available that have objectively been developed to investigate complex 3-D nature of spine motion, in real-time and in context of active physiologic load-bearing. Though techniques based on DFIS and XROMM motion visualizing tools have used MRI based modeling and DFIS based weight-bearing motion tracking systems, these methods still involve the use of ionizing radiation for capturing images of the motion. Moreover, x-ray based fluoroscopy images need complex algorithms for image corrections before the superimposition of models (rotoscoping) can be accomplished for all images (Figure 26). Therefore, manual segmentation based spine modeling methods integrated with the DFIS-based analysis of real-time complex combinations of vertebral motion can be challenging to be put into use in routine clinical use.

To summarize, currently available x-ray based imaging systems that study complex lumbar spine motion are mostly 2-D image acquisition and analysis. Advanced systems that investigate 3-D real-time lumbar spine motion still involve ionizing radiation exposure to body tissues. Although MRI based techniques are available for routine usage to investigate anomalous spine motion, real-time assessment techniques have not been available that can quantify lumbar spine motion in all the six degrees of freedom. In the next section I discuss in some detail our approach to develop a 3-D modeling based technique that may allow us direct visualization and quantification of segmental spine motion. The technique developed out of this dissertation work aims to assess *in-vivo* complex dynamic spine motion with the application of MRI sequences that allow imaging of objects in motion within an externally calibrated MR imaging volume. Additionally, application of a technique that reproduces the animation of the real-time spine motion will allow the frame-by-frame break-up of the motion permitting us to further analyze the motion in context of 2-D as well as the 3-D coupled motion. We

also envisage that imaging real-time human spine motion in weight-bearing MR systems will allow us to apply our technique to study segmental motion patterns in a more physiological load-bearing context.

The direction of developing analytical techniques and protocols for spine motion assessment in this dissertation work is an improvement in currently existing techniques in the sense that it proposes the usage of MRI-only imaging platform thereby eliminating the risk of ionizing radiation induced tissue injury. More specifically, the principle idea of this research will be to introduce the application of an MRI sequence used to image objects in motion. This work will also test the feasibility of using biplanar MR imaging (instead of orthogonal fluoroscopy) for imaging static translations and rotations to analyze 3-D motion in the study objects. The quantification will use animation techniques for the analysis of the motion. Additionally, in light of constant upgrades in faster imaging and computational techniques, modern MR scanners with capabilities of faster real-time imaging can potentially be used with the dynamic quantification technique being developed in this work for regular and relevant clinical applications (146, 473). In the next section I discuss some of the approach and specifics of the dissertation work. Specifically, I discuss the background information on the selection of the 3-D modeling and the MR imaging sequences used in the study, the methodology for testing the feasibility and reliability using basic geometrical objects (Aim1) and for probing the accuracy of the technique involving experiments with a porcine spine model (Aim 2) to quantify pre-determined translation and rotation displacements between the 3-D models on an MRI-only platform (7, 8, 23, 287, 355, 475).

Part V. Approaching the Proposed Dissertation Work: Technique Conceptualization, Feasibility, Reliability and Accuracy Testing

The use of MRI in diagnostic imaging to investigate aberrant motion patterns and segmental mobility uses two basic approaches. The most common approach is to measure dimensions of anatomical structures in the spine and to look for localized pathological changes at the symptomatic level. The other approach for using MRI is the quantitative assessment of inter-vertebral translation and rotational displacements at end-of-range flexion-extension positions. This evaluation is, mostly, performed in the sagittal plane scans of the lumbar spine that also provides an opportunity to assess the disc health and other anatomically relevant structures in context of the reported LBP. The use of MRI to scan moving objects within the scanning volume applies a technique based on computation of accumulated phase-contrast of nuclei of the scanned tissue moving in and out of the imaging plane. Imaging of such moving tissues is performed with a technique called motion-triggered cine MRI where the scanning is triggered and timed by synchronizing the activation of the MRI sequences to a metronome or heartbeats of the individual. Images are typically captured with either an EKG or a phonocardiogram linked to the MRI machine computer. The sequences have typically been used for assessing ventricular motion, coronary or aortic blood flow across the cardiac cycle, as facilitated by the visualization of the stream of images and simultaneous during specific phases of the cardiac cycle as seen by the EKG. The use of such a sequence can also determine and quantifies the direction and the amplitude of the moving object in context of the co-ordinate system assigned to the imaging volume (73, 299, 313, 314). Advanced techniques based on the cine-MRI sequences have been called dynamic-MRI sequences that use real-time ultrafast imaging techniques and do not require any motion triggering. These sequences are in fact, based on the application

of very short examination time and yield good image quality. The nature of the dynamic MRI limits the TE to a very short duration by ultrafast sequences that image the moving object (314). Accordingly, these sequences require short TRs generated with powerful gradient magnets that also control rapid rf pulse amplitudes, fast flip angles for generating a gradient-echo with a steady state precession of protons. Short TRs are integral to the sequences that use the magnetic field inhomogeneity to acquire high-contrast images with good temporal resolution (41). The imaging sequence that will be used in this work also represents a steady state gradient-echo sequence (2D HYCE S sequence) where the TR of the image is specifically encoded to be short. This sequence is also sensitive to inhomogeneity of the magnetic field, as well as to static inhomogeneity of the B_o. The rf and gradient time evolution for 2D HYCE S sequences is similar to other fast dynamic sequences in terms of the timings for the slice selecting gradient, the phase encoding gradient and the frequency encoding gradient. The sampling frequency in the streaming sequence is optimized for each selection of the TR, in line with the RF pulse and capacity of the field gradient to obtain the maximum image signal to noise (S/N) ratio. The TE (echo time) assigned to the sequence is the same as TR/2. The maximum thickness of the slice selected in this sequence is allowed up to 10mm.

In the preceding sections of this chapter we have reviewed that aberrant segmental motion instability of spine may be best defined in the dynamic perspective where the segmental motion is analyzed as it moves through the complete ROM. This analysis may provide information that is crucial to explain the association of spine mobility and LBP, both from the clinical and biomechanical perspectives. Such analyses serve as a platform where visualization of distinct and demonstrable ‘structural’ etiologies of LBP can be approached from a more ‘functional’ perspective of segmental

spine motion. Understanding the clinical presentation of LBP, for example, secondary to spondylolisthesis and intervertebral disc degeneration from a perspective of biomechanical stability of the spine may enhance our current understanding of the patho-physiology of LBP(359, 401, 413, 452). Accordingly, a more dynamic relationship of the force-displacement behavior at any given point within the spine ROM has been suggested as a possible approach for understanding the causes of LBP. As a result, more and more imaging protocols (as is being developed in this study) are being explored to track spine motion (179, 459). Since currently available imaging techniques applied for the assessment of inter-vertebral displacements in the clinical set-up constitute the diagnosis of static anatomy of the spine, the outcome of this dissertation work in the long run focuses on developing a potential tool for quantifying spine segmental kinematics using an MR-only technique (240, 255, 344, 401, 433, 452, 467). Specifically, the technique does not use ionizing radiation for its analysis, can potentially perform motion visualization both from single and biplanar perspectives, can be used in the weigh-bearing mode situation thereby enhancing its utility and application in the clinical setting (144, 295).

Defining clinical instability at the lumbar spine. Several researchers have used cadaveric models to analyze the accuracy and repeatability of spine motion quantifying techniques used experimentally to investigate lumbar spine motion characteristics (120, 350, 433). Several studies have also reported a number of variables that may influence the accuracy of the techniques in question. Variables such as image quality, differences in the approach of quantification, method of data acquisition and calculation of the kinematics may all have their influence on the quantified results (89, 120, 179, 346, 351, 398, 433, 474). Most of these techniques have been tested in the laboratory and not been extensively validated with concomitant

and regular use in the clinical setting. Since most of the clinical diagnosis of LBP is based on palpatory examination and analysis of static spine images, it is not surprising that about 80-90% of all LBP patients do not demonstrate any detectable patho-anatomical origin for their LBP and about 15% of them have an identifiable anatomical pathology explaining their symptoms, with ~30% of such patients believed to have some sort of spine-motion dysfunction based on clinical evaluation and end-of-range imaging (4, 21, 108). White and Panjabi, and Pope and Panjabi have defined clinical spine instability as “the loss of the ability of the spine under physiologic loads to maintain its pattern of displacement so that there is no initial or additional neurological deficit, no major deformity, and no incapacitating pain” (360, 459, 460). A translation of greater than 4 mm of one vertebra relative to another in the sagittal plane has been considered to be the most reliable indicator of spine instability at the lumbar region (344). Accordingly, the specific norm adopted by clinicians has followed a similar outlook for diagnosing segmental instability, as defined by the American Academy of Orthopedic Surgeons, “an abnormal response to applied loads characterized by motion in the motor segment beyond normal constraints” (144, 179). However, regardless of the suspected association of excessive spine motion and LBP, absolute correlation with the degree of instability and the severity of LBP (indicating a liner relationship of the load-displacement curve) has not yet been conclusively proven (144, 179, 256, 401, 467). The lack of precise *in-vivo* spine motion quantification techniques is responsible for this lack of consensus in defining clinical stability from an image-analysis perspective (311, 312). Accordingly, there have been reports of over- or under-diagnosis of instability induced LBP and consequently, of surgical interventions that minimize the ill effects of such an instability. Therefore, procedures such as lumbar inter-vertebral fusions have possibly demonstrated variable outcomes in patients where such instrumentations had been

performed to modify segmental kinematics, reduce pain levels and to alter segmental motion in associated spine segments (164, 256, 433).

Experimental models for segmental motion assessment. By the turn of the twentieth century, the use of roentgenograms was becoming popular as tools to detect disruptions in the structural integrity of the spine. Researchers were using x-rays for morphometric studies of anatomy of human spines (54). In 1944 Knuttson popularized the end-range (maximum flexion and maximum extension) radiograph technique for the sagittal plane inter-vertebral translation analysis that eventually established the criteria used till date to define spine instability in the clinical setting (234). Additionally, in the mid-twentieth century, improvements in earlier proposed techniques were undertaken with the inclusion of quantifying inter-vertebral angles and end-of-range rotation being an important criterion for such assessments. Comparison of such parameters in the sagittal plane were attempted to detect differences between symptomatic and asymptomatic patients with LBP (25, 54, 462). As x-ray imaging and video-fluoroscopy techniques advanced in the 1980's with the ability of acquiring images of moving objects in real-time, these techniques were stating to be used for LBP diagnostic (roentgenography) or interventional (fluoroscopy) purposes, mostly in the 2-dimensional perspective (115, 120, 170, 398, 430).

The need to study the more complex nature of coupled-motion in the spine necessitated the development of a biplanar imaging technique that used two x-ray sources from two different planes (418). The technique entailed imaging of the end-range static positions of the spine from two different orientations. Sagittal and coronal plane images of the spine were processed by digitizing the images with the selection of nine anatomical landmarks on each vertebra in each image. The calibration of these points in each perspective view of the spine was used to develop a three-dimensional

coordinate system for the imaging space. Linear transformation of the coordinates of each of these points was obtained from their positions at different static positions of the imaged spine. Relative 3-dimensional translations and rotations of the vertebrae were then computed from the displacements of landmarks observed from the orthogonal views obtained from the biplanar images (346, 349, 350). Development of the two-plane fluoroscopy technique helped the progression from a biplanar static observation of the end-range motion of the spine to the acquisition of biplanar dynamic images. The images cast on the image intensifier were recorded as a stream of images (de-constructed video footage) for analysis, as some uniplanar fluoroscopy studies had applied earlier for quantification of real-time lumbar spine motion (69-71, 89, 129, 337). Therefore, the assessment of *in-vivo* spine motion was completed in a more physiological context that included physiologic spine-loading, involved the passive and active spine stabilizing systems and was acquired during actual voluntary motion (144, 255, 312, 433). Further advancement of such visualization has led to the development of customized 3-D models in combination with video dual-fluoroscopy of active movement trials o the lumbar spine (256, 401, 452, 467). This technique used x-rays as the imaging source and was capable of calculating three-dimensional real-time coupled-motion of spine segments in individuals performing active movements within the fluoroscopy imaging space. Regardless of the uniqueness of this DFIS technique, it uses x-ray exposure and as such repeated or regular application of this technique will not be possible in human subjects for due to potentially hazardous radiation exposure with such application. On the other hand, although the use of MRI was being put to use and was a technique that eliminated x-ray exposure, such imaging was not performed in physiologic load-bearing conditions and did not have the ability to image actively moving objects within the machine (144, 295).

Repeatability and accuracy of techniques. Results from *in-vivo* studies measuring absolute spine ROM at the cervical, thoracic and the lumbar regions, or kinematic assessments of segmental ROM at the lumbar spine have been variable. Such variability has mostly resulted from two important reasons. Firstly, the limitation of the image resolution, orientation and geometrical distortion embedded in the 2-D rendition of 3-D objects in the images and other physiological limitation such as individual variability in the ROMs may have resulted in such wide range of outcomes (141, 170, 312). Additionally, assessment of displacements in 2-D did not capture coupled inter-vertebral motion profiles of lumbar vertebrae and the variability observed with inter-vertebral motion in some studies may have resulted from dividing the full ROM of the spine merely into three segments (cervical, thoracic or lumbar) without considering the individual characteristics of each regional ROM separately (25, 459, 462). In pursuit of formulating the radiological and clinical definition of spine instability, assessment of inter-vertebral displacements were bring developed in the earlier half of the twentieth century, mostly using sagittal plane imaging and using the superior or inferior endplates of adjacent vertebra as anatomical landmarks for such quantification (46, 115, 142, 462). Some of these studies had reported inconsistent observations due to potential limitations involved with the techniques (142). Advancements in the techniques in terms of improvements in repeatability and accuracy of the results involved the usage of additional landmarks for quantification and improvement in image resolution (170). Introduction of automated digitization of specific image features related to the displacements have yielded consistent results. The use of cut-offs such as Root Mean Square (RMS) values of <2 mm for translation and 1.5^{o} for rotation as indicators of instability have been reported to be more acceptable parameters for diagnosis. Breen *et al*. have reported mean absolute errors of 0.56±0.37^{o} for the coronal plane and

0.84±0.87° for the sagittal plane rotation as of critical importance in rotation stability of lumbar segments (120, 337). Additionally, similar RMS error values have been reported to be critical for rotational stability obtained from a 2-dimensional fluoroscopic evaluation, after performing corrections for optical (0.46±0.28°) for (89). However, the value of this was reported to be more than doubled without the correction, even when the images were digitized for quantification indicating the importance of image quality and distortion correction as a determining factor in such quantification. The reliability and accuracy of such measurements have been reported to be closer to the to the actual values of experimental displacements and have been shown to go up with selection of the exact anatomical landmarks selected for manual digitization (54). Highly improved outcomes depended on techniques that used the selection of four corner points of a vertebra for digitization on the mid-sagittal plane and then calculated the midpoints of the sides for further quantification (141). The same method was applied to measure changing endplate angles between two adjacent vertebrae across the string of images to calculate the rotational displacements. Some studies have reported calculating inter-vertebral translation as the distance between the perpendicular projections to the centers of two adjacent vertebra drawn from the bisector of the segmental angle at a given vertebral level, the bisetrix (details discussed in Chapter 5). The measure of this value was standardized by calculating a ratio by dividing that number with the length of the adjacent end-plate. This method resulted in better resolution of their radiographic images and repeated digitization of the landmarks as an important process for enhancing the accuracy of the results, as reported by some other studies (141, 171, 337, 433).

Recent advancements have moved towards generating 3-D data in spine using additional segmented models of the vertebrae superimposed upon the x-ray images of the motion to quantify and analyze their movement patterns (256, 401, 467). The

vertebral models are first registered with the fluoroscopic images and assigned joint co-ordinate systems between the vertebral elements. These registrations are performed for each image frame in the stream of images representing the entire video. The three-dimensional coordinate systems assigned to the vertebral models yield the kinematic measurements between the vertebral elements as the images are displayed in a separate image-viewing software (144, 256, 401, 467). Similar studies using MRI and static imaging of a spine that was axially rotated through different rotated trunk positions has reported small errors in tracking the rotational parameter through the entire ROM of ten healthy individuals (144). Comparing manual with the currently applied semi-automate and automated voxel based volume rendition techniques for segmentation and motion analysis systems have reported a non-significant differences in assessment of rotation and translation parameters between semi-manual quantitative motion analysis (QMA) and digitized manual techniques (144, 351). Comparison of displacement quantification errors between the manual and QMA techniques using the standard errors of measurement (SEM) offers relatively larger divergent values, including substantially higher intra-observer and inter-observer reliability values for the QMA technique (474). Regardless of diversity of the levels of agreement between these techniques, the use of standardized values within each technique to determine the relative kinematic changes in the lumbar inter-vertebral displacements have reported to better assist clinicians to diagnose and objectively measure the outcomes of interventions in lumbar instability in instance where techniques based on orthogonal fluoroscopy (Roentgen Stereo-photogrammetry/RSA) were performed (details discussed in Chapter 3) (79, 429, 442). Since anomalous behavior of spine is not limited to a purported exaggerated displacement at the end-range-of–motion, small and aberrant inter-vertebral motion within the segmental ROM may be a cause of pain and hence, accurate and reliable

methods that may objectively validate any existing association between LBP and altered segmental motion at the symptomatic region.

Statistical analyses for reliability and accuracy assessment. The other reason for discrepancy between results of quantification studies is the type of statistical approach selected for analyzing the results. One method of describing the results have been in terms of reporting the standard deviations from several quantification trials and several rounds of image processing to provide an estimate of the variance associated with the outcomes of a method (223). Literature reporting standard deviations (SD) from assessments of translations range from of 0.5 to 0.7 mm for translation and ~1.0^{o} for rotation. These studies attempted to measure the accuracy of techniques involving humans or other replicable models mostly including x-ray exposure for imaging (54, 69-71, 89, 141, 170, 208, 350, 398, 430, 452). Some of these reports have attempted to validate techniques measuring *in-vivo* inter-vertebral motion with experimental cadaveric models that were moved through a pre-determined distances within the imaging volume (430). We shall discuss in details in the next chapter on the limitation of using techniques based on tracking surface markers to quantify inter-vertebral motion. Variability associated with imaging techniques, especially radiographic imaging, have involved RMS errors in translation and for rotational measures associated with positioning of the spine models in the radiographic imaging plane, with simulation of a physiological imaging scenario by placing an animal tissue or water as an optical medium between the vertebrae and the x-ray source, and with uncorrected optical distortions present in the x-ray images (69, 70, 89, 350). Some authors have reported SDs of 0.4 - 0.8 mm for translation and 0.74 -1.64^{o} for rotation observed through a range of 5-15^{o} of flexion-extension images at different levels of the lumbar spine whereas others have reported errors of less than 1^{o} with ~0.3^{o} SD in quantifying sagittal and coronal plane rotations at

5º increments through a range of 20º (54, 141). Some researchers have attributed differences observed in their respective observations to the selection of their designs and statistical approaches for the reporting (141, 433). However, quite a few studies did not report any comparison between their outcomes and the results of other relevant studies, although a general overview of these studies revealed that regardless of the manual or automated evaluation of spine kinematics, rotations were more accurately quantified than translations (208, 351, 418). Additionally, the displacements analysis results with RMS errors of less than 0.5 mm for translation and 1.0º for rotation with standard deviations less than 0.5 mm and 0.75º respectively have been reported in available literature on the accuracy levels for techniques for such assessments (170, 208, 351, 418). Analysis of intra- and inter-observer data from within the same or between separate studies can provide important information on the reliability and accuracy of such quantification techniques, as reported by several studies that have attempted to develop quantification techniques and applied them as intra- and inter-observer differences (120, 295, 351, 398, 474). Reporting of Intra-class correlation coefficients (ICC) have been used as additional tools to compare between observer measurements in studies, with a value of 0 being no agreement and 1 being complete agreement between assessments. Some studies, as a norm, do only report percent differences between observations standard statistical technique for calculating a method's repeatability (120).

Summary of the statistical approach and technical improvements associated with the dissertation work. The primary focus of this dissertation work was to test the feasibility and reliability of the technique with the use of a pair of geometrical objects and a pair of porcine motion segments respectively. The feasibility of the techniques was determined by assessment of displacement between two solid body

objects that were moved within the scanning volume of the MRI through pre-determined translations and rotations. The reliability of displacement data obtained from two rotoscoping sessions (scanned using two MR sequences) was verified by calculating the ICC, CV and the Bland-Altman analysis. For the main part of the experiments, two porcine motion-segments were used to further demonstrate the reliability of the quantification technique being developed that was based on a rotoscoping process involving matching-up of morphological landmarks between the 3-D models and corresponding areas visible in the background images. These models used for imaging translation and rotation displacement trials with eight data points sampled (without replacement) from the proposed -5 mm to 5 mm range of motion. To avoid skewing of the samples, the range of translation in both the sagittal and the coronal planes were divided into two blocks (-5 mm to -1 mm and 1 to 5 mm) and four data points selected without replacement from each block. Similarly, the range of sagittal plane (flexion-extension) rotation was divided into four blocks (-5 to -1, 1 to 5, 6 to10, and 11 to15 degrees). Two samples were selected without replacement from each of these blocks. The range of coronal plane rotation (lateral bending) was blocked into four segments (-10 to -6, -5 to -1, 1 to 5, and 6 to10 degrees). Two data points were selected without replacements from each of these four blocks. For the flexion-extension trials eight translation trial points were permutated to generate a series of thirty-two trials (2 levels of spines and 2 levels of sequences). For the rotation displacement, eight data points were sampled without replacement from the proposed -5º to +15º range of motion. The order of these eight rotation trials were permutated to generate a series of thirty-two trials (2 levels of spines and 2 levels of sequences). For the lateral bending translation displacement, eight data points were sampled without replacement from the proposed -5

mm to 5 mm range of motion on both sides of the neutral position. The order of these eight translation trials were permutated to generate a series of thirty-two trials (2 levels of spines and 2 levels of sequences). For the rotation displacement, eight data points were sampled without replacement from the proposed -10º to +10º range of motion across the neutral position. The order of these eight rotation trial points were permutated to generate a series of thirty-two trials (2 levels of spines and 2 levels of sequences). All displacement trials were quantified twice with a gap of at least one week between the two assessments by a single, blinded rater (or two raters, contingent to the availability of time and resources). The magnitudes and directions of displacements were coded and the rater was blinded for the type of trial. Statistically, the accuracy of the main part of the experiment involving the porcine spine model was measured by creating the following linear mixed-effects model Bias = $ß_0$ + $ß_1$Displacement + $ß_2$Sequence + $b_{Session}$ + b_{spine} +ε, where bias was the difference between true and observed values (Bias = YTrue – Y). βo was the intercept, and β_1 and β_2 the regression coefficients representing the displacement and pulse fixed effects. $b_{session}$ and b_{spine} represented spine and assessment random effects, and ε represents the residuals. This formula evaluated accuracy as any non-zero intercept or coefficients. That is, β_0 of 0.2 indicated bias of 0.2 mm with sequence A, while β_2 of 0.5 indicated additional bias introduced by sequence B, relative to sequence A. Any interaction between the levels of spine, session and orientation of the scans were calculated by the linear mixed effects model. Average percentage error of the technique was obtained by dividing the absolute value of Bias by the true value and multiplied by 100: Average % error = (YTrue – Y)/YTrue * 100. Intra-Class Correlation Coefficients (ICCs) were calculated to ascertain the reliability of the technique.

Between-session ICCs were calculated separately for the two sequences and the orientation (coronal and sagittal) used in the study. Reliability was also tested by computing the coefficient of variations (CV) between the two sessions as the intra-rater reliability. The use of the regression model also allowed the examination the agreement between outcomes from the use of the T_1 and 2D HYCE S sequence both for the plane of motion and for translation and rotation. Trials were obtained from blocks of intervals created within the range of motion in order to maintain uniformity of selection of data points through the entire range of translation or rotation in both the coronal and sagittal plane experiments. The rater was blinded for the type of trial quantified during the analysis. The magnitudes of displacements in this work had been selected after comparing the range of motion tested in other studies and the accepted displacements considered as indicators of lumbar instability (54, 70, 89, 120, 170, 171, 179, 346, 351, 398, 459, 474). Additionally, the hybrid 2D HYCE S streaming sequence used in this study was a steady state sequence that is capable of dynamic MR imaging. Although the current study was limited to the use of the 2D HYCE S sequence in a static context, it nevertheless validated the capability of its usage in capturing images of satisfactory and reliable resolution that can be used with the technique reported here, for quantifying inter-vertebral motion. Additionally, the Intra and inter-observer assessments used for analysis determined the repeatability of the technique that was also supported by the calculation of the between-session ICCs.

Our technique was one of the first ones applied segmentation methods to generate 3-D models of the porcine spine segments, calibrated the MR imaging volume to scan the movement trials and simultaneously registered the 3-D models to the T_1 and 2D HYCE S images to measure the displacements. Our technique provides the option of imaging and analysis of the displacements from the two orthogonal perspectives.

Additionally, we envisioned that the reliability and accuracy of out technique was thought to be further enhanced by using MR imaging instead of fluoroscopy as the MR images allowed us to use ‘slices’ of images instead of 2-D x-ray images. The use of slices permitted to match the positions of the 3-D models with the anatomical landmarks on the background images better than that would have been possible with digitally uncorrected x-ray images (89, 120). Also, the use of short TE, TRs and suitable pixel size allowed us to enhance the image quality (433). The current project set out to address the feasibility of developing a quantification technique based on an MRI-only approach for creating segmented 3-D models, acquiring MRI scans of the spine models moved through pre-determined distances relative to each other and using the rotoscoping technique for quantifying the motion. Techniques using ionizing radiation need adjustment of the exposure dosage depending upon the frame-rate of data capture, the total number of frames, overall duration of the imaging, the field-size of the images, the size of the patient and the thickness/density of the body part of interest, and exposure settings on the hardware used. Unlike fluoroscopic imaging, MR scanning used in this study did not used any ionizing radiation. Additionally, unlike fluoroscopy the MR images used were very thin slices and did not require complex algorithms to correct geometrical distortions for nonlinear pinch-cushion effects. From a long-term perspective, the goal of this work was to create foundational research to enable the development of an MRI-only based technique for accurate and reliable analysis of segmental spine motion in the future.

Chapter 3. Development of a Morphology-Based Modeling Technique for Tracking Solid-Body Displacements: Examining the Reliability of a Potential MRI-Only Approach for Joint Kinematics Assessment

The material in this chapter has been published in the BMC Medical Imaging journal (274).

Abstract

Single or biplanar video radiography and Roentgen stereophotogrammetry (RSA) techniques used for the assessment of *in-vivo* joint kinematics involves application of ionizing radiation, which is a limitation for clinical research involving human subjects. To overcome this limitation, our long-term goal is to develop a magnetic resonance imaging (MRI)-only, three dimensional (3-D) modeling technique that permits dynamic imaging of joint motion in humans. Here, we present our initial findings, as well as reliability data, for an MRI-only protocol and modeling technique. We developed a morphology-based motion-analysis technique that uses MRI of custom-built solid-body objects to animate and quantify experimental displacements between them. The technique involved four major steps. First, the imaging volume was calibrated using a custom-built grid. Second, 3-D models were segmented from axial scans of two custom-built solid-body cubes. Third, these cubes were positioned at pre-determined relative displacements (translation and rotation) in the magnetic resonance coil and scanned with a T_1 and a fast contrast-enhanced pulse sequences. The digital imaging and communications in medicine (DICOM) images were then processed for animation. The fourth step involved importing these processed images into an animation software, where they were displayed as background scenes. In the same step, 3-D models of the cubes were imported into the animation software, where the user manipulated the models to match their outlines in the

scene (rotoscoping) and registered the models into an anatomical joint system. Measurements of displacements obtained from two different rotoscoping sessions were tested for reliability using coefficient of variations (CV), intraclass correlation coefficients (ICC), Bland-Altman plots, and Limits of Agreement analyses. Between-session reliability was high for both the T_1 and the contrast-enhanced sequences. Specifically, the average CVs for translation were 4.31% and 5.26% for the two pulse sequences, respectively, while the ICCs were 0.99 for both. For rotation measures, the CVs were 3.19% and 2.44% for the two pulse sequences with the ICCs being 0.98 and 0.97, respectively. A novel biplanar imaging approach also yielded high reliability with mean CVs of 2.66% and 3.39% for translation in the x- and z-planes, respectively, and ICCs of 0.97 in both planes. This work provides basic proof-of-concept for a reliable marker-less non-ionizing-radiation-based quasi-dynamic motion quantification technique that can potentially be developed into a tool for real-time joint kinematics analysis.

(*Note: Alphabetic subheadings of all figures related to this chapter presented in the figures section are provided at the bottom of the figure panels).*

Introduction

Visualization of skeletal elements is central to three-dimensional (3-D) kinematic analysis of joint motion. Indirect methods based on tracking surface landmarks (using reflective markers attached to the skin surface) within a calibrated volume (stereophotogrammetry) can contain artifacts (errors of transformation) due to integumentary displacements relative to actual skeletal motion (79, 81, 84, 112, 378). Direct visualization of bony elements during joint motion are typically accomplished *via* fluoroscopy or cineradiography. Unfortunately, both of these techniques require the use of ionizing radiation, and outcomes from these techniques are restricted mostly to two-

dimensional (2-D) analyses as the majority of these systems use single-plane imaging (68, 469). Emergence of the roentgen stereophotogrammetry (RSA) technique has enabled *in-vivo* measurement of complex 3-D skeletal kinematics from a series of radiographs acquired with biplanar, orthogonal fluoroscopy (38, 79, 397). Although this technique is accurate, it commonly requires surgical implantation of markers in bones (52, 65, 112, 283, 397), although model-based RSA techniques have recently begun to appear in the literature (53, 202, 245).

Recording a series of joint-motion images using x-ray fluoroscopy and then manually superimposing 3-D models of the same skeletal elements to match corresponding outlines in the x-ray images has been used to quantify *in-vivo* joint motion. (114, 213, 469, 479). More recently, Gatesy *et al*. reported using the scientific rotoscoping (SR) motion analysis technique, which involves biplanar fluoroscopy to image skeletal movements, creation of 3-D models of joint skeleton from high-resolution computed tomography (CT) scans, followed by model-to-image matching and registration (rotoscoping) performed over several frames of images yielding skeletal motion animation and 3-D kinematic data (39, 68, 153, 154). SR was developed from the X-Ray Reconstruction of Moving Morphology (XROMM) motion quantification technique, which tracks implanted markers digitized in biplanar fluoroscopic images captured within a calibrated imaging volume, instead of utilizing the model superimposition technique (68). Though accurate, both SR and XROMM techniques require corrections of geometrical distortions in images prior to the animation (29, 52, 283, 392, 429). While x-ray-based motion analysis techniques like SR, XROMM, and RSA are clearly novel and advanced, their translation to clinical research (i.e., human subjects research) has been limited due to health-related concerns associated with the radiation exposure (64, 200, 229, 250, 300).

From a clinical research perspective, understanding *in vivo* skeletal motion is of interest to both scientists and clinicians (136, 176, 258). More specifically, x-ray-based diagnostic imaging techniques measuring human inter-vertebral displacements have focused mostly on imaging the spine at static end-of-range positions (121, 155, 176, 292, 338, 344, 348, 455, 474). However, qualitative and quantitative assessments of spinal motion have been enhanced by quantitative radiographic techniques that track displacements of pre-assigned coordinate points of specific anatomic locations on orthographic spinal images and by real-time joint-motion evaluation with XROMM-like techniques (using CT/magnetic-resonance-imaging-based 3-D models) and RSA (with per-operative implanted vertebral markers) in human subjects (29, 300, 344, 347, 349, 391, 401, 426, 470, 472). Regrettably, these approaches still require exposure to ionizing radiation and, at times, require marker implantation on the bones.

Magnetic resonance imaging (MRI), when used for quantifying inter-vertebral motion, has mostly been restricted to the analysis of end-of-range sagittal-plane displacements (92, 228, 254). However, dynamic cine-phase contrast (cine-PC) or fast-phase contrast (fast-PC) imaging with ultra-fast gradient echo sequences have been employed for evaluating joint kinematics, especially in ankle, knee, or shoulder motion (47, 97, 127, 366, 371, 400, 453). The main approach for these techniques has been the use of pulse sequences that permit volume extraction from full 3-D motion datasets at selected time points along the range of motion (ROM). However, these techniques can be time-consuming. Additionally, the use of cine-PC sequences require a repeated, cyclic, velocity-controlled motion to be performed at the joint of interest during scanning to make the motion synchronized with velocity-encoded motion capture (126, 127). Also, these images have low resolution and may present motion artifacts (97, 107, 126). More recently, the combined use of segmented 3-D anatomical models (from high resolution,

~15 mins duration, static axial scans) registered to low resolution, volumetric images acquired at different joint positions using high speed (~40 sec) T_1 sequences has been reported (127). Although such techniques acquire multi-position data with much greater speed, the segmentation of these low-resolution images still require multi-slice images of the experimental quasi-dynamic joint positions. Accordingly, recent advancements in these methods have focused on the acquisition of faster and fewer slices of joint motion (without compromising image resolution) for model-to-image registration and without reducing the accuracy of the technique (time-accuracy tradeoff).

Currently, no modeling techniques exist for quantification of inter-vertebral joint displacements using single-plane or orthogonal magnetic-resonance (MR) image templates for 3-D model registration. Accordingly, our long-term goal is to develop a 3-D model-based technique that permits fast dynamic MR imaging of the human lumbar spine using an open-bore weight-bearing musculoskeletal MRI. Our study focuses on the lumbar spine as LBP is one of the most common reasons for seeking medical care world-wide and accounts for over 3.7 million physician visits per year in the United States alone (276, 280, 322, 390, 460). As such, LBP is arguably one of the most debilitating and costly health disorders, and the development of technologies to aid scientists and clinicians in better understanding the etiology of LBP—as well as in monitoring the effects of therapeutic interventions— is desperately needed.

As a first step towards our long-term goal, we present in this article our initial research and development findings for an MRI-only protocol involving imaging (using a standard T_1 and a fast contrast-enhanced MRI sequences), a series of pre-determined displacements between solid-body models, 3-D models (segmenting T_1 weighted axial scans), and a morphology-based rotoscoping strategy for animation and quantification of the displacements. The use of the contrast-enhanced sequence will allow us, firstly, to

test the feasibility and reliability of its use as a fast imaging tool and secondly, to compare its outcome with that of the standard high-resolution T_1 images. The feasibility and reliability of this MRI-based technique is discussed here, and we anticipate further developing this technique into a motion-assessment tool for the lumbar spine and other di-arthrodial joints.

Materials and Methods

General overview of the experimental design. The experiment involved scanning a pair of wooden cubes placed at pre-determined positions (displacement trials) relative to each other in a custom-calibrated coil of an open-MRI system (0.3 Tesla; Esaote G-scan Brio, Genoa, Italy). Additional axial images of the solid cubes were acquired and segmented using the AVIZO software (Hillsboro, OR, USA) to create 3-D virtual models of the cubes. Next, the MR images of the displacement trials and the 3-D cube models were transferred into an animation software (AutoDesk MAYA, San Rafael, CA, USA); and animations of these displacement trials were performed to quantify the relative motion incurred by the solid bodies. The technique involved four principal steps (Figure 27A). First, the imaging volume of the MRI coil was calibrated using a custom-built grid (Figure 28A). Second, 3-D models were segmented out from axial scans of the solid-body cubes (Figure 2B ii-v). Third, the solid bodies were positioned at pre-determined displacements (Figure 27B) relative to each other in the MRI coil and scanned (Figure 28B i); and the digital imaging and communications in medicine (DICOM) images were pre-processed into gray-scale TIF format. Fourth, these images were imported into the animation software using calibration data acquired from the grid used in the first step. These images were displayed as a series of background scenes in the animation environment (Figure 28C & D i-iii). Next, the 3-D models were imported into the animation software and manually manipulated by the user to “register” the

models to their outlines visible in the background images (Figure 28C & D). Lastly, inter-cube translational and rotational displacements were calculated using this technique. All measurements required for fabricating the grid and solid-body cubes and for measuring the experimental displacements during scanning were performed by a digital caliper (sensitivity = 0.02 mm) (Global Industrial, Port Washington, NY, USA). The details of each step are described below.

Calibrating the MRI Imaging Volume. The volume of the MRI coil was calibrated using a custom-built calibration grid (Figure 28A). Four square Perspex fiber plates (area = 80 mm^2; thickness = 2 mm) (Modular-Movement Tray-Set, Games Workshop/NG, UK) were serially stacked with a distance of 30 mm between each plate with three wooden dowels drilled across the plates and glued at all their contact points for stability. Before fixing the dowels, sixteen holes, each 2 mm in diameter, were drilled into each plate in a 4X4 array. Adjacent holes were drilled 20 mm apart from each other. Each hole was fitted with a 2-mm-diameter water bead using a small amount of glue. Three additional beads were embedded into two adjacent plates to define x, y, and z coordinates of the grid (Figure 28A) (466). The x- and z-axes were located in the same plane representing the plane of the grid plates, whereas the y-axis extended perpendicular to the plane of grid plates (Figure 28A). These coordinates were assigned as per the joint coordinate system (JCS) defined by the Standardization and Terminology Committee of the International Society of Biomechanics for studying inter-vertebral motion (466). To facilitate visualization of the beads in the MR images, the grid was submerged in a 1% saline solution for 30 seconds and then air dried for 2 minutes prior to scanning. The y-axis of the grid was placed along the longer axis of the MRI coil bore (DPA Wrist Coil, Esaote, Genoa, Italy). Four non-contiguous axial 3-mm-thick slices were acquired parallel to and across the grid in a way that each slice image included a

single plate with all the 16 beads of a plate in view using a Fast Spin Echo T_2 sequence (repetition time [TR] = 7810 ms, time to echo [TE] = 120 ms, field of view [FOV] = 200 x 200, Matrix = 256 × 256; resolution = 0.78 mm; voxel dimension = 1.82 mm^3). The four DICOM files were then transferred to the AVIZO software, where all the beads were segmented and images of all segmented individual plates were stored in the TIF format using Photoshop software (Adobe Systems Inc., San Jose, California) for later use in Step 4. Additionally, the surface rendition of the segmented beads representing a composite view of the entire grid was saved as an .OBJ file for digitization in Step 4.

Constructing and segmenting the solid-body cubes. Two solid-body cubes, with sides measuring ~40 mm, were cut from a wood block (Figure 28B). Hourglass shaped holes (7-mm base diameters) were drilled through the center of both cubes with a stepped-cone drill. These holes were drilled to create a distinct morphological feature within the cubes and to facilitate the rotoscoping and model-to-scene matching process in a later step. The cubes measured close to the average transverse dimensions of the first lumbar vertebral body in humans, and the hourglass feature simulated the appearance of the vertebral canal in a motion segment (39, 83, 329, 380). Adjacent edges of the cubes were marked with a 20-mm scale with 1.0 mm graduations (Figure 28B). A neutral position was defined as zero displacement between the mid-lines of the scales. The relative positions between these mid-lines on the scales were manipulated by the user to perform the translation trials with a range of 20 mm in either direction of the neutral position. The opposite sides of the cubes were marked with a protractor to measure inter-cube rotations on both sides of a 0º neutral position at increments of 5º through 90º of rotational displacement. Additionally, 3-D cube models were manually segmented in AVIZO using contiguous high resolution (pixel = 0.78 mm) axial T_1

weighted scans (TR = 810 ms, TE = 30 ms, FOV = 200 × 200, Matrix = 256 × 256) (Figure 28B).

Displacement trials. The solid-body cubes were immersed in ~1% saline for 30 seconds, wiped dry, and positioned within the MR coil. The long axes of the hourglass-shaped holes in both the cubes were placed along the y-axis of the imaging volume and scanned in the neutral position. The single-plane translations and rotations were performed in the z-plane of the imaging volume. The axis for the rotation trials was formed by the x-plane. The cubes were placed and fixed by double-sided tape on a flat foam platform in the coil to avoid shifting during scans. After scanning the neutral position, the platform was pulled out of the coil; and the cubes were re-positioned for the next trail, with the displacements verified by the Vernier caliper before the platform was re-positioned inside the MRI coil (Figure 28B). A gap of ~10 mm was maintained between adjacent edges of the cubes during translation, a distance representing the average dimension of a human lumbar disc space (198). For the rotation trials, the center of rotation (COR) of the rotating cube was kept 50 mm away from the center of the stationary cube. A high-resolution (0.78 mm) T_1 weighted sequence (TR = 810 ms, TE = 30 ms, FOV = 220 × 220, Matrix = 256 × 256, slices = 3, gap = 0, thickness = 5 mm, scan time = ~2 mins/scan) and a fast contrast-enhanced streaming sequence with resolution 0.98 mm (2D hybrid contrast enhanced streaming sequence [2D HYCE S]; thickness = 8 mm, slice = 1, scan time = ~10 s/scan) were used to acquire single-slice images of displaced positions in the mid-sagittal (zy-) plane with the central core of both cubes in view (Figure 28C). The trials included translations between 0.0 – 20 mm in 5 mm increments (n = 35 trials; 7 trials/displacement) and rotations ranging between 0° to 20° in 5° increments (n = 30 trials; 6 trials/displacement) on both sides of the neutral position [Table 4]. Biplanar translations were scanned in static positions after the cubes

were displaced both in the z- and x-planes through a range of 5 mm increments in a 0.0 to 20 mm range (n = 20; 4 trials/displacement). All trials were number-coded and randomly performed in three separate scanning sessions each designated for translational, rotational, and biplanar trials, respectively. For the biplanar trials, additional orthogonal slices were acquired with the central parts of both cubes in view.

Animation of the imaging volume and quantification in MAYA (68, 154, 324)**.**The MAYA software was used to create the animation environment. The environment essentially represented the calibrated MR imaging volume. The software also provided a "camera-view" for the user to view the cube models and the background scene in the calibrated animation environment (Figure 28D). The user manually manipulated the 3-D models to match and register them to their outlines seen in the background scenes. The steps for creating the animation environment are as follows:

Creating a MAYA framespec file (68)**.** The composite grid .OBJ file created in Step 1 was transferred to MAYA, all the beads were serially numbered according to their actual positions in the grid system, and the centroid points for each segmented bead was calculated by the program. Next, the values of the coordinate points for each bead centroid were calculated in the context of all other beads, representing the entire grid volume. The x, y, and z values of all bead coordinate points were merged together to generate the MAYA 'framespec' file to be used for the next step of grid digitization.

Digitizing the beads*.* A MEL-script (MAYA Embedded Language-script) command was run in Matlab. An image of a grid plate previously segmented in AVIZO and stored in a TIF format in Step 1 was opened using the Matlab program, and all beads in the plate were digitized serially by clicking over their central points. Next, the framespec file created in the previous step was loaded into the program to yield the Direct Linear Transformation (DLT) coefficient values for the concerned plate (68, 154).

All four plates were digitized sequentially to generate the DLT coefficient value for each plate image. The program allowed automated corrections for minimization of errors and to contain coefficient values < 1 (154). This step was repeated for all four plates, and each step yielded a plate coefficient value and a “xyz point” .csv file specific to the concerned digitized plate. The data points of the xyz-point files from all the four plates were collated to generate a common “four-plate xyz point” .csv file for the grid (466). Next, the four-plate xyz-point and the framespec files were loaded into the Matlab program using the MEL-script. One of the segmented plate-images were opened in the Matlab and re-digitized. The four-plate xyz-point file was loaded into the program, and the MEL-script was re-run to generate a “MayaCam”.csv file that was used to re-create the MR imaging within the animation software and to create the camera-view for the user.

Rotoscoping, animation, and quantification. The animation scene was created using the MayaCam file. After the animation environment was created, the background scene was introduced by importing the TIF format images of the trials into MAYA (Figure 28C & D). These images were clustered into a series of frames, with each series representing a specific trial type. Next, the two 3-D cube models were imported into MAYA using a scaling factor of 0.1 (from segmentation environment in mm to the animation environment in cm). The models were manipulated with the computer mouse and keyboard functions to achieve maximum geometrically alignment and match between the 3-D model and corresponding image outlines in the background scene. The sharp external boundaries and outlines of the hourglass silhouettes within the solid bodies were utilized to facilitate the model-to-scene match (Figure. 28C & D). This process was called rotoscoping.

Once rotoscoping in the first frame of the scene (neutral position in the series) was achieved, an Anatomical Joint Axis (AJX) was assigned to the solid bodies. The image of the background scene was then advanced to the next frame and the rotoscoping repeated; this process was repeated for all remaining trial images. For the biplanar translations, two orthogonal camera views were created to provide background scenes of displacements from two different, the x- and z-plane, perspectives (Figure 28D). Although the animation software generated solid-body motion data for all rotoscoped image frames in all six degrees of freedom, only applicable single-plane measures were extracted for analysis and reporting. Two sessions (S1 and S2) of rotoscoping and displacement quantification were performed separately for translational, rotational, and biplanar motion by a single observer (NKM). All trials were number coded, and the rater was blinded to the displacement type and the pulse sequence used for the scan. The AJX created in Session 1 was used for rotoscoping in the corresponding Session 2. The approximate time for rotoscoping (Step 4(c)) a series of image frames representing a specific trial type, e.g., a seven-translation series, in this study was ~40 minutes including matching of the neutral position at the start and extracting displacement data from the series at the end.

Statistical analysis. Test–retest reliability for the outcomes involving the T_1 and 2D HYCE S sequences from the two sessions were determined by coefficient of variation (CV), t-test, intraclass correlation coefficients (ICC) (two-way random effects model with a single measure of reliability), and 95% limits of agreement (LOA) analyses. Variability between the outcomes from a single displacement quantified in two different sessions was analyzed using CV. For example, if a particular displacement was quantified as 11.5 mm in Session 1 and 10.8 mm in Session 2, the CV was calculated as: Standard Deviation of the two sessions divided by the mean of the two sessions

times 100. Thus, for this example, the CV = (0.5/11.15) × 100 = 4.44%. The sessions were performed at an interval of one week. Additionally, we used dependent sample t-tests to compare the values between testing sessions.

ICC was calculated using a (2, 1) two-way random effects model with a single measure of reliability computed over the variance observed in the two sessions. A (2, 1) model was chosen as it allows the determination of any existing systematic bias. The statistical software SPSS (SPSS Inc., Version 21.0, Chicago, IL, USA) was used to calculate the ICC. The main objective of the statistical analysis was to ascertain the reliability of this technique. The relative reliability was assessed by calculating the ICC, which assesses the reproducibility of a measurement relative to a sample of repeated measurements. The absolute stability of a measure typically defines the contribution of the main-error component in the observed variance. To fully understand the absolute stability or reliability of a measure, it is essential to understand the contribution of different components of the measurement error. (35, 94). Accordingly, the measurement error was broken into two components. The first component was defined as the systematic bias, and the second was termed the random error. The systematic bias denoted the contribution of any learning effect on the part of the assessor in explaining the between-session variability of the data, whereas the random error explained a biological or mechanical effect (35, 56). The first step was to generate Bland-Altman plots using the between-session means and differences data. The correlation (R^2) between the absolute differences and the means of the between-session values was calculated to determine the spread of the dependent variable. R^2 values between 0 and 0.1 represented homoscedasticity, suggesting that there was no correlation between the size of the error and the size of the measured variable. Heteroscedasticity was considered to be present with R^2 values > 0.1 and indicated that the degree of error

increased with increase in the values of the measured variable along the scale, e.g., the error term increased as the technique attempted to measure larger displacements (translation/rotation) in the experiment (35, 56, 94, 227). Finally, the ratio LOA was calculated for verification of the absolute reliability of the measure using the following equation: ratio LOA = [(SDdiffs/AVGmeans) × 1.96] × 100, where *SDdiffs* was defined as the Standard Deviation of the difference of scores (Session 1 and Session 2), *AVGmeans* represented the average of the mean scores (Session 1 and Session 2) for each measurement, and the factor 1.96 specified the inclusion of 95% of observations of the differences in scores. The ratio LOA was interpreted as the highest percentage by which two tests will differ due to measurement error in either the positive or negative direction (35).

Results

Summary of results. Descriptive statistics and CV and ICC reliability measures obtained from the T_1 and 2D HYCE S images for each type of displacement are provided in Table 4. A high degree of between-session reliability was observed for both the T_1 and the contrast-enhanced dynamic pulse sequences. Specifically, the average CVs for translation were 4.31% and 5.26% for the two pulse sequences, respectively, while the ICCs were 0.99 for both sequences. For rotation measures, the CVs were 3.19% and 2.44% for the two pulse sequences with the ICCs being 0.98 and 0.97, respectively. A novel biplanar imaging approach also yielded high reliability, with mean CVs of 3.39% and 2.66% noted for translation in the z- and x-plane, respectively, along with ICCs of 0.97 in both planes. Additionally, all but one displacement variables showed homoscedastic relationships with the Bland-Altman's LOA analysis of the between-session measurements and demonstrated a relatively low degree of systematic bias.

Translation trials. Analysis of the between-session measurements of each of the two sequences, applying a paired sample 2-tailed t-test, did not show any significant differences in means between the T_1 ($p > 0.98$) and the 2D HYCE S ($p > 0.84$) pulse sequences. The reliability of the measured variables demonstrated high levels of consistency, with the T_1 sequence having CVs ranging from 1.1 to 14.63% and an ICC of 0.99. For the 2D HYCE S sequence, the CVs ranged from 1.6 to 13.5%, and the ICC was also 0.99. The Bland-Altman plot with 95% confidence interval (±1.96*standard deviation [SD]) analysis of the between-session data showed that all cases had a test-retest difference within ±1.24 mm (mean/bias=0.02mm) and ±1.59 mm (mean/bias=-0.34 mm) for the T_1 and the 2D HYCE S sequences, respectively (Figure 29A). The LOA analysis for translation indicated a relatively low degree of systematic bias in the between-session differences ($p = 0.98$ and 0.84) and a homoscedastic relationship between the differences and averages of the between-session measurements for both T_1 and the 2D HYCE S pulse sequences respectively ($R^2 = 0.07$ and $R^2 = 0.03$) (Figure 29A). The homoscedasticity indicated that the random errors did not increase with the increase of the measured displacement values. The follow-up ratio LOA analysis demonstrated a systematic bias in the order of 0.02 and -0.34 and random error of ±14.14 and ±13.68 for the T_1 and 2D HYCE S sequences, respectively. The ratio LOA analysis for translation suggested that the between-session measurement errors obtained with the technique did not exceed 14.15% and 13.34% in either the positive or negative direction with the use of T_1 and the 2D HYCE S pulse sequences, respectively.

Rotation trials. Analysis of the between-session measurements of the two sequences applying a paired sample 2-tailed t-test did not show any significant mean differences for the T_1 ($p > 0.94$) and the 2D HYCE S ($p > 0.96$) sequences. The reliability of the measured variables demonstrated high levels of consistency, with the T_1

sequence having CVs ranging from 1.2 to 7.6% and an ICC of 0.98. For the 2D HYCE S sequence, the CVs ranged from 1.05 to 7.6%, and the ICC was 0.98. The Bland-Altman plot with 95% confidence interval (±1.96*SD) analysis of the between-session data showed that all cases had a test-retest difference within ±1.27º (mean/bias= -0.14º) and ±0.65º (mean/bias=0.09º) for the T_1 and the 2D HYCE S sequences, respectively. The LOA analysis for the rotation trials indicated a relatively low degree of systematic bias in the between-session differences (p = 0.94 and 0.96) and a homoscedastic relationship between the differences and averages of the between-session measurements for both T_1 and the 2D HYCE S pulse sequences respectively (R^2=0.06 and 0.04) (Figure 29B). A homoscedastic relationship indicated that the random errors did not increase with the increase of the measured values. The follow-up ratio LOA analysis indicated a systematic bias in the order of -0.15 and -0.09 and random error of ±14.55 and ±20.10 for the T_1 and 2D HYCE S sequences, respectively. The ratio LOA analysis for rotation suggested that the between-session measurement errors obtained with the technique did not exceed 14.40% and 20.01% in either the positive or negative direction using the T_1 and the 2D HYCE S pulse sequences, respectively.

Comparing outcomes between the pulse sequences. Analysis of the difference between the averages of Session 1 and Session 2 translations obtained by T_1 and 2D HYCE S pulse sequences did not show any significant results using an independent sample 2-tailed t-test (p = 0.83). The Bland-Altman plot with 95% confidence interval (±1.96*SD) analysis of the between-sequence data showed a test-retest difference within ±1.50 mm (mean/bias=0.35 mm) (Figure 30A). A small heteroscedastic relationship observed in the translation measures indicated that the T_1 vs 2D HYCE S between-sequence difference in measured translations increased with assessments of larger magnitudes of translation (R^2=0.24). The follow-up ratio LOA

analysis demonstrated a systematic bias in the order of 0.35 and random error of ±13.41. The ratio LOA analysis for translation suggested that between-sequence measurement errors were within 13.77% in either the positive or negative direction.

Analysis of the difference between the averages of Session 1 and Session 2 rotations obtained by T_1 and 2D HYCE S pulse sequences did not show any significant results using an independent sample 2-tailed t-test ($p = 0.98$). The Bland-Altman plot with 95% confidence interval (±1.96*SD) analysis of the between-sequence data showed a test-retest difference within ±0.95º (mean/bias = 0.02º) (Figure 30A). A homoscedastic relationship observed in the rotation measures indicated that the between-sequence random errors did not increase with assessments of larger magnitudes of translation (R^2=0.03). The follow-up ratio LOA analysis demonstrated a systematic bias in the order of 0.03 and random error of ±14.28. The LOA ratio analysis for rotation suggested that the between-sequence measurement errors with the T_1 and 2D HYCE S pulse sequences were within 14.31% in either the positive or negative direction.

Biplanar trials. Analysis of the between-session measurements with a paired sample 2-tailed t-test did not show any significant difference for the z- ($p = 0.79$) and x ($p = 0.73$) planes. The reliability of the measured variables demonstrated high levels of consistency, with the z-plane having CVs ranging from 1.51 to 6.15% and an ICC of 0.97. The CVs for the x-plane measurements ranged from 1.32 to 3.95%, and the ICC was 0.97. The Bland-Altman plot with the 95% confidence interval (±1.96*SD) analysis of the biplanar between-session data showed that all displacements had a test-retest difference within ±1.41mm (mean/bias= -0.04 mm) and ±2.70 mm (mean/bias = 0.10) for the x- and z-planes, respectively (Figure 30B). The LOA analysis for the biplanar trials demonstrated a relatively low degree of systematic bias in the between-session differences ($p = 0.79$ and 0.73) and a systematic bias in the order of -0.04 and -0.01 and

random error of ±10.87 and ±21.03 for the z- and for the x-planes, respectively. The ratio LOA analysis for translation suggested that the between-session measurement errors obtained with the technique did not exceed 21.03% and 10.76 % in either the positive or negative direction for the x- and z-planes, respectively. The ratio LOA analysis for the biplanar translation trials showed a homoscedastic relationship between the differences and averages of the between-session measurements for the z-plane (R^2=0.04), indicating that the random errors did not increase with the increase of the measured values. The x-plane data, however, showed a marginal heteroscedastic relationship (R^2=0.11), indicating that the random errors did marginally increase with the increase of the measured values (Figure 30B).

Discussion

In this study, we describe a novel MRI-based approach that is conceptually similar to some fluoroscopy-based modeling protocols with the major difference of not requiring exposure to ionizing radiation, which has obvious implications for clinical research (39, 68, 479). While this is the first step in the development of an MRI-based protocol of this nature, our initial work indicates that this technique has promise as we have successfully developed a logical and rational approach to the quantification of motion and have also demonstrated relative and absolute reliability. Below we discuss our findings within the context of the extant literature as well as our future directions.

As stated above, the primary innovation of this work is that it represents an MRI-only, morphology-based modeling technique for tracking solid-body displacements, which is similar to fluoroscopy-based approaches, such as RSA, SR, and XROMM, and static x-ray-based techniques. The scope of application of these fluoroscopy-based techniques is limited due to the ionizing radiation exposure. For instance, obtaining serial

measures involving significant radiation exposure over time in research studies requiring oversight by an institutional review board (or other analogous committees charged with approving, monitoring and reviewing biomedical research involving humans) could raise questions about the cost-to-benefit ratio, particularly in light of the Institute of Medicine's recommendation on avoiding unnecessary medical radiation throughout life (229, 300). Accordingly, we believe that an MRI-only-based modeling technique for investigating joint kinematics has significant advantages, particularly for the advancement of clinical research.

Available MRI modeling techniques have usually applied multi-slice imaging of the objects of interest to capture the experimental displacements introduced into these objects in the scanning environment. Our study has uniquely attempted a morphology-based single-plane and an orthogonal imaging protocol to quantify experimentally induced displacements in our models. Additionally, we have used a fast-scanning protocol with dynamic contrast-enhanced pulse sequence and compared its outcome to a standard high-resolution T_1 imaging. Both these methods have demonstrated high-levels of reliability in quantifying displacements in objects within the MR imaging volume. These findings provide basic proof-of-concept for the notion that a reliable non-ionizing-radiation-based motion quantification technique can potentially be used to characterize a quasi-static visualization of joint kinematics from a single and biplanar approach. The use of dynamic sequence and image processing can be further explored to attempt quantification of joint kinematics in synchronized motion. Additionally, while our single-plane technique does not objectively address detecting out-of-plane motion, inclusion of the orthogonal imaging in the biplanar approach helps manual positioning of the model to match the corresponding out-of-plane shifts of the image silhouettes.

While our initial development results are promising, our study has some limitations. First, we have used static two-dimensional imaging for quantification purposes; and we do not know whether comparable levels of reliability would have been observed if the dynamic pulse sequence were used to scan the solid-bodies in real-time during an un-synchronized motion with subsequent quantification of these images using the technique reported here. The approach we chose was based on technology currently available; to our knowledge, an MRI-compatible device that would permit real-time manipulation of motion is not commercially available, and the custom development of such a device would require significant resources. Second, the current approach required manual segmentation and post-processing, which is very time intensive. Accordingly, we do not know how the use of semi-automatic protocols or automatic iterative segmentation algorithms would have changed our results. Third, while we reported high levels of reliability for a novel biplanar imaging modality (i.e., quantification of motion in two planes, or coupled motion), the orthogonal images obtained for this analysis were not acquired simultaneously (i.e., an image slice was first acquired in one plane and then acquired for the corresponding orthogonal plane) due to the inherent limitation of MR imaging to do so. While this is not necessarily a limitation of the current work, it could pose a limitation for future work that seeks to acquire simultaneous multi-planar images of motion. Lastly, we only assessed reliability and did not assess accuracy. We are currently conducting experiments that will assess accuracy of our technique in a porcine spine model.

Conclusions

In summary, this work provides basic proof-of-concept for a reliable non-ionizing-radiation-based marker-less imaging technique that can potentially be used to quantify quasi-dynamic displacements between joint elements. Additionally, this morphology-

based MRI-only technique could be explored further as a tool for real-time joint kinematics analysis. Acknowledgement: All MEL scripts and animation related software tools were used from XROMM resources developed at and made available by the Brown University, RI, USA.

Chapter 4. Quantification of Intervertebral Displacement with a Novel MRI-Based Modeling Technique: Assessing Accuracy and Reliability with a Porcine Spine Model

Abstract

The purpose of this study was to develop a novel magnetic resonance imaging (MRI)-based modeling and model-to-image matching technique for measuring intervertebral displacement in the spine. We present the accuracy and reliability of developmental work using a porcine spine model. We fitted porcine lumbar vertebral segments in a custom-built apparatus placed within an externally calibrated imaging volume of an open-MRI scanner. The apparatus allowed movement of the vertebrae through pre-assigned magnitudes of sagittal and coronal translation and rotation. The induced displacements were imaged with a static (T_1) and a fast dynamic (2D HYCE S) pulse sequences. These images were imported into animation software, in which the images form a background 'scene.' Three-dimensional models of vertebrae were created using static axial scans from the specimen and then transferred into the animation environment. In the animation environment, the user rotoscoped the models (manually moved the models to perform model-to-'scene' matching) to fit the models to their outlines. Next, the vertebral models were registered into anatomical joint axes in the animation software used to quantify the experimental displacements. Accuracy of the technique was calculated as 'bias' using a linear mixed effects model, average percentage error and root mean square errors (RMSE). Between-session reliability was tested by computing coefficient of variation (CV) and intra-class correlation coefficient (ICC). The model demonstrated a bias of 0.36 mm (±0.11) with the 2D HYCE S sequence at zero displacement. The bias increased by a factor of 0.008 mm for every 1

mm increase in the actual displacement. Additionally, the bias reduced by 0.06 mm with the change of sequence to T_1 from the dynamic 2D HYCE S sequence. Average percentage errors for the T_1 sequence was 12.5% and 14.9% for coronal and sagittal translation, and 10.78% and 16% for coronal and sagittal rotation, respectively. The percentage errors for the 2D HYCE S were 19.48% and 15.13% for coronal and sagittal translation, and 14.8% and 20.2% for coronal and sagittal rotation, respectively. Additionally, RMSEs of 0.31 mm, 0.40 mm, 0.68^0 and 0.72^0 were observed for translation and rotation measured in the coronal and sagittal planes using the T_1 sequence. RMSEs of 0.49 mm, 0.55 mm, 0.85^0 and 0.92^0 were observed for translation and rotation measured in the coronal and sagittal planes using the 2D DHYCE S sequence. Between-session ICCs (2,1) were 0.97 and 0.94, respectively for the T_1 and 2D HYCE S pulse sequences. No significant between-session differences in translation measurements were detected between imaging sequences, spine motion-segment pairs, or scan orientations. Strong correlation in the between-session translation measurements was detected for translation (Pearson's correlation coefficients of 0.90 and 0.88 for the T_1 and 2D HYCE S pulse sequences respectively). High coefficient of determination between the measured and actual translations were also observed with the use of both the sequences (R^2 of 0.94 and 0.90 for the T_1 and 2D HYCE S pulse sequences respectively). The model demonstrated a fixed bias of 0.62^0 (±0.12) with the 2D HYCE S sequence. The bias increased by a factor of 0.04^0 for each degree of increase in the actual rotation displacement performed. The bias reduced by 0.13^0 with the change of sequence to the T_1. Between-session ICCs (2,1) were 0.97 and 0.98, respectively for the T_1 and 2D HYCE S pulse sequences. No significant between-session differences in rotation measurements were detected between imaging sequences, spine

motion-segment pairs, or scan orientations. Strong correlation in the between-session rotation measurements was detected (Pearson's correlation coefficients of 0.97 and 0.95 for the T_1 and 2D HYCE S pulse sequences respectively). High coefficient of determination between the measured and actual rotations were also observed with the use of both the sequences (R^2 of 0.97 and 0.95 for the T_1 and 2D HYCE S pulse sequences respectively). To conclude, this novel quasi-dynamic approach to quantifying intervertebral relationship demonstrates a reasonable degree of accuracy and reliability using the model-to-image matching technique with both static and dynamic sequences in a porcine model. Future work is required to explore multi-planar assessment of real-time spine motion and to examine the reliability of our approach in humans.

(Note: Alphabetic subheadings of all figures related to this chapter presented in the figures section are provided at the bottom of the figure panels).

Introduction

Visualization of skeletal motion is of great interest to a substantial number of musculoskeletal scientists, as well as physicians. Radiological diagnosis of joint instability, for instance, is best achieved by direct visualization of pathological displacement between associated skeletal elements (301, 470). Indirect methods visualizing skeletal displacement often measure changes occurring between markers attached to bony landmarks on the skin. Although these techniques are performed within a calibrated volume in space, errors may be introduced by inconsistent skin movement relative to motion of the skeleton itself (79, 81, 112, 251, 378). Accordingly, direct visualization modalities, such as functional radiography, quantitative fluoroscopy, cineradiography, and computed tomography (CT), have offered options for assessment of static arthrodial displacement and joint motion (36, 300, 470). Unfortunately, these

techniques require the use of ionizing radiation, and the quantifiable outcomes of these methods are primarily restricted to two-dimensional (2-D) analysis of static images of displaced joint components (68, 469).

Several analytical techniques and approaches are available or are being developed to study patterns of joint displacement at multiple positions or to analyze real-time motion. Acquisition of single-plane images using x-rays plus manual positioning of skeletal three-dimensional (3-D) models to the outlines of the acquired x-ray images permit analysis of dynamic *in-vivo* relationship of joints (213, 469, 479). Similarly, the scientific rotoscoping (SR) motion analysis technique uses biplanar fluoroscopic imaging and 3-D skeletal modeling, followed by model-to-image matching (rotoscoping) that allows extraction of 3-D kinematic data from these models (39, 68, 152, 154). Nevertheless, in addition to the drawback of x-ray exposure, usage of such techniques requires complex corrections of geometrical distortion and motion-blur in the images (29, 52, 283, 300, 429). Recent advancements in the roentgen/radio stereophotogrammetry (RSA) technique, involving orthogonal radiographic imaging of joint motion, permit assessment of joint kinematics, as well as the detection of pathological micromotion in orthopedic implants (38, 79, 225, 397). Despite its accuracy, RSA commonly requires surgical implantation of markers in the articular skeleton (52, 65, 84, 112, 283, 397). However, model-based RSA techniques have recently begun to appear in the literature (53, 202, 245, 442). Additionally, some newer techniques have used fluoroscopy and a variety of 3-D model creating approaches (CT/magnetic resonance imaging [MRI]) for such analysis (344, 401, 426, 472). While SR, RSA, and other x-ray based techniques are clearly novel, they have limited application in clinical use and experimental human research because of health-related concerns associated with x-rays (168, 200, 229, 250).

Amongst all modalities, MRI has evolved as the preferred tool for musculoskeletal imaging, primarily because of its outstanding spatial resolution and avoidance of exposure to ionizing radiation (55). Because of technical limitations, musculoskeletal MRI has been predominantly used as a tool for static 2-D imaging of joints. However, cine-phase contrast (cine-PC) or fast-phase contrast (fast-PC) sequences have been used for real-time imaging of human blood flow and cardiac motion (41, 118, 209, 407). Use of these magnetic resonance (MR) sequences requires performance of a repeated, cyclic, velocity-controlled motion at the area of interest during scanning—a requirement that might be challenging to meet while scanning a painful joint (97, 107, 126). The utility of such MRI-based techniques has been tested to evaluate joint motion, but these attempts have been mostly restricted to use in the assessment of ankle, knee, or shoulder joints (42, 47, 66, 366, 371, 399, 400, 453). Typically, visualization of dynamic (real-time) or static multi-position (quasi-dynamic) joint motion requires a series of complex, time-consuming processes, including (i) volumetric extraction of images from time points along the full 3-D motion dataset, (ii) automated segmentation of the models, and (iii) running iterative algorithms for model-to-image registration (97, 107, 126, 127). Additionally, dynamic MR images have lower resolution and may exhibit motion artifact, as a result of the time-accuracy tradeoff (107, 127). Accordingly, recent advancements in these MRI-based motion tracking methods focus not only on faster scans but also on acquiring fewer slices from moving objects of interest for faster data-extraction and quicker model-to-image registration (97, 107).

We have recently reported a morphology-based model-to-image registration technique for quantifying displacements in solid-body objects (274). More specifically, this MRI-only technique uses single or biplanar (orthogonal) images for manual image-to-model registration, with high between-session reliability. In the earlier study, our aim

was to present a developmental, proof-of-concept work of an imaging and modeling technique that could quantify solid-body (i.e., wooden cubes) displacement. Here, we present the accuracy and reliability of an MRI-based 3-D model superimposition technique developed to objectively quantify experimental intervertebral displacement in porcine vertebral specimens. We have focused on quantification of intervertebral displacement in the lumbar spine for two major reasons. First, LBP accounts for over 3.7 million physician visits per year in the United States alone, with the prediction that 90% of all adults will experience LBP during their lifetime (276, 460). Approximately 50% of these individuals will have recurrent back pain, and about 10% will suffer pain-related disabilities (280, 322). Second, conventional diagnostic imaging performed for qualitative and quantitative assessment of vertebral instability in human degenerative disc disease has primarily focused on evaluating end-of-range intervertebral displacement in the sagittal plane (176, 338, 344, 363, 474). The technique presented in the current study quantifies multi-positional, intervertebral translation and rotation across a wide range of motion in both the sagittal and coronal planes, using standard static and fast contrast-enhanced sequences. Use of such imaging, 3-D modeling, and morphology-based model-to-image registration technique to quantify intervertebral motion is novel in the literature. As our long-term goal, we anticipate further developing this technique into a tool for dynamic MR imaging of the human lumbar spine, applying synchronized motion imaging and image processing techniques to an open-bore weight-bearing musculoskeletal MRI system.

Materials and Methods

General study overview. Figure 31 depicts a general overview of the study design. The experiment involved scanning a pair of porcine lumbar motion-segments

with the vertebrae placed at different positions (displacements) relative to each other, within an open-MRI system (0.25 Tesla; Esaote G-scan Brio, Genoa, Italy). These displacements were performed using an MRI-compatible custom built apparatus that permitted predetermined magnitudes of intervertebral translations and rotations. All displacements were performed in the lumbar coil after the scanning volume of the coil was calibrated using a custom-built grid system; calibration was performed only once, before commencing any of the study displacement trials. Axial images of the spine specimens were acquired and segmented using the AVIZO software (Hillsboro, OR, USA) to create virtual 3-D vertebral models. Thereafter, the images of the displacements and the 3-D vertebral models were transferred into the animation software AutoDesk MAYA (San Rafael, CA, USA) to recreate the animations of the series of intervertebral displacements and to quantify the relative motion between the vertebrae.

As the first step, the imaging volume of the MRI coil was calibrated using a custom-built grid (Figure 32A). Second, stand-alone axial scans of the vertebrae acquired at the commencement of the displacement trials were segmented to create virtual 3-D models of the spine segments. Next, a pair of corresponding vertebrae of a motion-segment was secured within a custom-built apparatus (Figure 32B&C) that allowed the upper vertebra to be either translated or rotated through predetermined magnitudes relative to the lower one. The spine segments were scanned using two different sequences (details given below) at each displaced position, and the Digital Imaging and Communications in Medicine (DICOM) images were converted into gray-scale tagged image format (TIF) images (pixel size = 0.85 mm). The images were then imported into the animation software. These displacements were placed in the animation ‘scene’ (referred to as the ‘background’) (Figure 32D), followed by importing the 3-D models into the MAYA program, in which the user manually manipulated (rotoscoped)

the models to match (register) their corresponding outlines in the slice. All measurements used while creating the grid were performed with a digital caliper (sensitivity = 0.01 mm) (Global Industrial, Port Washington, NY, USA).

Details of study steps. A summary of the steps outlined below has been described in our previous work (274).

Step 1. Calibrating the MR imaging volume. The volume of the lumbar MRI coil was calibrated (Figure 32A) with a custom-built calibration grid. Four square Perspex fiber plates (20 x 20 mm; thickness = 2 mm) (Modular-Movement Tray-Set, Games Workshop/NG, UK) were serially stacked with a distance of 35 mm between each plate. The plates were stabilized by five wooden dowels drilled across the plates, and glue was applied at all points of contact between the dowels and the plates. Sixteen 2-mm diameter holes (in a 4 × 4 array) were drilled in each plate with adjacent holes separated by 25 mm. Each hole was fitted with a 2-mm water-bead using glue. Three additional beads were drilled into two adjacent plates to localize the x, y, and z coordinates in the grid for use during segmentation at a later stage (Figure 32A) (466). The x- and y-axes were situated in the plane of the grid plates. The z-axis extended perpendicular to the plates. The coordinates assigned to the grid followed the definitions of the joint coordinate system recommended by the Standardization and Terminology Committee of the International Society of Biomechanics, in the context of the orientation of intervertebral translations and rotations executed in our study (466). To facilitate visualization of the beads in the images, the grid was submerged in a 1% saline solution for 30 seconds and then air dried for 1 minute prior to scanning. The x-axis of the grid was positioned along the anterior-posterior axis of the lumbar coil (DPA Lumbar Coil, Esaote, Genoa, Italy) and represented the craniocaudal axis of our motion-segments in the apparatus during all displacement trials (Figure 32A&C). Four consecutive non-

contiguous slices parallel to the grid plates were acquired to scan the grid. Each of these eight slices contained 16 beads in view. The four slices together contained all 64 beads were acquired using a fast spin echo T_2 sequence (TR = 7810 ms, TE = 120 ms, FOV = 220 × 220, matrix = 256 × 256, thickness = 3 mm). These images were then segmented in AVIZO for later use in Step 5.

Step 2. Fabrication of the displacement apparatus. The MRI-compatible apparatus (Figure 32B) included a clamp system consisting of a semicircular (top) and a full horizontal (bottom) ring system. The semicircular ring was attached to the full ring at the two ends of the diameter of the full ring by two pegs. The upper semicircular ring accommodated an inner clamp that could rotate within (and in the plane of) the outer ring. The upper vertebra was fixed to a vertical pair of screws in the inner clamp. This clamp system was positioned on a wider base ring. The entire assembly with the base ring was located on top of a three-base-plate system, in which the lowermost plate was stationary and contained a pair of vertically oriented screws to fix the lower vertebra. The upper two plates were hollowed-out at their centers to allow passage of the vertical screws. The upper two plates could slide orthogonally in relation to each other in two degrees of freedom (side-to-side, and anterior-posterior). The uppermost plate was grooved on the inside of its upper rim to firmly support the clamp and the base-ring system. A Vernier scale system was available on the base plate to measure the experimental displacements. The lowermost plate was mounted on a wooden platform that was fixed with Velcro to the base of the lumbar MRI coil to for stabilization. The movement of the base plates allowed 10-mm orthogonal translations of the upper vertebrae within the clamp system, and the clamp ring permitted rotation of the upper vertebra in three degrees of freedom, as measured by a protector attached to the ring. Sufficient space was made available within the ring system for orthogonal translation

and sagittal (flexion-extension) and coronal (lateral bending) rotation of the upper vertebra to encompass the range of motion defined as cut-off points for the clinical and radiological diagnosis of spine instability (54, 71, 89, 120, 171, 172, 351, 398, 474).

The semicircular and the horizontal rings were 3-D printed with a MakerBot Printer (Brooklyn, New York) using polylactic acid of the highest quality, 40% infill, and 5 shells to ensure the high accuracy and stiffness required for our experiments. The base plates, inner clamp, and base-ring of the apparatus were constructed of Delrin (Fig. 32B & C). Nylon set screws were used to fix the vertebrae to the apparatus and for locking the base plates in their displacements. The materials used for fabrication possessed a high modulus of elasticity and stiffness and did not distort MR images.

Step 3. Constructing and segmenting the porcine spine motion-segments. Two fresh adult porcine spines were purchased from a local slaughterhouse. Porcine specimens were chosen for their similarities to the shape and size of the human spine, specifically in the areas used for morphological rotoscoping in this study (76, 83, 199). Two lumbar vertebral segments (adjacent vertebrae) were dissected from each of the lumbar spines and refrigerated at -20^{o}C. Each segment was scanned on four different sessions on 4 separate days. The vertebrae were fixed with screws, with a space of approximately 15 mm between end-plates to approximate the average human disc height at that spinal level (198). The specimens were thawed approximately 3 hours before being attached to the plates. Drying was prevented by covering the specimens with a piece of gauze that was intermittently misted with saline solution during the sessions. Contiguous axial T_1 weighted scans (TR = 810 ms, TE = 30 ms, Fov = 220 × 220, matrix = 256 × 256) of the vertebral pair were acquired for manual segmentation and 3-D model creation at a later stage. Prior to the displacement trials, the vertebral pairs were scanned orthogonally in the non-displaced, neutral position.

Step 4. Displacement trials. The apparatus was secured within the lumbar coil with the aid of a rigid wooden platform (Figure 32B) that was fixed to the base of the lumbar coil with Velcro straps to maintain consistent placement of the apparatus and minimize motion during the scans. The craniocaudal axis of the motion-segment was oriented in the y-axis of the calibrated imaging volume. Translations and rotations were performed in the sagittal and coronal planes of the spine motion-segments. For the rotation trials, the center of rotation (COR) passed approximately through the lower end-plate of the upper vertebral body. Eight translations and eight rotations were performed in each sagittal (flexion-extension) and coronal (lateral bending) plane. In order to ensure an evenly distributed data set, the magnitude of each displacement was selected from several bins that were created within the range of motion of interest [Table 5]. A total of 32 displacements were scanned using two sequences for each of the two motion-segment pairs, generating a set of 128 images. Separate daily sessions were conducted to scan a different type of displacement, in a specific plane, each day for a given motion-segment pair; a total of eight sessions were required to complete the scanning. For each displacement trial, the apparatus was removed from the MRI console and translated or rotated as needed for the next displacement trial. The accuracy of the changes was verified using a Vernier scale placed along the sides of the base plates and confirmed using a digital caliper. Rotation displacements were measured using the protractor attached to the apparatus vertical ring, a goniometer, and an angular Vernier scale placed on the outer clamp (resolution $1/10^{th}$ of a millimeter). A contrast-enhanced streaming sequence (2D HYCE S; thickness = 8 mm, slice = 1, scan time = ~10 secs/scan) and a T_1 weighted sequence (TR = 810 ms, TE = 30 ms, Fov = 220 × 220, Matrix = 256 × 256, slices = 3, gap = 0, thickness = 5 mm, scan time = ~2 mins/scan)

were used for imaging. Slices for the translation and rotation trials were scanned in the mid-sagittal and mid-coronal planes, with both vertebrae in view (Fig. 33).

Step 5. Animation and quantification. The MAYA software was used to create a 'camera-view' (Maya Camera) of the MR imaging volume within the animation environment (68, 154, 323). This Maya Camera was created for the user to 'view' the displacement trials as a series of the background images in the animation 'scene' (Figure 33C). The Camera was first created and calibrated, then rotoscoping, animation, and quantification were performed.

Creating a MAYA framespecs file. The grid images acquired in Step 1 were segmented in AVIZO, creating an OBJ file for the grid. This image was then transferred to and opened in MAYA (Figure 33E). The centroids of each bead were serially numbered and assigned local coordinate points, thereby defining the volume of the grid and fixing the orientation of the grid axes in space. All coordinate points from the beads were merged to generate a 'framespecs' file for the grid to be used in the next step, digitization (68).

Digitizing the beads. The Matlab program uses a Maya Embedded Language (MEL)-script command to open and digitize each grid-plate image in order to create a direct linear transformation (DLT) coefficient file for each plate (68, 154). A grid-plate image segmented in AVIZO (Step 1; four axial and four sagittal slices, Ortho-Slice views) and saved in TIF format (Photoshop; Adobe Systems Inc. San Jose, California) was opened in Matlab, and the beads were numbered in sequence. Once numbered, the MAYA framespecs file created in Step 5(a) was loaded to calibrate the beads. This process calculated the DLT coefficient for the plate and returned a 'xyz points' file for each plate. The 'xyz points' files of all four plates (oriented in the same direction) were collated to generate a single four-plate 'xyz point' file for the plates. Next, any one of the

plate images was opened using the Matlab MEL-script, and the beads were numbered according to their positions in the grid. The framespecs file was then loaded into the grid calibration. This process yielded an error coefficient for the grid calibration (0.36 in this study) (Figure 33F). A coefficient value < 1 was considered favorable for use during further steps in animation (154). The digitization also yielded a MAYAcam file for creating the camera-view for the animation 'scene'(466).

Rotoscoping. The background animation 'scene' was created by importing the trial TIF images into MAYA. The scaling factor for this import was adjusted by a factor of 0.1 to account for the switch between MRI (mm) and MAYA (cm). Next, the vertebral models of the motion-segments were imported into MAYA and manipulated manually (rotoscoped) by the user to match and fit them into the corresponding vertebral image in the background 'scene'. Once the models matched the images in one frame, the rotoscoping was 'saved' and the background 'scene' was advanced to the next displacement image frame. The outlines of the vertebral canal silhouette, the spinous processes, and the transverse processes observed in the background images were utilized to fit the corresponding morphology of the 3-D models (Figure 33C&D).

Animation and quantification. The rotoscoping outcome of the first frame of the background 'scene' was considered to be the 'neutral' position, and a joint axis was assigned to the intervertebral joint. Once rotoscoping was performed for all displacement trials in a given sequence, the outputs from the animation were generated, and the joint axis data were exported as .csv files. Although the animation software output calculated vertebral displacements in six degrees of freedom, we only extracted displacement data in the plane applicable to our experimental trials for analysis and reporting. Two rotoscoping sessions (S1 and S2), separated by a gap of 1 week, were conducted by a single blinded observer (NKM) who quantified the trial results. All displacement images

were coded for the magnitude of displacement, type of sequence used for scanning, and pair of motion-segments used for the trials. Absolute values of quantified displacements, regardless of their directions, were used for analysis.

Experimental manipulations. Table 5 shows an overview of the displacement trials. The range of translation in both the sagittal and the coronal planes were divided into two bins (-5 mm to -1 mm and 1 mm to 5 mm), and four data points were randomly selected without replacement from each bin, to avoid skewing of the samples. Similarly, the range of sagittal plane rotation (flexion-extension) was divided into four blocks (-5 º to -1 º, 1º to 5 º, 6º to 10º, and 11º to 15º), and two samples were randomly selected without replacement from each of these blocks. The range of coronal plane rotation (lateral bending) was likewise divided into four blocks (-10 º to -6 º, -5º to -1º, 1º to 5º, and 6º to 10º), with two data points randomly selected without replacement from each of these four blocks.

The order of the selected displacements was permutated to generate a series of 32 trials (translations and rotations in the sagittal and coronal planes). Each displacement was performed for both pairs of spine-motion segments and each displacement was scanned separately using the two pulse sequences. The total number of displacement trial images generated was 128. These images were rotoscoped twice in two separate sessions for quantification thereby extracting data from a total of 288 images (including 32 'neutral' frames, one neutral frame in each type of trial sequence).

Statistical analysis. *Accuracy* was measured by creating the following linear mixed-effects model: $\text{Bias}=\beta_0+\beta_1\text{Displacement}+\beta_2\text{Pulse}+b_{\text{Session}}+b_{\text{Spine}}+\varepsilon$, where *Bias* was calculated as the difference between true and observed values ($Bias = Y_{True} - Y$); β_o was the intercept; β_1 and β_2 represented the regression coefficients of the actual

displacements and sequence fixed effects, respectively; $b_{session}$ and b_{Spine} represented the session and spine random effects; and ε represented the residuals. This formula evaluated accuracy as any non-zero intercept or coefficient. That is, a β_0 of 0.2 indicated a bias of 0.2 mm with the 2D HYCE S pulse sequence as the reference, whereas a β_2 of 0.5 indicated additional bias introduced by T_1 pulse sequence, relative to the T_1 pulse. Average percentage error was obtained by dividing *Bias* by the true value and multiplying by 100: Average % error = $(Y_{True} - Y)/Y_{True} * 100$. Additionally, root mean square errors of the quantified displacements, by sequence and by type of displacement performed, were calculated as a measure of accuracy. Relationships between the quantified and original displacements were ascertained by calculating the coefficient of displacements and this was performed separately for the two imaging sequences.

Between-session intra-class correlation coefficients (ICCs) were calculated separately for the two sequences to ascertain the reliability of the assessments. Reliability was also tested by computing the coefficient of variation (CV) between the two sessions. The student's t-test was used to analyze the between-session differences in outcome variables for the two sequences, two pairs of spine motion-segments, and two orientations (coronal vs sagittal) of the scans. Additionally, the strengths of the relationship between the measurements obtained during the two sessions were calculated with Pearson's correlation coefficient for each sequence and for each orientation.

Results

Translation trials. The linear mixed effects model (REML criterion) was used for analysis [Table 6]. The bias of the technique was calculated using the equation Bias = $ß_0 + ß_1 Displacement + ß_2 Sequence + b_{Session} + b_{Spine} + ε$, where the actual displacement and

the two sequences were taken as the fixed effects and the sessions and the spines as the random effects respectively. The model (repeated covariance type=scaled identity, covariance type=compound symmetry) demonstrated an intercept constant ß$_0$ of 0.36 mm (±0.11) contributing significantly (p=0.008) to the bias at a zero actual translational displacement with the 2D HYCE S sequence used as the reference sequence [Table 6A]. Additionally, increasing the actual displacement by one unit (1 mm) increased the measurement bias by a factor of 0.008 mm. This change in the bias was not statistically significant (p=0.69). The change in bias reduced by 0.06 mm with the change of sequence to T_1 from the dynamic 2D HYCE S sequence. This change was not statistically significant (p=0.34). The random effects parameters session and spine had a significant effect on the bias observed in the technique used for quantifying translational displacements (p=0.78) [Table 6B]. Average percentage of error of translation quantified by the technique by sequence and by orientation of the images (calculated as Quantified ~ Actual displacement/Actual displacement *100) show comparatively higher accuracy for the T_1 sequence (12.5% and 14.9% for coronal and sagittal translation, respectively) than the 2D HYCE S sequence (19.4% and 15.1% for coronal and sagittal translation, respectively) [Table 7]. Quantified translations demonstrated RMSEs of 0.31 mm and 0.40 mm in the coronal and sagittal planes for the T_1 sequence, and RMSEs of 0.49 mm and 0.55 mm in the coronal and sagittal planes for the 2D HYCE S sequence [Table 7]. High coefficient of determination between the measured and actual translations were also observed with the use of both the sequences (R^2 of 0.94 and 0.90 for the T_1 and 2D HYCE S pulse sequences respectively) (Figure 34).

In terms of reliability, the between-session ICCs (2,1) were 0.97 and 0.94, respectively for the T_1 and 2D HYCE S pulse sequences for coronal translation. Between-session ICCs were 0.96 and 0.95, respectively for the T_1 and 2D HYCE S pulse

sequences for sagittal translation. Comparisons of translation measurements (between-sessions data) as coefficient of variation (CV) calculated between the pulse sequences used, pairs of motion-segments tested, and imaging perspectives (sagittal and coronal) acquired are shown in Table 8. No significant between-session differences in translation measurements were detected between imaging sequences, spine motion-segment pairs, or scan orientations. Strong correlations in the overall between-session translation measurements were detected (Pearson's correlation coefficients of 0.90 and 0.88 for the T_1 and 2D HYCE S pulse sequences respectively) (Figure 35). More specifically, between-session Pearson's correlation coefficients for coronal plane translations were calculated to be 0.97 and 0.90 for the T_1 and 2D HYCE S sequences, respectively. Pearson's correlation coefficients for sagittal plane translations were 0.93 and 0.92 for the T_1 and 2D HYCE S sequences, respectively.

Rotation trials. The linear mixed effects model (REML criterion) was used for analysis [Table 9]. The bias (i.e., accuracy) of the technique was calculated using the equation $\text{Bias} = ß_0 + ß_1\text{Displacement} + ß_2\text{Sequence} + b_{\text{Session}} + b_{\text{Spine}} + \varepsilon$, where the actual displacement and the two sequences were taken as the fixed effects and the sessions and the spines as the random effects respectively. The model (repeated covariance type=scaled identity, covariance type=compound symmetry) demonstrated an intercept constant $ß_0$ of 0.62º (±0.12) contributing significantly (p=0.00) to the bias at a zero actual rotational displacement with the 2D HYCE S sequence used as the reference sequence [Table 9A]. Additionally, increasing the actual displacement by one unit (1 degree) increased the measurement bias by a factor of 0.04º. This change in the bias was statistically significant (p=0.00). The change in bias reduced by 0.13º with the change of sequence to the T_1 from the dynamic 2D HYCE S sequence. This change was

not statistically significant (p=0.08). The random effects parameters session and spine did not have any significant effect on the bias observed in the technique used for quantifying rotational displacements (p=0.78) [Table 9B]. Average percentage of error of translation quantified by the technique by sequence and by orientation of the sequence (calculated as Quantified ~ Actual displacement/Actual displacement *100) show comparatively higher accuracy for the T_1 images (10.78% and 16% for coronal and sagittal rotation, respectively), than the 2D HYCE S sequence (14.82% and 20.20% for coronal and sagittal rotation respectively) [Table 7]. Quantified rotations demonstrated RMSEs of 0.68^0 and 0.72^0 in the coronal and sagittal planes for the T_1 sequence, and RMSEs of 0.85^0 and 0.92^0 in the coronal and sagittal planes for the 2D HYCE S sequence [Table 7]. High coefficient of determination between the measured and actual rotations were also observed with the use of both the sequences (R^2 of 0.97 and 0.95 for the T_1 and 2D HYCE S pulse sequences respectively) (Figure 36).

In terms of reliability, the between-session ICCs (2,1) were 0.97 and 0.91, respectively for the T_1 and 2D HYCE S pulse sequences for coronal rotation. Between-session ICCs were 0.98 and 0.97, respectively for the T_1 and 2D HYCE S pulse sequences for sagittal rotation. Comparisons of rotation measurements (between sessions data) as coefficient of variation (CV) calculated between the pulse sequences used, pairs of motion-segments tested, and imaging perspectives (sagittal and coronal) acquired are shown in Table 8. No significant between-session differences in translation measurements were detected between imaging sequences, spine motion-segment pairs, or scan orientations Very strong correlation in the overall between-session rotation measurements was detected (Pearson's correlation coefficients of 0.97 and 0.95 for the T_1 and 2D HYCE S pulse sequences respectively) (Figure 37). More specifically, between-session Pearson's correlation coefficients for coronal plane rotations were

calculated to be 0.95 and 0.86 for the T_1 and 2D HYCE S sequences, respectively. Pearson's correlation coefficients for sagittal plane translations were 0.98 and 0.97 for the T_1 and 2D HYCE S sequences, respectively.

Discussion

Given the limitations of routine end-of-range static spinal imaging in providing clinically useful information on dynamic intervertebral relationships for diagnosing lumbar instability, we have reported a quantitative technique that permits the assessment of intervertebral displacement across a wide range of translation and rotation movements. More specifically, in light of the multiple differential diagnoses available for non-specific LBP and the drawback of frequent usage of ionizing radiation-based diagnostic imaging, we have presented our results of a novel MRI-only motion tracking technique for quantifying spinal motion, which avoids radiation exposure. We have also compared outcomes of our imaging technique using a static T_1 high resolution sequence and a fast 2D HYCE S dynamic sequence. The latter sequence can be used to scan dynamic movements of the spine. Therefore, application of this sequence in conjunction with image processing, MRI-based modeling, and a 3-D model superimposition technique may permit us to further develop this method as a tool for assessing intervertebral kinematics in the load-bearing human spine.

The results of this study demonstrate a relatively high degree of accuracy and reliability with our technique, which was comparable to the accuracy and reliability of many previous methods used to measure translation and rotation displacement (351, 398, 434, 474). Most of these earlier reports involved the use of x-ray-based techniques to quantify intervertebral motion. A few studies have involved MRI-based quantification methods that measured single-plane displacement, however. These studies was

performed in the recumbent, non-weight-bearing position (228, 351, 398, 433, 434, 472, 474). Our technique has two distinct advantages compared to techniques that use complex volume extraction from multi-planar scans for the purpose of reconstructing quasi-dynamic motion in 3-D skeletal models: (i) acquisition of single image slices for model-image registration in our technique considerably reduces the scanning time with the contrast-enhanced, as well as the static sequence, and (ii) although our technique relies on single-plane image acquisition, model-to-image superimposition with the help of morphology-based rotoscoping potentially enhances the precision of model-to-'scene' matching. The apparatus used in this study allowed only single-plane movements in the models. However, the precise morphology-based model superimposition used in this technique should be able to track additional in-plane shifts of the object of interest by matching anatomical landmarks in the model to corresponding contours in the background 'scene.' More specifically, in the context of applying our technique to single-slice sagittal-plane measurements routinely used in diagnostic imaging to detect spine instability, our method can potentially quantify concomitant in-plane translation and rotation with matching models with corresponding in-plane shifts of vertebral body angle, end-plate, and spinous process images. The animation software we used measured displacements in all degrees of freedom. However, our analyses included measurements only from the plane of experimental displacement. One of the most useful features of this technique is its ability to select image slices in any preferred orientation in space. This freedom of image-slice selection in a quasi-dynamic multi-position analysis of motion allows scanning of objects from any orthogonal perspective. Accordingly, as we have reported earlier, orthogonal images used to create background 'scenes' facilitate precise model-to-contour matching and help track orthogonal out-of-plane shifts in the background images.

To our knowledge, this is the first study reporting the use of an MRI-only morphology-based image registration technique. The advantage of using the slice-based model-to-image registration technique over voxel-based MRI approaches is that the former uses far less time in image acquisition that can be of great value while working with painful joints. The most innovative aspect of this work is possibly the usage of the 2D HYCE S pulse sequence for imaging. Results obtained from the quantification of 2D HYCE S images showed reasonably comparable reliability and accuracy in comparison to results from the T_1 sequences. The results from using this streaming sequence provide a foundation for examining the reliability of this technique for spine motion quantification in humans. Additionally, the application of the technique (using the 2D HYCE S sequence) in individuals in a weight-bearing positional MRI systems while performing dynamic spine motion may potentially permit analysis of real-time inter-vertebral and overall spine motion.

Accuracy levels of sophisticated x-ray based techniques like the RSA used for detecting micro-motions in joint prostheses have been in the order of tenths of a millimeter (77, 272). X-ray and fluoroscopy techniques and voxel-based CT/MRI model registration approaches applied to quantify segmental spine motion report lesser degrees of accuracy (26, 318). More specifically, the fluoroscopy based RSA and XROMM techniques are very accurate with the latter having a mean absolute accuracy of ±0.04 mm for tracking dynamic translations (39, 68). An MRI based study with segmented three-dimensional vertebral models used for automated superimposition (with a voxel-based registration technique) over static images of the neck taken at different positions reports root mean square errors (RMSE) of rotational accuracy at 0.24° for flexion–extension, 0.31° for lateral bending, and 0.43° for axial rotation. The accuracy reported in this study was validated using experimental MRI phantoms.

Translational accuracy in this study was reported as root mean square errors with values of 0.52 mm for supero-inferior, 0.51 mm for antero-posterior, and 0.41 mm for lateral translation, over the tested range of neck motion (208). Evaluation of post-surgical orthognathic changes studied by using CT scans has reported accuracies of 0.05 (±0.21) mm and 0.047 (±0.26) mm with separate voxel-based and a surface-based registration technique, respectively. Both the approaches have indicated accuracies of 0.29 (±0.33) mm and 0.23 (±0.56) mm respectively for soft tissue superimpositions (26). The estimated bias at zero displacements reported in our study (0.35 mm and 0.30 mm for the T_1 and 2D HYCE S sequences respectively) for translation and (0.63^0 and 0.49^0 for the T_1 and 2D HYCE S sequences respectively) for rotation. This constant offset in the quantified displacements denotes a systematic error at zero displacement for the technique. This error calculated by the model may have arisen due to several reasons (discussed elsewhere) and may be addressed appropriately to reduce the overall accuracy of the technique. However, the current RMSE values of our technique calculated with the use of T_1 (RMSE of 0.31 mm and 0.40 mm in the coronal and sagittal planes for translation and 0.68º and 0.72º in the coronal and sagittal planes for rotation) and with the 2D HYCE S (RMSE of 0.49 mm and 0.55 mm in the coronal and sagittal planes for translation and 0.85^0 and 0.92^0 in the coronal and sagittal planes for rotation) sequences respectively, demonstrate comparable results with the voxel-based MRI study noted above. Moreover, the overall percentage error associated with the current accuracy levels of our technique with the T_1 (~12-15% and ~11-16% for translation and rotation respectively) and with the 2D HYCE S (~15-20% for translation and rotation trials) suggest that though the application of our technique for detecting very small displacements may not be feasible, its use may be acceptable in a number of contexts

(clinical settings as well as research settings) depending upon the range of error that is permissible within the question being addressed. More specifically, our technique may be applied in situations where the anticipated effect size exceeds the expected error. The approach presented herein is clearly not as accurate as many of the gold-standard existing techniques; however, it does not require surgical implantation of beads or exposure to ionizing radiation, which holds many obvious advantages.

There are limitations in our study that should be noted. One limitation was opting for a quasi-dynamic approach for testing the accuracy and reliability of our technique instead of acquiring images of synchronized real-time vertebral motion using a motorized MRI-compatible apparatus. This was a logistic limitation, as customization or procurement of such sophisticated equipment was beyond the scope of funding for this work. Although the use of single-plane imaging for creating the background 'scene' may be considered a limitation, the technique in its current form, using a morphology-based rotoscoping approach, permits reasonably accurate and reliable model-to-image superimposition for tracking both sagittal and coronal plane intervertebral motion. Future developmental work is certainly required, and focusing on using higher resolution fast imaging sequences for accurate assessment of relatively smaller displacements is warranted. Establishing advanced registration algorithms to enhance the precision of model superimposition is another potential direction of future research.

It should be noted that we did observe some degree of systematic bias in the results (as denoted by the significant fixed intercept $ß_0$ values). There are a number of potential reasons contributing to this systematic bias, which could be corrected for improved accuracy in the future or, perhaps, mathematically. The first potential reason for some systematic bias relates to the calibration of the MRI volume space (431). Developers and researchers working with the RSA technique have shown that using a

combination of different grids for such calibration may improve the overall accuracy of the technique (77). More specifically, Cai *et al*., demonstrated that using equal bead spacing with different number of beads, and different bead spacing with equal number of beads for their calibration cubes improved the simulation of the imaging volume during digitization (77). Additionally, these investigators demonstrated greater accuracy of the superimposition of joint phantom models with pre-fitted markers, with images acquired from models that only had the positional markers in them. This was achieved with inclusion of additional projection images for calibration of the image space (from uniplanar to biplanar approach). Improvements with reduction of the size and increase in the number of the beads used for calibration have also been attributed to improvement of accuracy and precision outcomes of fluoroscopic techniques (319, 386). Therefore, in context of our technique, greater precision of bead placement in fabricating the grid system could be a starting point for improving accuracy and reducing the bias in the system. Also, using a multiplanar approach to scan our grid (more than the two orthogonal planes used in this study), segment and digitize them for calibration purposes may improve the simulation of the imaging volume within the animation software. Using smaller bead-sizes may be another consideration for improving the calibration approach. Lastly, reduction in the values of the DLT coefficient for the individual grid plates and the overall grid cube (digitized in any particular plane) may be achieved by more accurate bead placement in the grid. Moreover, comparing and accounting for the differences in coefficient values obtained from digitizing grid plates in relative orthogonal planes may yield important information that may be used as a factor for potential correction in the overall bias ($ß_0$) encountered in this study. Another potential reason for some systematic bias could relate to the rotoscoping approach. For instance, using more than a one-camera view (even for single-plane analysis) to view the animation may help reduce the

current offset. Biplanar (orthogonal or adjacent parallel plane) approach for rotoscoping may be helpful to reduce any parallax error arising from the single-plane model-to-image matching. Accuracy of the model-to-image matching approach has been demonstrated to improve with addition of viewing planes into the model registration process (305, 418, 442). Additionally, any rater-bias or error introduced in the rotoscoping technique should be accounted for, in reducing this fixed effect of error.

Conclusions

To our knowledge, this is the first reported MRI-based 3-D modeling technique that has compared the outcomes from high (slow) and low (fast) resolution imaging to quantify intervertebral displacements using an animation platform for model-to-image registration.

Chapter 5. Effects of Spine Loading In a Patient with Post-Decompression Lumbar Disc Herniation: Observations Using an Open Weight-Bearing MRI

The material presented in this chapter has been published in the European Spine Journal (275).

Abstract

Our objective was to use an open weight-bearing MRI to identify the effects of different loading conditions on the inter-vertebral anatomy of the lumbar spine in a post-discectomy recurrent lumbar disc herniation (RLDH) patient. A 43-year-old male with a left-sided L5-S1 post-decompression re-herniation underwent MR imaging in three spine-loading conditions: i) supine, ii) weight-bearing on standing (WB), and iii) WB with 10% of body mass axial loading (WB+AL) (5% through each shoulder). A segmentation-based proprietary software was used to calculate and compare linear dimensions, angles and cross sections across the lumbar spine. The L5 vertebrae showed a 4.6 mm posterior shift at L5-S1 in the supine position that changed to an anterior translation >2.0 mm on WB. The spinal canal sagittal thickness at L5-S1 reduced from supine to WB and WB+AL (13.4, 10.6, 9.5 mm) with corresponding increases of 2.4 and 3.5 mm in the L5-S1 disc protrusion with WB and WB+AL, respectively. Change from supine to WB and WB+AL altered the L5-S1 disc heights (10.2, 8.6, 7.0 mm), left L5-S1 foramen heights (12.9, 11.8, 10.9 mm), L5-S1 Segmental Angles (10.3^{o}, 2.8^{o}, 4.3^{o}), Sacral Angles (38.5^{o}, 38.3^{o}, 40.3^{o}), L1-L3-L5 Angles (161.4^{o}, 157.1^{o}, 155.1^{o}), and the dural sac cross sectional area (149, 130, 131 mm^{2}). Notably, the adjacent L4-L5 segment demonstrated a retro-listhesis >2.3 mm on WB. We observed that with weight-bearing, measurements indicative of spinal canal narrowing could be detected. These findings suggest that

further research is warranted to determine the potential utility of weight-bearing MRI in clinical decision making.

(Note: Alphabetic subheadings of all figures related to this chapter presented in the figures section are provided at the bottom of the figure panels).

Introduction

Lumbar disc herniation (LDH) secondary to degenerative disc disease is a common occurrence, with as many as 40% of adults with disc herniation experiencing LDH-induced LBP (93, 352). Although conservative treatment results in regression of the size of the herniated disc tissue in a good number of cases, about 20% of LDH patients with unresolved radicular pain require surgical treatment (80, 99). Around 5-18% of LDH patients undergoing primary lumbar discectomy and decompression surgery have been observed to develop recurrent lumbar disc herniation (RLDH), arising as a complication from the primary surgery (80, 222, 420). Typically, RLDH is defined as a recurrence of herniation at the same site of the prior operation, or at the same level on the ipsi- or contralateral side, with at least 6 months of pain-free post-operative period (122, 421).

Different imaging techniques have been used for evaluating primary or secondary disc herniation (43, 162). Specifically, Gadolinium enhanced magnetic resonance imaging (MRI) with fat saturation, turbo-spin echo, inversion recovery sequences have been used to detect the presence of extruding disc tissue (93, 156). Predominantly, pre-operative assessments for LDH, or for revision surgeries in RLDH, mostly depend upon the evaluation of encroachments into the spinal canal and the lateral foramen from protruding disc fragments. Patient evaluations have rarely relied on quantification of dynamic changes in inter-vertebral anatomy secondary to physiological spine-loading (80, 265, 421).

Only a few imaging studies have investigated the effects of axial spine loading in healthy individuals and an even a smaller number have focused on symptomatic LDH patients (85, 109, 128, 187, 212, 215, 330, 456). Almost all of these studies had induced axial spine loading in the supine position and by using an external MRI-compatible compression device to analyze changes in spinal canal dimensions and shifts in disc protrusion sizes with such loading. Additionally, the loading protocols followed in these MRI studies were, at best, simulations of more physiologic loading conditions observed with upright weight-bearing postures of the spine and therefore some of these results have demonstrated differences when compared to those obtained from actual weight-bearing radiographs (109, 187, 224, 330, 421, 423). More recently a few studies have reported MR imaging of the spine in weight-bearing upright positions (128, 215, 216, 385, 428). Additionally, majority of such reports have tested non-LBP individuals (215, 216, 385), whereas some others have focused on non-specific LBP cohorts (428, 457). To the best of our knowledge, MR image analysis with different axial loading conditions of the lumbar spine in a RLDH patient had never been reported. Accordingly, our objective was to use an open weight-bearing MRI to identify the effects of different loading conditions on the inter-vertebral anatomy of the lumbar spine in a post-discectomy RLDH patient.

Case Report

The patient: A 43-year-old male (183 cm, 91 kg,) presenting with weakness in the left leg and foot involving the L5-S1 distribution. He had been diagnosed with a left L5-S1 herniation two years prior and had undergone a single-level, open discectomy with laminar decompression one year prior to reporting to our facilities with symptom recurrence. On a Numeric Pain Rating Scale (1-10), he reported an average score of 7

for the last 7 days prior to the scan, with the pain being most aggravated in the supine position.

MR Imaging Protocol: The patient was imaged using a G Scan Brio weight-bearing MRI (Esaote S.p.A., Genova, Italy), which is an open-field magnet (0.25 Tesla) with the ability to rotate from supine to a fully upright, weight-bearing (WB) position in 3° increments. The patient was initially imaged in an upright, weight-bearing position (84° tilt of the gantry) with his feet shoulder width apart, strapped securely at his pelvis. This position is recommended in the literature as a safe position that allows optimal WB of the spine without compromising postural stability (147). Next, the patient was brought to a recumbent position by tilting the table to the horizontal position and imaged in the supine position (0°). Lastly, the patient was imaged again in the WB position while additional loads equivalent to 10% of his body weight (9.1 kg) was supported over his shoulders i.e., containers filled with 5% of body weight, placed in two canvass tote bags, and one bag (4.55 kg) was placed over each shoulder, in a weight bearing + axial loading (WB+AL) position. Sagittal MR images of the entire lumbar spine were acquired at all the three spine loading conditions using a Fast Spin Echo T_2 sequence (TR=3520ms; TE=125ms; number of acquisition=1; Matrix=288 x 234; FOV=320 x 320; Oversampling=185%; Slice thickness=4 mm; Gap=1 mm; acquisition time: 4min 41s). Scanning time and sequences used for imaging performed in this study were similar to those reported from earlier studies and took less than 5 minutes of scanning at each position (428). Scores of 6, 7 and 9 were recorded on the pain rating scale during imaging in the supine, weight-bearing, and weight-bearing+ axial loading conditions, respectively. We also acquired additional images of the spine for purposes other than those specified for this study. The total time taken to situate the patient at different

positions, allowing ~5 minutes before initiating the scan, acquisition of all images and a few minutes of rest in between, was ~90 minutes.

MRI Analysis: Images were transferred to a proprietary image analysis software system (OrthoCAD, Esaote S.p.A., Genova, Italy). The outlines of all lumbar and the first sacral vertebral bodies including the spinal canal were semi automatically segmented using the 3-D segmentation software. Segmentation was performed across all image slices acquired with one blinded investigator (NKM) segmenting the trials. All images were inspected for disc protrusion, evidence of spine stenosis and lateral foramen narrowing. The software yielded volumetric contour models of the segmented elements of the vertebrae and the spinal canal. Semi-automated quantification of several linear, angular and cross-sectional area (CSA) parameters was performed across all the three loading conditions, and compared. Following parameters were calculated [Table 10 and 11]:

- Inter-vertebral Listhesis: Calculated as the distance between the adjacent corners of contiguous vertebrae in a motion segment (Figure 38A).
- Inter-vertebral Translation: Calculated as the distance (on the median bisector) between the perpendicular projections to the centers of two adjacent vertebra drawn from the median bisector of the segmental angle at a given vertebral level (Figure 38B). This parameter evaluates the relative displacements between adjacent vertebrae relative to its baseline value measured in the supine position [Table 10].
- Spinal Canal Sagittal Thickness: The maximum mid-sagittal diameter of the dural sac.

- Disc Height: Measured at the point of maximum distance between the superior and the inferior end-plates.
- Left Intervertebral Foramen Height: Measured as the height of the foramen demarcated by the assessor over the sagittal images.
- Intervertebral Segmental Angles: The angle between the end-plates between adjacent vertebrae.
- L5-S1 Segmental Angle: The segmental angle between the L5-S1 end-plates.
- Lordosis Angle: The angle between the superior plate of L1 and S1.
- Sacral Angle: The angle between the horizontal plane and the sacral endplate.
- L1-L3-L5 Angle: The angle formed by the line joining the centers of the L1, L3 and L5 vertebrae.
- Left inter-vertebral Foramen CSA: Measured as the vertical-plane sectional area of the lateral canals. The area of each foramen was manually demarcated by using a pencil tool in the software.
- The spinal canal CSA: Calculated as the sectional area in the axial plane.

Sagittal-plane protrusion of the L5-S1 disc beyond the posterior limit of the vertebrae were objectively measured using the ‘ruler’ tool in software [Zone: L5-S1, Table 10] and presented as the increase in sagittal-plane posterior disc protrusions measured form the disc-tip to the perpendicular bisectors drawn to the adjacent L5-S1 vertebral corners with WB and WB+AL (taking the value at the supine position=zero/baseline). A new parameter named the Absolute Vertebral Translation was formulated as the displacement (forward or backward) incurred by the superior member of each vertebral segment with the change in spine position from the supine to the WB and then to the WB+AL positions. This ‘absolute’ translation parameter was calculated assuming the

inter-vertebral translation in the supine position to represent a zero displacement. A negative sign to the value indicated a backward translation of the vertebral body and vice versa.

Results

The descriptive statistics observed for all parameters evaluated are displayed in Table 10 and 11. One of the most prominent findings was a notable posterior shift of the L5 (4.6 mm) on the S1 in the supine position (Inter-vertebral Listhesis and Inter-vertebral Translation in Table 10). The L5 shifted anteriorly on standing, and with axial loading of the spine (Listhesis: from 4.6 to 3.2 to 2.9 mm). However, the L4 at the L4-L5 junction demonstrated a posterior translation with WB and then a slight anterior shift on WB+AL (Listhesis in Table 10: from 3.1 to 4.1 to 3.8 mm). Some other noticeable observations were as follows. (i) Slight increases in spinal canal sagittal thickness at some vertebral levels were noticed on WB [Table 10] (428). However, marked narrowing of this dimension was noted at the level of L5-S1 junction on WB and with WB+AL (Figure 39A). (ii) Reduction in the L5-S1 Left Intervertebral Foramen Height (to <10 mm) with WB+AL. (iii) Acute shortening of the L5-S1 angle on standing and reduced disc height at the same level, with WB. (iv) In co116mparison to the supine position, the posterior mid-sagittal bulge of the protruding L5-S1 disc demonstrated increases of 2.4 and 3.5 mm with WB and WB+AL, respectively. Lastly, (v) dimensions of the left inter-vertebral foramina CSAs increased slightly with WB at all levels, whereas it was reduced to 98 mm^2 at the L5-S1 space (Figure 39B), the spinal canal CSA demonstrated critical narrowing (>15 mm^2) (109) at the L5-S1 level from the supine to WB positions (Figure 39B). Figures 40 and 41 show the other changes occurring in dimensional changes in disc heights, listhesis and absolute translations, as well a changes observed in lateral

foramen, spinal canal cross sectional area (CSA) and sagittal spinal canal thickness with three loading conditions in the lumbar spine.

Discussion

This work represents one of the first attempts to quantify changes in inter-vertebral morphology, lateral foramen and spinal canal dimensions in response to physiological loading of the spine, specifically in context of recurrent disc herniation. We found that in the supine position the posterior limit of the L5 vertebra demonstrated a prominent backward shift with relation to the S1 vertebral body, when compared to the WB and WB+AL. This posterior shift of the L5 and reported accentuation of pain may have resulted from the loss of dorsal support elements in the spine secondary to the earlier surgical decompression procedure. This posterior shift of the L5 vertebrae, however, did not alter the spinal canal sagittal thickness nor the CSA possibly due to the absence of the laminae removed with the prior decompression. Marked reduction noticed in L5-S1 disc height on WB and the formation of bony spurs at the anterior edge of the inferior L5 end-pate (Figure 36B) may be suggestive of segmental instability (203). Additionally, the L4 vertebra at the adjacent L4-L5 segment demonstrated a paradoxical pattern of displacement. WB resulted in a backward slide of the L4 over the L5 vertebral body, whereas additional loading with the WB+AL resulted in an anterior translation shift of the L4. Altered motion patterns at neighboring vertebral levels on loading may indicate initial stages of adjacent-segment pathology, as commonly evidenced with LDH or RLDH (128, 218).

Studies with instrumented axial spine loading in the supine position have reported clinically significant (>15 mm^2), multi-level narrowing of the spinal canal in a wide variety of LBP patients using MR imaging, often with re-enactment of the pain

during such loading (85, 109, 187). The range of magnitude and duration of instrumented spine loading in these studies demonstrate large variability. Instrumented spine loading up to 50% of body-weight and the duration anywhere between 5-50 minutes of standing or additional axial loading have been applied to affect quantifiable deformation of the spinal canal anatomy (109, 215, 385). In our case study, notable narrowing of the L5-S1 spinal canal CSA, the left lateral foramen CSA, and the left L5-S1 intervertebral foramina heights could be demonstrated with ~10 min of WB. However, only smaller changes were noticed with ~10 min of additional spine loading (i.e., the WB+AL conditioning). In our case, standing alone brought about the critical changes in the canal spaces and accentuation of the disc protrusion. Notable changes were observed when comparing the supine and WB parameters. Since additional L5-S1 disc protrusion, spinal canal dimensions and aberrant L4/L5 translations could be detected comparing the supine and WB images, WB MRI may be considered as an option for the evaluation of crucial parameters required for clinical decision-making.

In summary, we observed that with weight-bearing MRI, measurements indicative of spinal canal narrowing could be detected. These findings suggest that that further research is warranted to determine the potential utility of weight-bearing MRI in clinical decision making.

Chapter 6. Conclusions and Future Directions

Conclusions

Low back pain results from a myriad of identifiable causes or may arise from a non-detectable etiology. In about half of patients with an 'undetected' cause responsible for their LBP are thought to have some sort of instability in their spine. A range of stabilization exercises or expensive surgical treatments such as vertebral fusions focus to reduce or eliminate inter-vertebral motion in the affected spine segment to overcome the dysfunction in natural stabilization of the vertebrae. Though evidence points towards a strong association between degenerative disc disease, spine pain and segmental instability, a pathognomic relationship between radiologic evidence of disc degeneration or instability and pain symptoms in non-specific LBP patients is yet to be established. A major limitation in establishing or disapproving this relationship is the currently available approaches for quantifying spine kinematics in the clinical setting. Most of the available techniques do not provide assessments of inter-vertebral relationship in the dynamically moving spine and most of the common techniques used in clinics require exposure to x-ray radiation (e.g., dual fluoroscopy). This innovative imaging work was conceived with an idea to remodel and restructure the XROMM technique (described in Chapter 3) and apply it a new technique applicable for an MR imaging platform for the assessment of spine segmental motion. The initial idea of developing orthogonal fluoroscopy for assessment of spine kinematics involved potential multiple exposures to x-ray radiation. This was a concern for using such technique for research involving human volunteers as the use of high radiation equipment is not permitted for scientific investigations in certain states in the US, including ours, Ohio. Additionally, joint kinematics evaluation tools based on x-rays such as quantitative fluoroscopy and functional radiography have been

the routine diagnostic approaches for the assessment of vertebral instability assessment. Accordingly, my focus was to develop a quantification technique that moved away from the x-ray approach to a radiation-free MRI platform that would be safe to be applied in research as well as in the clinical field.

Thus, I pivoted to the idea of using the MRI as a substitute to orthogonal x-ray imaging, which represented a major innovative in MR musculoskeletal imaging. After several rounds of refinements in the imaging and image modeling technique developed here, it is suggestive of becoming even a better alternative to the x-ray technique. This is because of several reasons. While working through the AIM 1 (feasibility and reliability), it has become apparent that the rotoscoping technique can be used not only with single slice acquisitions, acquisition of additional multi-planar images at a given static displacement may enhance the accuracy of the rotoscoping outcomes. The selection of these additional orthogonal planes for visualizing a given inter-vertebral displacement (virtually in any desired plane) potentially allows greater freedom to the user to include desired anatomical landmarks within the selected image slices. Additionally, setting up of orthogonal camera views in the Maya animation software permits the user to map out-of-plane motion in vertebrae of interest. The use of morphology-based rotoscoping enables the user to potentially choose any major anatomical landmarks of preference for rotoscoping, thereby increasing the accuracy of model-to-image matching in the trial scans. The use of the porcine spines for AIM 2 has provided evidence that accurate quantification of the spine displacements could be achieved with the technique. The innovative idea of building of calibration grids to calibrate the volume of the imaging space has not been done earlier. The accuracy of the quantification also depended on the accuracy of the volume calibration of the MR coils. The major achievement of this project was to create a technique and unique workflow that permits quantification of un-

ipalanar and biplanar motion in rigid bodies and spine elements without the use of ionizing radiation. Though voxel-based-morphometry (VBM) techniques are available for use in functional MR imaging, the concept and usage of external calibration technique applied in our study was very unique for two major reasons. First, VBM methods and simultaneous 3-D image reconstruction techniques require acquisition of strict isotropic scanned images to ensure spatial resolution of the final reconstructed images. The reconstruction also requires acquisition of multiple isotropic image slices that scan the entire object volume. Our study, on the other hand, uses morphology selective anisotropic single image slices in the single or orthogonal plane, without performing any reconstruction of image volumes. Therefore, minimization of effective slice numbers drastically reduces the scan time without compromising the resolution of the images in our approach. Secondly, we have greatly minimized the computation time for calculating the displacements (solid-body or the porcine vertebrae) by introducing the data processing and animation platform that are pre-loaded with segmentation and motion analysis algorithms, when compared to the VBM approach that requires complex and lengthy computations.

AIM 1 and AIM 2 of the project represent one of the first attempts to apply a MRI-only technique for quantification of inter-vertebral motion with 3-D modeling and animation. Especially, the use of motion capturing hybrid 2D HYCE S sequence will permit us to apply the technique to skeletal motion analysis in humans as a step ahead from being restricted to analyzing positional changes in vertebrae from static images (acquired at the end-ranges of movement) to developing a tool to enable mapping of spine motion in a more dynamic context. Application of this technique may facilitate validation of accuracy and reliability of spine motion imaging and clinical techniques usually applied detect abnormalities in the lumbar spine segment motion. In the light of

fast progress in made in the discipline of MRI sequence development, this work in combination of real-time, high-resolution image acquisition, can develop into a novel approach for quantification of lumbar spine motion. In conclusion the work described in AIM 1 has successfully shown that it is feasible to use an innovative non-ionizing, MRI based 3-D modeling technique to quantify biplanar translational and rotational motion, in solid-body objects. The work described in AIM 2 of this project has enabled us to quantify *ex-vivo* inter-vertebral motion in porcine spine segments with reasonable accuracy and reliability across single-rater quantification sessions. Accomplishment in executing AIM 2 of this dissertation has validated our technique for reliability and accuracy. The third exploratory aim proposed to examine changes in inter-vertebral motion under different spine loading conditions in a case of recurrent disc herniation, using commercially available, semi-automatic segmentation software (OrthoCAD®, Esaote SpA). The technique used to scan the patient in an open-MR system in the supine and then in progressive loading spine-position shows that this particular technique is non-claustrophobic for the patient, and can detect a number of geometrical properties of the vertebral bodies and spinal canal that can be calculated to objectively asses the use of a MRI based semi-automated segmentation technique as a proof of concept tool that picks up changes in inter-vertebral morphology introduced due to differential loading of the lumbar spine.

Significant time and resources were allotted to work out the feasibility of the technique using several pilot trials for this purpose. The outcomes of this novel work in terms of validating a non-radiation based MR imaging and analysis protocol was close to what was initially expected. Outcomes of AIM 2 provide the foundation for future development of even more reliable and accurate technique to permit quantification of *in vivo* vertebral motion. This technique developed exclusively on a MRI-based 3-D

animation technique may be considered a safe tool that can be used for advancement of our understanding about normal and pathological motion in spine or other different joints in the body. In the long-term these findings have the potential to change the concepts of diagnosis and treatment in the fields of physical medicine and rehabilitation, orthopedics, as well as physical therapy, especially in context of LBP.

Future Directions

The discussion sections of Chapters 3, 4 and 5 of this document as well as the conclusion segment above have suggested a number of avenues for future research toward improving techniques and approaches for the assessment spine kinematics. Below, I will provide three broad perspectives on future directions for studies on spine kinematics, mostly as further development and refinement of the techniques such as the one that has evolved from this dissertation work and their potential applications to enhance our understanding of motion of joints in general and in studying inter-vertebral kinematics in particular.

Improvement and application of the current technique. This dissertation work is one of the pioneering efforts to develop a quantification technique that allows 3-D animation for assessment of complex spine motion on a MR imaging platform. Due to the current limitation of costs and time, and for investigating the preliminary feasibility (Aim1), reliability and accuracy of the developed technique, uncoupled spine motion was used as experimental displacements for the study. However, given the ability of the animation to track movement of the 3-D models in all 6 degrees of freedom in space, this technique can potentially be applied to map out-of-plane motion in images acquired in appropriate planes needed for such quantification. Therefore, the next logical steps in improving this technique should focus on (i) quantifying real-time inter-vertebral motion

in a dynamically moving spine where coupled motion in motion-segments can be elicited using robotic equipment with feedback mechanisms. Such MRI-compatible equipment should be capable of generating sustainable torques across the spine joints to induce pre-determined ranges of flexion-extension or lateral bending moments in experimental models. Such motion can be imaged using dynamic streaming sequences (e.g., the 2D HYCE S sequence used in this work), and the vertebral displacements can then be analyzed using 3-D animation. An alternative to this could be imaging and quantifying dynamic motion of the spine in human volunteers who could perform standardized bending tasks inside the magnet. (ii) This technique permits the creation of more than one view or perspective of looking at a given spine motion. Maya Cameras can potentially be created having a single-plane, orthogonal plane or multiple slice (at different levels but in the same plane) views of a motion trial. Future studies can apply a combination of these views to enhance the accuracy of the model-to-image matching (rotoscoping). Development of faster multi-slice and multi-plane imaging sequences can be applied to acquire minimum number of images of a trial for the morphology-based rotoscoping approach developed in this work. Accordingly, this novel approach should be immensely helpful to potentiate the utilization of a great number of anatomical landmarks available close to joint skeletons for accurate 3-D rotoscoping in high resolution MR images. (iii) Currently available voxel-based 3-D reconstruction of MR images is time consuming and susceptible to motion-artefacts. The technique developed in this study, on the other hand, does not need complex corrective measures and acquires minimum number of image slice at a much faster rate. Therefore, clinical application for quantifying joint displacements using this technique in individuals with joint pain will be more favorable when compared to volume based reconstruction techniques. Application of advanced and faster dynamic MR sequences in imaging spine

motion in the weight-bearing position (as positioned in Aim 3) will enhance the temporal resolution of data acquired in motion trails with the improvement of the frame capture rates closer to the current rates of acquisition in quantitative fluoroscopic techniques. (iv) Lastly, the relevance of the developed technique to be used for experimental application and for comparison with other techniques like the RSA cannot be over-emphasized. Given the level of reliability and accuracy results of the technique in detecting sagittal single-plane displacements, is expected that the use of this technique may be explored in its current form in a clinical setting. The process and the quantification time for the trials can be shortened with automation of some major steps in the technique. The use of stronger magnetic field strengths may increase the accuracy and reliability of this technique. Use of open MRI systems for clinical and research data collection may be explored in situations where the individual being examined is more comfortable, feels less claustrophobic during scanning, and imaged in weight-bearing spine position so that potential unexpected inter-segmental behavior secondary to axial loading of the trunk can be unmasked. Use of MRI compatible EMG systems to detect muscle onsets and fatiguing patterns in conjunction with muscle functional MRI may be used to study the relationships between pain, muscle function and inter-vertebral displacements in health and in disease.

Scope of improvement in image-based analytical techniques. A number of segmentation techniques used with MR and computed tomography (CT) imaging may be developed as fully automated processes to enhance accuracy in model reconstruction (27, 252). Further, development of automated digitization and registration processes can significantly reduce image processing time required for trial reconstruction. Development of isotropic real-time imaging options may facilitate faster multi-axial data acquisition of

moving joints, rapid reconstruction of models, real-time animation and quantification of joint motion.

Clinical correlation of quantified inter-vertebral motion. Accurate, dynamic and 3-D motion analysis is the long-term goal. Abnormalities in lumbar inter-vertebral motion detected with functional radiography or fluoroscopy may or may not be associated with LBP. In cases where radiologic abnormal motion co-exists with LBP, it is not yet clear if the abnormal motion is the primary reason of pain or is a result of other factors triggering the pain. Although evidence suggests a link between aberrant vertebral motion in degenerative disc disease and back pain, the temporal relationship between the onset and duration of pain episodes and radiologically detected motion anomaly has not yet determined except for a very few studies (128, 241). Additionally, clinically detected exaggerated spine motion (e.g., with the prone instability testing) in the lumbar spine has not yet been validated or correlated with radiological observations. One of the primary reasons for existent gaps in delineating mechanistic relationships between back pain and aberrant segmental motion is the lack of techniques that can be safely and frequently used for the evaluation of *in-vivo* skeletal motion in humans. Most of the common imaging tools used for this purpose apply ionizing radiation exposure which ultimately limit their use. Techniques like functional radiography do not enable real-time 3-D evaluation of spine motion, thereby restricting wider application of such techniques in analyzing planar or coupled spine motion patterns in symptomatic LBP. In this dissertation I have developed a novel imaging technique and modelling approach that can potentially be applied to analyze inter-vertebral motion using real-time data acquisition on an MRI-only platform. Application of multi-planar image acquisition approach to the current technique will further improve the accuracy of quantification and will enhance our understanding of the association between vertebral motion and LBP.

References

1. Abbott JH, Mccane B, Herbison P, Moginie G, Chapple C, and Hogarty T. Lumbar segmental instability: a criterion-related validity study of manual therapy assessment. *BMC musculoskeletal disorders* 6: 56, 2005.

2. Abumi K, Panjabi MM, and Duranceau J. Biomechanical evaluation of spinal fixation devices. Part III. Stability provided by six spinal fixation devices and interbody bone graft. *Spine* 14: 1249-1255, 1989.

3. Abumi K, Panjabi MM, Kramer KM, Duranceau J, Oxland T, and Crisco JJ. Biomechanical evaluation of lumbar spinal stability after graded facetectomies. *Spine* 15: 1142-1147, 1990.

4. Ackerman SJ, Polly DW, Jr., Knight T, Holt T, and Cummings J. Management of sacroiliac joint disruption and degenerative sacroiliitis with nonoperative care is medical resource-intensive and costly in a United States commercial payer population. *ClinicoEconomics and outcomes research : CEOR* 6: 63-74, 2014.

5. Ackerman SJ, Polly DW, Jr., Knight T, Schneider K, Holt T, and Cummings J. Comparison of the costs of nonoperative care to minimally invasive surgery for sacroiliac joint disruption and degenerative sacroiliitis in a United States Medicare population: potential economic implications of a new minimally-invasive technology. *ClinicoEconomics and outcomes research : CEOR* 5: 575-587, 2013.

6. Adamovich S, Levin M, and Feldman A. Merging different motor patterns: coordination between rhythmical and discrete single-joint movements. *Experimental brain research* 99: 325-337, 1994.

7. Adams GR, Duvoisin MR, and Dudley GA. Magnetic resonance imaging and electromyography as indexes of muscle function. *Journal of applied physiology* 73: 1578-1583, 1992.

8. Adams GR, Harris RT, Woodard D, and Dudley GA. Mapping of Electrical Muscle Stimulation Using Mri. *Journal of applied physiology* 74: 532-537, 1993.

9. Adams MA. Mechanical testing of the spine. An appraisal of methodology, results, and conclusions. *Spine* 20: 2151-2156, 1995.

10. Adams MA, and Dolan P. Spine biomechanics. *Journal of biomechanics* 38: 1972-1983, 2005.

11. Adams MA, and Dolan P. A technique for quantifying the bending moment acting on the lumbar spine in vivo. *Journal of biomechanics* 24: 117-126, 1991.

12. Adams MA, Dolan P, and Hutton WC. The lumbar spine in backward bending. *Spine* 13: 1019-1026, 1988.

13. Adams MA, and Hutton WC. The effect of posture on the role of the apophysial joints in resisting intervertebral compressive forces. *The Journal of bone and joint surgery British volume* 62: 358-362, 1980.

14. Adams MA, and Hutton WC. Has the Lumbar Spine a Margin of Safety in Forward Bending. *Clinical biomechanics* 1: 3-6, 1986.

15. Adams MA, and Hutton WC. The mechanical function of the lumbar apophyseal joints. *Spine* 8: 327-330, 1983.

16. Adams MA, and Hutton WC. Prolapsed intervertebral disc. A hyperflexion injury 1981 Volvo Award in Basic Science. *Spine* 7: 184-191, 1982.

17. Adams MA, Hutton WC, and Stott JR. The resistance to flexion of the lumbar intervertebral joint. *Spine* 5: 245-253, 1980.

18. Adams MA, May S, Freeman BJ, Morrison HP, and Dolan P. Effects of backward bending on lumbar intervertebral discs. Relevance to physical therapy treatments for low back pain. *Spine* 25: 431-437; discussion 438, 2000.

19. Adams MA, Mcnally DS, and Dolan P. 'Stress' distributions inside intervertebral discs. The effects of age and degeneration. *The Journal of bone and joint surgery British volume* 78: 965-972, 1996.

20. Ahmadi A, Maroufi N, Behtash H, Zekavat H, and Parnianpour M. Kinematic analysis of dynamic lumbar motion in patients with lumbar segmental instability using digital videofluoroscopy. *European spine journal : official publication of the European Spine Society, the European Spinal Deformity Society, and the European Section of the Cervical Spine Research Society* 18: 1677-1685, 2009.

21. Airaksinen O, Brox JI, Cedraschi C, Hildebrandt J, Klaber-Moffett J, Kovacs F, Mannion AF, Reis S, Staal JB, Ursin H, Zanoli G, and Pain CBWGOGFCLB. Chapter 4. European guidelines for the management of chronic nonspecific low back pain. *European spine journal : official publication of the European Spine Society, the European Spinal Deformity Society, and the European Section of the Cervical Spine Research Society* 15 Suppl 2: S192-300, 2006.

22. Al-Rawahi M, Luo J, Pollintine P, Dolan P, and Adams MA. Mechanical function of vertebral body osteophytes, as revealed by experiments on cadaveric spines. *Spine* 36: 770-777, 2011.

23. Alexiev AR. Some differences of the electromyographic erector spinae activity between normal subjects and low back pain patients during the generation of isometric trunk torque. *Electromyography and clinical neurophysiology* 34: 495-499, 1994.

24. Alini M, Li W, Markovic P, Aebi M, Spiro RC, and Roughley PJ. The potential and limitations of a cell-seeded collagen/hyaluronan scaffold to engineer an intervertebral disc-like matrix. *Spine* 28: 446-454; discussion 453, 2003.

25. Allbrook D. Movements of the lumbar spinal column. *The Journal of bone and joint surgery British volume* 39-B: 339-345, 1957.

26. Almukhtar A, Ju X, Khambay B, Mcdonald J, and Ayoub A. Comparison of the accuracy of voxel based registration and surface based registration for 3-D assessment of surgical change following orthognathic surgery. *PloS one* 9: e93402, 2014.

27. Anderson DD, Segal NA, Kern AM, Nevitt MC, Torner JC, and Lynch JA. Reliability of semiautomated computational methods for estimating tibiofemoral contact stress in the Multicenter Osteoarthritis Study. *Computational and mathematical methods in medicine* 2012: 767469, 2012.

28. Andersson GB, Ortengren R, and Nachemson A. Intradiskal pressure, intra-abdominal pressure and myoelectric back muscle activity related to posture and loading. *Clinical orthopaedics and related research* 156-164, 1977.

29. Anderst WJ, Vaidya R, and Tashman S. A technique to measure three-dimensional in vivo rotation of fused and adjacent lumbar vertebrae. *The Spine Journal* 8: 991-997, 2008.

30. Antoniou J, Steffen T, Nelson F, Winterbottom N, Hollander AP, Poole RA, Aebi M, and Alini M. The human lumbar intervertebral disc: evidence for changes in the biosynthesis and denaturation of the extracellular matrix with growth, maturation, ageing, and degeneration. *The Journal of clinical investigation* 98: 996-1003, 1996.

31. Arbanas J, Klasan GS, Nikolic M, Cvijanovic O, and Malnar D. Immunohistochemical analysis of the human psoas major muscle with regards to the body side and aging. *Collegium antropologicum* 34 Suppl 2: 169-173, 2010.

32. Arbanas J, Klasan GS, Nikolic M, Jerkovic R, Miljanovic I, and Malnar D. Fibre type composition of the human psoas major muscle with regard to the level of its origin. *Journal of anatomy* 215: 636-641, 2009.

33. Arbanas J, Pavlovic I, Marijancic V, Vlahovic H, Starcevic-Klasan G, Peharec S, Bajek S, Miletic D, and Malnar D. MRI features of the psoas major muscle in patients with low back pain. *European spine journal : official publication of the European Spine Society, the European Spinal Deformity Society, and the European Section of the Cervical Spine Research Society* 22: 1965-1971, 2013.

34. Arokoski JP, Valta T, Airaksinen O, and Kankaanpää M. Back and abdominal muscle function during stabilization exercises. *Archives of Physical Medicine and Rehabilitation* 82: 1089-1098, 2001.

35. Atkinson G, and Nevill AM. Statistical methods for assessing measurement error (reliability) in variables relevant to sports medicine. *Sports medicine* 26: 217-238, 1998.

36. Auerbach JD, Wills BP, Mcintosh TC, and Balderston RA. Evaluation of spinal kinematics following lumbar total disc replacement and circumferential fusion using in vivo fluoroscopy. *Spine* 32: 527-536, 2007.

37. Axelsson P, Johnsson R, Strömqvist B, Arvidsson M, and Herrlin K. Posterolateral lumbar fusion. Outcome of 71 consecutive operations after 4 (2-7) years. *Acta Orthop Scand* 65: 309-314, 1994.

38. Axelsson P, and Karlsson BS. Intervertebral mobility in the progressive degenerative process. A radiostereometric analysis. *European spine journal : official publication of the European Spine Society, the European Spinal Deformity Society, and the European Section of the Cervical Spine Research Society* 13: 567-572, 2004.

39. Baier DB, and Gatesy SM. Three-dimensional skeletal kinematics of the shoulder girdle and forelimb in walking Alligator. *Journal of anatomy* 223: 462-473, 2013.

40. Barker PJ, Guggenheimer KT, Grkovic I, Briggs CA, Jones DC, Thomas CD, and Hodges PW. Effects of tensioning the lumbar fasciae on segmental stiffness during flexion and extension: Young Investigator Award winner. *Spine* 31: 397-405, 2006.

41. Barkhausen J, Ruehm SG, Goyen M, Buck T, Laub G, and Debatin JF. MR evaluation of ventricular function: true fast imaging with steady-state precession versus fast low-angle shot cine MR imaging: feasibility study. *Radiology* 219: 264-269, 2001.

42. Barrance PJ, Williams GN, Novotny JE, and Buchanan TS. A method for measurement of joint kinematics in vivo by registration of 3-D geometric models with cine phase contrast magnetic resonance imaging data. *Journal of biomechanical engineering* 127: 829-837, 2005.

43. Barrera MC, Alustiza JM, Gervas C, Recondo JA, Villanua JA, and Salvador E. Post-operative lumbar spine: comparative study of TSE T2 and turbo-FLAIR sequences vs contrast-enhanced SE T1. *Clinical radiology* 56: 133-137, 2001.

44. Basmajian JV. Control of individual motor units. A guide and preliminary reading for prospective subjects in single motor unit training experiments. *American journal of physical medicine* 52: 257-260, 1973.

45. Beazell JR, Mullins M, and Grindstaff TL. Lumbar instability: an evolving and challenging concept. *The Journal of manual & manipulative therapy* 18: 9-14, 2010.

46. Begg AC, and Falconer MA. Plain radiography in intraspinal protrusion lumbar intervertebral disks; a correlation with operative findings. *The British journal of surgery* 36: 225-239, 1949.

47. Behnam AJ, Herzka DA, and Sheehan FT. Assessing the accuracy and precision of musculoskeletal motion tracking using cine-PC MRI on a 3.0T platform. *Journal of biomechanics* 44: 193-197, 2011.

48. Belkoff SM, Mathis JM, Jasper LE, and Deramond H. The biomechanics of vertebroplasty. The effect of cement volume on mechanical behavior. *Spine* 26: 1537-1541, 2001.

49. Bergmark A. Stability of the lumbar spine. A study in mechanical engineering. *Acta orthopaedica Scandinavica Supplementum* 230: 1-54, 1989.

50. Bergmark A. Stability of the lumbar spine: a study in mechanical engineering. *Acta Orthopaedica* 60: 1-54, 1989.

51. Berven S, Tay BB, Colman W, and Hu SS. The lumbar zygapophyseal (facet) joints: a role in the pathogenesis of spinal pain syndromes and degenerative spondylolisthesis. *Semin Neurol* 22: 187-196, 2002.

52. Bey MJ, Kline SK, Tashman S, and Zauel R. Accuracy of biplane x-ray imaging combined with model-based tracking for measuring in-vivo patellofemoral joint motion. *Journal of orthopaedic surgery and research* 3: 38, 2008.

53. Bey MJ, Zauel R, Brock SK, and Tashman S. Validation of a new model-based tracking technique for measuring three-dimensional, in vivo glenohumeral joint kinematics. *Journal of biomechanical engineering* 128: 604-609, 2006.

54. Bifulco P, Cesarelli M, Allen R, Sansone M, and Bracale M. Automatic recognition of vertebral landmarks in fluoroscopic sequences for analysis of intervertebral kinematics. *Medical & biological engineering & computing* 39: 65-75, 2001.

55. Bitar R, Leung G, Perng R, Tadros S, Moody AR, Sarrazin J, Mcgregor C, Christakis M, Symons S, Nelson A, and Roberts TP. MR pulse sequences: what every radiologist wants to know but is afraid to ask. *Radiographics* 26: 513-537, 2006.

56. Bland JM, and Altman DG. Statistical methods for assessing agreement between two methods of clinical measurement. *Lancet* 1: 307-310, 1986.

57. Boden SD, Riew KD, Yamaguchi K, Branch TP, Schellinger D, and Wiesel SW. Orientation of the lumbar facet joints: association with degenerative disc disease. *The Journal of bone and joint surgery American volume* 78: 403-411, 1996.

58. Boden SD, and Wiesel SW. Lumbosacral segmental motion in normal individuals. Have we been measuring instability properly? *Spine* 15: 571-576, 1990.

59. Bogduk N. *Clinical and radiological anatomy of the lumbar spine*. Elsevier Health Sciences, 2012.

60. Bogduk N. The innervation of the lumbar spine. *Spine* 8: 286-293, 1983.

61. Bogduk N. A reappraisal of the anatomy of the human lumbar erector spinae. *Journal of anatomy* 131: 525-540, 1980.

62. Bogduk N, Tynan W, and Wilson AS. The nerve supply to the human lumbar intervertebral discs. *Journal of anatomy* 132: 39-56, 1981.

63. Bogduk N, Wilson AS, and Tynan W. The human lumbar dorsal rami. *Journal of anatomy* 134: 383-397, 1982.

64. Boice JD, Jr., Mandel JS, and Doody MM. Breast cancer among radiologic technologists. *Jama* 274: 394-401, 1995.

65. Bojan AJ, Bragdon C, Jonsson A, Ekholm C, and Karrholm J. Three-dimensional bone-implant movements in trochanteric hip fractures: Precision and accuracy of radiostereometric analysis in a phantom model. *Journal of orthopaedic research : official publication of the Orthopaedic Research Society* 33: 705-711, 2015.

66. Borotikar BS, Sipprell WH, 3rd, Wible EE, and Sheehan FT. A methodology to accurately quantify patellofemoral cartilage contact kinematics by combining 3-D image shape registration and cine-PC MRI velocity data. *Journal of biomechanics* 45: 1117-1122, 2012.

67. Boyd LM, and Carter AJ. Injectable biomaterials and vertebral endplate treatment for repair and regeneration of the intervertebral disc. *European spine journal : official publication of the European Spine Society, the European Spinal Deformity Society, and the European Section of the Cervical Spine Research Society* 15 Suppl 3: S414-421, 2006.

68. Brainerd EL, Baier DB, Gatesy SM, Hedrick TL, Metzger KA, Gilbert SL, and Crisco JJ. X-ray reconstruction of moving morphology (XROMM): precision, accuracy and applications in comparative biomechanics research. *Journal of experimental zoology Part A, Ecological genetics and physiology* 313: 262-279, 2010.

69. Breen A, Allen R, and Morris A. A digital videofluoroscopic technique for spine kinematics. *Journal of medical engineering & technology* 13: 109-113, 1989.

70. Breen A, Allen R, and Morris A. An image processing method for spine kinematics-preliminary studies. *Clinical biomechanics* 3: 5-10, 1988.

71. Breen AC, Allen R, and Morris A. Spine kinematics: a digital videofluoroscopic technique. *Journal of biomedical engineering* 11: 224-228, 1989.

72. Brickleyparsons D, and Glimcher MJ. Is the Chemistry of Collagen in Intervertebral Disks an Expression of Wolff Law - a Study of the Human Lumbar Spine. *Spine* 9: 148-163, 1984.

73. Brossmann J, Muhle C, Schroder C, Melchert UH, Bull CC, Spielmann RP, and Heller M. Patellar tracking patterns during active and passive knee extension: evaluation with motion-triggered cine MR imaging. *Radiology* 187: 205-212, 1993.

74. Brown SH, Gregory DE, Carr JA, Ward SR, Masuda K, and Lieber RL. ISSLS prize winner: Adaptations to the multifidus muscle in response to experimentally induced intervertebral disc degeneration. *Spine* 36: 1728-1736, 2011.

75. Buckwalter JA. Aging and degeneration of the human intervertebral disc. *Spine* 20: 1307-1314, 1995.

76. Busscher I, Ploegmakers JJW, Verkerke GJ, and Veldhuizen AG. Comparative anatomical dimensions of the complete human and porcine spine. *European Spine Journal* 19: 1104-1114, 2010.

77. Cai R, Yuan X, Rorabeck C, Bourne RB, and Holdsworth DW. Development of an RSA calibration system with improved accuracy and precision. *Journal of biomechanics* 41: 907-911, 2008.

78. Campbell-Kyureghyan N, Jorgensen M, Burr D, and Marras W. The prediction of lumbar spine geometry: method development and validation. *Clinical biomechanics* 20: 455-464, 2005.

79. Cappozzo A, Della Croce U, Leardini A, and Chiari L. Human movement analysis using stereophotogrammetry. Part 1: theoretical background. *Gait & posture* 21: 186-196, 2005.

80. Carragee EJ, Tanner CM, Khurana S, Hayward C, Welsh J, Date E, Truong T, Rossi M, and Hagle C. The rates of false-positive lumbar discography in select patients without low back symptoms. *Spine* 25: 1373-1380; discussion 1381, 2000.

81. Cereatti A, Della Croce U, and Cappozzo A. Reconstruction of skeletal movement using skin markers: comparative assessment of bone pose estimators. *Journal of neuroengineering and rehabilitation* 3: 7, 2006.

82. Chen WJ, Chiou WK, Lee YH, Lee MY, and Chen ML. Myo-electric behavior of the trunk muscles during static load holding in healthy subjects and low back pain patients. *Clinical biomechanics* 13: S9-S15, 1998.

83. Cheung JP, Shigematsu H, and Cheung KM. Verification of measurements of lumbar spinal dimensions in T1- and T2-weighted magnetic resonance imaging sequences. *The spine journal : official journal of the North American Spine Society* 14: 1476-1483, 2014.

84. Chiari L, Della Croce U, Leardini A, and Cappozzo A. Human movement analysis using stereophotogrammetry. Part 2: instrumental errors. *Gait & posture* 21: 197-211, 2005.

85. Choi KC, Kim JS, Jung B, and Lee SH. Dynamic lumbar spinal stenosis : the usefulness of axial loaded MRI in preoperative evaluation. *Journal of Korean Neurosurgical Society* 46: 265-268, 2009.

86. Cholewicki J, Juluru K, and Mcgill SM. Intra-abdominal pressure mechanism for stabilizing the lumbar spine. *Journal of biomechanics* 32: 13-17, 1999.

87. Cholewicki J, and Mcgill SM. Lumbar posterior ligament involvement during extremely heavy lifts estimated from fluoroscopic measurements. *Journal of biomechanics* 25: 17-28, 1992.

88. Cholewicki J, and Mcgill SM. Mechanical stability of the in vivo lumbar spine: implications for injury and chronic low back pain. *Clinical biomechanics* 11: 1-15, 1996.

89. Cholewicki J, Mcgill SM, Wells RP, and Vernon H. Method for measuring vertebral kinematics from videofluoroscopy. *Clinical biomechanics* 6: 73-78, 1991.

90. Cholewicki J, Panjabi MM, and Khachatryan A. Stabilizing function of trunk flexor-extensor muscles around a neutral spine posture. *Spine* 22: 2207-2212, 1997.

91. Cholewicki J, Panjabi MM, and Khachatryan A. Stabilizing function of trunk flexor-extensor muscles around a neutral spine posture. *Spine* 22: 2207-2212, 1997.

92. Chung SS, Lee CS, Kim SH, Chung MW, and Ahn JM. Effect of low back posture on the morphology of the spinal canal. *Skeletal radiology* 29: 217-223, 2000.

93. Cinotti G, Roysam GS, Eisenstein SM, and Postacchini F. Ipsilateral recurrent lumbar disc herniation. A prospective, controlled study. *The Journal of bone and joint surgery British volume* 80: 825-832, 1998.

94. Clark BC, Cook SB, and Ploutz-Snyder LL. Reliability of techniques to assess human neuromuscular function in vivo. *Journal of electromyography and kinesiology : official journal of the International Society of Electrophysiological Kinesiology* 17: 90-101, 2007.

95. Clark BC, Manini TM, Mayer JM, Ploutz-Snyder LL, and Graves JE. Electromyographic activity of the lumbar and hip extensors during dynamic trunk extension exercise. *Arch Phys Med Rehabil* 83: 1547-1552, 2002.

96. Clark BC, Pierce JR, Manini TM, and Ploutz-Snyder LL. Effect of prolonged unweighting of human skeletal muscle on neuromotor force control. *European journal of applied physiology* 100: 53-62, 2007.

97. Clarke EC, Martin JH, D'entremont AG, Pandy MG, Wilson DR, and Herbert RD. A non-invasive, 3-D, dynamic MRI method for measuring muscle moment arms in vivo: demonstration in the human ankle joint and Achilles tendon. *Medical engineering & physics* 37: 93-99, 2015.

98. Cole TC, Burkhardt D, Ghosh P, Ryan M, and Taylor T. Effects of spinal fusion on the proteoglycans of the canine intervertebral disc. *Journal of orthopaedic research : official publication of the Orthopaedic Research Society* 3: 277-291, 1985.

99. Connolly ES. Surgery for recurrent lumbar disc herniation. *Clinical neurosurgery* 39: 211-216, 1992.

100. Coppes MH, Marani E, Thomeer RT, and Groen GJ. Innervation of "painful" lumbar discs. *Spine* 22: 2342-2349; discussion 2349-2350, 1997.

101. Cresswell AG, Oddsson L, and Thorstensson A. The influence of sudden perturbations on trunk muscle activity and intra-abdominal pressure while standing. *Experimental brain research* 98: 336-341, 1994.

102. Crisco Iii JJ, and Panjabi MM. Postural biomechanical stability and gross muscular architecture in the spine. In: *Multiple muscle systems*Springer, 1990, p. 438-450.

103. Crisco JJ, 3rd, and Panjabi MM. The intersegmental and multisegmental muscles of the lumbar spine. A biomechanical model comparing lateral stabilizing potential. *Spine* 16: 793-799, 1991.

104. Crisco JJ, and Panjabi MM. Euler stability of the human ligamentous lumbar spine. Part I: Theory. *Clinical biomechanics* 7: 19-26, 1992.

105. Crisco JJ, Panjabi MM, Yamamoto I, and Oxland TR. Euler stability of the human ligamentous lumbar spine. Part II: Experiment. *Clinical biomechanics* 7: 27-32, 1992.

106. Crock HV. A reappraisal of intervertebral disc lesions. *Med J Aust* 1: 983-989, 1970.

107. D'entremont AG, Nordmeyer-Massner JA, Bos C, Wilson DR, and Pruessmann KP. Do dynamic-based MR knee kinematics methods produce the same results as static methods? *Magnetic resonance in medicine : official journal of the Society of Magnetic Resonance in Medicine / Society of Magnetic Resonance in Medicine* 69: 1634-1644, 2013.

108. Dagenais S, Caro J, and Haldeman S. A systematic review of low back pain cost of illness studies in the United States and internationally. *The spine journal : official journal of the North American Spine Society* 8: 8-20, 2008.

109. Danielson B, and Willén J. Axially loaded magnetic resonance image of the lumbar spine in asymptomatic individuals. *Spine* 26: 2601-2606, 2001.

110. Danneels L, Coorevits P, Cools A, Vanderstraeten G, Cambier D, Witvrouw E, and De Cuyper H. Differences in electromyographic activity in the multifidus muscle and the iliocostalis lumborum between healthy subjects and patients with sub-acute and chronic low back pain. *European Spine Journal* 11: 13-19, 2001.

111. De Kleuver M, Oner FC, and Jacobs WC. Total disc replacement for chronic low back pain: background and a systematic review of the literature. *European spine journal : official publication of the European Spine Society, the European Spinal Deformity Society, and the European Section of the Cervical Spine Research Society* 12: 108-116, 2003.

112. Della Croce U, Leardini A, Chiari L, and Cappozzo A. Human movement analysis using stereophotogrammetry. Part 4: assessment of anatomical landmark misplacement and its effects on joint kinematics. *Gait & posture* 21: 226-237, 2005.

113. Demoulin C, Crielaard JM, and Vanderthommen M. Spinal muscle evaluation in healthy individuals and low-back-pain patients: a literature review. *Joint, bone, spine : revue du rhumatisme* 74: 9-13, 2007.

114. Dial KP, Goslow GE, and Jenkins FA. The Functional-Anatomy of the Shoulder in the European Starling (Sturnus-Vulgaris). *Journal of morphology* 207: 327-344, 1991.

115. Dimnet J, Fischer LP, Gonon G, and Carret JP. Radiographic studies of lateral flexion in the lumbar spine. *Journal of biomechanics* 11: 143-150, 1978.

116. Dolan P, and Adams MA. The relationship between EMG activity and extensor moment generation in the erector spinae muscles during bending and lifting activities. *Journal of biomechanics* 26: 513-522, 1993.

117. Dolan P, Mannion AF, and Adams MA. Passive tissues help the back muscles to generate extensor moments during lifting. *Journal of biomechanics* 27: 1077-1085, 1994.

118. Draney MT, Herfkens RJ, Hughes TJR, Pelc NJ, Wedding KL, Zarins CK, and Taylor CA. Quantification of vessel wall cyclic strain using cine phase contrast magnetic resonance imaging. *Ann Biomed Eng* 30: 1033-1045, 2002.

119. Dunlop RB, Adams MA, and Hutton WC. Disc space narrowing and the lumbar facet joints. *The Journal of bone and joint surgery British volume* 66: 706-710, 1984.

120. Dvorak J, Panjabi MM, Chang DG, Theiler R, and Grob D. Functional radiographic diagnosis of the lumbar spine. Flexion-extension and lateral bending. *Spine* 16: 562-571, 1991.

121. Dvorak J, Panjabi MM, Novotny JE, Chang DG, and Grob D. Clinical validation of functional flexion-extension roentgenograms of the lumbar spine. *Spine* 16: 943-950, 1991.

122. Erbayraktar S, Acar F, Tekinsoy B, Acar U, and Guner EM. Outcome analysis of reoperations after lumbar discectomies: a report of 22 patients. *The Kobe journal of medical sciences* 48: 33-41, 2002.

123. Esses SI, and Moro JK. The value of facet joint blocks in patient selection for lumbar fusion. *Spine* 18: 185-190, 1993.

124. Fairbank J. Total disc replacement for chronic low back pain. *Bmj* 342: d2745, 2011.

125. Farfan HF. Effects of torsion on the intervertebral joints. *Can J Surg* 12: 336-341, 1969.

126. Fellows RA, Hill NA, Gill HS, Macintyre NJ, Harrison MM, Ellis RE, and Wilson DR. Magnetic resonance imaging for in vivo assessment of three-dimensional patellar tracking. *J Biomech* 38: 1643-1652, 2005.

127. Fellows RA, Hill NA, Macintyre NJ, Harrison MM, Ellis RE, and Wilson DR. Repeatability of a novel technique for in vivo measurement of three-dimensional patellar tracking using magnetic resonance imaging. *J Magn Reson Imaging* 22: 145-153, 2005.

128. Ferreiro Perez A, Garcia Isidro M, Ayerbe E, Castedo J, and Jinkins JR. Evaluation of intervertebral disc herniation and hypermobile intersegmental instability in symptomatic adult patients undergoing recumbent and upright MRI of the cervical or lumbosacral spines. *European journal of radiology* 62: 444-448, 2007.

129. Fiebert IM, Spyropoulos T, Peterman D, and Dotson L. Thoracic segmental flexion during cervical forward bending. *Journal of back and musculoskeletal rehabilitation* 3: 80-85, 1993.

130. Fisher MJ, Meyer RA, Adams GR, Foley JM, and Potchen EJ. Direct Relationship between Proton T2 and Exercise Intensity in Skeletal-Muscle Mr Images. *Investigative radiology* 25: 480-485, 1990.

131. Fitzgerald JA, and Newman PH. Degenerative spondylolisthesis. *The Journal of bone and joint surgery British volume* 58: 184-192, 1976.

132. Fleckenstein JL, Watumull D, Bertocci LA, Parkey RW, and Peshock RM. Finger-specific flexor recruitment in humans: depiction by exercise-enhanced MRI. *Journal of applied physiology* 72: 1974-1977, 1992.

133. Flicker PL, Fleckenstein JL, Ferry K, Payne J, Ward C, Mayer T, Parkey RW, and Peshock RM. Lumbar muscle usage in chronic low back pain. Magnetic resonance image evaluation. *Spine* 18: 582-586, 1993.

134. Ford D, Bagnall KM, Mcfadden KD, Greenhill B, and Raso J. Analysis of vertebral muscle obtained during surgery for correction of a lumbar disc disorder. *Acta anatomica* 116: 152-157, 1983.

135. Ford DM, Bagnall KM, Mcfadden KD, Greenhill BJ, and Raso VJ. Paraspinal muscle imbalance in adolescent idiopathic scoliosis. *Spine* 9: 373-376, 1984.

136. Freddolini M, Strike S, and Lee RY. Stiffness properties of the trunk in people with low back pain. *Human movement science* 36: 70-79, 2014.

137. Freeman MD, Woodham MA, and Woodham AW. The role of the lumbar multifidus in chronic low back pain: a review. *PM & R : the journal of injury, function, and rehabilitation* 2: 142-146; quiz 141 p following 167, 2010.

138. Freemont AJ, Peacock TE, Goupille P, Hoyland JA, O'brien J, and Jayson MI. Nerve ingrowth into diseased intervertebral disc in chronic back pain. *Lancet* 350: 178-181, 1997.

139. Fritz JM, Childs JD, and Flynn TW. Pragmatic application of a clinical prediction rule in primary care to identify patients with low back pain with a good prognosis following a brief spinal manipulation intervention. *BMC family practice* 6: 29, 2005.

140. Fritzell P, Hägg O, Wessberg P, Nordwall A, and Group SLSS. 2001 Volvo Award Winner in Clinical Studies: Lumbar fusion versus nonsurgical treatment for chronic low back pain: a multicenter randomized controlled trial from the Swedish Lumbar Spine Study Group. *Spine* 26: 2521-2532; discussion 2532-2524, 2001.

141. Frobin W, Brinckmann P, Leivseth G, Biggemann M, and Reikeras O. Precision measurement of segmental motion from flexion-extension radiographs of the lumbar spine. *Clinical biomechanics* 11: 457-465, 1996.

142. Froning EC, and Frohman B. Motion of the lumbosacral spine after laminectomy and spine fusion. Correlation of motion with the result. *The Journal of bone and joint surgery American volume* 50: 897-918, 1968.

143. Frymoyer JW, Hanley EN, Jr., Howe J, Kuhlmann D, and Matteri RE. A comparison of radiographic findings in fusion and nonfusion patients ten or more years following lumbar disc surgery. *Spine* 4: 435-440, 1979.

144. Fujii R, Sakaura H, Mukai Y, Hosono N, Ishii T, Iwasaki M, Yoshikawa H, and Sugamoto K. Kinematics of the lumbar spine in trunk rotation: in vivo three-dimensional analysis using magnetic resonance imaging. *European spine journal : official publication of the European Spine Society, the European Spinal Deformity Society, and the European Section of the Cervical Spine Research Society* 16: 1867-1874, 2007.

145. Fujimori T, Iwasaki M, Nagamoto Y, Matsuo Y, Ishii T, Sugiura T, Kashii M, Murase T, Sugamoto K, and Yoshikawa H. Kinematics of the thoracic spine in trunk lateral bending: in vivo three-dimensional analysis. *The spine journal : official journal of the North American Spine Society* 14: 1991-1999, 2014.

146. Gabr RE, Sun X, Pednekar AS, and Narayana PA. Automated patient-specific optimization of three-dimensional double-inversion recovery magnetic resonance imaging. *Magnetic resonance in medicine : official journal of the Society of Magnetic Resonance in Medicine / Society of Magnetic Resonance in Medicine* 2015.

147. Gallucci M, Limbucci N, Paonessa A, and Splendiani A. Degenerative disease of the spine. *Neuroimaging clinics of North America* 17: 87-103, 2007.

148. Gardner-Morse M, Stokes IA, and Laible JP. Role of muscles in lumbar spine stability in maximum extension efforts. *Journal of orthopaedic research : official publication of the Orthopaedic Research Society* 13: 802-808, 1995.

149. Gardner-Morse MG, and Stokes IA. The effects of abdominal muscle coactivation on lumbar spine stability. *Spine* 23: 86-91; discussion 91-82, 1998.

150. Gardner-Morse MG, and Stokes IA. Physiological axial compressive preloads increase motion segment stiffness, linearity and hysteresis in all six degrees of freedom for small displacements about the neutral posture. *Journal of orthopaedic research : official publication of the Orthopaedic Research Society* 21: 547-552, 2003.

151. Gardner-Morse MG, and Stokes IA. Structural behavior of human lumbar spinal motion segments. *Journal of biomechanics* 37: 205-212, 2004.

152. Gatesy S, and Alenghat T. A 3-D computer-animated analysis of pigeon wing movement. In: *American Zoologist*SOC INTEGRATIVE COMPARATIVE BIOLOGY 1313 DOLLEY MADISON BLVD, NO 402, MCLEAN, VA 22101 USA, 1999, p. 104A-104A.

153. Gatesy SM, and Baier DB. The origin of the avian flight stroke: a kinematic and kinetic perspective. 2009.

154. Gatesy SM, Baier DB, Jenkins FA, and Dial KP. Scientific rotoscoping: a morphology-based method of 3-D motion analysis and visualization. *Journal of experimental zoology Part A, Ecological genetics and physiology* 313: 244-261, 2010.

155. Gertzbein SD, Seligman J, Holtby R, Chan KW, Ogston N, Kapasouri A, and Tile M. Centrode characteristics of the lumbar spine as a function of segmental instability. *Clinical orthopaedics and related research* 48-51, 1986.

156. Gilbert JW, Martin JC, Wheeler GR, Storey BB, Mick GE, Richardson GB, Herder SL, Gyarteng-Dakwa K, and Broughton PG. Lumbar disk protrusion rates of symptomatic patients using magnetic resonance imaging. *Journal of manipulative and physiological therapeutics* 33: 626-629, 2010.

157. Gill KP, and Callaghan MJ. The measurement of lumbar proprioception in individuals with and without low back pain. *Spine* 23: 371-377, 1998.

158. Gollnick PD, Piehl K, and Saltin B. Selective glycogen depletion pattern in human muscle fibres after exercise of varying intensity and at varying pedalling rates. *The Journal of physiology* 241: 45-57, 1974.

159. Granata KP, and Marras WS. An EMG-assisted model of loads on the lumbar spine during asymmetric trunk extensions. *Journal of biomechanics* 26: 1429-1438, 1993.

160. Granata KP, and Orishimo KF. Response of trunk muscle coactivation to changes in spinal stability. *Journal of biomechanics* 34: 1117-1123, 2001.

161. Granata KP, Slota GP, and Wilson SE. Influence of fatigue in neuromuscular control of spinal stability. *Human factors* 46: 81-91, 2004.

162. Graver V, Haaland AK, Magnaes B, and Loeb M. Seven-year clinical follow-up after lumbar disc surgery: results and predictors of outcome. *British journal of neurosurgery* 13: 178-184, 1999.

163. Grimby L, and Hannerz J. Recruitment order of motor units on voluntary contraction: changes induced by proprioceptive afferent activity. *Journal of neurology, neurosurgery, and psychiatry* 31: 565-573, 1968.

164. Ha KY, Son JM, Im JH, and Oh IS. Risk factors for adjacent segment degeneration after surgical correction of degenerative lumbar scoliosis. *Indian journal of orthopaedics* 47: 346-351, 2013.

165. Hadlow SV, Fagan AB, Hillier TM, and Fraser RD. The Graf ligamentoplasty procedure. Comparison with posterolateral fusion in the management of low back pain. *Spine* 23: 1172-1179, 1998.

166. Häggmark T, and Thorstensson A. Fibre types in human abdominal muscles. *Acta Physiol Scand* 107: 319-325, 1979.

167. Haher TR, O'brien M, Dryer JW, Nucci R, Zipnick R, and Leone DJ. The role of the lumbar facet joints in spinal stability. Identification of alternative paths of loading. *Spine* 19: 2667-2670 discussion 2671, 1994.

168. Hammer GP, Scheidemann-Wesp U, Samkange-Zeeb F, Wicke H, Neriishi K, and Blettner M. Occupational exposure to low doses of ionizing radiation and cataract development: a systematic literature review and perspectives on future studies. *Radiation and environmental biophysics* 52: 303-319, 2013.

169. Handa T, Ishihara H, Ohshima H, Osada R, Tsuji H, and Obata K. Effects of hydrostatic pressure on matrix synthesis and matrix metalloproteinase production in the human lumbar intervertebral disc. *Spine* 22: 1085-1091, 1997.

170. Hanley EN, Matteri RE, and Frymoyer JW. Accurate roentgenographic determination of lumbar flexion-extension. *Clinical orthopaedics and related research* 145-148, 1976.

171. Harvey SB, and Hukins DW. Measurement of lumbar spinal flexion-extension kinematics from lateral radiographs: simulation of the effects of out-of-plane movement and errors in reference point placement. *Medical engineering & physics* 20: 403-409, 1998.

172. Harvey SB, Smith FW, and Hukins DW. Measurement of lumbar spine flexion-extension using a low-field open-magnet magnetic resonance scanner. *Investigative radiology* 33: 439-443, 1998.

173. Hasan Z. The Human Motor Control System's Response to Mechanical Perturbation: Should It, Can It and Does It Ensure Stability? *Journal of motor behavior* 37: 484-493, 2005.

174. Hasan Z. Role of proprioceptors in neural control. *Current opinion in neurobiology* 2: 824-829, 1992.

175. Hasan Z, and Enoka R. Isometric torque-angle relationship and movement-related activity of human elbow flexors: implications for the equilibrium-point hypothesis. *Experimental brain research* 59: 441-450, 1984.

176. Hasegewa K, Kitahara K, Hara T, Takano K, and Shimoda H. Biomechanical evaluation of segmental instability in degenerative lumbar spondylolisthesis. *European spine journal : official publication of the European Spine Society, the European Spinal Deformity Society, and the European Section of the Cervical Spine Research Society* 18: 465-470, 2009.

177. Hastreiter D, Ozuna RM, and Spector M. Regional variations in certain cellular characteristics in human lumbar intervertebral discs, including the presence of alpha-smooth muscle actin. *Journal of orthopaedic research : official publication of the Orthopaedic Research Society* 19: 597-604, 2001.

178. Hayashi T, Daubs MD, Suzuki A, Scott TP, Phan KH, Ruangchainikom M, Takahashi S, Shiba K, and Wang JC. Motion characteristics and related factors of Modic changes in the lumbar spine. *Journal of neurosurgery Spine* 1-7, 2015.

179. Hayes MA, Howard TC, Gruel CR, and Kopta JA. Roentgenographic evaluation of lumbar spine flexion-extension in asymptomatic individuals. *Spine* 14: 327-331, 1989.

180. Henneman E, Clamann HP, Gillies JD, and Skinner RD. Rank Order of Motoneurons within a Pool - Law of Combination. *Journal of neurophysiology* 37: 1338-1349, 1974.

181. Henneman E, Somjen G, and Carpenter DO. Excitability and inhibitability of motoneurons of different sizes. *Journal of neurophysiology* 28: 599-620, 1965.

182. Henneman E, Somjen G, and Carpenter DO. Functional Significance of Cell Size in Spinal Motoneurons. *Journal of neurophysiology* 28: 560-580, 1965.

183. Herkowitz HN, and Kurz LT. Degenerative lumbar spondylolisthesis with spinal stenosis. A prospective study comparing decompression with decompression and intertransverse process arthrodesis. *The Journal of bone and joint surgery American volume* 73: 802-808, 1991.

184. Herrmann CM, Madigan ML, Davidson BS, and Granata KP. Effect of lumbar extensor fatigue on paraspinal muscle reflexes. *Journal of electromyography and kinesiology : official journal of the International Society of Electrophysiological Kinesiology* 16: 637-641, 2006.

185. Hicks GE, Fritz JM, Delitto A, and Mishock J. Interrater reliability of clinical examination measures for identification of lumbar segmental instability. *Archives of Physical Medicine and Rehabilitation* 84: 1858-1864, 2003.

186. Hides J, Stanton W, Freke M, Wilson S, Mcmahon S, and Richardson C. MRI study of the size, symmetry and function of the trunk muscles among elite cricketers with and without low back pain. *British journal of sports medicine* 42: 809-813, 2008.

187. Hiwatashi A, Danielson B, Moritani T, Bakos RS, Rodenhause TG, Pilcher WH, and Westesson PL. Axial loading during MR imaging can influence treatment decision

for symptomatic spinal stenosis. *AJNR American journal of neuroradiology* 25: 170-174, 2004.

188. Hochhauser L, Kieffer SA, Cacayorin ED, Petro GR, and Teller WF. Recurrent postdiskectomy low back pain: MR-surgical correlation. *AJR American journal of roentgenology* 151: 755-760, 1988.

189. Hodges P, Holm AK, Hansson T, and Holm S. Rapid atrophy of the lumbar multifidus follows experimental disc or nerve root injury. *Spine* 31: 2926-2933, 2006.

190. Hodges PW. Core stability exercise in chronic low back pain. *The Orthopedic clinics of North America* 34: 245-254, 2003.

191. Hodges PW, Cresswell AG, Daggfeldt K, and Thorstensson A. In vivo measurement of the effect of intra-abdominal pressure on the human spine. *Journal of biomechanics* 34: 347-353, 2001.

192. Hodges PW, Eriksson AE, Shirley D, and Gandevia SC. Intra-abdominal pressure increases stiffness of the lumbar spine. *Journal of biomechanics* 38: 1873-1880, 2005.

193. Hodges PW, and Richardson CA. Contraction of the abdominal muscles associated with movement of the lower limb. *Physical therapy* 77: 132-142; discussion 142-134, 1997.

194. Hodges PW, and Richardson CA. Feedforward contraction of transversus abdominis is not influenced by the direction of arm movement. *Experimental brain research* 114: 362-370, 1997.

195. Hodges PW, and Richardson CA. Inefficient muscular stabilization of the lumbar spine associated with low back pain. A motor control evaluation of transversus abdominis. *Spine* 21: 2640-2650, 1996.

196. Holm S, Holm AK, Ekstrom L, Karladani A, and Hansson T. Experimental disc degeneration due to endplate injury. *Journal of spinal disorders & techniques* 17: 64-71, 2004.

197. Holm S, Indahl A, and Solomonow M. Sensorimotor control of the spine. *Journal of electromyography and kinesiology : official journal of the International Society of Electrophysiological Kinesiology* 12: 219-234, 2002.

198. Hong CH, Park JS, Jung KJ, and Kim WJ. Measurement of the normal lumbar intervertebral disc space using magnetic resonance imaging. *Asian spine journal* 4: 1-6, 2010.

199. Hong CH, Park JS, Jung KJ, and Kim WJ. Measurement of the Normal Lumbar Intervertebral Disc Space Using Magnetic Resonance Imaging. *Asian spine journal* 4: 1-6, 2010.

200. Hricak H, Brenner DJ, Adelstein SJ, Frush DP, Hall EJ, Howell RW, Mccollough CH, Mettler FA, Pearce MS, Suleiman OH, Thrall JH, and Wagner LK. Managing radiation use in medical imaging: a multifaceted challenge. *Radiology* 258: 889-905, 2011.

201. Hubley-Kozey CL, and Vezina MJ. Muscle activation during exercises to improve trunk stability in men with low back pain. *Archives of Physical Medicine and Rehabilitation* 83: 1100-1108, 2002.

202. Hurschler C, Seehaus F, Emmerich J, Kaptein BL, and Windhagen H. Comparison of the model-based and marker-based roentgen stereophotogrammetry methods in a typical clinical setting. *The Journal of arthroplasty* 24: 594-606, 2009.

203. Iguchi T, Kanemura A, Kasahara K, Sato K, Kurihara A, Yoshiya S, Nishida K, Miyamoto H, and Doita M. Lumbar instability and clinical symptoms: which is the more critical factor for symptoms: sagittal translation or segment angulation? *Journal of spinal disorders & techniques* 17: 284-290, 2004.

204. Indahl A, Kaige A, Reikeras O, and Holm S. Electromyographic response of the porcine multifidus musculature after nerve stimulation. *Spine* 20: 2652-2658, 1995.

205. Indahl A, Kaigle AM, Reikeras O, and Holm SH. Interaction between the porcine lumbar intervertebral disc, zygapophysial joints, and paraspinal muscles. *Spine* 22: 2834-2840, 1997.

206. Ishihara H, Mcnally DS, Urban JP, and Hall AC. Effects of hydrostatic pressure on matrix synthesis in different regions of the intervertebral disk. *Journal of applied physiology* 80: 839-846, 1996.

207. Ishii T, Mukai Y, Hosono N, Sakaura H, Fujii R, Nakajima Y, Tamura S, Iwasaki M, Yoshikawa H, and Sugamoto K. Kinematics of the cervical spine in lateral bending: in vivo three-dimensional analysis. *Spine* 31: 155-160, 2006.

208. Ishii T, Mukai Y, Hosono N, Sakaura H, Nakajima Y, Sato Y, Sugamoto K, and Yoshikawa H. Kinematics of the upper cervical spine in rotation: in vivo three-dimensional analysis. *Spine* 29: E139-144, 2004.

209. Iwai F, Sostman HD, Evans AJ, Nadel SN, Hedlund LW, Beam CA, Charles HC, and Spritzer CE. Cine Phase-Contrast Magnetic-Resonance-Imaging for Analysis of Flow Phenomena in Experimental Aortic Dissection. *Investigative radiology* 26: 1071-1078, 1991.

210. Jackson RP. The facet syndrome. Myth or reality? *Clinical orthopaedics and related research* 110-121, 1992.

211. Jacobs WC, Van Der Gaag NA, Kruyt MC, Tuschel A, De Kleuver M, Peul WC, Verbout AJ, and Oner FC. Total disc replacement for chronic discogenic low back pain: a Cochrane review. *Spine* 38: 24-36, 2013.

212. Jayakumar P, Nnadi C, Saifuddin A, Macsweeney E, and Casey A. Dynamic degenerative lumbar spondylolisthesis: diagnosis with axial loaded magnetic resonance imaging. *Spine* 31: E298-301, 2006.

213. Jenkins FA, Jr., Dial KP, and Goslow GE, Jr. A cineradiographic analysis of bird flight: the wishbone in starlings is a spring. *Science* 241: 1495-1498, 1988.

214. Jiang H, Russell G, Raso VJ, Moreau MJ, Hill DL, and Bagnall KM. The nature and distribution of the innervation of human supraspinal and interspinal ligaments. *Spine* 20: 869-876, 1995.

215. Jinkins JR, Dworkin JS, and Damadian RV. Upright, weight-bearing, dynamic-kinetic MRI of the spine: initial results. *European radiology* 15: 1815-1825, 2005.

216. Jinkins JR, Dworkin JS, Green CA, Greenhalgh JF, Gianni M, Gelbien M, Wolf RB, Damadian J, and Damadian RV. Upright, weight-bearing, dynamic-kinetic MRI of the spine pMRI/kMRI. *Riv Neuroradiol* 15: 333-357, 2002.

217. Johnson WE, Eisenstein SM, and Roberts S. Cell cluster formation in degenerate lumbar intervertebral discs is associated with increased disc cell proliferation. *Connective tissue research* 42: 197-207, 2001.

218. Johnsson KE, Redlund-Johnell I, Uden A, and Willner S. Preoperative and postoperative instability in lumbar spinal stenosis. *Spine* 14: 591-593, 1989.

219. Jonsson B. The functions of individual muscles in the lumbar part of the spinae muscle. *Electromyography* 10: 5-21, 1970.

220. Kaigle AM, Wessberg P, and Hansson TH. Muscular and kinematic behavior of the lumbar spine during flexion-extension. *Journal of spinal disorders* 11: 163-174, 1998.

221. Kalimo H, Rantanen J, Viljanen T, and Einola S. Lumbar muscles: structure and function. *Ann Med* 21: 353-359, 1989.

222. Kambin P, Cohen LF, Brooks M, and Schaffer JL. Development of degenerative spondylosis of the lumbar spine after partial discectomy. Comparison of laminotomy, discectomy, and posterolateral discectomy. *Spine* 20: 599-607, 1995.

223. Kanayama M, Abumi K, Kaneda K, Tadano S, and Ukai T. Phase lag of the intersegmental motion in flexion-extension of the lumbar and lumbosacral spine. An in vivo study. *Spine* 21: 1416-1422, 1996.

224. Kanno H, Ozawa H, Koizumi Y, Morozumi N, Aizawa T, Ishii Y, and Itoi E. Changes in lumbar spondylolisthesis on axial loaded MRI: Do they reproduce the positional changes in the degree of olisthesis observed on X-ray in the standing position? *The spine journal : official journal of the North American Spine Society* 2015.

225. Karrholm J. Roentgen stereophotogrammetry. Review of orthopedic applications. *Acta Orthop Scand* 60: 491-503, 1989.

226. Kawaguchi Y, Osada R, Kanamori M, Ishihara H, Ohmori K, Matsui H, and Kimura T. Association between an aggrecan gene polymorphism and lumbar disc degeneration. *Spine* 24: 2456-2460, 1999.

227. Kaya RD, Hoffman RL, and Clark BC. Reliability of a modified motor unit number index (MUNIX) technique. *Journal of electromyography and kinesiology : official journal of the International Society of Electrophysiological Kinesiology* 24: 18-24, 2014.

228. Keorochana G, Taghavi CE, Lee KB, Yoo JH, Liao JC, Fei Z, and Wang JC. Effect of sagittal alignment on kinematic changes and degree of disc degeneration in the lumbar spine: an analysis using positional MRI. *Spine* 36: 893-898, 2011.

229. Kesavachandran CN, Haamann F, and Nienhaus A. Radiation exposure of eyes, thyroid gland and hands in orthopaedic staff: a systematic review. *European journal of medical research* 17: 28, 2012.

230. Kiesel KB, Uhl TL, Underwood FB, Rodd DW, and Nitz AJ. Measurement of lumbar multifidus muscle contraction with rehabilitative ultrasound imaging. *Manual therapy* 12: 161-166, 2007.

231. Kirkaldy-Willis W, and Farfan H. Instability of the lumbar spine. *Clinical orthopaedics and related research* 165: 110-123, 1982.

232. Kirkaldy-Willis WH, and Farfan HF. Instability of the lumbar spine. *Clinical orthopaedics and related research* 110-123, 1982.

233. Kjos BO, Ehman RL, and Brant-Zawadzki M. Reproducibility of T1 and T2 relaxation times calculated from routine MR imaging sequences: phantom study. *AJR American journal of roentgenology* 144: 1157-1163, 1985.

234. Knutsson F. The instability associated with disk degeneration in the lumbar spine. *Acta Radiologica [Old Series]* 25: 593-609, 1944.

235. Kong MH, Hymanson HJ, Song KY, Chin DK, Cho YE, Yoon DH, and Wang JC. Kinetic magnetic resonance imaging analysis of abnormal segmental motion of the functional spine unit. *Journal of neurosurgery Spine* 10: 357-365, 2009.

236. Kong MH, Morishita Y, He W, Miyazaki M, Zhang H, Wu G, Hymanson HJ, and Wang JC. Lumbar segmental mobility according to the grade of the disc, the facet joint, the muscle, and the ligament pathology by using kinetic magnetic resonance imaging. *Spine* 34: 2537-2544, 2009.

237. Koshland G, and Hasan Z. Electromyographic responses to a mechanical perturbation applied during impending arm movements in different directions: one-joint and two-joint conditions. *Experimental brain research* 132: 485-499, 2000.

238. Koumantakis GA, Winstanley J, and Oldham JA. Thoracolumbar proprioception in individuals with and without low back pain: intratester reliability, clinical applicability, and validity. *The Journal of orthopaedic and sports physical therapy* 32: 327-335, 2002.

239. Kovacs FM, Seco J, Royuela A, Corcoll Reixach J, Abraira V, and Spanish Back Pain Research N. Predicting the evolution of low back pain patients in routine clinical practice: results from a registry within the Spanish National Health Service. *The spine journal : official journal of the North American Spine Society* 12: 1008-1020, 2012.

240. Kozanek M, Wang S, Passias PG, Xia Q, Li G, Bono CM, Wood KB, and Li G. Range of motion and orientation of the lumbar facet joints in vivo. *Spine* 34: E689-696, 2009.

241. Kulig K, Powers CM, Landel RF, Chen H, Fredericson M, Guillet M, and Butts K. Segmental lumbar mobility in individuals with low back pain: in vivo assessment during manual and self-imposed motion using dynamic MRI. *BMC musculoskeletal disorders* 8: 8, 2007.

242. Kuslich SD, Ulstrom CL, and Michael CJ. The tissue origin of low back pain and sciatica: a report of pain response to tissue stimulation during operations on the lumbar spine using local anesthesia. *The Orthopedic clinics of North America* 22: 181-187, 1991.

243. Kwok AW, Wang YX, Griffith JF, Deng M, Leung JC, Ahuja AT, and Leung PC. Morphological changes of lumbar vertebral bodies and intervertebral discs associated with decrease in bone mineral density of the spine: a cross-sectional study in elderly subjects. *Spine* 37: E1415-1421, 2012.

244. Lad SP, Huang KT, Bagley JH, Hazzard MA, Babu R, Owens TR, Ugiliweneza B, Patil CG, and Boakye M. Disparities in the outcomes of lumbar spinal stenosis surgery based on insurance status. *Spine* 38: 1119-1127, 2013.

245. Lai JY, Dai WL, Syu CB, Shih KS, Wang WT, and Lin SC. A new registration method for three-dimensional knee nearthrosis model using two X-ray images. *Computer methods in biomechanics and biomedical engineering* 13: 265-278, 2010.

246. Landel R, Kulig K, Fredericson M, Li B, and Powers CM. Intertester reliability and validity of motion assessments during lumbar spine accessory motion testing. *Physical therapy* 88: 43-49, 2008.

247. Lariviere C, Gagnon D, and Loisel P. A biomechanical comparison of lifting techniques between subjects with and without chronic low back pain during freestyle lifting and lowering tasks. *Clinical biomechanics* 17: 89-98, 2002.

248. Larivière C, Gagnon D, and Loisel P. The comparison of trunk muscles EMG activation between subjects with and without chronic low back pain during flexion-extension and lateral bending tasks. *Journal of electromyography and kinesiology : official journal of the International Society of Electrophysiological Kinesiology* 10: 79-91, 2000.

249. Latash ML, and Zatsiorsky VM. Joint stiffness: Myth or reality? *Human movement science* 12: 653-692, 1993.

250. Latini G, Dipaola L, Mantovani A, and Picano E. Reproductive effects of low-to-moderate medical radiation exposure. *Current medicinal chemistry* 19: 6171-6177, 2012.

251. Leardini A, Chiari L, Della Croce U, and Cappozzo A. Human movement analysis using stereophotogrammetry. Part 3. Soft tissue artifact assessment and compensation. *Gait & posture* 21: 212-225, 2005.

252. Lebow RL, Adogwa O, Parker SL, Sharma A, Cheng J, and Mcgirt MJ. Asymptomatic same-site recurrent disc herniation after lumbar discectomy: results of a prospective longitudinal study with 2-year serial imaging. *Spine* 36: 2147-2151, 2011.

253. Lee BW, Lee JE, Lee SH, and Kwon HK. Kinematic analysis of the lumbar spine by digital videofluoroscopy in 18 asymptomatic subjects and 9 patients with herniated nucleus pulposus. *Journal of manipulative and physiological therapeutics* 34: 221-230, 2011.

254. Lee SH, Daffner SD, Wang JC, Davis BC, Alanay A, and Kim JS. The change of whole lumbar segmental motion according to the mobility of degenerated disc in the lower lumbar spine: a kinetic MRI study. *European spine journal : official publication of the European Spine Society, the European Spinal Deformity Society, and the European Section of the Cervical Spine Research Society* 2014.

255. Lee SW, Wong KW, Chan MK, Yeung HM, Chiu JL, and Leong JC. Development and validation of a new technique for assessing lumbar spine motion. *Spine* 27: E215-220, 2002.

256. Li G, Wang S, Passias P, Xia Q, Li G, and Wood K. Segmental in vivo vertebral motion during functional human lumbar spine activities. *European spine journal : official publication of the European Spine Society, the European Spinal Deformity Society, and the European Section of the Cervical Spine Research Society* 18: 1013-1021, 2009.

257. Li G, Wuerz TH, and Defrate LE. Feasibility of using orthogonal fluoroscopic images to measure in vivo joint kinematics. *Journal of biomechanical engineering* 126: 314-318, 2004.

258. Licciardone JC, Gatchel R, and Dagenais S. Assessment and management of back pain. *JAMA internal medicine* 174: 478-479, 2014.

259. Lin JJ, Shih C, and Lin GY. Lumbar zygapophyseal joint injections in patients with chronic lower back pain. *Journal of the neurological sciences* 238: S500-S500, 2005.

260. Lipson SJ, and Muir H. 1980 Volvo award in basic science. Proteoglycans in experimental intervertebral disc degeneration. *Spine* 6: 194-210, 1981.

261. Loeb GE. Motoneurone task groups: coping with kinematic heterogeneity. *The Journal of experimental biology* 115: 137-146, 1985.

262. Lovely TJ, and Rastogi P. The value of provocative facet blocking as a predictor of success in lumbar spine fusion. *Journal of spinal disorders* 10: 512-517, 1997.

263. Luoto S, Taimela S, Hurri H, and Alaranta H. Mechanisms explaining the association between low back trouble and deficits in information processing. A controlled study with follow-up. *Spine* 24: 255-261, 1999.

264. Lurie JD, Doman DM, Spratt KF, Tosteson AN, and Weinstein JN. Magnetic resonance imaging interpretation in patients with symptomatic lumbar spine disc herniations: comparison of clinician and radiologist readings. *Spine* 34: 701-705, 2009.

265. Lurie JD, Moses RA, Tosteson AN, Tosteson TD, Carragee EJ, Carrino JA, Kaiser JA, and Herzog RJ. Magnetic resonance imaging predictors of surgical outcome in patients with lumbar intervertebral disc herniation. *Spine* 38: 1216-1225, 2013.

266. Lyons G, Eisenstein SM, and Sweet MB. Biochemical changes in intervertebral disc degeneration. *Biochimica et biophysica acta* 673: 443-453, 1981.

267. Macdonald DA, Moseley GL, and Hodges PW. The lumbar multifidus: does the evidence support clinical beliefs? *Manual therapy* 11: 254-263, 2006.

268. Macintosh JE, and Bogduk N. 1987 Volvo award in basic science. The morphology of the lumbar erector spinae. *Spine* 12: 658-668, 1987.

269. Macintosh JE, and Bogduk N. The attachments of the lumbar erector spinae. *Spine* 16: 783-792, 1991.

270. Macintosh JE, and Bogduk N. The biomechanics of the lumbar multifidus. *Clinical biomechanics* 1: 205-213, 1986.

271. Macintosh JE, Valencia F, Bogduk N, and Munro RR. The morphology of the human lumbar multifidus. *Clinical biomechanics* 1: 196-204, 1986.

272. Madanat R, Makinen TJ, Moritz N, Mattila KT, and Aro HT. Accuracy and precision of radiostereometric analysis in the measurement of three-dimensional micromotion in a fracture model of the distal radius. *Journal of orthopaedic research : official publication of the Orthopaedic Research Society* 23: 481-488, 2005.

273. Mahato NK. Disc spaces, vertebral dimensions, and angle values at the lumbar region: a radioanatomical perspective in spines with L5-S1 transitions Clinical article. *J Neurosurg-Spine* 15: 371-379, 2011.

274. Mahato NK, Montuelle S, Cotton J, Williams S, Thomas J, and Clark B. Development of a morphology-based modeling technique for tracking solid-body displacements: examining the reliability of a potential MRI-only approach for joint kinematics assessment. *BMC Med Imaging* 16: 38, 2016.

275. Mahato NK, Sybert D, Law T, and Clark B. Effects of spine loading in a patient with post-decompression lumbar disc herniation: observations using an open weight-

bearing MRI. *European spine journal : official publication of the European Spine Society, the European Spinal Deformity Society, and the European Section of the Cervical Spine Research Society* 2016.

276. Manchikanti L, Singh V, Falco FJ, Benyamin RM, and Hirsch JA. Epidemiology of low back pain in adults. *Neuromodulation : journal of the International Neuromodulation Society* 17 Suppl 2: 3-10, 2014.

277. Manniche C, Lundberg E, Christensen I, Bentzen L, and Hesselsoe G. Intensive dynamic back exercises for chronic low back pain: a clinical trial. *Pain* 47: 53-63, 1991.

278. Mannion AF. Fibre type characteristics and function of the human paraspinal muscles: normal values and changes in association with low back pain. *Journal of electromyography and kinesiology : official journal of the International Society of Electrophysiological Kinesiology* 9: 363-377, 1999.

279. Mannion AF, Dumas GA, Cooper RG, Espinosa FJ, Faris MW, and Stevenson JM. Muscle fibre size and type distribution in thoracic and lumbar regions of erector spinae in healthy subjects without low back pain: normal values and sex differences. *Journal of anatomy* 190 (Pt 4): 505-513, 1997.

280. March L, Smith EU, Hoy DG, Cross MJ, Sanchez-Riera L, Blyth F, Buchbinder R, Vos T, and Woolf AD. Burden of disability due to musculoskeletal (MSK) disorders. *Best practice & research Clinical rheumatology* 28: 353-366, 2014.

281. Maroudas A. Biophysical chemistry of cartilaginous tissues with special reference to solute and fluid transport. *Biorheology* 12: 233-248, 1975.

282. Marras WS, and Sommerich CM. A three-dimensional motion model of loads on the lumbar spine: II. Model validation. *Human factors* 33: 139-149, 1991.

283. Martin DE, Greco NJ, Klatt BA, Wright VJ, Anderst WJ, and Tashman S. Model-based tracking of the hip: implications for novel analyses of hip pathology. *The Journal of arthroplasty* 26: 88-97, 2011.

284. Mattila M, Hurme M, Alaranta H, Paljärvi L, Kalimo H, Falck B, Lehto M, Einola S, and Järvinen M. The multifidus muscle in patients with lumbar disc herniation. A histochemical and morphometric analysis of intraoperative biopsies. *Spine* 11: 732-738, 1986.

285. Mayer JM, Graves JE, Clark BC, Formikell M, and Ploutz-Snyder LL. The use of magnetic resonance imaging to evaluate lumbar muscle activity during trunk extension exercise at varying intensities. *Spine* 30: 2556-2563, 2005.

286. Mayer JM, Graves JE, Udermann BE, and Ploutz-Snyder LL. Quantification of the loading characteristics of the upper body and back extension strength on a variable angle Roman chair. *Journal of back and musculoskeletal rehabilitation* 16: 95-104, 2002.

287. Mayer TG, Smith SS, Keeley J, and Mooney V. Quantification of lumbar function. Part 2: Sagittal plane trunk strength in chronic low-back pain patients. *Spine* 10: 765-772, 1985.

288. Mccall IW, Park WM, and O'brien JP. Induced pain referral from posterior lumbar elements in normal subjects. *Spine* 4: 441-446, 1979.

289. Mcgill S, Juker D, and Kropf P. Appropriately placed surface EMG electrodes reflect deep muscle activity (psoas, quadratus lumborum, abdominal wall) in the lumbar spine. *Journal of biomechanics* 29: 1503-1507, 1996.

290. Mcgill SM. The biomechanics of low back injury: implications on current practice in industry and the clinic. *Journal of biomechanics* 30: 465-475, 1997.

291. Mcgill SM. Electromyographic activity of the abdominal and low back musculature during the generation of isometric and dynamic axial trunk torque: implications for lumbar mechanics. *Journal of orthopaedic research : official publication of the Orthopaedic Research Society* 9: 91-103, 1991.

292. Mcgill SM, and Cholewicki J. Biomechanical basis for stability: an explanation to enhance clinical utility. *The Journal of orthopaedic and sports physical therapy* 31: 96-100, 2001.

293. Mcgill SM, Grenier S, Kavcic N, and Cholewicki J. Coordination of muscle activity to assure stability of the lumbar spine. *Journal of electromyography and kinesiology : official journal of the International Society of Electrophysiological Kinesiology* 13: 353-359, 2003.

294. Mcgregor AH, Anderton L, Gedroyc WM, Johnson J, and Hughes SP. The use of interventional open MRI to assess the kinematics of the lumbar spine in patients with spondylolisthesis. *Spine* 27: 1582-1586, 2002.

295. Mcgregor AH, Anderton L, Gedroyc WMW, Johnson J, and Hughes SPF. Assessment of spinal kinematics using open interventional magnetic resonance imaging. *Clinical orthopaedics and related research* 341-348, 2001.

296. Mcgregor AH, Mccarthy ID, Dore CJ, and Hughes SP. Quantitative assessment of the motion of the lumbar spine in the low back pain population and the effect of different spinal pathologies of this motion. *European spine journal : official publication of the European Spine Society, the European Spinal Deformity Society, and the European Section of the Cervical Spine Research Society* 6: 308-315, 1997.

297. Meakin JR, Smith FW, Gilbert FJ, and Aspden RM. The effect of axial load on the sagittal plane curvature of the upright human spine in vivo. *Journal of biomechanics* 41: 2850-2854, 2008.

298. Mehta JS, Kochhar S, and Harding IJ. A slip above a slip: retrolisthesis of the motion segment above a spondylolytic spondylolisthesis. *European spine journal : official publication of the European Spine Society, the European Spinal Deformity*

Society, and the European Section of the Cervical Spine Research Society 21: 2128-2133, 2012.

299. Melchert UH, Schroder C, Brossmann J, and Muhle C. Motion-triggered cine MR imaging of active joint movement. *Magnetic resonance imaging* 10: 457-460, 1992.

300. Mellor FE, Thomas P, and Breen A. Moving back: The radiation dose received from lumbar spine quantitative fluoroscopy compared to lumbar spine radiographs with suggestions for dose reduction. *Radiography* 20: 251-257, 2014.

301. Mellor FE, Thomas PW, Thompson P, and Breen AC. Proportional lumbar spine inter-vertebral motion patterns: a comparison of patients with chronic, non-specific low back pain and healthy controls. *European spine journal : official publication of the European Spine Society, the European Spinal Deformity Society, and the European Section of the Cervical Spine Research Society* 23: 2059-2067, 2014.

302. Melrose J, Roberts S, Smith S, Menage J, and Ghosh P. Increased nerve and blood vessel ingrowth associated with proteoglycan depletion in an ovine anular lesion model of experimental disc degeneration. *Spine* 27: 1278-1285, 2002.

303. Milner-Brown HS, Stein RB, and Yemm R. The orderly recruitment of human motor units during voluntary isometric contractions. *The Journal of physiology* 230: 359-370, 1973.

304. Mimura M, Panjabi MM, Oxland TR, Crisco JJ, Yamamoto I, and Vasavada A. Disc degeneration affects the multidirectional flexibility of the lumbar spine. *Spine* 19: 1371-1380, 1994.

305. Miranda DL, Schwartz JB, Loomis AC, Brainerd EL, Fleming BC, and Crisco JJ. Static and dynamic error of a biplanar videoradiography system using marker-based and markerless tracking techniques. *Journal of biomechanical engineering* 133: 121002, 2011.

306. Mooney V, Gulick J, Perlman M, Levy D, Pozos R, Leggett S, and Resnick D. Relationships between myoelectric activity, strength, and MRI of lumbar extensor muscles in back pain patients and normal subjects. *Journal of spinal disorders* 10: 348-356, 1997.

307. Mooney V, and Robertson J. Facet Syndrome. *Clinical orthopaedics and related research* 149-156, 1976.

308. Moseley GL, Hodges PW, and Gandevia SC. Deep and superficial fibers of the lumbar multifidus muscle are differentially active during voluntary arm movements. *Spine* 27: E29-36, 2002.

309. Moseley GL, Nicholas MK, and Hodges PW. Does anticipation of back pain predispose to back trouble? *Brain : a journal of neurology* 127: 2339-2347, 2004.

310. Motiei-Langroudi R, Sadeghian H, and Seddighi AS. Clinical and magnetic resonance imaging factors which may predict the need for surgery in lumbar disc herniation. *Asian spine journal* 8: 446-452, 2014.

311. Muggleton JM, and Allen R. Insights into the measurement of vertebral translation in the sagittal plane. *Medical engineering & physics* 20: 21-32, 1998.

312. Muggleton JM, Kondracki M, and Allen R. Spinal fusion for lumbar instability: Does it have a scientific basis? *Journal of spinal disorders* 13: 200-204, 2000.

313. Muhle C, Brinkmann G, Brossmann J, Wesner F, and Heller M. Kinematic MR imaging of the ankle--initial results with ultra-fast sequence imaging. *Acta radiologica (Stockholm, Sweden : 1987)* 38: 885-889, 1997.

314. Muhle C, Brossmann J, and Heller M. Kinematic CT and MR imaging of the patellofemoral joint. *European radiology* 9: 508-518, 1999.

315. Myklebust JB, Pintar F, Yoganandan N, Cusick JF, Maiman D, Myers TJ, and Sances A. Tensile strength of spinal ligaments. *Spine* 13: 526-531, 1988.

316. Nachemson AL. Disc pressure measurements. *Spine* 6: 93-97, 1981.

317. Nachemson AL, Schultz AB, and Berkson MH. Mechanical properties of human lumbar spine motion segments. Influence of age, sex, disc level, and degeneration. *Spine* 4: 1-8, 1979.

318. Nada RM, Maal TJ, Breuning KH, Berge SJ, Mostafa YA, and Kuijpers-Jagtman AM. Accuracy and reproducibility of voxel based superimposition of cone beam computed tomography models on the anterior cranial base and the zygomatic arches. *PloS one* 6: e16520, 2011.

319. Nebergall AK, Rader K, Palm H, Malchau H, and Greene ME. Precision of radiostereometric analysis (RSA) of acetabular cup stability and polyethylene wear improved by adding tantalum beads to the liner. *Acta Orthopaedica* 86: 563-568, 2015.

320. Niggemann P, Kuchta J, Grosskurth D, Beyer HK, Hoeffer J, and Delank KS. Spondylolysis and isthmic spondylolisthesis: impact of vertebral hypoplasia on the use of the Meyerding classification. *Brit J Radiol* 85: 358-362, 2012.

321. Nitz AJ, and Peck D. Comparison of muscle spindle concentrations in large and small human epaxial muscles acting in parallel combinations. *The American surgeon* 52: 273-277, 1986.

322. North RB, Shipley J, Wang H, and Mekhail N. A review of economic factors related to the delivery of health care for chronic low back pain. *Neuromodulation : journal of the International Neuromodulation Society* 17 Suppl 2: 69-76, 2014.

323. Nyakatura JA, and Fischer MS. Functional morphology and three-dimensional kinematics of the thoraco-lumbar region of the spine of the two-toed sloth. *The Journal of experimental biology* 213: 4278-4290, 2010.

324. Nyakatura JA, and Fischer MS. Three-dimensional kinematic analysis of the pectoral girdle during upside-down locomotion of two-toed sloths (Choloepus didactylus, Linne 1758). *Frontiers in zoology* 7: 21, 2010.

325. O'sullivan P. Diagnosis and classification of chronic low back pain disorders: maladaptive movement and motor control impairments as underlying mechanism. *Manual therapy* 10: 242-255, 2005.

326. Oegema TR, Jr., Johnson SL, Aguiar DJ, and Ogilvie JW. Fibronectin and its fragments increase with degeneration in the human intervertebral disc. *Spine* 25: 2742-2747, 2000.

327. Ogston NG, King GJ, Gertzbein SD, Tile M, Kapasouri A, and Rubenstein JD. Centrode patterns in the lumbar spine. Baseline studies in normal subjects. *Spine* 11: 591-595, 1986.

328. Osti OL, Vernon-Roberts B, Moore R, and Fraser RD. Annular tears and disc degeneration in the lumbar spine. A post-mortem study of 135 discs. *The Journal of bone and joint surgery British volume* 74: 678-682, 1992.

329. Ostrofsky KR, and Churchill SE. Sex determination by discriminant function analysis of lumbar vertebrae. *J Forensic Sci* 60: 21-28, 2015.

330. Ozawa H, Kanno H, Koizumi Y, Morozumi N, Aizawa T, Kusakabe T, Ishii Y, and Itoi E. Dynamic changes in the dural sac cross-sectional area on axial loaded MR imaging: is there a difference between degenerative spondylolisthesis and spinal stenosis? *AJNR American journal of neuroradiology* 33: 1191-1197, 2012.

331. Paassilta P, Lohiniva J, Goring HH, Perala M, Raina SS, Karppinen J, Hakala M, Palm T, Kroger H, Kaitila I, Vanharanta H, Ott J, and Ala-Kokko L. Identification of a novel common genetic risk factor for lumbar disk disease. *Jama* 285: 1843-1849, 2001.

332. Pal GP, and Routal RV. Mechanism of change in the orientation of the articular process of the zygapophyseal joint at the thoracolumbar junction. *Journal of anatomy* 195 (Pt 2): 199-209, 1999.

333. Pal GP, and Routal RV. A study of weight transmission through the cervical and upper thoracic regions of the vertebral column in man. *Journal of anatomy* 148: 245-261, 1986.

334. Pal GP, and Routal RV. Transmission of weight through the lower thoracic and lumbar regions of the vertebral column in man. *Journal of anatomy* 152: 93-105, 1987.

335. Pal GP, Routal RV, and Saggu SK. The orientation of the articular facets of the zygapophyseal joints at the cervical and upper thoracic region. *Journal of anatomy* 198: 431-441, 2001.

336. Palepu V, Kodigudla M, and Goel VK. Biomechanics of disc degeneration. *Advances in orthopedics* 2012: 726210, 2012.

337. Panjabi M, Chang D, and Dvorak J. An analysis of errors in kinematic parameters associated with in vivo functional radiographs. *Spine* 17: 200-205, 1992.

338. Panjabi MM. Clinical spinal instability and low back pain. *Journal of Electromyography and Kinesiology* 13: 371-379, 2003.

339. Panjabi MM. A hypothesis of chronic back pain: ligament subfailure injuries lead to muscle control dysfunction. *European spine journal : official publication of the European Spine Society, the European Spinal Deformity Society, and the European Section of the Cervical Spine Research Society* 15: 668-676, 2006.

340. Panjabi MM. The stabilizing system of the spine. Part I. Function, dysfunction, adaptation, and enhancement. *Journal of spinal disorders* 5: 383-389; discussion 397, 1992.

341. Panjabi MM. The stabilizing system of the spine. Part II. Neutral zone and instability hypothesis. *Journal of spinal disorders* 5: 390-396; discussion 397, 1992.

342. Panjabi MM, Krag MH, and Chung TQ. Effects of disc injury on mechanical behavior of the human spine. *Spine* 9: 707-713, 1984.

343. Parthan A, Evans CJ, and Le K. Chronic low back pain: epidemiology, economic burden and patient-reported outcomes in the USA. *Expert review of pharmacoeconomics & outcomes research* 6: 359-369, 2006.

344. Passias PG, Wang S, Kozanek M, Xia Q, Li W, Grottkau B, Wood KB, and Li G. Segmental lumbar rotation in patients with discogenic low back pain during functional weight-bearing activities. *The Journal of bone and joint surgery American volume* 93: 29-37, 2011.

345. Patwardhan AG, Havey RM, Carandang G, Simonds J, Voronov LI, Ghanayem AJ, Meade KP, Gavin TM, and Paxinos O. Effect of compressive follower preload on the flexion-extension response of the human lumbar spine. *Journal of orthopaedic research : official publication of the Orthopaedic Research Society* 21: 540-546, 2003.

346. Pearcy M, Portek I, and Shepherd J. Three-dimensional x-ray analysis of normal movement in the lumbar spine. *Spine* 9: 294-297, 1984.

347. Pearcy MJ. Stereo radiography of lumbar spine motion. *Acta Orthop Scand Suppl* 212: 1-45, 1985.

348. Pearcy MJ, and Bogduk N. Instantaneous axes of rotation of the lumbar intervertebral joints. *Spine* 13: 1033-1041, 1988.

349. Pearcy MJ, and Hindle RJ. New method for the non-invasive three-dimensional measurement of human back movement. *Clinical biomechanics* 4: 73-79, 1989.

350. Pearcy MJ, and Whittle MW. Movements of the lumbar spine measured by three-dimensional X-ray analysis. *Journal of biomedical engineering* 4: 107-112, 1982.

351. Pearson AM, Spratt KF, Genuario J, Mcgough W, Kosman K, Lurie J, and Sengupta DK. Precision of lumbar intervertebral measurements: does a computer-assisted technique improve reliability? *Spine* 36: 572-580, 2011.

352. Peloquin JM, Yoder JH, Jacobs NT, Moon SM, Wright AC, Vresilovic EJ, and Elliott DM. Human L3L4 intervertebral disc mean 3-D shape, modes of variation, and their relationship to degeneration. *Journal of biomechanics* 47: 2452-2459, 2014.

353. Penning L. Psoas muscle and lumbar spine stability: a concept uniting existing controversies. Critical review and hypothesis. *European spine journal : official publication of the European Spine Society, the European Spinal Deformity Society, and the European Section of the Cervical Spine Research Society* 9: 577-585, 2000.

354. Pette D, and Staron RS. Myosin isoforms, muscle fiber types, and transitions. *Microsc Res Tech* 50: 500-509, 2000.

355. Ploutz-Snyder LL, Tesch PA, Crittenden DJ, and Dudley GA. Effect of unweighting on skeletal muscle use during exercise. *Journal of applied physiology* 79: 168-175, 1995.

356. Pollintine P, Dolan P, Tobias JH, and Adams MA. Intervertebral disc degeneration can lead to "stress-shielding" of the anterior vertebral body: a cause of osteoporotic vertebral fracture? *Spine* 29: 774-782, 2004.

357. Pollintine P, Luo J, Offa-Jones B, Dolan P, and Adams MA. Bone creep can cause progressive vertebral deformity. *Bone* 45: 466-472, 2009.

358. Pollintine P, Przybyla AS, Dolan P, and Adams MA. Neural arch load-bearing in old and degenerated spines. *Journal of biomechanics* 37: 197-204, 2004.

359. Pope MH, Frymoyer JW, and Krag MH. Diagnosing instability. *Clinical orthopaedics and related research* 60-67, 1992.

360. Pope MH, and Panjabi M. Biomechanical definitions of spinal instability. *Spine* 10: 255-256, 1985.

361. Pope MH, Pflaster DS, and Krag MH. Biomechanics of lumbar disk disease. *Instructional course lectures* 41: 187-192, 1992.

362. Pope MH, Wilder DG, Stokes IA, and Frymoyer JW. Biomechanical testing as an aid to decision making in low-back pain patients. *Spine* 4: 135-140, 1979.

363. Portek I, Pearcy MJ, Reader GP, and Mowat AG. Correlation between radiographic and clinical measurement of lumbar spine movement. *British journal of rheumatology* 22: 197-205, 1983.

364. Potvin JR, and O'brien PR. Trunk muscle co-contraction increases during fatiguing, isometric, lateral bend exertions. Possible implications for spine stability. *Spine* 23: 774-780; discussion 781, 1998.

365. Price TB, Kamen G, Damon BM, Knight CA, Applegate B, Gore JC, Eward K, and Signorile JF. Comparison of MRI with EMG to study muscle activity associated with dynamic plantar flexion. *Magnetic resonance imaging* 21: 853-861, 2003.

366. Quick HH, Ladd ME, Hoevel M, Bosk S, Debatin JF, Laub G, and Schroeder T. Real-time MRI of joint movement with TrueFISP. *J Magn Reson Imaging* 15: 710-715, 2002.

367. Radebold A, Cholewicki J, Panjabi MM, and Patel TC. Muscle response pattern to sudden trunk loading in healthy individuals and in patients with chronic low back pain. *Spine* 25: 947-954, 2000.

368. Raj PP. Intervertebral disc: anatomy-physiology-pathophysiology-treatment. *Pain practice : the official journal of World Institute of Pain* 8: 18-44, 2008.

369. Rantanen J, Rissanen A, and Kalimo H. Lumbar muscle fiber size and type distribution in normal subjects. *European spine journal : official publication of the European Spine Society, the European Spinal Deformity Society, and the European Section of the Cervical Spine Research Society* 3: 331-335, 1994.

370. Raue U, Trappe TA, Estrem ST, Qian HR, Helvering LM, Smith RC, and Trappe S. Transcriptome signature of resistance exercise adaptations: mixed muscle and fiber type specific profiles in young and old adults. *Journal of applied physiology* 112: 1625-1636, 2012.

371. Rebmann AJ, and Sheehan FT. Precise 3-D skeletal kinematics using fast phase contrast magnetic resonance imaging. *J Magn Reson Imaging* 17: 206-213, 2003.

372. Reeves NP, and Cholewicki J. Expanding our view of the spine system. *European spine journal : official publication of the European Spine Society, the European Spinal Deformity Society, and the European Section of the Cervical Spine Research Society* 19: 331-332, 2010.

373. Reeves NP, and Cholewicki J. Modeling the human lumbar spine for assessing spinal loads, stability, and risk of injury. *Critical reviews in biomedical engineering* 31: 73-139, 2003.

374. Reeves NP, Cholewicki J, and Milner TE. Muscle reflex classification of low-back pain. *Journal of electromyography and kinesiology : official journal of the International Society of Electrophysiological Kinesiology* 15: 53-60, 2005.

375. Reeves NP, Cholewicki J, and Narendra KS. Effects of reflex delays on postural control during unstable seated balance. *Journal of biomechanics* 42: 164-170, 2009.

376. Reeves NP, Narendra KS, and Cholewicki J. Spine stability: lessons from balancing a stick. *Clinical biomechanics* 26: 325-330, 2011.

377. Reeves NP, Narendra KS, and Cholewicki J. Spine stability: the six blind men and the elephant. *Clinical biomechanics* 22: 266-274, 2007.

378. Reinschmidt C, Van Den Bogert AJ, Nigg BM, Lundberg A, and Murphy N. Effect of skin movement on the analysis of skeletal knee joint motion during running. *Journal of biomechanics* 30: 729-732, 1997.

379. Revel M, Poiraudeau S, Auleley GR, Payan C, Denke A, Nguyen M, Chevrot A, and Fermanian J. Capacity of the clinical picture to characterize low back pain relieved by facet joint anesthesia. Proposed criteria to identify patients with painful facet joints. *Spine* 23: 1972-1976; discussion 1977, 1998.

380. Rhoad RC, Klimkiewicz JJ, Williams GR, Kesmodel SB, Udupa JK, Kneeland JB, and Iannotti JP. A new in vivo technique for three-dimensional shoulder kinematics analysis. *Skeletal radiology* 27: 92-97, 1998.

381. Richardson SM, Walker RV, Parker S, Rhodes NP, Hunt JA, Freemont AJ, and Hoyland JA. Intervertebral disc cell-mediated mesenchymal stem cell differentiation. *Stem cells* 24: 707-716, 2006.

382. Risch SV, Norvell NK, Pollock ML, Risch ED, Langer H, Fulton M, Graves JE, and Leggett SH. Lumbar strengthening in chronic low back pain patients. Physiologic and psychological benefits. *Spine* 18: 232-238, 1993.

383. Roberts S, Eisenstein SM, Menage J, Evans EH, and Ashton IK. Mechanoreceptors in intervertebral discs. Morphology, distribution, and neuropeptides. *Spine* 20: 2645-2651, 1995.

384. Roberts S, Urban JP, Evans H, and Eisenstein SM. Transport properties of the human cartilage endplate in relation to its composition and calcification. *Spine* 21: 415-420, 1996.

385. Rodriguez-Soto AE, Jaworski R, Jensen A, Niederberger B, Hargens AR, Frank LR, Kelly KR, and Ward SR. Effect of load carriage on lumbar spine kinematics. *Spine* 38: E783-791, 2013.

386. Ryd L, Yuan X, and Lofgren H. Methods for determining the accuracy of radiostereometric analysis (RSA). *Acta Orthop Scand* 71: 403-408, 2000.

387. Saltin B, Bangsbo J, Graham TE, and Johansen L. Metabolism and Performance in Exhaustive Intense Exercise - Different Effects of Muscle Glycogen Availability, Previous Exercise and Muscle Acidity. *Med Sport Sci* 34: 87-114, 1992.

388. Sapsford RR, and Hodges PW. Contraction of the pelvic floor muscles during abdominal maneuvers. *Arch Phys Med Rehabil* 82: 1081-1088, 2001.

389. Sato K, Wakamatsu E, Yoshizumi A, Watanabe N, and Irei O. The configuration of the laminas and facet joints in degenerative spondylolisthesis. A clinicoradiologic study. *Spine* 14: 1265-1271, 1989.

390. Schaefer C, Sadosky A, Mann R, Daniel S, Parsons B, Tuchman M, Anschel A, Stacey BR, Nalamachu S, and Nieshoff E. Pain severity and the economic burden of neuropathic pain in the United States: BEAT Neuropathic Pain Observational Study. *ClinicoEconomics and outcomes research : CEOR* 6: 483-496, 2014.

391. Schneider G, Pearcy MJ, and Bogduk N. Abnormal motion in spondylolytic spondylolisthesis. *Spine* 30: 1159-1164, 2005.

392. Schueler BA. The AAPM/RSNA physics tutorial for residents: general overview of fluoroscopic imaging. *Radiographics : a review publication of the Radiological Society of North America, Inc* 20: 1115-1126, 2000.

393. Schwarzer AC, Aprill CN, Derby R, Fortin J, Kine G, and Bogduk N. The false-positive rate of uncontrolled diagnostic blocks of the lumbar zygapophysial joints. *Pain* 58: 195-200, 1994.

394. Schwarzer AC, Aprill CN, Derby R, Fortin J, Kine G, and Bogduk N. The Relative Contributions of the Disc and Zygapophyseal Joint in Chronic Low-Back-Pain. *Spine* 19: 801-806, 1994.

395. Schwarzer AC, Wang SC, Bogduk N, Mcnaught PJ, and Laurent R. Prevalence and clinical features of lumbar zygapophysial joint pain: a study in an Australian population with chronic low back pain. *Annals of the rheumatic diseases* 54: 100-106, 1995.

396. Schwarzer AC, Wang SC, O'driscoll D, Harrington T, Bogduk N, and Laurent R. The ability of computed tomography to identify a painful zygapophysial joint in patients with chronic low back pain. *Spine* 20: 907-912, 1995.

397. Selvik G. Roentgen stereophotogrammetric analysis. *Acta radiologica (Stockholm, Sweden : 1987)* 31: 113-126, 1990.

398. Shaffer WO, Spratt KF, Weinstein J, Lehmann TR, and Goel V. 1990 Volvo Award in clinical sciences. The consistency and accuracy of roentgenograms for measuring sagittal translation in the lumbar vertebral motion segment. An experimental model. *Spine* 15: 741-750, 1990.

399. Sheehan FT, Zajac FE, and Drace JE. In vivo tracking of the human patella using cine phase contrast magnetic resonance imaging. *Journal of biomechanical engineering* 121: 650-656, 1999.

400. Shellock FG, Mink JH, Deutsch A, and Pressman BD. Kinematic magnetic resonance imaging of the joints: techniques and clinical applications. *Magnetic resonance quarterly* 7: 104-135, 1991.

401. Shin JH, Wang S, Yao Q, Wood KB, and Li G. Investigation of coupled bending of the lumbar spine during dynamic axial rotation of the body. *European spine journal : official publication of the European Spine Society, the European Spinal Deformity Society, and the European Section of the Cervical Spine Research Society* 22: 2671-2677, 2013.

402. Shirazi-Adl A. Strain in fibers of a lumbar disc. Analysis of the role of lifting in producing disc prolapse. *Spine* 14: 96-103, 1989.

403. Sihvonen T, Partanen J, and Hanninen O. Averaged (rms) surface EMG in testing back function. *Electromyography and clinical neurophysiology* 28: 335-339, 1988.

404. Silfies SP, Cholewicki J, Reeves NP, and Greene HS. Lumbar position sense and the risk of low back injuries in college athletes: a prospective cohort study. *BMC musculoskeletal disorders* 8: 129, 2007.

405. Smith E, Hoy DG, Cross M, Vos T, Naghavi M, Buchbinder R, Woolf AD, and March L. The global burden of other musculoskeletal disorders: estimates from the Global Burden of Disease 2010 study. *Annals of the rheumatic diseases* 73: 1462-1469, 2014.

406. Soderberg GL, and Barr JO. Muscular function in chronic low-back dysfunction. *Spine* 8: 79-85, 1983.

407. Spottiswoode BS, Zhong X, Lorenz CH, Mayosi BM, Meintjes EM, and Epstein FH. Motion-guided segmentation for cine DENSE MRI. *Medical image analysis* 13: 105-115, 2009.

408. Staron RS, Hagerman FC, Hikida RS, Murray TF, Hostler DP, Crill MT, Ragg KE, and Toma K. Fiber Type Composition of the Vastus Lateralis Muscle of Young Men and Women. *Journal of Histochemistry & Cytochemistry* 48: 623-629, 2000.

409. Staron RS, Hikida RS, Hagerman FC, Dudley GA, and Murray TF. Human skeletal muscle fiber type adaptability to various workloads. *Journal of Histochemistry & Cytochemistry* 32: 146-152, 1984.

410. Staron RS, Hikida RS, Hagerman FC, Dudley GA, and Murray TF. Human skeletal muscle fiber type adaptability to various workloads. *J Histochem Cytochem* 32: 146-152, 1984.

411. Staron RS, and Johnson P. Myosin polymorphism and differential expression in adult human skeletal muscle. *Comp Biochem Physiol B* 106: 463-475, 1993.

412. Stephens JA, and Stuart DG. The motor units of cat medial gastrocnemius: speed-size relations and their significance for the recruitment order of mortor units. *Brain research* 91: 177-195, 1975.

413. Stokes IA, and Frymoyer JW. Segmental motion and instability. *Spine* 12: 688-691, 1987.

414. Stokes IA, and Gardner-Morse M. Stability increase of the lumbar spine with different muscle groups: a biomechanical in vitro study. *Spine* 20: 2168-2169, 1995.

415. Stokes IA, Gardner-Morse MG, and Henry SM. Abdominal muscle activation increases lumbar spinal stability: analysis of contributions of different muscle groups. *Clinical biomechanics* 26: 797-803, 2011.

416. Stokes IA, Henry SM, and Single RM. Surface EMG electrodes do not accurately record from lumbar multifidus muscles. *Clinical biomechanics* 18: 9-13, 2003.

417. Stokes IA, and Iatridis JC. Mechanical conditions that accelerate intervertebral disc degeneration: overload versus immobilization. *Spine* 29: 2724-2732, 2004.

418. Stokes IA, Wilder DG, Frymoyer JW, and Pope MH. 1980 Volvo award in clinical sciences. Assessment of patients with low-back pain by biplanar radiographic measurement of intervertebral motion. *Spine* 6: 233-240, 1981.

419. Stokes MJ, Cooper RG, Morris G, and Jayson MI. Selective changes in multifidus dimensions in patients with chronic low back pain. *European spine journal : official publication of the European Spine Society, the European Spinal Deformity Society, and the European Section of the Cervical Spine Research Society* 1: 38-42, 1992.

420. Suk KS, Lee HM, Moon SH, and Kim NH. Recurrent lumbar disc herniation: results of operative management. *Spine* 26: 672-676, 2001.

421. Swartz KR, and Trost GR. Recurrent lumbar disc herniation. *Neurosurg Focus* 15: E10, 2003.

422. Szpalski M, Gunzburg R, and Mayer M. Spine arthroplasty: a historical review. *European spine journal : official publication of the European Spine Society, the European Spinal Deformity Society, and the European Section of the Cervical Spine Research Society* 11 Suppl 2: S65-84, 2002.

423. Szypryt EP, Twining P, Wilde GP, Mulholland RC, and Worthington BS. Diagnosis of lumbar disc protrusion. A comparison between magnetic resonance imaging and radiculography. *The Journal of bone and joint surgery British volume* 70: 717-722, 1988.

424. Taghipour-Darzi M, Ebrahimi-Takamjani E, Salavati M, Mobini B, and Zekavat H. Reliability of quality measures of movement in lumbar spine flexion-extension radiography. *Journal of back and musculoskeletal rehabilitation* 22: 149-156, 2009.

425. Taimela S, Kankaanpää M, and Luoto S. The effect of lumbar fatigue on the ability to sense a change in lumbar position. A controlled study. *Spine* 24: 1322-1327, 1999.

426. Tan Y, Aghdasi BG, Montgomery SR, Inoue H, Lu C, and Wang JC. Kinetic magnetic resonance imaging analysis of lumbar segmental mobility in patients without significant spondylosis. *European spine journal : official publication of the European Spine Society, the European Spinal Deformity Society, and the European Section of the Cervical Spine Research Society* 21: 2673-2679, 2012.

427. Taneja R, Dighe M, Kanal KM, Richardson ML, Mitsumori LM, and Dubinsky TJ. Utility of multiplanar and three-dimensional reconstructions from computed tomography performed for maternal indications for visualizing fetal anatomy and estimating gestational age. *Journal of computer assisted tomography* 35: 446-453, 2011.

428. Tarantino U, Fanucci E, Iundusi R, Celi M, Altobelli S, Gasbarra E, Simonetti G, and Manenti G. Lumbar spine MRI in upright position for diagnosing acute and chronic low back pain: statistical analysis of morphological changes. *Journal of orthopaedics and traumatology : official journal of the Italian Society of Orthopaedics and Traumatology* 14: 15-22, 2013.

429. Tashman S, Kolowich P, Collon D, Anderson K, and Anderst W. Dynamic function of the ACL-reconstructed knee during running. *Clinical orthopaedics and related research* 454: 66-73, 2007.

430. Taylor J, and Twomey L. Sagittal and horizontal plane movement of the human lumbar vertebral column in cadavers and in the living. *Rheumatology and rehabilitation* 19: 223-232, 1980.

431. Tersi L, and Stagni R. Effect of calibration error on bone tracking accuracy with fluoroscopy. *J Biomech Eng* 136: 054502, 2014.

432. Tessitore E, Molliqaj G, Schatlo B, and Schaller K. Clinical evaluation and surgical decision making for patients with lumbar discogenic pain and facet syndrome. *European journal of radiology* 84: 765-770, 2015.

433. Teyhen DS, Flynn TW, Bovik AC, and Abraham LD. A new technique for digital fluoroscopic video assessment of sagittal plane lumbar spine motion. *Spine* 30: E406-413, 2005.

434. Teyhen DS, Flynn TW, Childs JD, Kuklo TR, Rosner MK, Polly DW, and Abraham LD. Fluoroscopic video to identify aberrant lumbar motion. *Spine* 32: E220-229, 2007.

435. Thelen DG, Ashton-Miller JA, and Schultz AB. Lumbar muscle activities in rapid three-dimensional pulling tasks. *Spine* 21: 605-613, 1996.

436. Thelen DG, Schultz AB, and Ashton-Miller JA. Co-contraction of lumbar muscles during the development of time-varying triaxial moments. *Journal of orthopaedic research : official publication of the Orthopaedic Research Society* 13: 390-398, 1995.

437. Thomas JS, and France CR. The relationship between pain-related fear and lumbar flexion during natural recovery from low back pain. *European spine journal : official publication of the European Spine Society, the European Spinal Deformity Society, and the European Section of the Cervical Spine Research Society* 17: 97-103, 2008.

438. Thomas JS, France CR, Lavender SA, and Johnson MR. Effects of fear of movement on spine velocity and acceleration after recovery from low back pain. *Spine* 33: 564-570, 2008.

439. Thomas JS, Lavender SA, Corcos DM, and Andersson GB. Trunk kinematics and trunk muscle activity during a rapidly applied load. *Journal of electromyography and kinesiology : official journal of the International Society of Electrophysiological Kinesiology* 8: 215-225, 1998.

440. Thorstensson A, and Carlson H. Fibre types in human lumbar back muscles. *Acta Physiol Scand* 131: 195-202, 1987.

441. Todorov E, and Jordan MI. Optimal feedback control as a theory of motor coordination. *Nature neuroscience* 5: 1226-1235, 2002.

442. Trozzi C, Kaptein BL, Garling EH, Shelyakova T, Russo A, Bragonzoni L, and Martelli S. Precision assessment of model-based RSA for a total knee prosthesis in a biplanar set-up. *The Knee* 15: 396-402, 2008.

443. Tucci JT, Carpenter DM, Pollock ML, Graves JE, and Leggett SH. Effect of reduced frequency of training and detraining on lumbar extension strength. *Spine* 17: 1497-1501, 1992.

444. Umbel JD, Hoffman RL, Dearth DJ, Chleboun GS, Manini TM, and Clark BC. Delayed-onset muscle soreness induced by low-load blood flow-restricted exercise. *European journal of applied physiology* 107: 687-695, 2009.

445. Urban JP, and Mcmullin JF. Swelling pressure of the lumbar intervertebral discs: influence of age, spinal level, composition, and degeneration. *Spine* 13: 179-187, 1988.

446. Van Der Meulen MC, and Huiskes R. Why mechanobiology? A survey article. *Journal of biomechanics* 35: 401-414, 2002.

447. Van Dieen JH, Cholewicki J, and Radebold A. Trunk muscle recruitment patterns in patients with low back pain enhance the stability of the lumbar spine. *Spine* 28: 834-841, 2003.

448. Van Dieen JH, Selen LP, and Cholewicki J. Trunk muscle activation in low-back pain patients, an analysis of the literature. *Journal of electromyography and kinesiology : official journal of the International Society of Electrophysiological Kinesiology* 13: 333-351, 2003.

449. Vink P, Van Der Velde EA, and Verbout AJ. A functional subdivision of the lumbar extensor musculature. Recruitment patterns and force-RA-EMG relationships under isometric conditions. *Electromyography and clinical neurophysiology* 27: 517-525, 1987.

450. Vlaeyen JW, and Linton SJ. Fear-avoidance and its consequences in chronic musculoskeletal pain: a state of the art. *Pain* 85: 317-332, 2000.

451. Walker BF, and Williamson OD. Mechanical or inflammatory low back pain. What are the potential signs and symptoms? *Man Ther* 14: 314-320, 2009.

452. Wang S, Passias P, Li G, Li G, and Wood K. Measurement of vertebral kinematics using noninvasive image matching method-validation and application. *Spine* 33: E355-361, 2008.

453. Ward SR, Shellock FG, Terk MR, Salsich GB, and Powers CM. Assessment of patellofemoral relationships using kinematic MRI: Comparison between qualitative and quantitative methods. *J Magn Reson Imaging* 16: 69-74, 2002.

454. Weeks DL, Forget R, Mouchnino L, Gravel D, and Bourbonnais D. Interaction between attention demanding motor and cognitive tasks and static postural stability. *Gerontology* 49: 225-232, 2003.

455. Weiler PJ, King GJ, and Gertzbein SD. Analysis of sagittal plane instability of the lumbar spine in vivo. *Spine* 15: 1300-1306, 1990.

456. Weishaupt D, and Boxheimer L. Magnetic resonance imaging of the weight-bearing spine. *Seminars in musculoskeletal radiology* 7: 277-286, 2003.

457. Weishaupt D, Schmid MR, Zanetti M, Boos N, Romanowski B, Kissling RO, Dvorak J, and Hodler J. Positional MR imaging of the lumbar spine: does it demonstrate nerve root compromise not visible at conventional MR imaging? *Radiology* 215: 247-253, 2000.

458. Wetzel FT, Mcnally TA, and Phillips FM. Intradiscal electrothermal therapy used to manage chronic discogenic low back pain: new directions and interventions. *Spine* 27: 2621-2626, 2002.

459. White AA, 3rd, and Panjabi MM. The basic kinematics of the human spine. A review of past and current knowledge. *Spine* 3: 12-20, 1978.

460. Whitehurst DG, Bryan S, Lewis M, Hay EM, Mullis R, and Foster NE. Implementing Stratified Primary care Management for low Back Pain: Cost Utility

Analysis alongside a Prospective, Population-based, Sequential Comparison Study. *Spine* 2015.

461. Wilder DG, Aleksiev AR, Magnusson ML, Pope MH, Spratt KF, and Goel VK. Muscular response to sudden load. A tool to evaluate fatigue and rehabilitation. *Spine* 21: 2628-2639, 1996.

462. Wiles P. Movements of the Lumbar Vertebrae during Flexion and Extension: (Section of Orthopaedics). *Proceedings of the Royal Society of Medicine* 28: 647-651, 1935.

463. Wilke HJ, Wolf S, Claes LE, Arand M, and Wiesend A. Stability increase of the lumbar spine with different muscle groups. A biomechanical in vitro study. *Spine* 20: 192-198, 1995.

464. Windhorst U. Muscle proprioceptive feedback and spinal networks. *Brain research bulletin* 73: 155-202, 2007.

465. Wisleder D, Smith MB, Mosher TJ, and Zatsiorsky V. Lumbar spine mechanical response to axial compression load in vivo. *Spine* 26: E403-409, 2001.

466. Wu G, Siegler S, Allard P, Kirtley C, Leardini A, Rosenbaum D, Whittle M, D'lima DD, Cristofolini L, Witte H, Schmid O, Stokes I, Standardization, and Terminology Committee of the International Society Of B. ISB recommendation on definitions of joint coordinate system of various joints for the reporting of human joint motion--part I: ankle, hip, and spine. International Society of Biomechanics. *Journal of biomechanics* 35: 543-548, 2002.

467. Xia Q, Wang S, Kozanek M, Passias P, Wood K, and Li G. In-vivo motion characteristics of lumbar vertebrae in sagittal and transverse planes. *Journal of biomechanics* 43: 1905-1909, 2010.

468. Xia Q, Wang S, Passias PG, Kozanek M, Li G, Grottkau BE, Wood KB, and Li G. In vivo range of motion of the lumbar spinous processes. *European spine journal : official publication of the European Spine Society, the European Spinal Deformity Society, and the European Section of the Cervical Spine Research Society* 18: 1355-1362, 2009.

469. Yamazaki T, Watanabe T, Nakajima Y, Sugamoto K, Tomita T, Yoshikawa H, and Tamura S. Improvement of depth position in 2-D/3-D registration of knee implants using single-plane fluoroscopy. *IEEE transactions on medical imaging* 23: 602-612, 2004.

470. Yang JS, Cho YJ, Kang SH, and Choi HJ. Dynamic Radiographic Results of Different Semi-Rigid Fusion Devices for Degenerative Lumbar Spondylolisthesis: "Dynamic Rod" vs. "Dynamic Screw Head". *Turkish neurosurgery* 26: 268-273, 2016.

471. Yang KH, and King AI. Mechanism of facet load transmission as a hypothesis for low-back pain. *Spine* 9: 557-565, 1984.

472. Yao Q, Wang S, Shin JH, Li G, and Wood K. Motion characteristics of the lumbar spinous processes with degenerative disc disease and degenerative spondylolisthesis. *Eur Spine J* 22: 2702-2709, 2013.

473. Yazdani S, Yusof R, Riazi A, and Karimian A. Magnetic resonance image tissue classification using an automatic method. *Diagnostic pathology* 9: 1, 2014.

474. Yeager MS, Cook DJ, and Cheng BC. Reliability of computer-assisted lumbar intervertebral measurements using a novel vertebral motion analysis system. *The spine journal : official journal of the North American Spine Society* 14: 274-281, 2014.

475. Yue G, Alexander AL, Laidlaw DH, Gmitro AF, Unger EC, and Enoka RM. Sensitivity of muscle proton spin-spin relaxation time as an index of muscle activation. *Journal of applied physiology* 77: 84-92, 1994.

476. Zedka M, Prochazka A, Knight B, Gillard D, and Gauthier M. Voluntary and reflex control of human back muscles during induced pain. *The Journal of physiology* 520: 591-604, 1999.

477. Zemke KJ, Muller-Fahrnow A, Jany KD, Pal GP, and Saenger W. The three-dimensional structure of the bifunctional proteinase K/alpha-amylase inhibitor from wheat (PK13) at 2.5 A resolution. *FEBS letters* 279: 240-242, 1991.

478. Zetterberg C, Andersson GB, and Schultz AB. The activity of individual trunk muscles during heavy physical loading. *Spine* 12: 1035-1040, 1987.

479. Zhu Z, Massimini DF, Wang G, Warner JJP, and Li G. The accuracy and repeatability of an automatic 2D–3-D fluoroscopic image-model registration technique for determining shoulder joint kinematics. *Medical engineering & physics* 34: 1303-1309, 2012.

480. Zielinski KA, Henry SM, Ouellette-Morton RH, and Desarno MJ. Lumbar multifidus muscle thickness does not predict patients with low back pain who improve with trunk stabilization exercises. *Arch Phys Med Rehabil* 94: 1132-1138, 2013.

Table 1. Typical values of Neutral zones (in degrees), Elastic zones (in degrees), and NZR (%) for some levels through the spine.

	Flexion				Extension				One-side lat. bend				One-side ax rotation			
	NZ	EZ	ROM	NZR	NZ	EZ	ROM	NZR	NZ	EZ	ROM	NZR	NZ	EZ	ROM	NZR
C0-C1	1.1	2.4	3.5	31.4	1.1	19.9	21.0	5.2	1.5	4.0	5.5	27.3	1.6	5.6	7.2	22.2
C1-C2	3.2	8.3	11.5	27.8	3.2	7.7	10.9	29.4	1.2	5.5	6.7	17.9	29.6	9.3	38.9	76.1
Low cervical	10.4	6.9	17.3	60.1	3.6	3.5	7.1	50.7	9.3	4.3	13.6	68.4	5.8	9.2	15.0	38.7
Lumbar	1.5	6.1	7.6	19.7	1.5	2.3	3.8	39.5	1.6	5.0	6.6	24.2	0.7	1.7	2.4	29.2
L5-S1	3.0	7.0	10.0	30.0	3.0	4.8	7.8	38.5	1.8	3.7	5.5	32.7	0.4	1.0	1.4	28.6

NZ = neutral zone, EZ = elastic zone, ROM = range of motion, NZR = neutral zone ratio.

Table adapted from Panjabi MM. The stabilizing system of the spine. Part II. Neutral zone and instability hypothesis. J Spinal Disord. 1992 Dec;5(4):390-6. Used with permission.

Table 2. Orientation and force distribution of the lumbar fascicles of the Erector Spinae muscle in cadaver specimen.

The parameter OP represents the fascicle length as seen in the radiographs. BS=lateral displacement of the caudal attachment as seen in the postero-anterior (PA) views. Ψ=obliquity of the fascicle with respect to the longitudinal axis of the vertebra of origin as seen in the PA view. γ= same as (Ψ) as seen in lateral view.

Orientation and Force Distribution of the Lumbar Fascicles of Erector Spinae as Seen in Cadavers (N = 5) and Clinical Radiographs (N = 21)

Fascicle (by origin)			*Orientations (Mean Degrees & SD)*								*Proportions of Force Exerted (%)*		
			Cadavers				*Clinical*						
	BC	*OP*	*ψ*	*SD*	*γ*	*SD*	*ψ*	*SD*	*γ*	*SD*	*Long.*	*Post.*	*Lat.*
Longissimus thoracis pars lumborum													
L1	17	224	4	0.8	20	0.6	5	1.6	21	1.9	0.88	0.12	0.01
L2	15	191	5	1.6	26	1.5	7	2.4	25	1.8	0.81	0.18	0.01
L3	11	140	9	2.6	33	2.0	9	2.3	31	2.6	0.72	0.26	0.02
L4	15	89	14	2.6	40	1.3	16	2.5	40	2.4	0.56	0.40	0.05
L5	3	44	27	3.3	46	4.4	26	4.1	48	2.9	0.42	0.49	0.10
Iliocostalis lumborum pars lumborum													
L1	9	224	3	1.2	20	1.7	5	2.2	20	1.8	0.88	0.12	0.01
L2	8	152	5	2.4	24	0.8	5	2.5	23	1.8	0.85	0.15	0.01
L3	4	102	5	2.4	30	3.1	7	2.8	29	2.2	0.75	0.23	0.01
L4	3	54	15	2.4	38	1.5	16	3.3	39	3.0	0.57	0.37	0.05

Table and content for Table legend adapted from Macintosh JE, Bogduk N. The attachments of the lumbar erector spinae. Spine. 1991; 16(7):783-92. Used with permission.

Table 3.Type distribution and sizes (mean diameters) as recorded at different sites of the lumbar muscles.
Inter-individual standard deviations are given in parentheses.

	MFd (L4–5) (n = 21)	MFs (n = 12)	ILd (n = 12)	ILs (n = 12)	MFd (L3–4) (n = 12)	MFd (L5–S1) (n = 12)
Type 1 (%)	62.6	57.4	66.6	66.5	69.6	61.7
Type 1 diameter (µm)	54.0 (9.2)	57.1 (10.8)	55.9 (10.2)	57.1 (15.2)	52.9 (7.2)	57.8 (10.2)
Type 2 diameter (µm)	35.4 (8.8)	33.8 (7.0)	35.2 (9.2)	35.3 (10.7)	33.9 (12.1)	34.5 (7.8)

MFd, Deep multifidus; MFs, superficial multifidus; ILd, deep iliocostalis lumborum; ILs, superficial iliocostalis lumborum
Differences between biopsy regions statistically insignificant

Table and content for table legend adapted from Rantanen J, Rissanen A, Kalimo H. Lumbar muscle fiber size and type distribution in normal subjects. European spine journal: official publication of the European Spine Society, the European Spinal Deformity Society, and the European Section of the Cervical Spine Research Society. 1994;3(6):331-5. Used with permission.

Table 4. Actual displacements scanned and their quantified values.
Mean values and standard deviations, between-session average coefficient of variation (CV) and intra-class correlation coefficients (ICC) for the solid-body displacements.

		Scanned Displacements	Mean± SD for S1 (mm)	Mean± SD for S2 (mm)	Mean CV (%)	ICC (95% CI)
Single (z-) plane	Translation in T_1 (n=7/displacement)	0.0 mm	0.90±0.64	0.73±0.47	14.63	0.99 (0.98-0.99)
		5.0 mm	5.53±0.32	5.30±0.44	1.07	
		10.0 mm	11.60±0.41	11.30±0.45	2.80	
		15.0 mm	15.01±0.54	15.27±0.52	1.22	
		20.0 mm	20.84±0.43	21.13±0.53	1.81	
	Translation in 2D HYCE S (n=7/displacement)	0.0 mm	1.09±0.69	1.32±0.65	13.50	0.97 (0.98-0.99)
		5.0 mm	5.34±0.75	5.20±0.40	4.68	
		10.0 mm	10.35±0.59	10.97±0.59	4.12	
		15.0 mm	14.70±1.05	15.20±0.60	2.39	
		20.0 mm	19.79±0.72	20.25±0.44	1.61	
	Rotation in T_1 (n=6/displacement)	0º	0.21±0.18º	0.22±0.13º	2.29	0.98 (0.97-0.99)
		5º	5.43±0.77º	4.89±0.64º	7.41	
		10º	10.14±0.95º	10.38±0.75º	1.67	
		15º	14.44±1.22º	15.15±1.72º	3.37	
		20º	20.60±0.59º	20.95±0.64º	1.19	
	Rotation in 2D HYCE S (n=6/displacement)	0º	0.11±0.05º	0.12±0.09º	7.59	0.98 (0.97-0.99)
		5º	5.08±0.11º	5.01±0.06º	1.10	
		10º	10.39±0.17º	10.56±0.35º	1.17	
		15º	14.92±0.35º	15.20±0.21º	1.30	
		20º	20.20±0.63º	20.51±0.42º	1.05	
Biplanar (z- & x-planes)	Translation in 2D HYCE S z- plane (n=4/displacement)	0.0 mm	0.65±0.31	0.92±0.61	3.61	0.97 (0.98-0.99)
		5.0 mm	5.44±0.42	5.03±0.32	6.15	
		10.0 mm	10.54±0.59	11.29±0.61	4.84	
		15.0 mm	14.99±0.31	14.71±0.99	1.32	
		20.0 mm	20.94±0.89	21.39±0.98	1.51	
	Translation in 2D HYCE S x- plane (n=4/displacement)	0.0 mm	0.88±0.52	0.83±0.41	3.95	0.97 (0.98-0.99)
		5.0 mm	5.33±0.33	5.12±0.45	2.80	
		10.0 mm	11.40±0.28	10.95±0.50	2.82	
		15.0 mm	15.06±0.48	15.58±0.40	2.41	
		20.0 mm	20.88±0.58	21.27±0.69	1.32	

Table 5. Overview of the number of displacement trials in each plane for the differing displacement values.

All displacements were scanned twice, once with the T_1 sequence and once with the fast contrast-enhanced 2D HYCE S pulse sequence. All scans were performed on two sets of porcine spine motion-segments, yielding 128 (32 × 2 × 2) image frames representing the displacements. Each image frame generated a displacement data point. All 128 displacements were quantified twice, in two separate sessions with 1 week between sessions.

Plane	Translation (mm)		Rotation (degrees)				
	-5 to -1	1 to 5	-10 to -6	-5 to -1	1 to 5	6 to 10	11 to 15
Coronal	4	4	2	2	2	2	-
Sagittal	4	4	-	2	2	2	2

Table 6. Table showing the output of the linear mixed effects model analysis in SPSS for translational displacements.

A. Shows the estimates and levels of significance of the Sequence and the Actual displacements as the fixed effects parameters of the model. ***B.*** Shows the levels of significance of the Session and Spine as the random effects in the model.

A. Estimates of Fixed Effects

Parameter	Estimate	Std. Error	df	t	Sig.	95% Confidence Interval	
						Lower Bound	Upper Bound
Intercept	.356664	.111686	11.075	3.193	.008	.111050	.602278
Sequence	-.058811	.059079	11.075	-.995	.341	-.188734	.071113
Disp_A	.008051	.019990	11.075	.403	.695	-.035911	.052012

B. Estimates of Covariance Parameters

Parameter		Estimate	Std. Error	Wald Z	Sig.	95% Confidence Interval	
						Lower Bound	Upper Bound
Repeated Measures	Variance	.070336	.010677	6.588	.000	.052236	.094709
Intercept + Session + Spine [subject = ID]	CS diagonal offset	.150422	.005527	27.215	.000	.139970	.161655
	CS covariance	-.050140	.000000	.	.	.	.

Table 7. Table showing the average% error and the root mean square errors (RSME) of translation and rotation quantified by the technique (by sequence and orientation of the images).
The average error was calculated as: Quantified ~ Actual displacement/Actual displacement *100. The standard deviations are shown in parentheses.

	T_1		2D HYCE S	
	Coronal	**Sagittal**	**Coronal**	**Sagittal**
Translation Average % Error	12.50% (17.86)	14.97% (17.66)	19.48% (17.86)	15.13% (11.35)
Rotation Average % Error	10.78 % (9.28)	16.0% (15.25)	14.82% (9.73)	20.20% (18.19)
RMSE Translation	0.31 mm	0.40 mm	0.49 mm	0.55 mm
RMSE Rotation	0.68º	0.72º	0.85º	0.92º

Table 8. Comparisons of between-session measurements.
Translation and rotation for each pulse sequence, pair of motion-segments tested, and imaging perspective (sagittal and coronal) shown. None of the 2-tailed pairwise t test comparisons show a significant value at the *p=0.05* level. (CV=coefficient of variation)

Displacement	**Statistic**	***Between-session Comparisons**		
		By Sequence (2D HYCE S, T_1)	**By Spine (Spine 1, Spine 2)**	**By Orientation (Coronal, Sagittal)**
Translation	**CV%**	16.58, 9.36	10.28, 15.66	14.23, 11.71
Rotation	**CV%**	13.33, 7.28	10.50, 10.01	11.01, 9.59

* Session1 versus Session 2
CV = coefficient of variation

Table 9. Table showing the output of the linear mixed effects model analysis in SPSS for rotational displacements.

A. Shows the estimates and levels of significance of the Sequence and the Actual displacements as the fixed effects parameters of the model. ***B.*** Shows the levels of significance of the Session and Spine as the random effects in the model.

A. Estimates of Fixed Effects

Parameter	Estimate	Std. Error	df	t	Sig.	95% Confidence Interval	
						Lower Bound	Upper Bound
Intercept	.629690	.126022	65.600	4.997	.000	.378049	.881330
Sequence	-.132278	.070716	65.600	-1.871	.066	-.273482	.008926
Disp_A	.044565	.008775	65.600	5.078	.000	.027042	.062088

B. Estimates of Covariance Parameters

Parameter		Estimate	Std. Error	Wald Z	Sig.	95% Confidence Interval	
						Lower Bound	Upper Bound
Repeated Measures	Variance	.130916	.023133	5.659	.000	.092594	.185099
Intercept + Session + Spine [subject = ID]	CS diagonal offset	.000000	.000000	.	.	.	.
	CS covariance	.001181	.001482	.797	.425	-.001724	.004086

Table 10. Lumbar and lumbo-sacral linear (in mm) and angular (in degrees) parameters across the three spine-loading conditions.

LINEAR	**Lumbar Levels**	**Supine**	**Weight Bearing (WB)**	**Weight Bearing + 10% body mass (WB+AL)**
1. Inter-vertebral Listhesis[#]	L1-L2	2.5	2.4	2.2
	L2-L3	3.3	2.9	2.1
	L3-L4	3.3	2.7	1.8
	L4-L5	3.1	**4.1**	3.8
	L5-S1	**4.6**	3.2	2.9
2. Inter-vertebral Translation[##]	L1-L2	3.0	3.1	3.6
	L2-L3	3.1	3.3	2.5
	L3-L4	2.9	3.9	3.1
	L4-L5	3.2	**5.2**	3.4
	L5-S1	**4.2**	2.1	2
3. Spinal Canal Sagittal Thickness	*Zone:* L1-L2	13.0	13.08	12.9
	Zone: L2-L3	13.2	14.4	12.4
	Zone: L3-L4	12.2	13.6	12.7
	Zone: L4-L5	13.5	14.3	14.2
	Zone: L5-S1	**13.4**	10.6(2.4)	**9.5**(3.5)
4. Disc Height	L1-L2	14.06	13.47	13.1
	L2-L3	14.88	14.84	13.54
	L3-L4	15.54	15.14	13.93
	L4-L5	14.98	13.81	13.22
	L5-S1	10.29	8.61	**7.06**
5. Left Intervertebral Foramen Height	L1-L2	18.21	17.88	15.71
	L2-L3	18.96	17.93	17.09
	L3-L4	19.92	18.16	17.65
	L4-L5	20.74	15.71	16.43
	L5-S1	12.92	10.89	**9.95**

#measured as the distance between the postero-inferior corners of the superior vertebra to the postero-superior corner of the lower vertebra. The positive values indicate overhanging of the superior vertebra the inferior one at that level. ##measured as the distance between perpendicular planes drawn at the central points of the adjacent vertebrae (see Figure 1B). Numbers in parentheses in *Zone: L5-S1* represent in the increase in sagittal-plane posterior disc protrusions measured form the convex disc tips to the perpendicular bisectors drawn to the adjacent L5-S1 vertebral corners with WB and WB+AL (taking the supine value=zero/baseline). Notable changes are represented in bold.

Table 11. Lumbar and lumbo-sacral angular parameters (in degrees) and cross sectional area (CSA) (in mm^2) dimensions across the three spine-loading conditions.

ANGULAR	**Lumbar Levels**	**Supine**	**Weight Bearing (WB)**	**Weight Bearing + 10% body mass**
1. Inter-vertebral Segmental Angles	L1-L2	3.5	8.3	4.0
	L2-L3	2.8	10.7	7.5
	L3-L4	7.3	7.3	9.3
	L4-L5	7.5	12.9	11.2
2. L5-S1 Segmental Angle	L5-S1	10.3	**2.8**	4.3
3. Lordosis Angle	L5-S1	53.4	59.2	57.5
4. Sacral Angle	S1	38.5	38.3	40.3
5. L1-L3-L5 Angle	L1-L5	161.4	157.1	155.1
CSA	**Lumbar Levels**	**Supine**	**Weight Bearing (WB)**	**Weight Bearing + 10% body weight**
1. Left inter-vertebral Foramen CSA	L1-L2	120	127	121
	L2-L3	101	107	104
	L3-L4	110	115	111
	L4-L5	111	113	118
	L5-S1	106	**98**	100
2. Spinal Canal CSA	*Zone*: L1-L2	155	146	142
	Zone: L2-L3	163	144	138
	Zone: L3-L4	168	143	152
	Zone: L4-L5	164	155	159
	Zone: L5-S1	149	**130**	**131**

Notable changes are represented in bold.

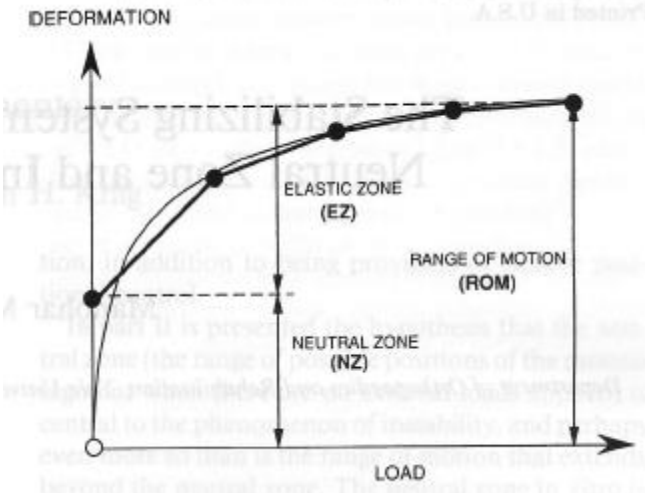

Figure 1. Nonlinear load-deformation curve in soft tissue or joint.
The Neutral zone (NZ) is highly flexible whereas the Elastic Zone (EZ) stiff. NZ+EZ=Range of Motion (ROM).

Figure and content for figure legend adapted from Panjabi MM. The stabilizing system of the spine. Part II. Neutral zone and instability hypothesis. Journal of spinal disorders 5: 390-396; discussion 397, 1992. Used with permission.

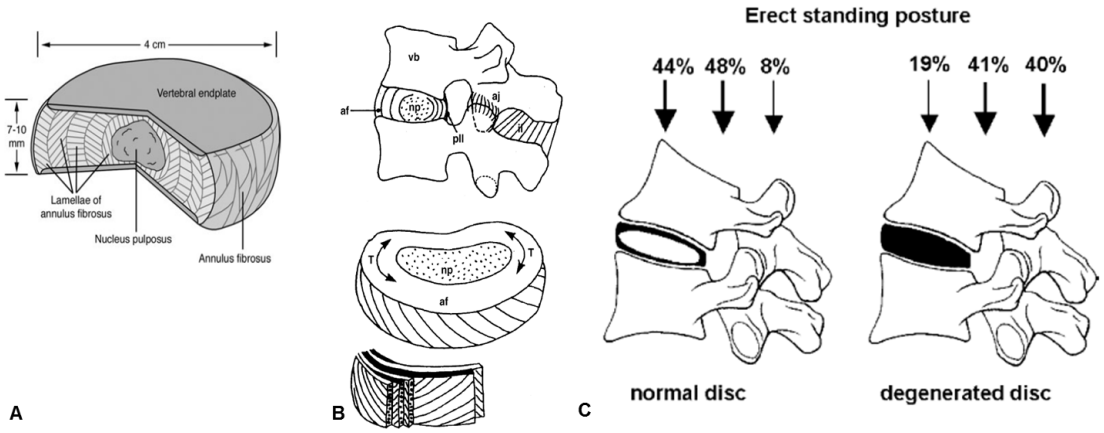

Figure 2. Anatomy of the inter-vertebral disc.
A. Cut out section of a normal disc showing the central nucleus pulposus and the fibrous annulus fibrosus. ***B.*** Generation of hoop stress (T) on compressive loading allowing equal distribution of forces at the endplate. ***C.*** Load shifts shown between the anterior & posterior sections of the vertebral body and the facet joints. Note the loading difference at the facte joints in normal and degenerated disc conditions. np=Nucleus pulposus; af=annulus fibrosus; pll=posterior longitudinal ligament; aj=apophyseal joint; il=interspinous ligament.

Figure and content for figure legend adapted from Raj PP. Raj PP. Intervertebral disc: anatomy-physiology-pathophysiology-treatment. Pain practice: the official journal of World Institute of Pain 8: 18-44, 2008. Used with permission.

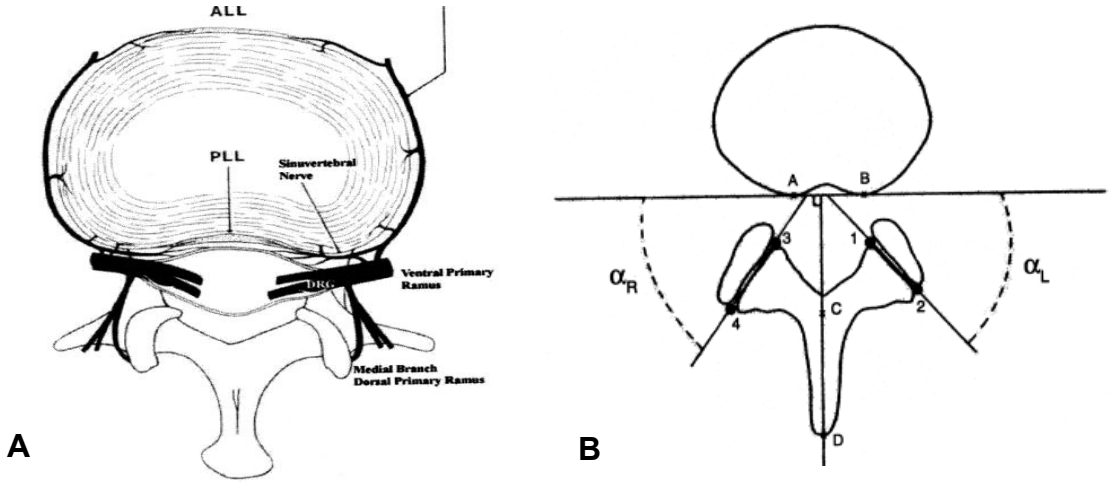

Figure 3. Innervation of Disc and Facet Joints and Facet Topism.
A. Top view of a vertebrae showing ALL (anterior longitudinal ligament), PLL (posterior longitudinal ligament), and sensory distribution of the ventral and dorsal primary rami to vertebral tissues of the motion segment. ***B.*** Facet topism. Angular differences between the two facet articular surfaces α_R and α_L.

Figure and content for figure legend adapted from Berven S, Tay BB, Colman W, Hu SS. The lumbar zygapophyseal (facet) joints: a role in the pathogenesis of spinal pain syndromes and degenerative spondylolisthesis. Semin Neurol. 2002; 22(2):187-96.Used with permission.

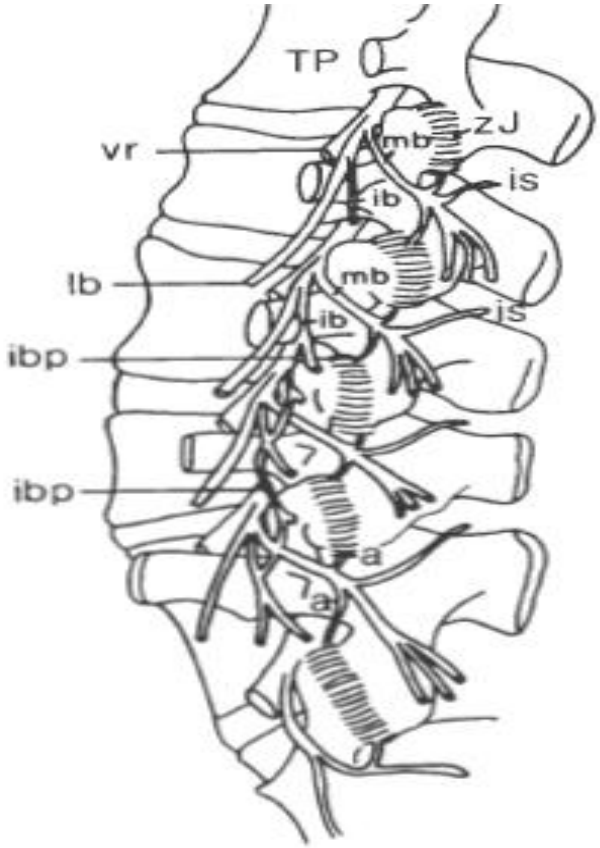

Figure 4. **Schematic representation of the innervation sources of the paraspinal muscles, facet joints (zJ).**
zJ= facet joints; vr=ventral rami; lb=lateral branches; mb=medial branches; ibp=intermediate branch plexus; is=interspinous branch; a=articular branch; TP=transverse processes.

Figure and content for figure legend adapted from Kalimo H, Rantanen J, Viljanen T, *et al*. Lumbar muscles: Structure and function. Ann Med 1989; 21:353–9. Used with permission.

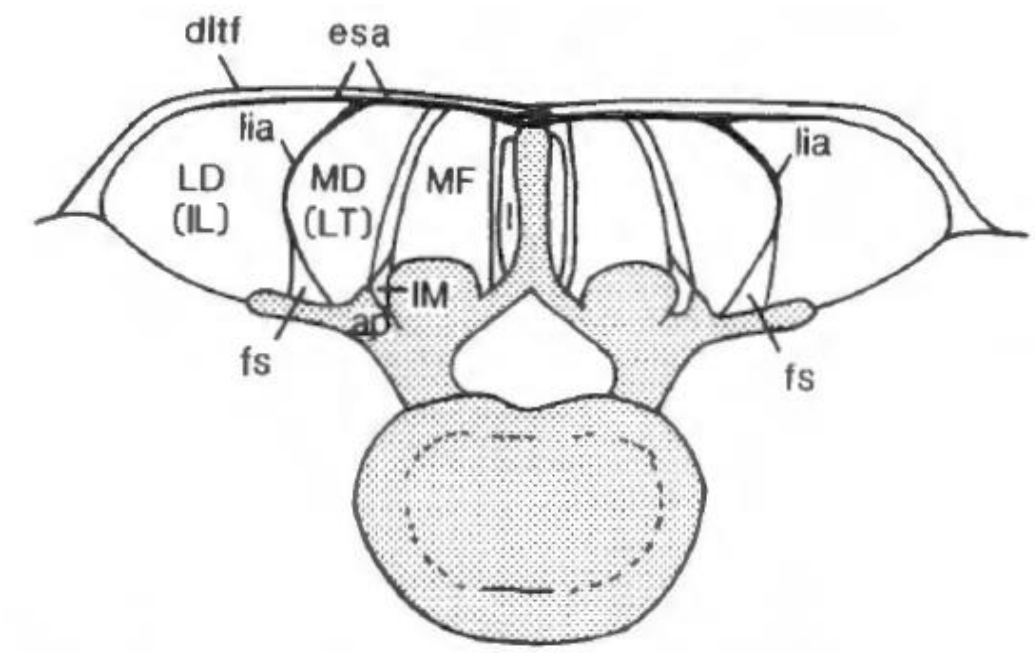

Figure 5. Schematic repreentation of transverse section through the back muscles (at L4).
MF=multifidus; MD=medial division of Erector Spinae, LT=longissimus; LD= lateral division of Erector Spinae, IL=ilio-costalis; I=interspinalis; esa=erector spinae aponeurosis; lia=lumbar intermuscular aponeurosis; fs=fat filled space; ap=accessory process; IM=intertransversii muscles; dltf=dorsal thoraco-lumbar facsia.

Figure and content for figure legend adapted from Kalimo H, Rantanen J, Viljanen T, *et al*. Lumbar muscles: Structure and function. Ann Med 1989; 21:353–9. Used with permission.

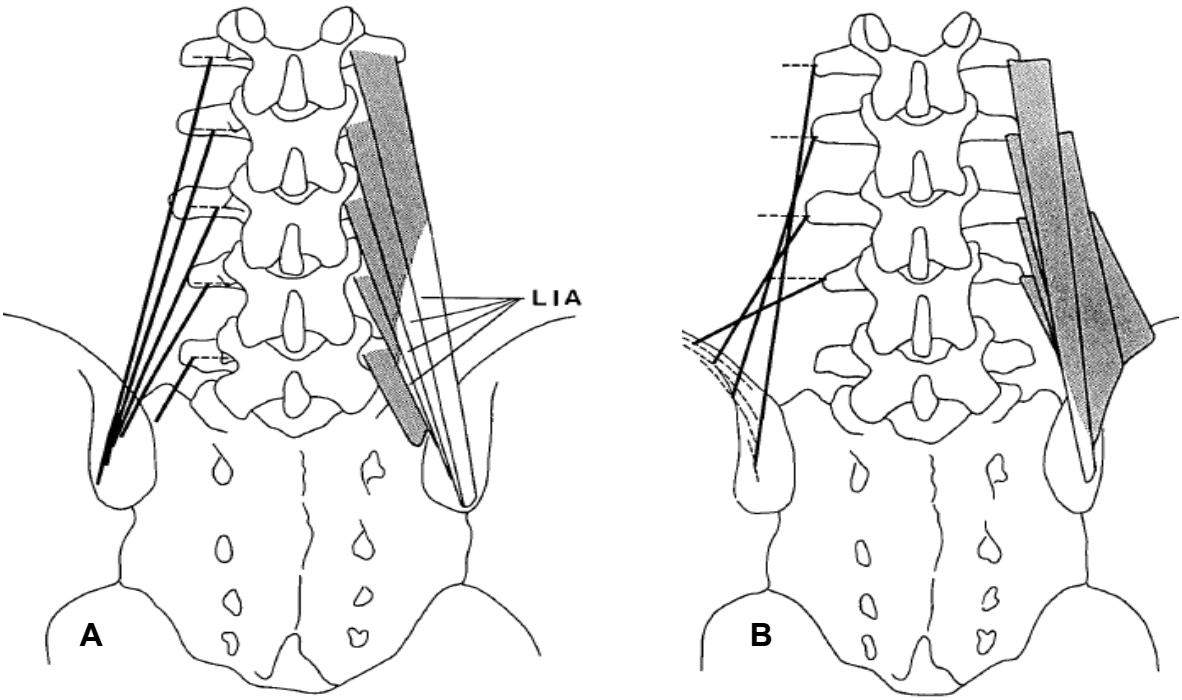

Figure 6. Schematic diagram of the fascicular attachnments of the parts of the Erector Spinae (ES).
A. Shows the lumbar part medial division of the erector spinae (ES) (Longissimus thoracis pars lumborum). ***B.*** Shows the lumbar part of the lateral division of the ES called the Ilio-costalis pars lumborum. LIA=lumbar intermuscular septum.

Figure and content for figure legend adapted from Macintosh JE, and Bogduk N. 1987 Volvo award in basic science. The morphology of the lumbar erector spinae. Spine 12: 658-668, 1987. Used with permission.

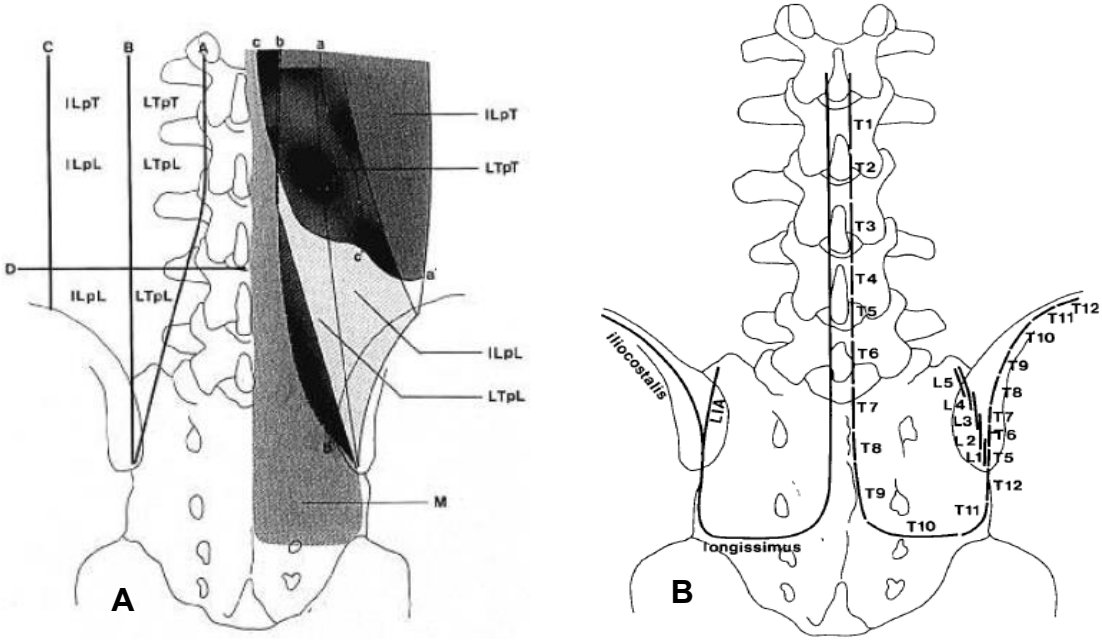

Figure 7. Orientation of components of the back muscles.
A. Schematic representation of caudal attachment og the thoracic and lumabr parts of the longissimus and ilio-costalis on the dorsal aspects of the sacrum and ilium. ***B.*** Topographic anatomy of the multifidus and the four parts of the ES.

Figure and content for figure legend adapted from Macintosh JE, Bogduk N. 1987 Volvo award in basic science. The morphology of the lumbar erector spinae. Spine. 1987;12(7):658-68. Used with permission.

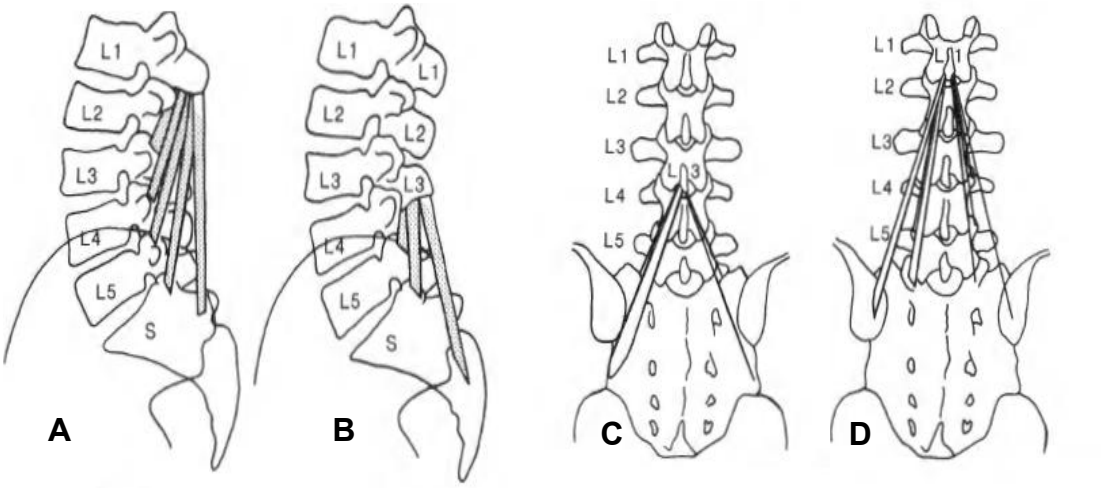

Figure 8. Schematic representation of muscle fascicular bands of multifidus. The fascicles arising from the L1 and L3 vertebrae to show the disposition of the fascicles.

Figure and content for figure legend adapted from Kalimo H, Rantanen J, Viljanen T, Einola S. Lumbar muscles: structure and function. Ann Med. 1989;21(5):353-9. Used with permission.

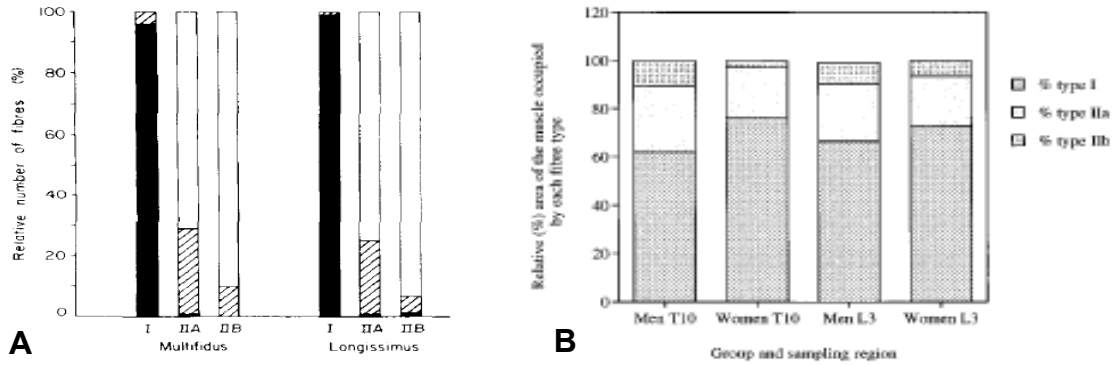

Figure 9. Distribution of Muscle Fibre-types in the thoraco-lumbar back muecles. ***A.*** Relative number (mean) of muscle fibres of each type (I, IIA and IIB) within each individual muscle sample that were independently rated. Dark (black), cross-hatched (medium) or light (colourless) staining intensity for NADH-diaphorase. ***B.*** Relative occupation of each type of fibre at the T10 and L3 levels.

Figure and content for figure legend adapted from Mannion AF, Dumas GA, Cooper RG, Espinosa FJ, Faris MW, Stevenson JM. Muscle fibre size and type distribution in thoracic and lumbar regions of erector spinae in healthy subjects without low back pain: normal values and sex differences. Journal of anatomy. 1997;190 (Pt 4):505-13. Used with permission.

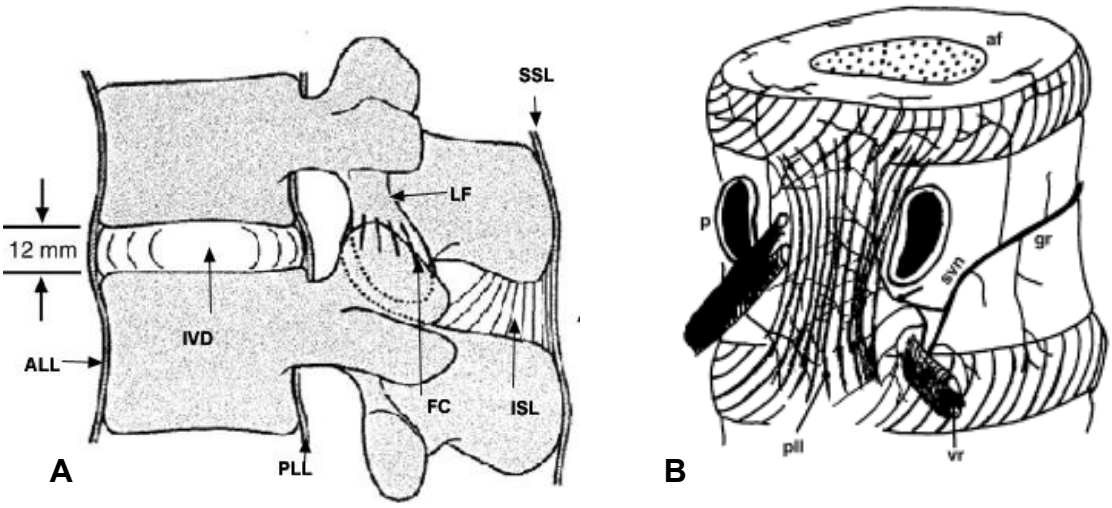

Figure 10. Ligaments associated with a Motion-Segment.
A. Illustration of the spinal ligaments in profile. ALL=anterior longitudinal ligament; PLL=posterior longitudinal ligament; IVD=inter-vertebral disc; LF=ligamentum flavum; FC=facet capsule; ISL=inter-spinous ligament; SSL=supra-spinal ligament. ***B.*** PLL as seen schematically from behind. af=annulus fibrosus; vr=ventral rami; svn=sinuvertebral nerve; gr=grey ramus; p=pedicle.

Figure and content for figure legend adapted from Adams MA, and Dolan P. Spine biomechanics. Journal of biomechanics 38: 1972-1983, 2005. Used with permission.

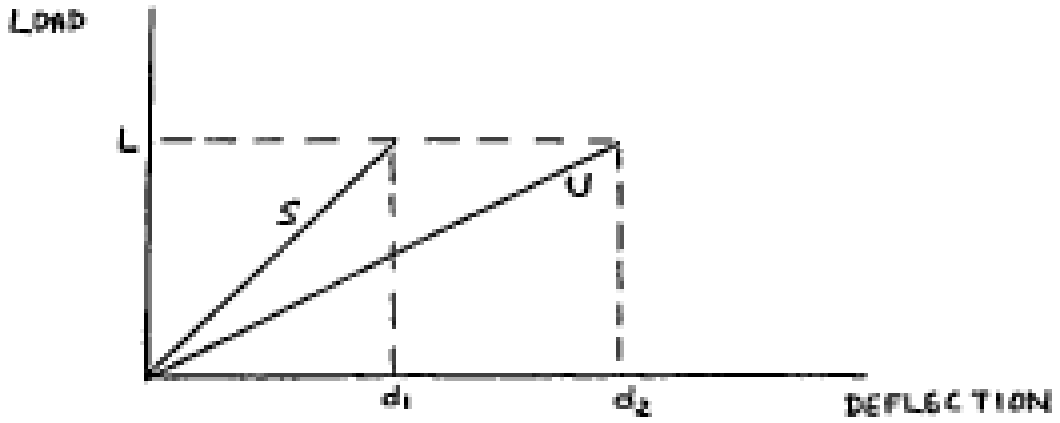

Figure 11. Common measure of stiffness and stability as displayed by the load displacement relationship.
Application of the same magnitude of load (L) results in a greater displacement (d_2) in a relatively more unstable system (U) than the displacement (d_1) in a relatively more stable system (S). This relationship is often equated unequivocally to the stiffness and stability of the spine system.

Figure and content for figure legend adapted from Pope MH, and Panjabi M. Biomechanical definitions of spinal instability. Spine 10: 255-256, 1985. Used with permission.

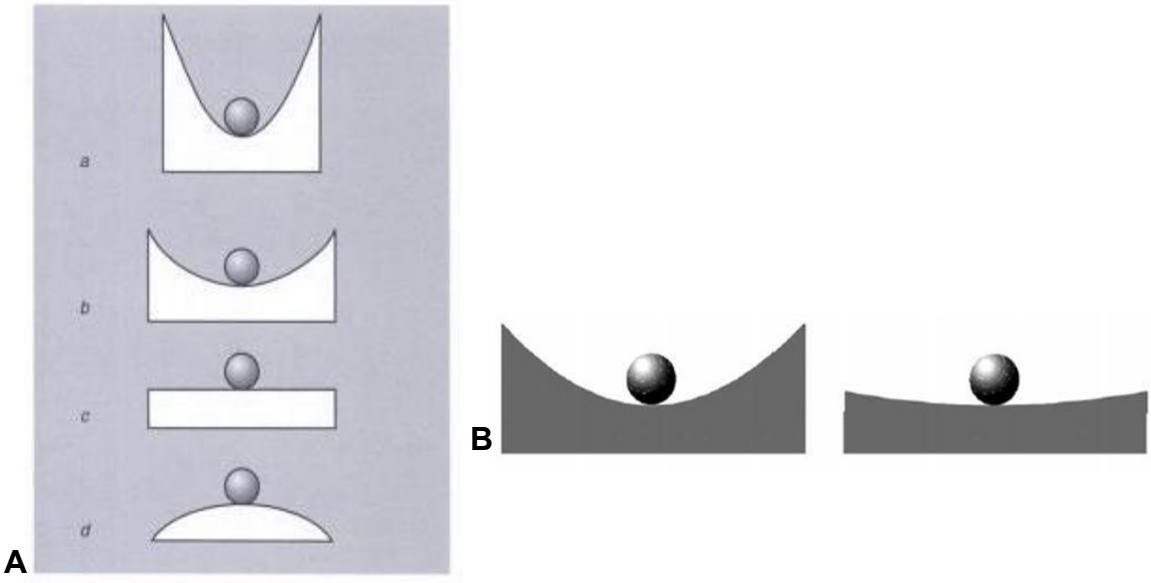

Figure 12. The energy-well concept of stability.
A. The ball and well examples demonstrate that the system on the top is more stable in comparison due to the least potential energy associated with the system in comparison to those below. The steepness of the walls in the example represents greater stiffness of the system, and therefore thought to impart greater stability to the ball. **B.** The ball and well example demonstrates that the system on the left is more robust than the one on the right.

Figure and content for figure legend adapted from Reeves NP, Narendra KS, and Cholewicki J. Spine stability: the six blind men and the elephant. Clinical biomechanics 22: 266-274, 2007. Used with permission.

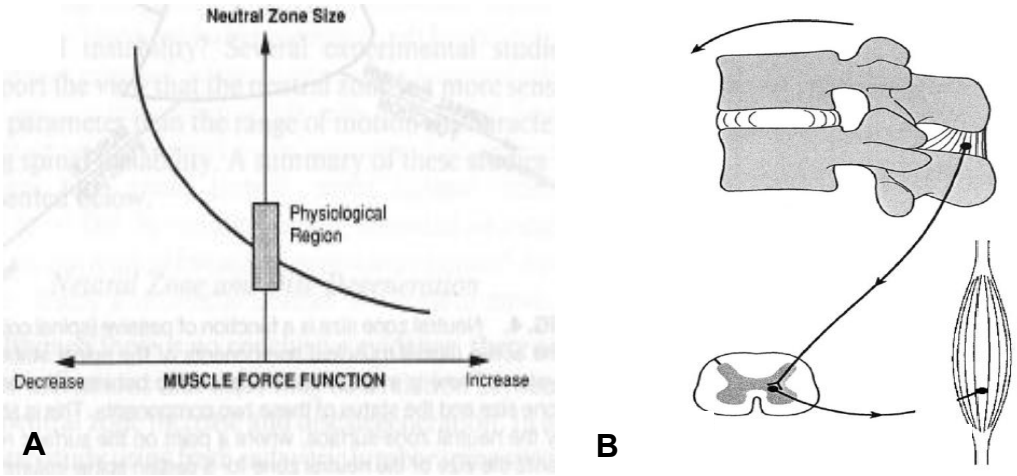

Figure 13. **The role of lumbar muscles as stiffness modulators of the segments as shown to regulate physiological Neutral Zones with increase or decrease in muscle activity.**
Basic construct of muscle control for spinal stability. ***A.*** Propriceptive feedback shown to come from the interspinous ligaments during spine flexion. ***B.*** Reflex activation of back extension.

Figure and content for figure legend adapted from Panjabi MM. The stabilizing system of the spine. Part II. Neutral zone and instability hypothesis. Journal of spinal disorders 5: 390-396; discussion 397, 1992, and Adams MA, and Dolan P. Spine biomechanics. Journal of biomechanics 38: 1972-1983, 2005. Used with permission.

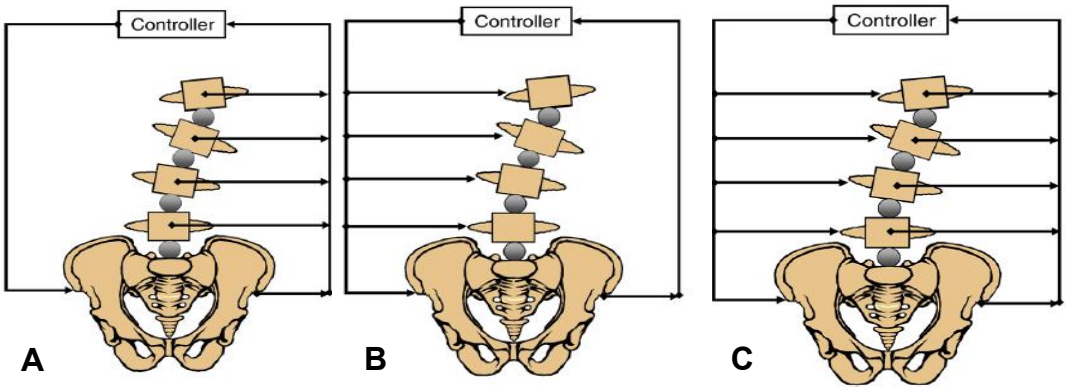

Figure 14. Controller hypothesis for spine motor adjustments.
A. Multiple output single control; ***B.*** Single output multiple control; ***C.*** Multiple output multiple control.

Figure and content for figure legend adapted from Reeves NP, Narendra KS, and Cholewicki J. Spine stability: lessons from balancing a stick. Clinical biomechanics 26: 325-330, 2011. Used with permission.

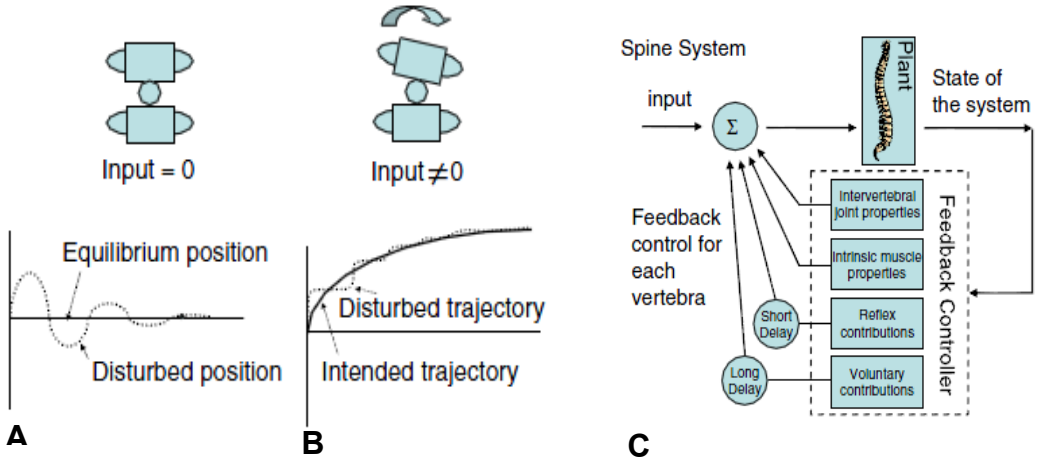

Figure 15. Changes in equilibrium of segmental spine configurations in two different contexts.
A. In a static context changes show as equilibrium and disturbed positions; ***B.*** In a dynamic context shown as intended and disturbed trajectories. In a stable spine, the disturbed configurations quickly resolve into the equilibrium or the intended ones. ***C.*** Multiple feedback controller system of the lumbar spine stabilizing mechanism.

Figure and content for figure legend adapted from Reeves NP, Narendra KS, and Cholewicki J. Spine stability: the six blind men and the elephant. Clinical biomechanics 22: 266-274, 2007. Used with permission.

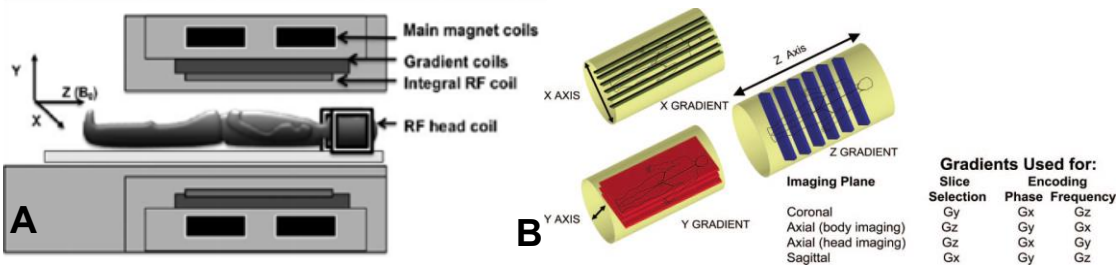

Figure 16. Schematic demonstrating the relative positions of the different magnet coils comprising the MR machine.
A. The patient is positioned within the bore of the machine and is surrounded by coils that lie concentric to each other and in the following order (from furthest to closest to the patient): main magnet coils, gradient coils and radiofrequency (RF) coils. For neuroimaging, a further RF coil is placed around the patient's head to improve signal to noise ratio. ***B.*** Schematic and table show the x-, y-, and z-axis gradients (Gx, Gy, and Gz, respectively) that are used for section selection and for phase and frequency encoding during acquisitions in the most common imaging planes.

Figure and content for figure legend adapted from Currie S, Hoggard N, Craven IJ, Hadjivassiliou M, and Wilkinson ID. Understanding MRI: basic MR physics for physicians. Postgraduate medical journal 89: 209-223, 2013 ; Bitar R, Leung G, Perng R, Tadros S, Moody AR, Sarrazin J, McGregor C, Christakis M, Symons S, Nelson A, and Roberts TP. MR pulse sequences: what every radiologist wants to know but is afraid to ask. Radiographics : a review publication of the Radiological Society of North America, Inc 26: 513-537, 2006. Used with permission.

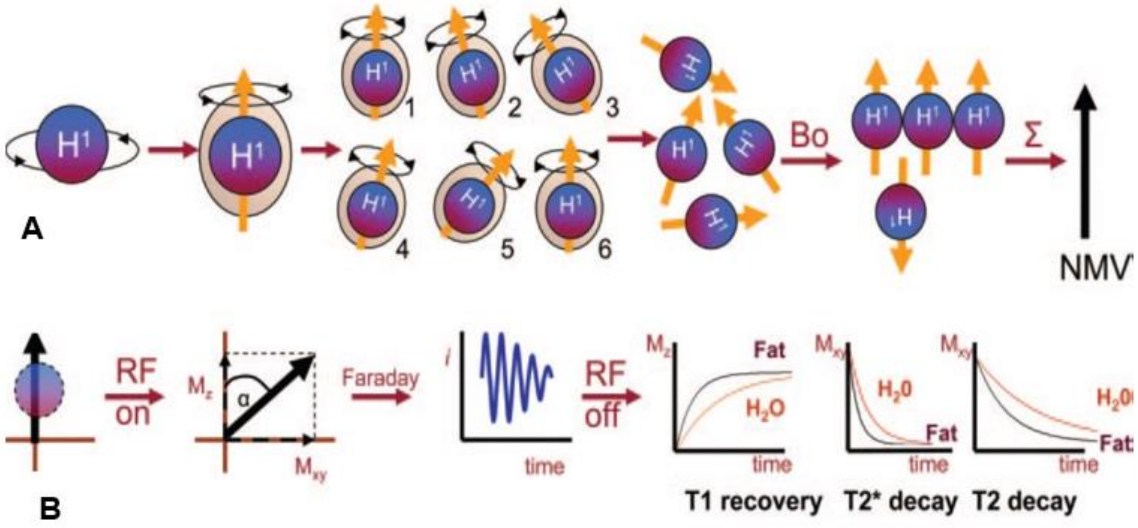

Figure 17. Basic physics of the MR signal.
A. As 1H nuclei spin, they induce their own magnetic field (tan), the direction (magnetic axis) of which is depicted by an arrow (yellow). The 1H nuclei initially precess with a wobble at various angles (1–6), but when they are exposed to an external magnetic field (B_0), they align with it. The sum of all magnetic moments is called the net magnetization vector (NMV). ***B.*** When an RF pulse is applied, the net magnetization vector is flipped at an angle (α), which produces two magnetization components: longitudinal magnetization (Mz) and transverse magnetization (Mxy). As the transverse magnetization precesses around a receiver coil, it induces a current (i). When the RF generator is turned off, T1 recovery and T2 and T2* decay occur.

Figure and content for figure legend adapted from Bitar R, Leung G, Perng R, Tadros S, Moody AR, Sarrazin J, McGregor C, Christakis M, Symons S, Nelson A, and Roberts TP. MR pulse sequences: what every radiologist wants to know but is afraid to ask. Radiographics : a review publication of the Radiological Society of North America, Inc 26: 513-537, 2006. Used with permission.

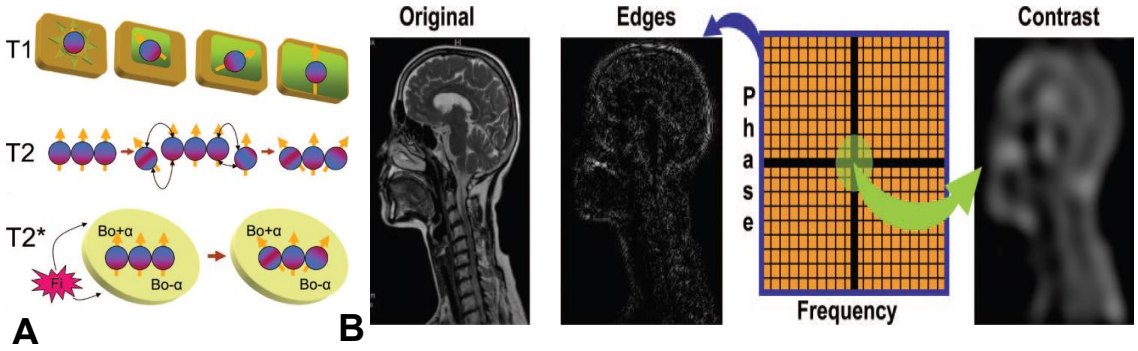

Figure 18. Magnetization relaxation and decay.
A. (Top) T_1 recovery (spin-lattice relaxation) involves recovery of the longitudinal magnetization (yellow) because of the release of energy (green) into the environment. The lattice is indicated in tan. (Middle) T2 decay (spin-spin relaxation) is decay of the transverse magnetization because of the interaction of the individual magnetic fields of spinning nuclei. Note that all nuclei initially spin in phase (as indicated by the similar position of the red bands at the bottom of each circle), then move out of phase (with red bands in different positions). (Bottom) T2* decay is decay of the transverse magnetization because of magnetic field inhomogeneity (Fi). α= flip angle, B_0= external magnetic field. ***B.*** Schematic and corresponding MR images (original) show the characteristics determined by data at the periphery of k-space (ie, spatial resolution, or definition of edges) and those determined by data at the center of k-space (ie, gross form and image contrast).

Figure and content for figure legend adapted from Bitar R, Leung G, Perng R, Tadros S, Moody AR, Sarrazin J, McGregor C, Christakis M, Symons S, Nelson A, and Roberts TP. MR pulse sequences: what every radiologist wants to know but is afraid to ask. Radiographics : a review publication of the Radiological Society of North America, Inc 26: 513-537, 2006. Used with permission.

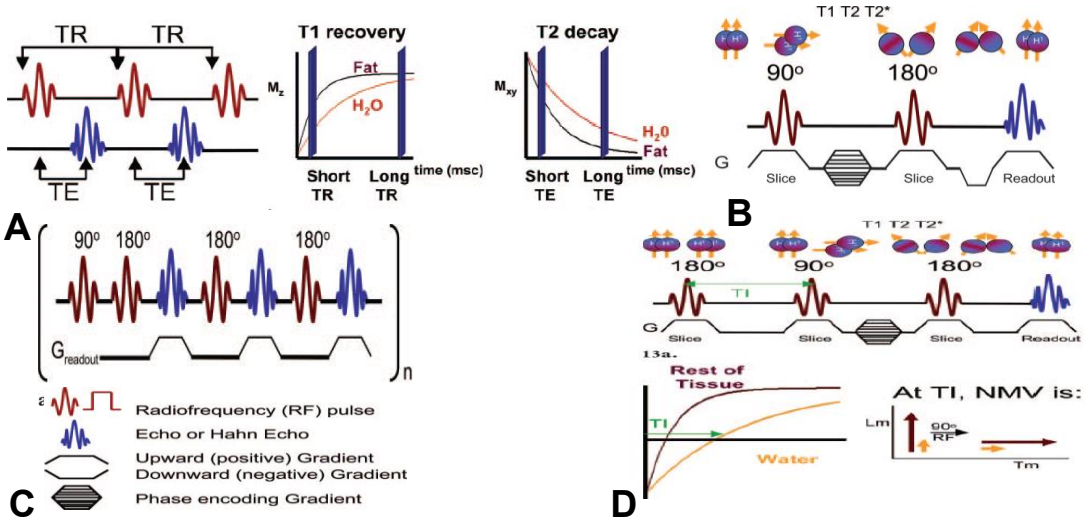

Figure 19. Basic anatomy of MRI sequences:
A. Schematic representation of TR and TE with the graphs showing the effects of short and long TR (left) and short and long TE (right) on T_1 recovery and T_2 decay in fat and water: TR relates to T_1 and affects T_1 weighting, whereas TE relates to T_2 and affects T_2 weighting. Msc= milliseconds, Mxy= transverse magnetization, Mz= longitudinal magnetization. ***B.*** Application of an SE pulse sequence. (a) Diagram shows the application of an initial pulse at a 90° flip angle to redirect the net magnetization vector into the transverse plane; a subsequent interval of T_1, T_2, and T_2* relaxation, accompanied by the gradual dephasing of the transverse magnetization; and a second pulse applied at a flip angle of 180° to bring the spinning nuclei again into phase so that an echo is produced. Note the locations of the section-selective (Slice) and phase- and frequency encoding (Readout) gradients (G). ***C.*** Fast SE pulse sequence. G = gradient, n =number of repetitions. Definitions of common symbols used in pulse sequence diagrams (below). ***D.*** Conventional inversion-recovery sequence diagram shows a 180° preparatory pulse applied to null the signal from either fat or water. At a predetermined inversion time (TI), a 90° pulse is applied, and the SE sequence is continued. G= gradient. Diagrams show T_1 recovery in water and in tissue with use of a conventional inversion-recovery sequence. Nulling of the water signal is seen at TI, when there is virtually no net magnetization vector (NMV) in water. When the 90° pulse flips the net magnetization vector into the transverse plane, little or no transverse magnetization (Tm) is present, and, therefore, no signal is detected in water. Lm= longitudinal magnetization.

Figure and content for figure legend adapted from Bitar R, Leung G, Perng R, Tadros S, Moody AR, Sarrazin J, McGregor C, Christakis M, Symons S, Nelson A, and Roberts TP. MR pulse sequences: what every radiologist wants to know but is afraid to ask. Radiographics : a review publication of the Radiological Society of North America, Inc 26: 513-537, 2006. Used with permission.

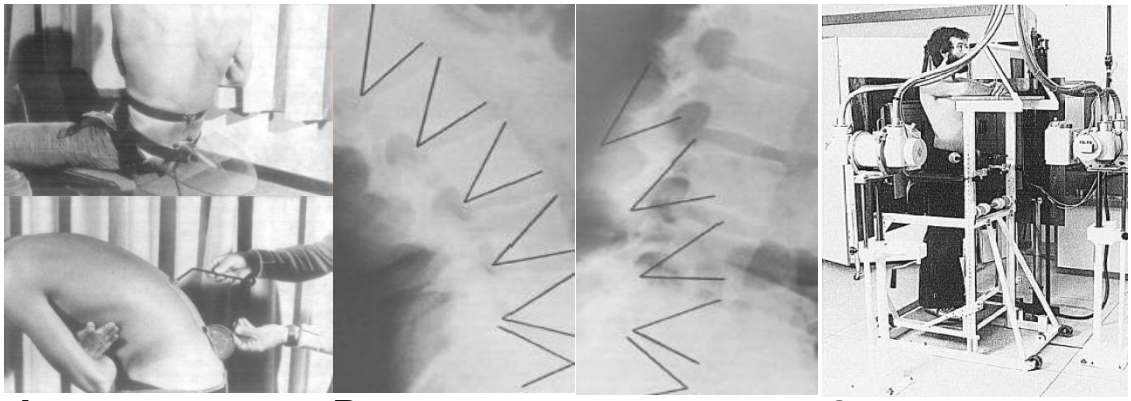

Figure 20. Spine displacement Measurement Techniques.
A. Axial rotation measurement by use of a lumbar rotameter (top); Flexion measurement by use of a lumbar spondylometer (bottom); ***B.*** Radiographic Measurement Technique***:*** Roentgenogram in sagittal plane in extended (left) and in sagittal plane in the flexed position; ***C.*** Schematic showing kinematic measurement technique developed by Pearcy *et al*.in 1985.

Figure and content for figure legend adapted from Taylor J, Twomey L., 1980. Sagittal and horizontal plane movement of the human lumbar vertebral column in cadavers and in the living. Rheumatology and Rehabilitation 19, 223-232; Hanley, Jr, E., Matteri, R., Frymoyer, J., 1976. Accurate Roentgenographic Determination of Lumbar Flexion-Extension. Clinical Orthopaedics and Related Research 115, 145-148; Pearcy, M., Portek, I., Shepher, J., 1985. Pearcy M, Portek I, and Shepherd J. Three-dimensional x-ray analysis of normal movement in the lumbar spine. Spine 9: 294-297, 1984. Used with permission.

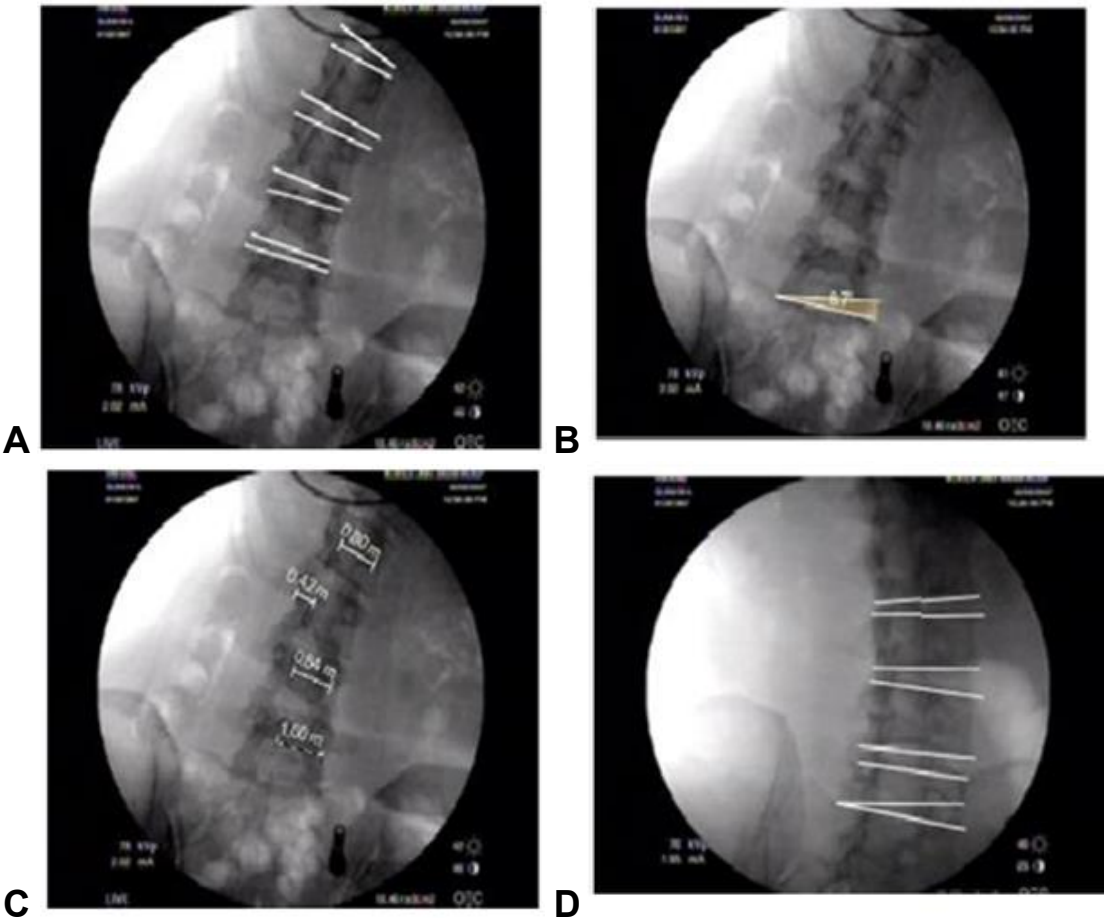

Figure 21. Images from a DFIS video fluoroscope.
A. Direction and degree of extension in lateral flexion. ***B.*** Direction and degree of sacral descent in lateral flexion. ***C.*** Rotation of the spinous process on lateral flexion. The distance from the spinous process to the lateral margin of the vertebrae is to be noted. ***D.*** Direction and degree of extension in rotation.

Figure and content for figure legend adapted from Lee BW, Lee JE, Lee SH, Kwon HK. Kinematic analysis of the lumbar spine by digital video-fluoroscopy in 18 asymptomatic subjects and 9 patients with herniated nucleus pulposus. J Manipulative Physiol Ther. 2011 May;34(4):221-30. Used with permission.

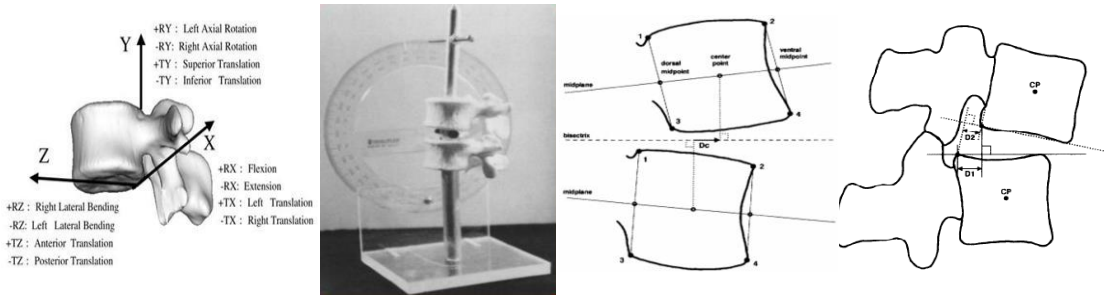

Figure 22. Inter-vertebral displacements: Perspectives for measuring translation and rotational motion.
A. Coordinate system used for defining kinematic measurements. ***B.*** Example setup of testing the accuracy of a measurement technique using a cadaveric model. ***C.*** Schematic showing kinematic measurement technique developed by Frobin *et al*. Example of a protocol to measure dorsoventral displacement from a lateral radiograph of the lumbar spine. Displacement Dl is determined as the distance of the projection of the dorsal corner of the cranial vertebra from the respective dorsal corner of the caudal vertebra; displacement is measured along the tangent to the endplate of the caudal vertebra (continuous line). This protocol, however, is not symmetric with respect to the two vertebrae. If a tangent is drawn to the endplate of the cranial vertebra and the rule is followed accordingly (dotted lines), a different displacement D2 results. Furthermore, if both vertebrae are imagined to rotate simultaneously, but in opposite directions about their appertaining center points CP, so that no net dorso-ventral translation occurs, Dl and D2 change nevertheless. These findings suggest that the current definition of 'displacement' may not be optimally chosen.

Figure and content for figure legend adapted from Fujii, R., Sakaura, H., Mukai, Y., Hosono, N., Ishii, T., Iwasaki, M., Yoshikawa, H., Sugamoto, K., 2007. Kinematics of the lumbar spine in trunk rotation: in vivo three-dimensional analysis using magnetic resonance imaging. European Spine Journal 16, 1867-1874; Cholewicki, J., McGill, S., Wells, R., Vernon, H., 1991. Method for measuring vertebral kinematics from videofluoroscopy. Clinical Biomechanics 6, 73-78; Frobin, W., Brinckmann, P., Leivseth, G., Biggemann, M., Reikeras, O., 1996. Precision measurement of segmental motion from flexion-extension radiographs of the lumbar spine. Clinical Biomechanics 11 (8), 457-465. Used with permission.

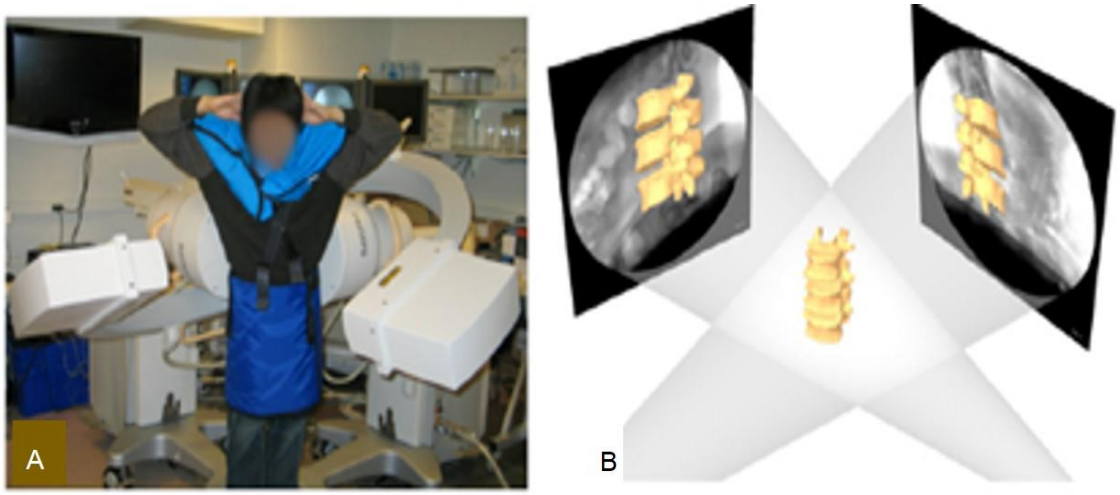

Figure 23. Biplanar Fluoroscopy-Modeling technique for quantification of lumbar inter-vertebral motion.
A. Performance of maximum flexion within the DFIS set up with minimum hip joint movement. ***B.*** The projection of the DFIS acquired image frames in a software environment to allow manual positioning (rotoscoping) of the MR generated 3-D model within the fluoroscope images, one frame at a time.

Figure and content for figure legend adapted from Xia Q, Wang S, Kozanek M, Passias P, Wood K, and Li G. In-vivo motion characteristics of lumbar vertebrae in sagittal and transverse planes. Journal of biomechanics 43: 1905-1909, 2010. Used with permission.

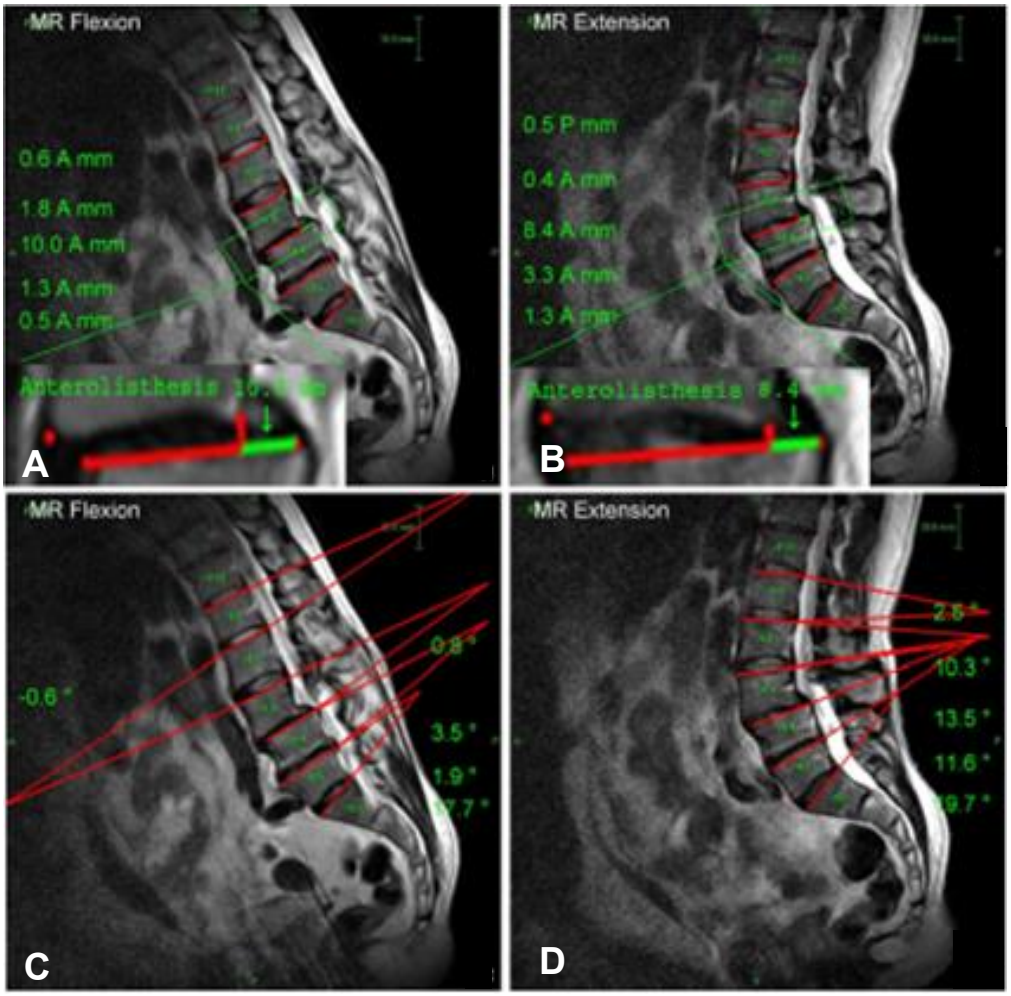

Figure 24. Images from a sagittal MR scan, as used for motion quantification. ***A***. Intervertebral translation in flexion. **B**. Intervertebral translation in extension. ***C.*** Rotational changes at specific vertebral levels in flexion (left) and ***D.*** In extension.

Figure and content for figure legend adapted from Tan Y, Aghdasi BG, Montgomery SR, Inoue H, Lu C, Wang JC. Kinetic magnetic resonance imaging analysis of lumbar segmental mobility in patients without significant spondylosis. Eur Spine J. 2012 Dec;21(12):2673-9. Used with permission.

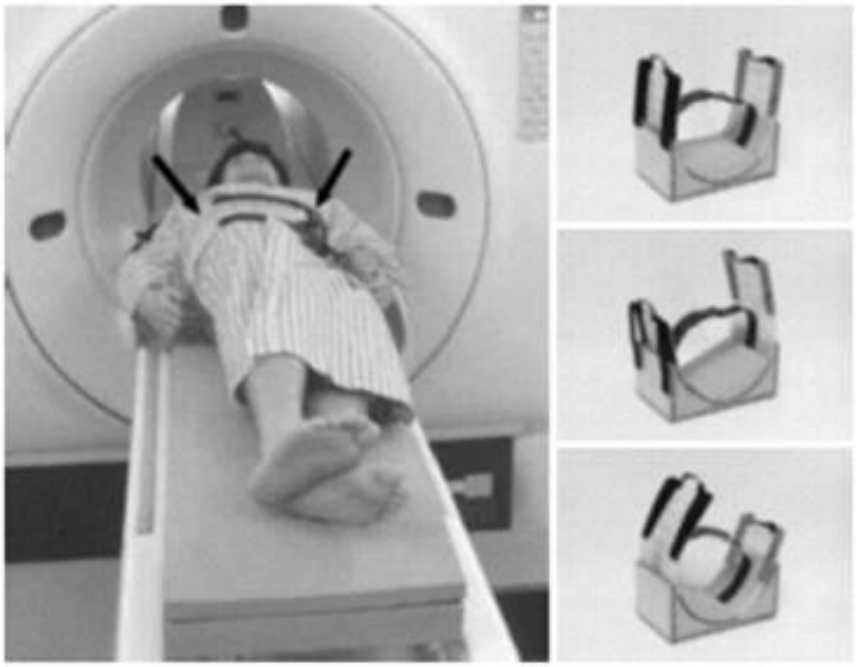

Figure 25. Positional MR technique involving static rotational displacements. A devise was designed to rotate the trunk as reproducibly as possible. MR imaging was taken at nine positions, one in the neutral plane and at 15, 30, 45 and at maximum rotation. The maximum trunk rotation was defined as the position in which the trunks were rotated as much as possible without the bilateral shoulders pulled away from the MR table.

Figure and content for figure legend adapted from Fujii R, Sakaura H, Mukai Y, Hosono N, Ishii T, Iwasaki M, Yoshikawa H, Sugamoto K. Kinematics of the lumbar spine in trunk rotation: in vivo three-dimensional analysis using magnetic resonance imaging. Eur Spine J. 2007; 16(11):1867-74. Used with permission.

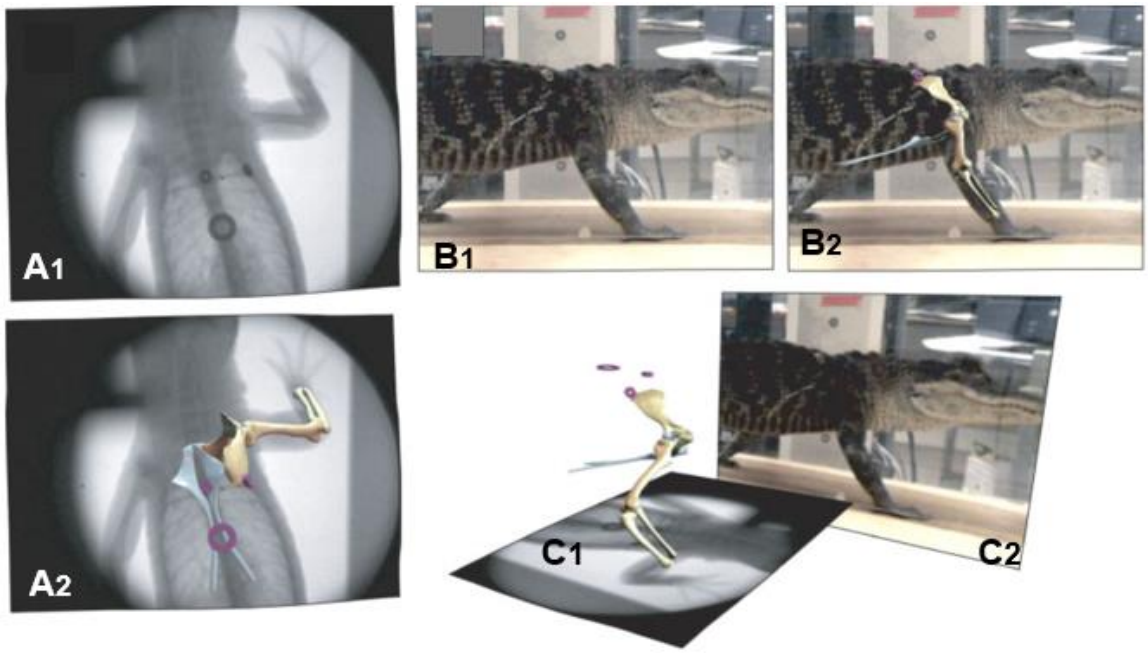

Figure 26. Overview of the morphology based XROMM technique using the scientific rotoscoping (SR) of alligator walking.
A. Dorsal x-ray views of the walking (top and bottom panels, A1 and A2). ***B.*** Walking as seen in lateral standard video used for animation and quantification of the right sided pectoral girdle and the forelimb marionette (B1 and B3). ***C.*** Shows the right forelimb marionette within a rotoscoping environment against orthogonally placed dorsal radiographic (C1) and a video (C2) frames. Our study uses a pair of orthogonal MRI views of the quantification of the biplanar translation trials in Aim1. A single-plane approach has been used for the quantification of inter-vertebral translation-rotation motion in Aim 2, for rotoscoping.

Figure and content for figure legend adapted from Gatesy, S. M., Baier, D. B., Jenkins, F. A., & Dial, K. P. (2010). Scientific rotoscoping: a morphology-based method of 3-D motion analysis and visualization. J Exp Zool A Ecol Genet Physiol, 313(5), 244-261. Used with permission.

A

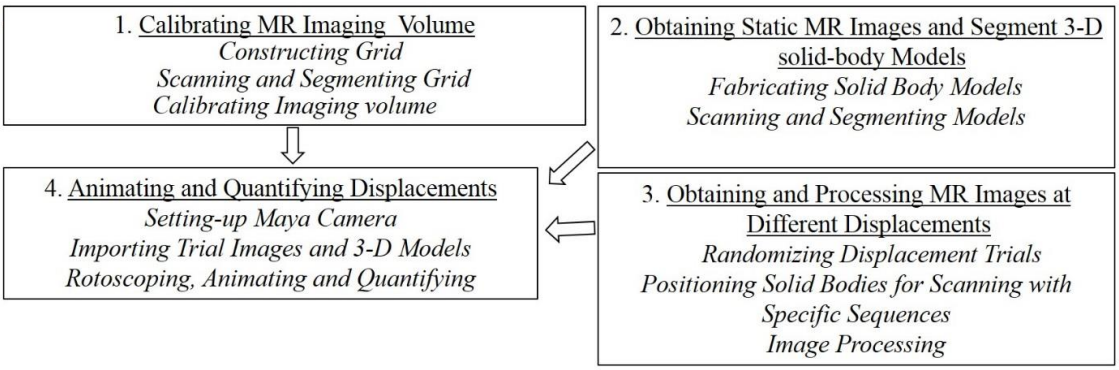

B

Planes	Displacements	
	Translation (0 to 20 mm / 5 mm increment)	Rotation (0° to 20° / 5° increment)
Single (z- plane)	n=35; 7 trials/displacement	n=30; 6 trials/displacement
Biplanar (z- and x- planes)	n=20; 4 trials/displacement	---

Figure 27. Steps involved in the technique and types of displacements quantified. ***A***. Overview of the quantification technique. ***B.*** Number of trials for each type of displacement performed. Note that for each displacement paradigm, data from two different pulse sequences were obtained.

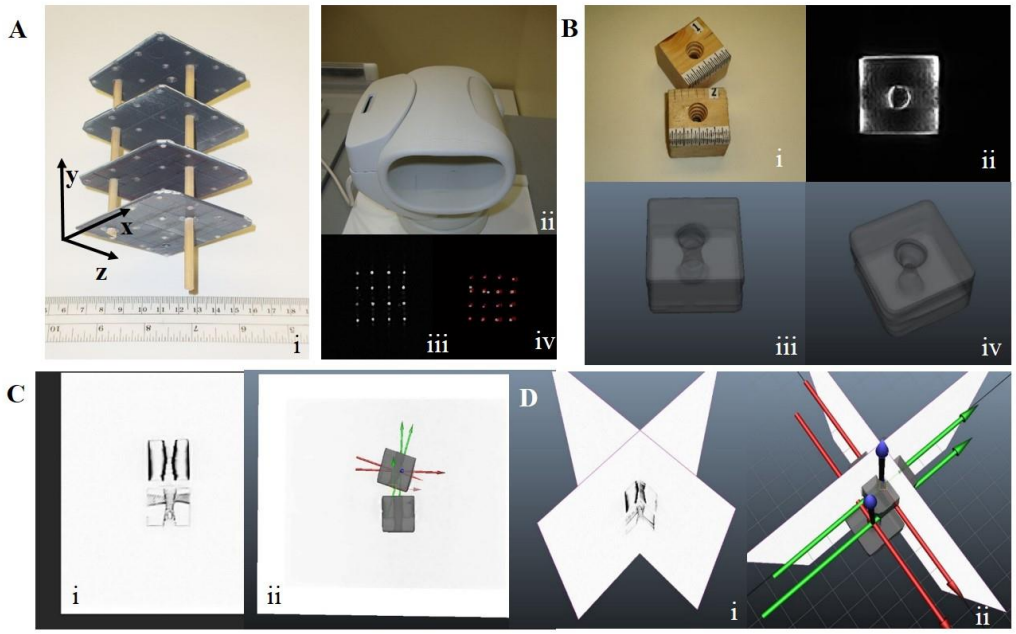

Figure 28. Overview of the animation processes leading to the quantification of a single-plane and biplanar displacements.
A. Imaging volume calibration: (i) the calibration grid with orientation of the plates in space, (ii) MRI coil with orientation of the imaging volume, (iii) & (iv) pre- and post-digitized bead images from the grid. ***B***. (i) shows positioning of a translation trial. The solid-body models are spaced ~10 mm apart flat on a foam platform. The lower cube has been translated by 0.5 mm to the right relative to the upper cube, indicated by a wooden pointer (asterisk) and measured by the caliper. The orientation of the displacement has been shown by the coordinate axis. (ii) View of the wooden cubes. (iii) High-resolution axial T_1 image slice through a cube. (iv) Representative 3-D model of a segmented cube. (v) Model as viewed after being imported into the animation environment. ***C.*** (i) Representative image from a single-plane translation trial with the T_1 sequence. (ii) Representative image from a single-plane rotation trial with the contrast-enhanced sequence. ***D.*** (i) Representative single-plane rotoscoping "scene." The image slice (white background) lies obliquely across the figure. The solid-body shadow is visible with its outline in the image slice (lower arrow). Upper half of the superimposed cube model is visible (upper arrow) with the anatomical axis. (ii) Image frame from a translation trial viewed from the top of the animation scene. The two cube models are cut through by the image slice (dark horizontal plane) across the hourglass holes within the models. (iii) Orthogonal image slices with registered 3-D models.

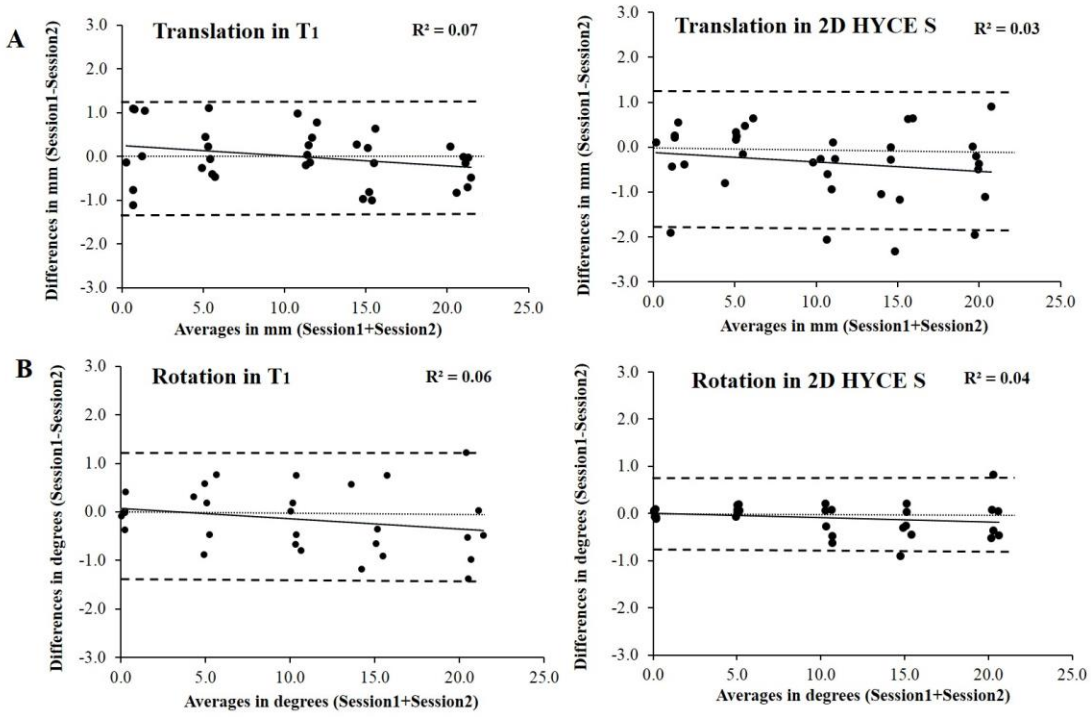

Figure 29. Bland–Altman plots for the translation and rotation trials.
A: Plots of the translation displacements quantified with the two sequences. The dashed lines representing the 95% confidence interval of test-retest differences for all translations show that the between-session differences were within ±1.24 mm (mean/bias=0.02 mm) and ±1.59 mm (mean/bias= -0.34 mm) for the T_1 (left) and the 2D HYCE S (right) sequences, respectively. ***B:*** Plots of the rotation displacements quantified with the two sequences. The dashed lines representing the 95% confidence interval of all rotations show that the test-retest differences were within ±1.27º (mean/bias= -0.14º) and ±0.65º (mean/bias=0.09º) for the T_1 (left) and the 2D HYCE S (right) sequences, respectively. The central narrow line denotes zero difference mark. The dark line at the center represents the trend line. Homoscedasticity (R^2 values < 0.1) indicated that the between-session differences in the measurements did not increase with an increase in the magnitude of the measured displacement. Heteroscedasticity was represented by R^2 values > 0.1, indicating that the between-session differences in the measurements increased with an increase in the magnitude of the measured displacement.

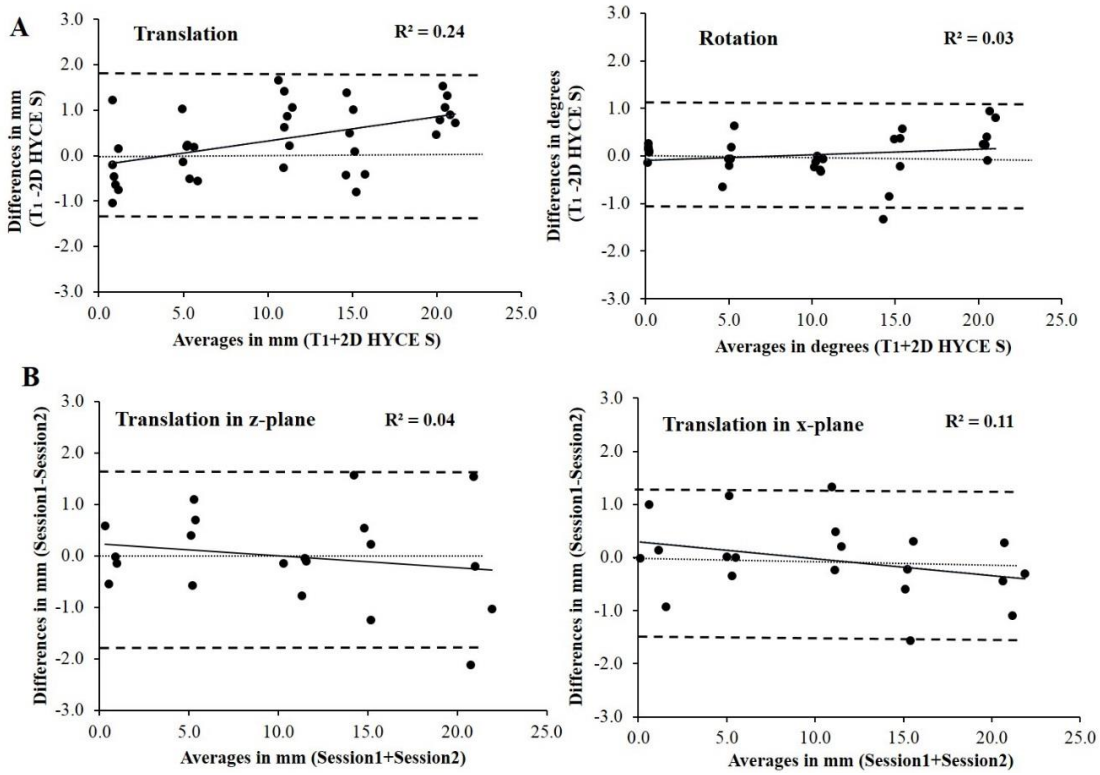

Figure 30. Bland–Altman plots comparing the measurements between two sequences, and outcomes of biplanar translations using 2D HYCE S sequence. ***A.*** Plots comparing outcomes using T_1 and the 2D HYCE S sequences. The dashed lines representing the 95% confidence intervals show that the between-session differences in the measurements obtained with the T_1 and the 2D HYCE S sequences fell within ±1.85 mm (mean/bias = 0.35 mm) for translations (left) and within $\pm 0.95^0$ (mean/bias= 0.02^0) for all rotations (right) quantified. ***B.*** Bland–Altman plots for biplanar 2D HYCE S translations. The dashed lines representing the 95% confidence intervals show that the test-retest differences for translations fell within ±1.77 mm (mean/bias = -0.01 mm) and ±1.41 mm (mean/bias= -0.04 mm) for the z- and x-planes, respectively. The central narrow line denotes zero difference mark. The dark line at the center represents the trend line. Homoscedasticity (R^2 values < 0.1) indicated that the random errors did not increase with an increase in the magnitude of the measured values. Homoscedasticity (R^2 values < 0.1) indicated that the differences in the measurements did not increase with the increase in the magnitude of the measured displacement. Heteroscedasticity was represented by R^2 values > 0.1, indicating that the differences in the measurements increased with the increase in the magnitude of the measured displacement.

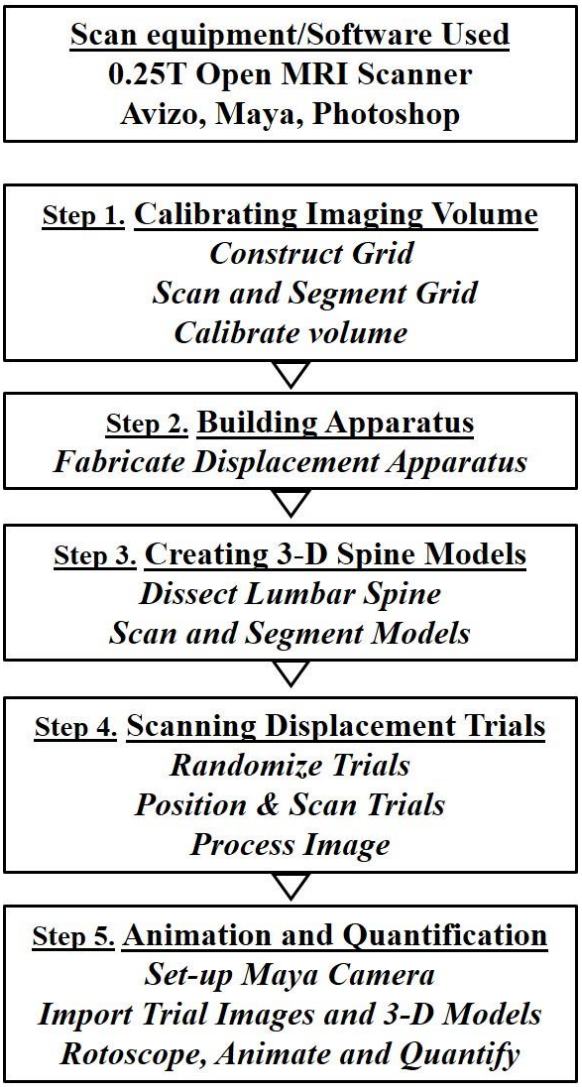

Figure 31. Workflow of the reported technique showing the steps leading to animation and quantification.

Calibration of imaging volume, building of the displacement apparatus, and dissection of the spine models were completed before execution of the trials. Scanning for static axial images for model segmentation was performed at the beginning of the first trial session.

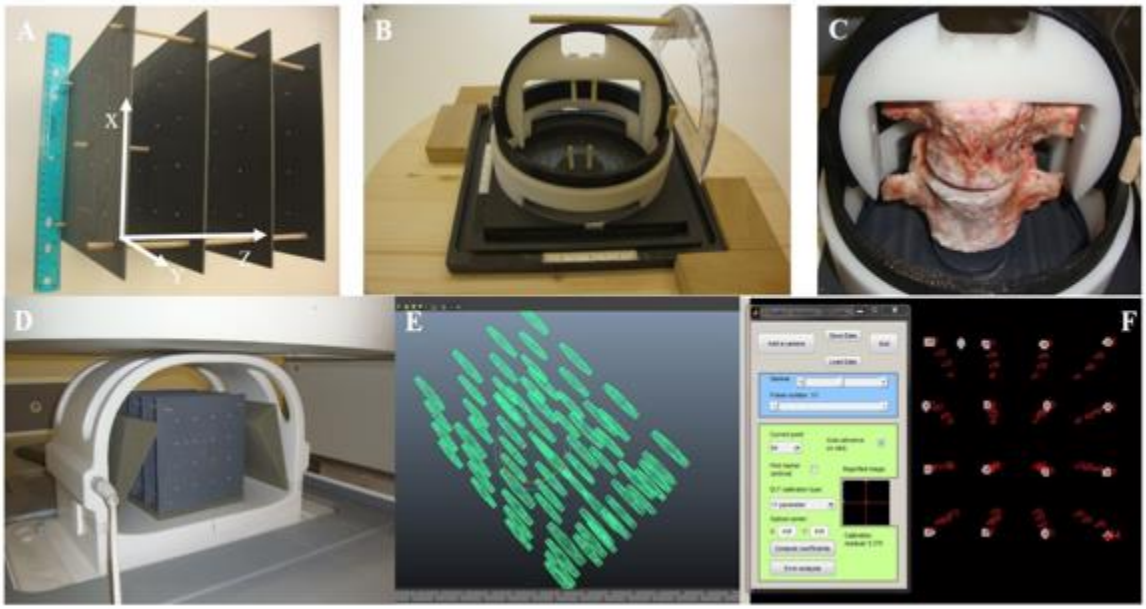

Figure 32. The grid, displacement apparatus and calibration outputs.
Clockwise from top left: ***A.*** The four-plate grid system shown with the coordinates for bead numbering. ***B.*** The assembled displacement apparatus shown mounted on the wooden platform. The clamp system consists of a semicircular (top) and a full horizontal (bottom) ring system (black). The upper semicircular ring accommodates the inner clamp (white) system that can rotate in the plane of the outer (black) ring. The upper vertebra is fixed to the vertical pair of screws in the white clamp. The upper half ring is connected to the lower full black ring orthogonally at two joints that allow the upper ring to change its vertical angulation as required. This clamp system is positioned on a wider-base axial rotating ring. The entire assembly with the base ring is located on top of a three-base-plate system in which the lowermost plate is stationary and provides a pair of screws to fit the lower vertebra. The upper two plates are hollowed at their centers and can slide orthogonally in relation to each other. The uppermost plate is grooved on its upper surface to firmly support the clamp and the base-ring system. Note the Vernier scale system used to measure the actual experimental displacements. ***C.*** The apparatus assembly shown with a pair of porcine motion-segments attached to the device. ***D.*** Scanning the grid plates. ***E.*** View of the segmented grid beads in the animation software MAYA, in which the centroids for each bead are calculated to generate the framespecs.csv file. ***F.*** Digitized grid plate showing the beads in the 3-dimensional perspective, according to the coordinate system assigned, and the calibration coefficient outputs, as calculated by MEL-script.

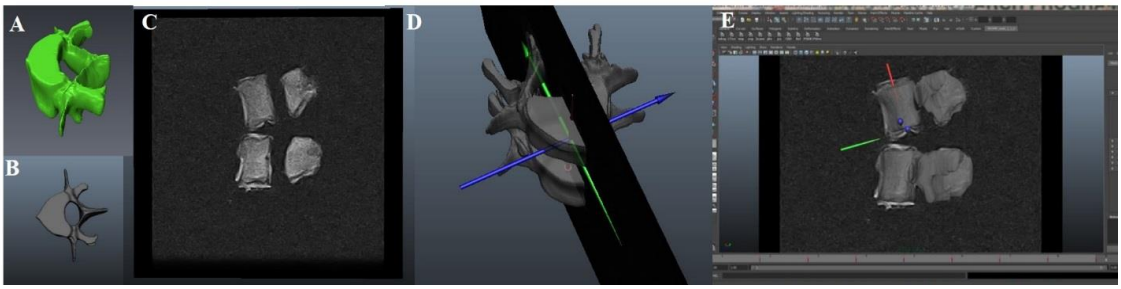

Figure 33. Segmentation, scene and rotoscoping.
A. View of a segmented vertebra using AVIZO software. ***B.*** 3-dimensional model as viewed in the animation software. ***C.*** Representative image from a rotation trial acquired with a fast contrast-enhanced MRI sequence. ***D.*** Projection image from one of the animation frames, as seen from above. Notice the animation background 'scene' or image slice stretching obliquely across the figure from top left to bottom right. Observe the models cutting across the scene as a model-to-image match is being performed in the sagittal plane. ***E.*** Screenshot of a representative animation image from a rotation trial showing a motion-segment model registered to the image scene.

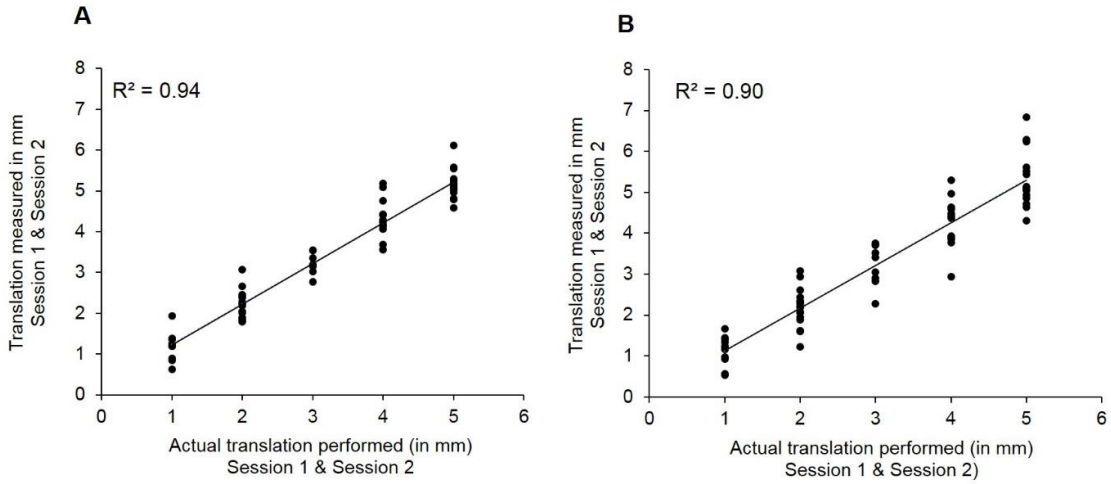

Figure 34. Relationship between translations quantified in both rotoscoping sessions and the actual translations performed.
A. Translational displacements measured using a T_1 sequence. ***B.*** Translational displacements measured using a 2D HYCE S sequence.

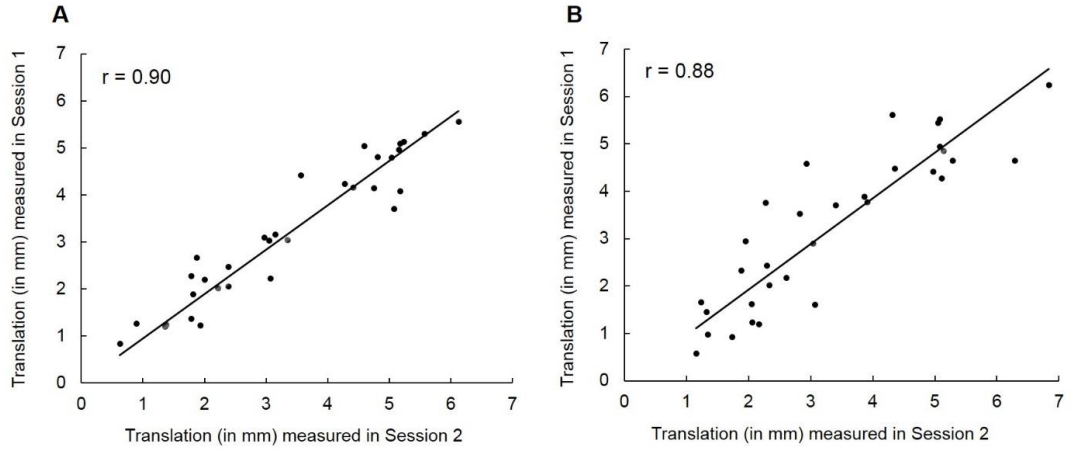

Figure 35. Strength of relationship between translations quantified in the two rotoscoping sessions.
A. Translational displacements measured using a T_1 sequence. ***B.*** Translational displacements measured using a 2D HYCE S sequence. r = Pearson's correlation coefficient.

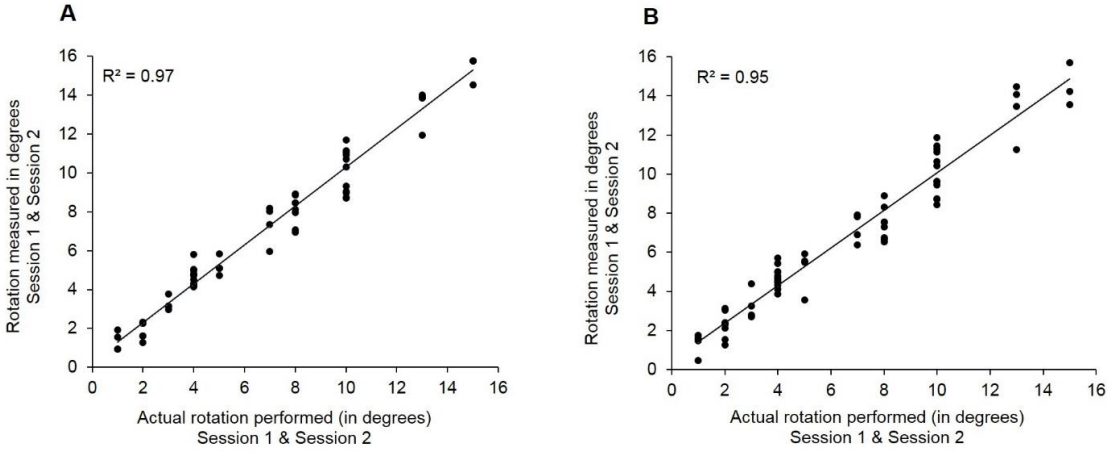

Figure 36. Relationship between rotations quantified in both rotoscoping sessions and the actual rotations performed.
A. Rotational displacements measured using a T_1 sequence. ***B.*** Rotational displacements measured using a 2D HYCE S sequence.

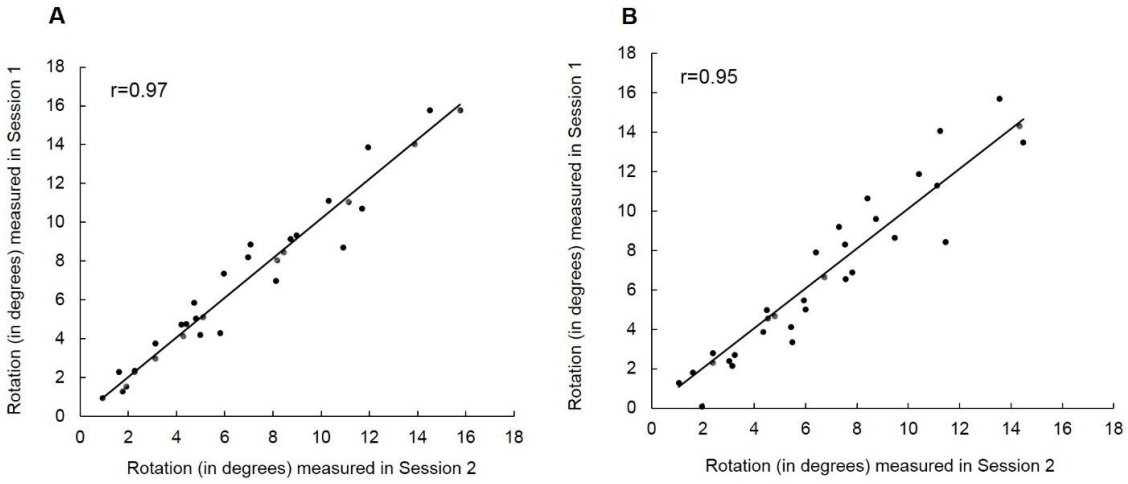

Figure 37. Strength of relationship of between rotations quantified in the two rotoscoping sessions.
A. Rotational displacements measured using a T_1 sequence. ***B.*** Rotational displacements measured using a 2D HYCE S sequence. r = Pearson's correlation coefficient.

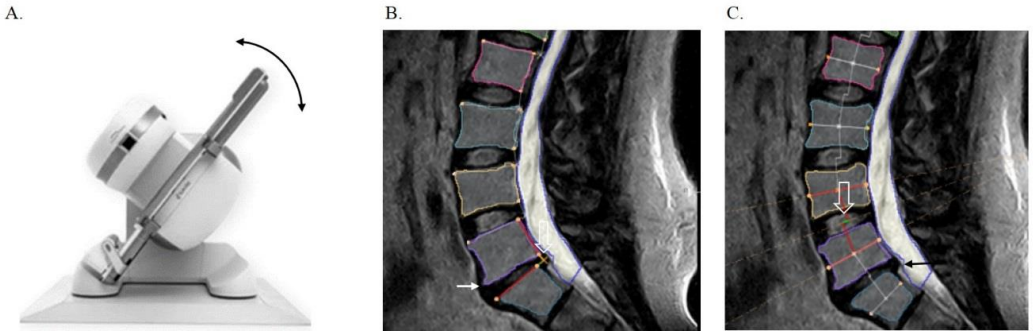

Figure 38. Weight-bearing MRI and Orthocad measurements parameters.
A. Photo of the weight-bearing (WB) MRI (G-Scan Brio) with the ability to rotate from supine to a fully upright, weight-bearing position in 1° increments. ***B.*** Sagittal view of the segmented vertebrae in WB. Open arrow shows the 'Intervertebral Listhesis' parameter that is calculated as the distance between the adjacent corners at the posterior ends of contiguous vertebrae. Arrow demonstrates the bony spur at the anterior end of the lower vertebral edge of L5. ***C.*** Open arrow demonstrates the 'Translation' parameter calculated as the distance between the two perpendicular projections drawn to the centers of two adjacent vertebrae from the median bisector of the segmental angle at a given vertebral level (L4-L5, here). The arrow points to the bulging L5-S1 disc on WB.

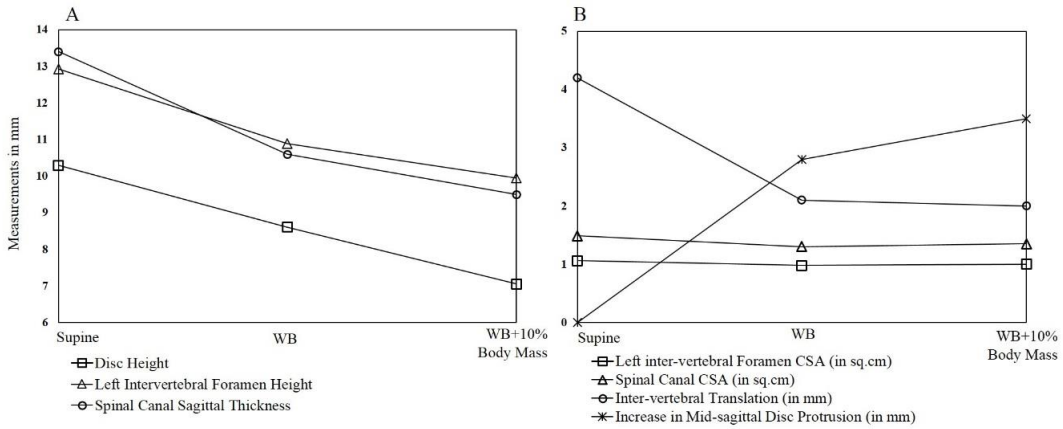

Figure 39. Parameters as measured at the L5-S1 segment in the supine, WB (weight bearing) and the WB+AL (weight bearing and additional loading).
A. Changes in disc heights, Intervertebral Foramen Height (left side) and L5-S1 sagittal plane dimension. ***B.*** Alterations in L5-S1 left inter-vertebral foramen cross sectional area (CSA), L5-S1 spinal canal CSA (in cm^2), Inter-vertebral Translation calculated as the distance (on the median bisector) between the perpendicular projections to the centers of two adjacent vertebra drawn from the median bisector of the segmental angle at a given vertebral level, and the change in sagittal-plane posterior disc protrusion measured form the disc-tip to the perpendicular bisectors drawn to the adjacent L5-S1 vertebral corners (represented here taking the value of the supine position=zero/baseline).

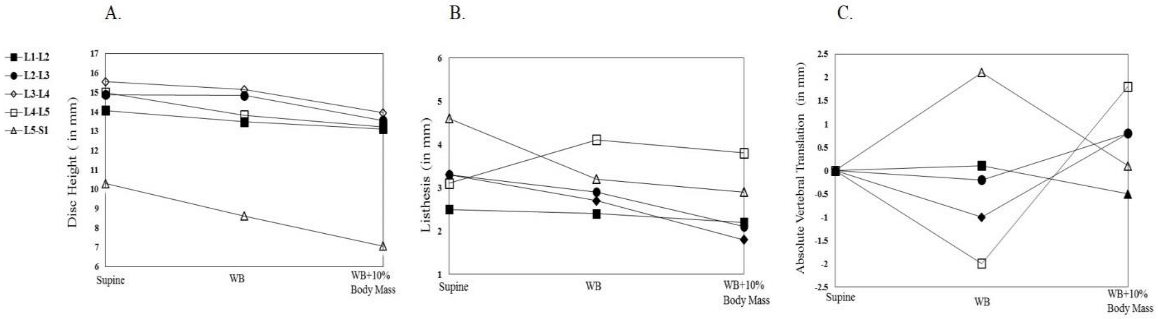

Figure 40. Dimensional changes in disc heights, listhesis and absolute translations with three loading conditions.
A. Changes in disc heights across the three imaging conditions. Note the reduction at the L5-S1 level with progressive weight-bearing (WB) load. ***B.*** Changes in listhesis across the three imaging conditions. Note the reduction at the L5-S1 with WB and the increase at the L4-L5 space with WB. ***C.*** Changes in absolute translation across the three imaging conditions. Note the large linear displacements at L5-S1 and L4-L5 (in opposite directions) with WB, and the relatively large shift with WB+AL at L4-L5.

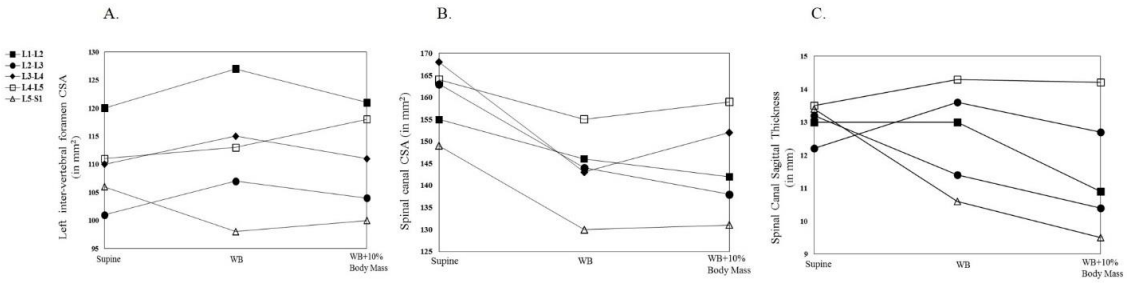

Figure 41. Dimensional changes in lateral foramen, spinal canal cross sectional area (CSA) and sagittal spinal canal thickness with three loading conditions. ***A.*** Changes in left inter-vertebral foramen CSA across the three weight-bearing (WB) conditions. Note the reduction with WB at the L5-S1 level. ***B.*** Changes in spinal canal CSA across the three WB conditions. Note the change at L5-S1, L3-L4 and L4-L5 with WB, and increase at the L3-L4 level with WB+AL. ***C***. Changes in spinal canal sagittal thickness across the three loading conditions. Sagittal dimension of the spinal canal. Note the marginal increase in this dimension at the upper three levels with WB, and gradual decline lowest two levels with WB and WB+AL.

Thesis and Dissertation Services